Clumped isotope analysis of carbonates: analytical aspects, calibration and application to Silurian brachiopod shells and diagenetic phases from Gotland/Sweden

Dissertation
submitted in fulfilment of the requirements for the degree of
Doctor of Philosophy

Institute of Geosciences
Department of Paleontology
Johann Wolfgang Goethe-University
Frankfurt/Main

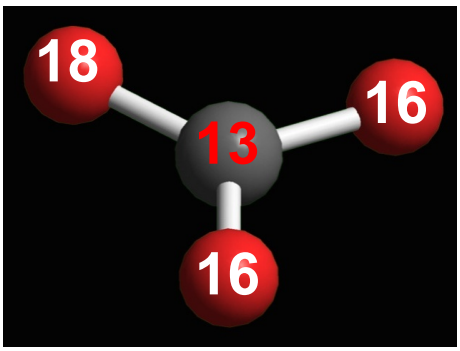

by Ulrike Wacker
from Nürnberg

Frankfurt (August 2014)

(D30)

Vom Fachbereich 11 der Johann Wolfgang Goethe-Universität als Dissertation angenommen.

Dekan: Prof. Dr. Andreas Junge

Gutachter: Dr. habil. Jens Fiebig
Prof. Dr. Stefano M. Bernasconi

Datum der Disputation:

TABLE OF CONTENTS

List of Figures iv
List of Tables vi
Acknowledgements vii

Abstract 1

1 Introduction 3
1.1 Carbonate clumped isotope paleothermometry 4
1.2 Recent developments in clumped isotope analysis and paleothermometry 7
1.2.1 Data reduction and interlaboratory comparison 7
1.2.2 Calibration of the carbonate clumped isotope thermometer 9
1.3 Acid digestion, gas preparation and clumped isotope analysis performed in Frankfurt 10
1.3.1 Phosphoric acid digestion 11
1.3.2 Purification of analyte gas 12
1.3.3 Mass spectrometric analysis 14
1.4 Application of clumped isotope thermometry to Silurian carbonates 15
1.5 Objectives and outline of the thesis 17

2 Background effects on Faraday collectors in gas-source mass spectrometry and implications for clumped isotope measurements 19
2.1 Introduction 20
2.2 Experimental 22
2.2.1 Mass Spectrometers 22
2.2.2 Background determination on masses 44-49 23
2.2.3 Clumped isotope notation 27
2.3 Results 28
2.3.1 Negative backgrounds on Faraday cups 28
2.3.2 Significance of the mass 49 signal of CO_2 measured through a 10^{12} Ω resistor 29
2.4 Discussion 31
2.5 Background correction procedures 32
2.6 Conclusions and implications 38
2.7 Acknowledgements 39
2.8 Supplementary Information 40

3 Clumped isotope analysis of carbonates: comparison of two different acid digestion techniques 42
3.1 Introduction 43
3.2 Experimental 45
3.2.1 Samples and sample preparation 45
3.2.2 Acid digestion 46
3.2.3 CO_2 cleaning procedure 47
3.2.4 Measurements 47
3.2.5 Data processing 48
3.3 Results 50
3.4 Discussion 53
3.4.1 Correlation between sample size and Δ_{47} values 53
3.4.2 Potential occurrence of contaminants in sample-derived CO_2 54
3.4.3 Incomplete gas yield 56
3.4.4 Potential variations of fractionation factors during acid digestion 57
3.4.5 Secondary re-equilibration 59
3.4.6 Difference in the acid fractionation factors between 90 and 25 °C 61
3.4.7 Implications for discrepant calibrations 62

3.5 Conclusions 63
3.6 Acknowledgments 63
3.7 Supplementary Information 64

4 Empirical calibration of the clumped isotope paleothermometer using calcites of various origins 67
4.1 Introduction 68
4.2 Materials and methods 71
4.2.1 Sample material 71
4.2.1.1 Eggshell of an ostrich 72
4.2.1.2 Spondylus sp. 72
4.2.1.3 Dyscolia wyvillei 73
4.2.1.4 Cold seep carbonate 74
4.2.1.5 Foraminifera 75
4.2.2 Acid digestion, gas purification, mass spectrometric analysis and data reduction 77
4.3 Results 79
4.3.1 Standard materials 80
4.3.2 Regression line and statistical analyses 81
4.3.3 Replication of measurements 83
4.4 Discussion 84
4.4.1 Comparison of our calibration with previously published studies 84
4.4.2 Potential reasons for discrepant calibrations at 90 °C and 25 °C digestion temperatures 88
4.4.2.1 Scaling of Δ_{47} data 88
4.4.2.2 Phosphoric acid fractionation: sensitive to the bulk or clumped isotopic composition of carbonates? 89
4.4.2.3 Partial re-equilibration of CO_2 at either 25 or 90 °C 90
4.4.3 Disequilibrium precipitation 92
4.4.4 Isotopic mixing 94
4.5 Conclusions 95
4.6 Acknowledgements 96
4.7 Supplementary Information 96
4.8 Appendices 105

5 Empirical calibration of the clumped isotope paleothermometer based on aragonite: preliminary results 108
5.1 Introduction 109
5.2 Material and Methods 110
5.2.1 Sample material 110
5.2.2 Acid digestion and gas preparation 111
5.2.3 Isotopic analysis 111
5.2.4 Data reduction 112
5.3 Results 113
5.3.1 Reference material 114
5.3.2 Calibration samples and authigenic aragonite 114
5.3.3 Regression line 114
5.4 Discussion and Outlook 115
5.4.1 Comparison with relevant published calibrations based on natural carbonates 115
5.4.2 Authigenic aragonite 117
5.5 Acknowledgements 117
5.6 Supplementary Information 118

6 Clumped isotope analysis applied to Silurian carbonates (Gotland/Sweden): deciphering both the alteration degree of fossil brachiopod shells and diagenetic processes 126
6.1 Introduction 127
6.2 Materials and methods 131
6.2.1 Sample material 131
6.2.2 Microscopic analyses 131
6.2.3 Sample material for elemental and isotopic analysis 132
6.2.4 Analyses of trace element concentrations 133
6.2.5 Isotopic analysis 134
6.2.6 $T(\Delta_{47})$ and $\delta^{18}O_w$ estimations 134
6.3 Results 135
6.3.1 Brachiopod shells 138
6.3.2 Diagenetic phases 142
6.4 Discussion 143
6.4.1 Preservation state of the investigated fossils 143
6.4.2 $T(\Delta_{47})$ and $\delta^{18}O_w$ reconstructions: pristine versus altered values 145
6.4.2.1 $T(\Delta_{47})$ and $\delta^{18}O$ estimates for Silurian ocean water 145
6.4.2.2 Diagenetic processes 151
6.5 Conclusions 156
6.6 Acknowledgements 156
6.7 Supplementary information 157

7 Summary and outlook 168
7.1 Summary 168
7.2 Outlook 171

8 References 174

Zusammenfassung 188

Curriculum Vitae 193

List of Figures

Page

Figure 1.1 Projection of raw Δ_{47} data to the absolute scale (8)
Figure 1.2 Comparison of several published calibration lines (10)
Figure 1.3 Acid digestion techniques for carbonate clumped isotope anaylsis (11)
Figure 1.4 Schematic illustration of the high-vayuum extraction line (12)
Figure 1.5 Scheme of the gas chromatography setup (13)
Figure 1.6 Scheme of the mass spectrometer (14)
Figure 1.7 Trends of the $\delta^{18}O$ and $\delta^{13}C$ curves for the Silurian (Gotland/Sweden) (15)

Figure 2.1 Peak shape for ETH and GU by accelaration voltage scanning (23)
Figure 2.2 Peak shape of m/z 47 for ETH and GU by HV scanning and different m/z 44 intensities (24)
Figure 2.3 Backgrounds for ETH and Gu; expanded view of Figure 2.2 (24)
Figure 2.4 Dependence of the backgrounds for ETH for all six beams measured on 2 d (25)
Figure 2.5 Dependence of the backgrounds for GU for all six beams (26)
Figure 2.6 Change in m/z 49 peak intensity with m/z 44 for ETH and GU (30)
Figure 2.7 Heated and 25 °C equilibrated gas line for ETH calculated with the background determined by either the software or with gas flowing in the MS (33)
Figure 2.8 Heated gas line for GU calculated with the background determined by either the software or with the backgrounds measured with gas flow into the source (33)
Figure 2.9 Correlation of the m/z 49 signal with the background determined on the left side of the m/z 47 peak for ETH and GU (36)
Figure 2.10 Correction of the heated gas line with the m/z 49 vs. background m/z 47 for ETH and GU (37)

Figure 3.1 Correlation plot of Δ_{47} values and sample size for *A. islandica* and NBS 19 (54)
Figure 3.2 Δ_{47} values plotted vs. $\Delta(\Delta_{48})$ (55)
Figure 3.3 Crossplots of $\delta^{18}O$, $\delta^{13}C$ and Δ_{47} values for *A. islandica* and NBS 19 (57)

Figure 4.1 Calcite calibration line determined in this study (82)
Figure 4.2 Comparison of several calibration regression lines (86)
Figure 4.3 Comparison of calibration lines determined for carbonates digested at 90 °C (87)
Figure A4.1 Comparison of calibration lines obtained from mean or single Δ_{47} values (106)
Figure A4.2 Calibration regression obtained from single Δ_{47} values (107)

Figure 5.1 Aragonite calibration line determined in this study (115)
Figure 5.2 Our aragonite calibration compared with lines based on digestions of natural carbonates at 90 °C and theoretical predictions (116)

Figure 6.1 Stratigraphic map of Gotland, sample localities and published $\delta^{18}O$ and $\delta^{13}C$ for brachiopod shells from Gotland (132)
Figure 6.2 Cathodoluminescent structures for the studied brachiopod shells (139)
Figure 6.3 Ultrastructural preservation states for the studied brachiopod shells (140)
Figure 6.4 Crossplots Δ_{47} ratios and element concentrations shells and diagenetic phases (141)
Figure 6.5 T(Δ_{47}) values of the analyzed brachiopod shells (146)
Figure 6.6 Ultrastructural preservation along ontogenetic shell transects and T(Δ_{47}) as well as $\delta^{18}O_w$ values estimated for samples of varying preservation (148)
Figure 6.7 Trace element concentrations of shells from Diupvik versus Δ_{47} values (150)
Figure 6.8 Alteration mechanisms of calcite during diagenesis and T(Δ_{47}) behaviour (152)
Figure 6.9 T(Δ_{47}) estimates for the different phases of each samples (153)
Figure 6.10 T(Δ_{47}) versus $\delta^{18}O$ as well as $\delta^{18}O_w$ values for the different phases (154)

Figure 7.1 $\delta^{11}B$ values of three depth transects of sample 17-1 (172)
Figure 7.2 $\delta^{11}B$ and $^{87}Sr/^{86}Sr$ ratios of the different phases of sample Val(1)-1 (173)

List of Tables

Page

Table 1.1 Relative Abundances of CO_2 and CO_3^{2-} isotopologues at random distribution (5)

Table 2.1 ETH data Fig. 2.7 (40)
Table S2.2 FRA data Fig. 2.8 (40)
Table S2.3 FRA data Fig. 10(A) (41)
Table S2.4 ETH data Fig. 10(B) (41)

Table 3.1 Isotopic results of digestions at 25 and 90 °C (50)
Table 3.2. Differences in acid fractionation factors between 90 and 25 °C (62)
Table S3.1 Heated and water equilibrated gas data (64)

Table 4.1 Sample material (72)
Table 4.2 Isotopic results (79)
Table 4.3 Numerical details of predictor and response variables (83)
Table 4.4 Published calibration equations including our results (87)
Table 4.5 Comparison of $\delta^{18}O_{calcite}$ with independently constrained $\delta^{18}O_{water}$ values (94)
Table S4.1 Heated and water equilibrated gas data (96)
Table S4.2 Isotopic data of samples and standards (99)

Table 5.1 Isotopic results of sample Material (113)
Table 5.2 Numerical details of predictor and response variables (115)
Table S5.1 Heated and water equilibrated gas data (118)
Table S5.2 Isotopic data of samples and standards (121)

Table 6.1 Geochemical data of the shells, micritic phases and sparitic cements (135)
Table S6.1 Heated and water equilibrated gas data (157)
Table S6.2 Isotopic data of samples and standards (160)

Acknowledgements

First of all I would like to thank Jens Fiebig who gave me the chance to work on this project and who adviced me in the last four years. I have benefited from his chemical and technical knowledge that greatly enlarged my skills to work with analytical methods. He, furthermore, supported me in difficult moments and gave me plenty of rope for choosing study material that was not related to the DFG proposal (i.e., the Silurian samples). In addition, he provided me to take part in several conferences and workshops which helped me to share information with colleagues and to establish contacts in the scientific community. Besides, thanks go to Bernd Schöne who was the second applicant of the DFG project. Sven Hofmann is acknowledged for technical support during lab work, thanks also to the glassblower Robert Röder. I appreciate the work of Niklas Löffler, Tina Lüdecke, Katharina Methner and Tanja Rutz who I have instructed about the clumped isotope technique and who were highly motivated and trustful.

I would like to thank the clumped isotope community for organizing workshops and sharing information with the group. I express my appreciation to John Eiler and Nami Kitchen who welcomed me to visit the clumped isotope lab at Caltech. They introduced me to their lab equipment and allowed me to use it. Also thanks to Hagit Affek and her group who showed me the clumped isotope lab at Yale University. These were important experiences at an early stage of my Ph.D. Moreover, I would like to thank Stefano Bernasconi for co-operation.

Biggest thanks go to all colleagues from the department of Earth Sciences in Frankfurt who I have met within the last four years. Social activities, a field trip to the Dolomites and scientific exchange had a positive impact on my work and my personal life. Special thanks to Axel Gerdes and Linda Marco, as well as Gernold Zulauf and Nicolas Thiemeyer for scientific experiments regarding $\delta^{11}B$ and $^{87}Sr/^{86}Sr$ as well as micro CT analyses; Alan Woodland is acknowledged for improving the English of the calibration paper. Furthermore, I would like to thank our secretary Conny Anhalt for her help with bureaucratic business and for organizing BBQs, Christmas parties, works outing, cocktail parties and much more.

Many friends, Ph.D. students and postdocs who contributed to a great time in Frankfurt and who helped me in difficult moments deserve thanks: Claudia and Klaus, Friedel, Lineth, Katha M., Tina, Sijo and Nimi, Erik, Micha, Fabian and Claudia, Matt, Stu, Maria, Nico, Filip, Iris, Jessi and Axel (and Sophia), Sietske, Alex, Karo, Katha C., Miri and Eike, André, Andreas and Voula (and Maja), Zahra and Justin, Christina, Anja, Tanja, Angela, Bas and Guillaume. Biggest thanks go to old and new friends who I have met on several conferences, especially Sarah, Melanie, Christoph, Manuel, Anna-Lena and Anne-Lise. Also greatest thanks to my best friends Sophia, Soraya and Irina; even though we could not get together for a while, our friendships did not change at all.

Special thanks go to my flat mates and friends Anke and Hayan for a very familiar time in Bockenheim. I wish you and Leo Fahed all the best. Thanks to Philipp (and Denise), Matthias and Hagen for being sympathetic and thoughtful in a short but busy time.

Furthermore, I would like to thank my crazy family Katrin, Bärbel, Birgit, Thomas, Karoline, Enys, Jochen, Amina, Ingrid, Burkhard, Marlis, Astrid and Marion. I have often missed you during the last four years and I have enjoyed the few and short moments when we have met.
Finally all my thanks go to my mum who cared for my sibblings and me, who enabled our education, teached us about ethics and who has always been with us in good and bad times. You supported me in tough times especially during the last ten years. Recently you gave me a helping hand in a very difficult situation, you handed out excellent adviced and you helped me to find my way again and to try new ways. In the end all your trust and support enabled me to finish this thesis. Danke Mama, muchas gracias!

Abstract

During this study clumped isotope analysis of carbonates was established at the Goethe University of Frankfurt, Germany. Therefore, preparation protocols and analytical parameters were elaborated to obtain precise and accurate Δ_{47} data. Briefly, analyte CO_2 was cleaned cryogenically using glass extraction lines to remove traces of water that enable re-equilibration of C–O bonds in the gases. Furthermore, analyte CO_2 was passed through a gas chromatograph (GC) to clean it from contaminants that produce isobaric interferences with m/z 47. Initially, phosphoric acid digestions of carbonates was conducted at 25 °C in McCrea-type reaction vessels. Afterwards samples were reacted at 90 °C using a common acid bath. Mass spectrometric analyses were performed using a MAT 253 equipped with a dual inlet system. Δ_{47} values were directly projected to the absolute scale using CO_2 gases equilibrated at distinct temperatures.

In cooperation with Stefano Bernasconi and his research group at ETH Zurich we studied the non-linearity that occurs for the measurement of m/z 47. This effect results from secondary electrons created by the m/z 44 beam. These electrons cause a negative background on the m/z 47 collector. A correction procedure was proposed that relies on the determination of the negative background on the m/z 47 Faraday cup. This approach might reduce time-consuming analyses of heated gases which were used so far to account for the observed non-linearity. However, the suggested correction of the negative background on the m/z 47 cup is only applicable if the slit width of the m/z 44 beam is significantly wider than that of the m/z 47 beam.

This thesis, furthermore, presents a comparison of the different phosphoric acid digestion techniques which are commonly used for carbonate clumped isotope analysis. For calcitic and aragonitic material digested at 25 °C in McCrea-type vessels we observed that the sample size has an effect on Δ_{47} data: higher mean Δ_{47} values and a larger scatter of data were received for samples <7 mg than for larger aliquots. For carbonate samples digested at 90 °C in a common acid bath no sample size effect was determined. We assume that secondary re-equilibration of CO_2 with water preferentially occurs at 25 °C producing the observed differences. However, a sample size effect can be avoided if reaction temperature is increased to 90 °C.

In order to make carbonate Δ_{47} data obtained from acid digestions at 90 °C comparable to Δ_{47} data received from reactions at 25 °C the difference of the acid fractionation factores ($\Delta_{47}{}^{*}{}_{25\text{-}90}$) between both temperatures has to be known. For the determination of the $\Delta_{47}{}^{*}{}_{25\text{-}90}$

value we have considered Δ_{47} data made at 25 °C from samples >7 mg only. For calicte and aragonite we obtained differences in fractionation factores of 0.075‰ and 0.066‰, respectively. These $\Delta_{47}{}^{*}{}_{25\text{-}90}$ values are coincident with the theoretical prediction of 0.069‰ proposed for calcite (Guo et al., 2009).

Moreover, this dissertation comprises a calibration study of the clumped isotope thermometer based on various natural calcites that grew between 9 and 38 °C. The samples include a brachiopod shell, a bivalve shell, an eggshell of an ostrich and foraminifera tests which formed from distinct biomineralizing processes. Furthermore we included an authigenic carbonate crystallized from biological-induced precipitation. The following linear relationship between $1/T^2$ and Δ_{47} was determined (with Δ_{47} in ‰ and T in K):

$\Delta_{47} = 0.0327\ (\pm\ 0.0026) \times 10^6 / T^2 + 0.3030\ (\pm\ 0.0308)$ $\quad (R^2 = 0.9915)$

This equation differs from the pioneering Ghosh et al. (2006a) calibration. However, our regression line is statistically indistinguishable from that of Henkes et al. (2013) which is based on aragonitic mollusks and calcitic brachiopod shells. Both studies have in common that calibration data were, at first, directly referenced to the absolute scale. In addition, both datasets rely on similar digestion techniques. Furthermore, the two calibrations are conform with the theoretical prediction of Guo et al. (2009).

The calcite calibration of the clumped isotope paleothermometer received in this study was applied to Δ_{47} data measured for Silurian brachiopods shells from Gotland/Sweden. Prior to isotopic analysis the fossils were intensively investigated for their preservation state (CL, SEM, trace elements). The lowest $T(\Delta_{47})$ values of ca. 28 to 33 °C were estimated from ultrastructurally well-preserved regions of some shells. For these samples also the lowest $\delta^{18}O_w$ values of Silurian seawater were determined. These estimates of ca. −1‰ confirm the assumption that the $\delta^{18}O$ value of the Silurian ocean was buffered to (0 ± 1)‰.

Nevertheless, most studied shells were characterized by a patchwork of pristine and altered shell portions resulting in elevated $T(\Delta_{47})$ values which plot mostly between 40 and 60 °C. Our results indicate that the clumped isotopic composition of the shells were altered at low water-rock ratios, not affecting the $\delta^{18}O$ values. Δ_{47} and $\delta^{18}O$ data of associated diagenetic phases (sparitic and micritic phases of the inner fillings of the fossils) provide evidence that the sparitic cements grew during several diagenetic events which occurred at different temperatures in fluid-buffered systems. We, furthermore, conclude that the micritic phases lithified at a very early diagenetic stage with the $\delta^{18}O$ values being most probably close to a Silurian seawater composition.

1 Introduction

The study of past climate is of utmost importance for predictions concerning future global climate change. Therefore, scientists of several disciplines search for indicators that help to decipher ancient climatic conditions. Sedimentological and ecological reconstructions, as well as geochemical data are combined in multiproxy studies. The results help to understand and to unravel mechanisms controlling global and regional climate trends, which are finally tested in models.

Water temperatures of ancient oceans are important indicators for climatic conditions having prevailed on Earth. The oldest method to determine absolute water temperatures relies on the oxygen isotope composition ($\delta^{18}O$) of minerals. If a crystal precipitates in oxygen isotopic equilibrium with ambient water the fractionation of the ^{18}O and ^{16}O isotope ratios between the mineral and the water depends on the temperature of growth as well as on the $\delta^{18}O$ value of the water (Urey, 1947). If the isotopic composition of the water can be constrained independently, growths temperatures of minerals and, therefore, past environmental conditions, can be reconstructed by determining the $\delta^{18}O$ values of the crystals. The $\delta^{18}O$ paleothermometer is widely applied to fossil material, especially to marine precipitates. However, sampled minerals mostly grew in water of unknown isotopic composition. Therefore, scientists have to refer to models that help to reconstruct $\delta^{18}O$ values of ancient ocean water (e.g., Muehlenbachs and Clayton, 1976; Gregory and Taylor, 1981; Gregory, 1991; Knauth and Roberts, 1991; Muehlenbachs, 1998; Veizer et al., 1999; Muehlenbachs et al. 2003; Kasting et al., 2006; Jaffrés et al., 2007; Turchyn et al. 2013). However, discrepant models regarding the evolution of the oxygen isotopic composition of seawater with time have been proposed (e.g., Muehlenbachs and Clayton, 1976; Veizer et al., 1999; Muehlenbachs et al. 2003; Kasting et al., 2006). As a consequence temperature reconstructions of the paleo-ocean have been accompanied with large uncertainties using the $\delta^{18}O$ paleothermometer. Several proxies were established since the 1990ies that enable an independent determination of ancient seawater temperatures and help to reconstruct $\delta^{18}O$ values of past ocean water. These are Sr/Ca ratios (Beck et al., 1992; Pfeiffer et al., 2006; Marshall and McCulloch, 2002) and Mg/Ca ratios (Nürnberg et al., 1996; Elderfield and Ganssen, 2000; Anand et al., 2003) of marine carbonates, as well as TEX_{86} measured on bulk sedimentary organic matter (Schouten et al., 2002; Wuchter et al., 2006; Kim et al., 2008). The most recent tool is the carbonate clumped isotope thermometer that was developed by John M. Eiler and his research group at California Institute of Technology (Caltech), Pasadena, USA (e.g., Ghosh et al., 2006a; Eiler, 2011).

1.1 Carbonate clumped isotope paleothermometry

Clumped isotope geochemistry got into the focus of several disciplines of Earth Sciences, e.g., paleoclimatic and paleoaltimetric reconstructions (e.g., Ghosh et al., 2006b; Came et al., 2007; Garzione et al., 2008; Huntington et al., 2010; Passey et al., 2010; Csank et al., 2011; Finnegan et al., 2011; Quade et al., 2011; Peters et al., 2013), atmospheric studies (e.g., Eiler and Schauble, 2004; Affek and Eiler, 2006; Yeung et al., 2009, 2012), as well as applications in petrology and investigations concerning diagenetic processes (e.g., Dennis and Schrag, 2010; Ferry et al., 2009; Huntington et al., 2011; Swanson et al., 2012). In contrast to conventional stable isotope analyses clumped isotope measurements addresses the abundances of isotopologues constituted by more than one heavy isotope (multiply-substituted isotopologues, Eiler and Schauble, 2004). Isotopologues characterized by two or more rare isotopes have unique chemical and physical properties which can help to understand distinct processes in nature in more detail (Eiler, 2007).

The analysis of clumped isotopes within natural gases is challenging because of their low abundance: more than one rare isotope is incoporated in only ≤10's per million molecules of a given population (Eiler, 2007, Table 1.1). Nevertheless, a method was developed which allows to determine the isotopic abundances of these rare masses (Eiler and Schauble, 2004).

So far, most geological applications of this new technique comprise carbonate clumped isotope thermometry. The ordering of isotopes in CO_3^{2-} groups of minerals is thermodynamically controlled. Bonds between heavy isotopes are lower in their zero-point energies than bonds between light isotopes (Bigeleisen and Mayer, 1947; Urey, 1947; Biegeleisen, 1955). Therefore, the abundance of isotopologues which contain bonds between heavy isotopes increases with decreasing temperature. Consequently, the measure of the abundance of clumped species provides information about thermal conditions during mineral growth (Ghosh et al., 2006a). The ordering of carbon and oxygen isotopes in a carbonate crystal is determined by the equilibrium constants of isotope exchange reactions. These equilibrium constants primarily depend on temperature. Carbonate clumped isotope thermometry relies on the isotope exchange reaction (1.1) involving the multiply substituted isotopologue $^{13}C^{18}O^{16}O_2^{2-}$:

$$Ca^{13}C^{16}O_3 + Ca^{12}C^{18}O^{16}O_2 = Ca^{13}C^{18}O^{16}O_2 + Ca^{12}C^{16}O_3 \quad (1.1)$$

So far, a direct measure of the abundances of carbonate groups which incorporate ^{13}C-^{18}O bonds within crystals is not possible. However, information concerning clumping of heavy isotopes in carbonates is preserved in CO_2 gas obtained from phosphoric acid digestion of the minerals (e.g., Ghosh et al., 2006a).

Table 1.1 *Relative abundances of CO_2 and CO_3^{2-} isotopologues at random distribution presuming $^{13}C/^{12}C$ ratios correspondent to V-PDB and $^{18}O/^{16}O$ as well as $^{17}O/^{16}O$ ratios equal to V-SMOW (after Ghosh et al., 2006a).*

Mass	*Isotope/Isotopologue*	*Relative Abundance*
C and O		
12	^{12}C	98.89%
13	^{13}C	1.11%
16	^{16}O	99.759%
17	^{17}O	370 ppm
18	^{18}O	0.204%
CO_2		
44	$^{16}O^{12}C^{16}O$	98.40%
45	$^{16}O^{13}C^{16}O$	1.10%
45	$^{17}O^{12}C^{16}O$	730 ppm
46	$^{18}O^{12}C^{16}O$	0.40%
46	$^{17}O^{13}C^{16}O$	8.19 ppm
46	$^{17}O^{12}C^{17}O$	135 ppb
47	$^{18}O^{13}C^{16}O$	45 ppm
47	$^{17}O^{12}C^{18}O$	1.5 ppm
47	$^{17}O^{13}C^{17}O$	1.5 ppb
48	$^{18}O^{12}C^{18}O$	4.1 ppm
48	$^{17}O^{13}C^{18}O$	16.7 ppb
49	$^{18}O^{13}C^{18}O$	46 ppb

Mass	*Isotopologue*	*Relative Abundance*
CO_3		
60	$^{12}C^{16}O^{16}O^{16}O$	98.20%
61	$^{13}C^{16}O^{16}O^{16}O$	1.10%
61	$^{12}C^{17}O^{16}O^{16}O$	0.11%
62	$^{12}C^{18}O^{16}O^{16}O$	0.60%
62	$^{13}C^{17}O^{16}O^{16}O$	12 ppm
62	$^{12}C^{17}O^{17}O^{16}O$	405 ppb
63	$^{13}C^{18}O^{16}O^{16}O$	67 ppm
63	$^{12}C^{17}O^{18}O^{16}O$	4.4 ppm
63	$^{13}C^{17}O^{17}O^{16}O$	4.54 ppb
63	$^{12}C^{17}O^{17}O^{17}O$	50 ppt
64	$^{12}C^{18}O^{18}O^{16}O$	12 ppm
64	$^{13}C^{17}O^{18}O^{16}O$	50 ppb
64	$^{12}C^{17}O^{17}O^{18}O$	828 ppt
64	$^{13}C^{17}O^{17}O^{17}O$	0.5 ppt
65	$^{13}C^{18}O^{18}O^{16}O$	138 ppb
65	$^{12}C^{17}O^{18}O^{18}O$	4.5 ppb
65	$^{13}C^{17}O^{17}O^{18}O$	9 ppt
66	$^{12}C^{18}O^{18}O^{18}O$	8 ppb
66	$^{13}C^{17}O^{18}O^{18}O$	51 ppt
67	$^{13}C^{18}O^{18}O^{18}O$	94 ppt

The measure of clumping in analyte CO_2 is expressed as the Δ_{47} value, which is the ratio between the abundances of mass 45 to 47 relative to mass 44 (R^{45}, R^{46}, R^{47}) and the correspondent random distribution ratios (R^{45*}, R^{46*}, R^{47*}):

$$\Delta_{47} = ((R^{47}/ R^{47*} - 1) - (R^{46}/ R^{46*} - 1) - (R^{45*}/ R^{45*} - 1)) * 1000 \quad \text{(in ‰)} \quad (1.2)$$

Applications

In several studies clumped isotope analysis was applied to ancient carbonates. In combination with the conventional $\delta^{18}O$ paleothermometer the proxy allows to determine both the temperatures and the $\delta^{18}O$ composition of ancient water. This advantage can help to solve given uncertainties regarding reconstructions of paleoenvironmental conditions in marine and terrestrial settings.

As noted above seawater temperatures offer important insights to the history of global climate. The $\delta^{18}O$ paleothermometer represents the proxy which has been most often addressed to reconstruct past environmental conditions. However, it is unclear, whether the oxygen isotopic composition of seawater has been buffered to (0 ± 1)‰ by low- and high-temperature alteration processes occurring at mid-ocean ridges (Muehlenbachs and Clayton, 1976; Gregory and Taylor, 1981; Gregory, 1991; Muehlenbachs, 1998; Muehlenbachs et al., 2003), or whether a secular change of $\delta^{18}O$ ratios has occurred with time (Veizer et al., 1997, 1999; Kasting et al., 2006). So far, clumped isotope data strengthen the assumption that the oxygen isotopic composition of Paleozoic seawater has been buffered to (0 ± 1)‰ (Came et al., 2007; Finnegan et al., 2011; Brand et al., 2012; Cummins et al., 2014). In addition, variations of the $\delta^{18}O$ value of the ocean caused by glaciation effects could be deciphered (Finnegan et al., 2011).

Besides, the clumped isotope paleothermometer is an important proxy for studies on pedogenic carbonates. The oxygen isotopic compositions of water from which soil carbonates precipitate vary largely dependent on regional conditions. Clumped isotope analysis can help (1) to decipher terrestrial climatic conditions (Passey et al., 2010), (2) to reconstruct paleoaltitudes and tectonic processes (e.g., Ghosh et al., 2006b; Huntington et al., 2010; Quade et al., 2011) and (3) to determine the season during which carbonate growth occurred (Peters et al., 2013).

Apart from paleoenvironmental reconstructions, the clumped isotope paleothermometer offers information concerning petrological studies and alteration meachanisms of carbonates during diagenesis (e.g., Dennis and Schrag, 2010; Ferry et al., 2011; Huntington et al., 2011; Loyd et al., 2012). Furthermore, processes of mineralization regarding isotopic equilibrium precipitation can be addressed (e.g., Affek et al., 2008; Daeron et al., 2011; Saenger et al., 2012; Kluge et al., 2014).

1.2 Recent developments in clumped isotope analysis and paleothermometry

1.2.1 Data reduction and interlaboratory comparison

Measured raw Δ_{47} values have to be corrected for a non-linearity of the mass spectrometer which otherwise affects the accuracy of Δ_{47} measurements (Huntington et al., 2009). This effect introduces a dependence of the Δ_{47} value of CO_2 gas on its bulk isotopic composition (δ^{47}). It has been proposed to monitor the non-linearity by measuring "heated gases" (Huntington et al., 2009). CO_2 enclosed in sealed quartz glass tubes is heated for at least 2 h at 1000 °C, so that the abundance of each isotopologue corresponds to a distribution close to stochastic. The "heated gas line" is determined in a plot of δ^{47} versus Δ_{47} values (sample gas versus reference gas). Raw Δ_{47} data have to be corrected for the slope of this line (Fig. 1.1: step 1 → 2).

Furthermore, raw Δ_{47} values are referenced to an internal scale depending on the clumped isotopic composition of the reference gas used for analysis. In order to make measured values comparable between different laboratories an absolute scale was developed. It is based on thermodynamic predictions of the extent of ^{13}C-^{18}O clumping in CO_2 gas (Dennis et al., 2011). A direct projection of Δ_{47} data to this scale is done via CO_2 gases equilibrated at a variety of temperatures (i.e., "heated gases" and water equilibrated gases). Measured non-linearity corrected Δ_{47} values received for CO_2 equilibrated at distinct temperatures are plotted versus Δ_{47} values theoretically predicted for gases at correspondent temperatures (Wang et al., 2004; Guo et al., 2009). This allows to construct the empirical transfer function (ETF) which is then applied to non-linearity corrected Δ_{47} values to finally receive absolute Δ_{47} values that are comparable between laboratories (Fig. 1.1; step 2 → 3). It is, furthermore, possible to reference Δ_{47} data to the absolute scale via a secondary transfer function using standard materials that have defined clumped isotope values. This option allows to project Δ_{47} values, which have been made before the establishment of the reference frame of Dennis et al. (2011), to the absolute scale.

Analyte CO_2 is obtained from phosphoric acid digestion of carbonate samples. Initially reactions were performed at 25 °C using sealed vessels (McCrea). Subsequently in several laboratories the digestion temperature was raised to 90 °C and the carbonates were digested in a common acid bath. In order to make Δ_{47} data of CO_2 obtained from samples digested at different temperatures comparable, the difference in acid fractionation between the two temperatures ($\Delta_{47}{}^{*}{}_{25-90}$) has to be applied (Fig. 1.1; step 3 → 4). The theoretical prediction of

the $\Delta_{47}{}^{*}{}_{25-90}$ value is 0.069‰ (Guo et al., 2009). This value is close to the empirical determination of Passey et al. (2010) who obtained a $\Delta_{47}{}^{*}{}_{25\text{-}90}$ value of 0.081‰. So far, this constant was applied to most published Δ_{47} data made at 90 °C. However, the value of Passey et al. (2010) is reported on the internal scale of Caltech. Furthermore, the correspondent analyses were performed at two different mass spectrometers. Later, Henkes et al. (2013) reported a difference in acid fractionation between 90 and 25 °C digestions of 0.092‰ which was directly referenced to the absolute scale. This $\Delta_{47}{}^{*}{}_{25-90}$ value is significantly higher than the theoretical prediction of Guo et al. (2009).

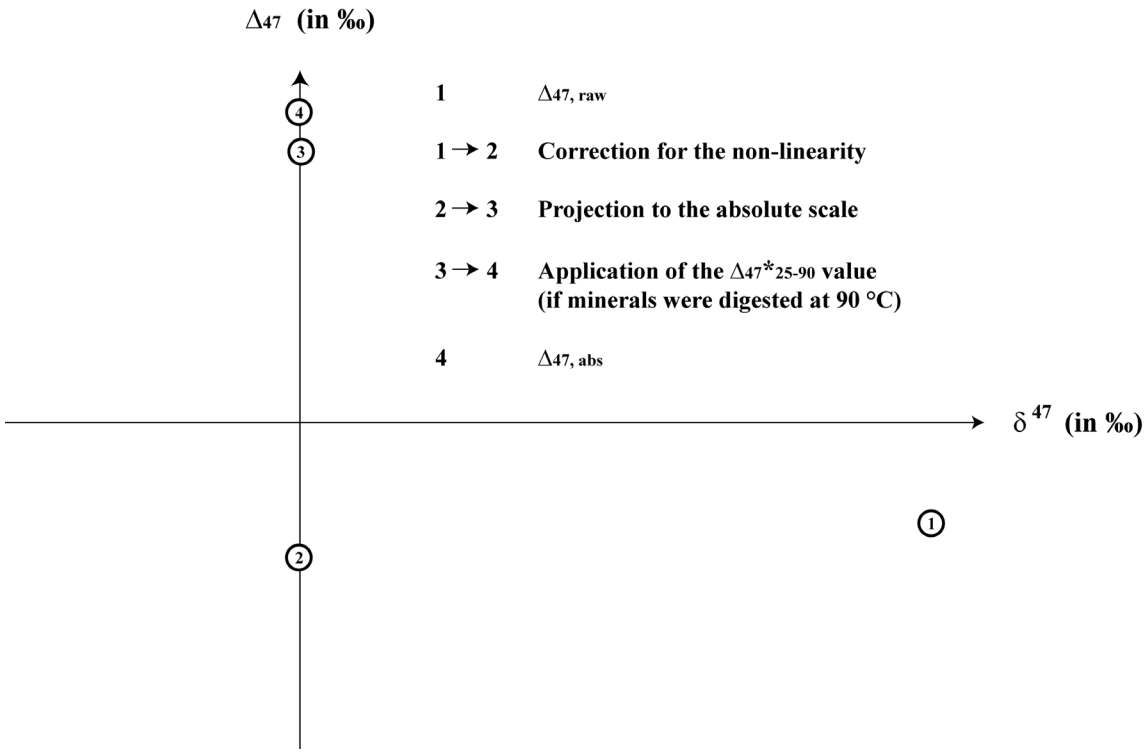

Figure 1.1 *Schematic illustration of the correction procedure to convert raw Δ_{47} data to the absolute scale (modified after Dennis et al., 2011). $\Delta_{47,\,raw}$ values are, at first, corrected for the non-linearity applying the slope correction determined by the heated gas line. Secondly, the ETF is applied to project data in the absolute reference frame based on theoretical predictions about equilibrium clumping in CO_2 gases. Finally, the $\Delta_{47}{}^{*}{}_{25-90}$ value has to be applied to clumped isotope data obtained from 90 °C digestions of minerals to make Δ_{47} values comparable to data from carbonates reacted at 25 °C.*

Clumped isotope analysis has been exclusively performed at Caltech for several years. However, the technique was established in further laboratories over the years. The increasing number of institutes measuring clumped isotopes requires intense interlaboratory comparisons to guarantee that reported Δ_{47} data are reliable. The most often used reference materials are

NBS 19 and Carrara marble. However, a comparison of average Δ_{47} values determined for NBS 19 reported from Caltech, Harvard, Yale and Johns Hopkins University revealed relatively large variations: the absolute difference between mean Δ_{47} values on the absolute scale is 0.031‰ and a standard deviation of 0.017‰ was received (Dennis et al., 2011). For comparison, the shot noise limit is generally ~0.008‰ (e.g., Huntington et al., 2009). Furthermore, no systematic trends were observed betweeb laboratories. For NBS 19 Harvard reported the lowest Δ_{47} average, but they determined the highest mean Δ_{47} value compared to the other laboratories for the standard DSC-45923 (Dennis et al., 2011). So far, the reasons for the deviations in reported Δ_{47} data are unknown. Further interlaboratory comparison has already been started, initiated by Stefano M. Bernasconi form ETH Zurich. A set of standard materials of a varying range in Δ_{47} and bulk isotopic compositions was prepared and was sent to several laboratories.

1.2.2 Calibration of the carbonate clumped isotope thermometer

As outlined above crystallization temperatures obtained from carbonate clumped isotope analysis were published in several studies. Nevertheless, these estimates should be evaluated critically as discrepant calibrations of the paleothermometer were obtained (Fig. 1.2). The first published calibration line relies on synthetic calcites that were precipitated between 0 and 50 °C (Ghosh et al., 2006a). This calibration was approved by Δ_{47} data for modern brachiopod shells and mollusks (Came et al., 2007), foraminifera (Tripati et al., 2010; Grauel et al., 2013), deep-sea corals (Thiagarajan et a., 2011), as well as synthetic calcites (Zaarur et al., 2013). Nevertheless, Dennis and Schrag (2010) reported a calibration based on synthetic calcites which yields a lower temperature sensitivity of Δ_{47} (flatter slope of the calibration line). An almost similar temperature sensitivity was determined in the study of Eagle et al. (2013) and Henkes et al. (2013) whose calibrations rely on modern mollusk and brachiopod shells. At least the slopes of the lines of Dennis and Schrag (2010), Eagle et al. (2013) and Henkes et al. (2013) are in agreement with the theoretical temperature sensitivity of the clumped isotope paleothermometer (Guo et al., 2009). However, the intercepts of all these calibration lines differ. It is still unknown why discrepant results were obtained in the different studies. No evidence for kinetic effects or analytical artifacts that might have affected carbonate growth or clumped isotope analysis have been found yet. So far, most published clumped isotope temperatures were estimated applying the Ghosh et al. (2006a) calibration line.

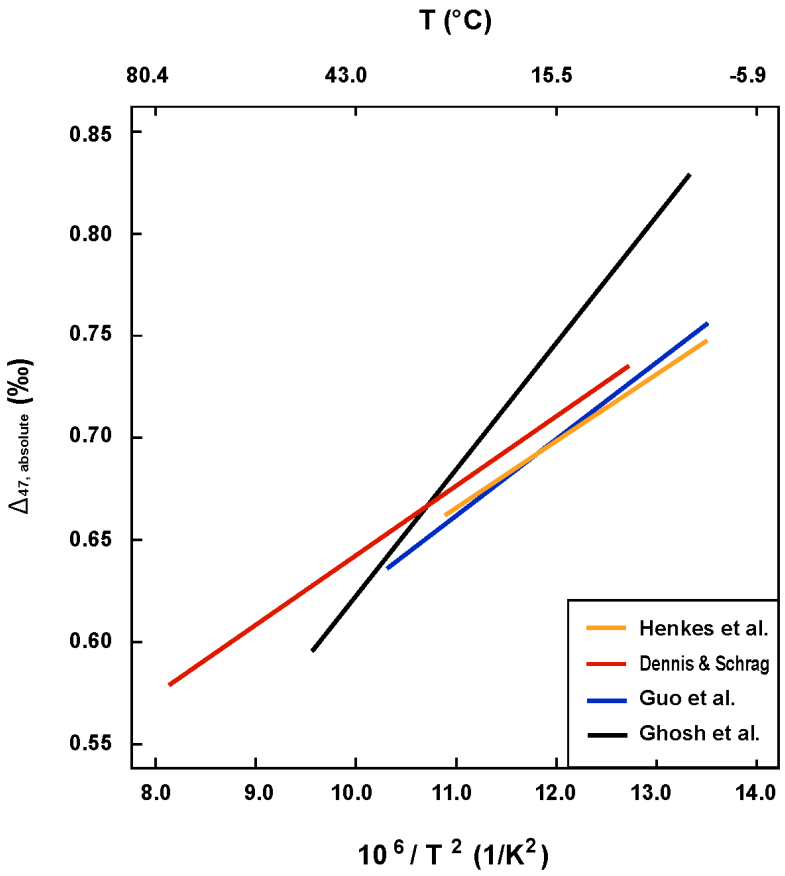

Figure 1.2 *Comparison of several published calibration lines of the carbonate clumped isotope thermometer (Δ_{47} data of Dennis and Schrag (2010) and Henkes et al. (2013) which are based on acid digestions of minerals at 90 °C were corrected for the difference in acid fractionation factors between 90 and 25 °C reactions applying the theoretical $\Delta_{47}{}^{*}{}_{25\text{-}90}$ value of Guo et al. (2009)). Though Δ_{47} values were directly or secondarily projected to the absolute scale discrepancies occurred. The Ghosh et al. (2006a) line based on synthetic calcite was confirmed by several studies on biogenic and synthetic carbonates (see text above). Nevertheless, it is not conform with the theoretical prediction of Guo et al. (2009). In contrast, the temperature sensitivity of Δ_{47} of the calibration of Dennis and Schrag (2010) is similar to that theoretically predicted by Guo et al. (2009); however, the intercept is significantly higher. Recently, Henkes et al. (2013) reported a calibration that is based on mollusk and brachiopod shells which is indistinguishable from the theoretical line. The reasons for these discrepancies are still unknown.*

1.3 Acid digestion, gas preparation and clumped isotope analysis performed in Frankfurt

One of the main target of this dissertation was the elaboration of gas preparation protocols for precise and accurate clumped isotope analysis at the Goethe University/Frankfurt. In the following, methodological aspects of this technique are briefly summarized. Detailed protocols regarding digestion of carbonates, gas preparation and mass spectrometric analysis, as well as data reduction used in this laboratory are reported in the “Methods section” of each chapter.

1.3.1 Phosphoric acid digestion

For the first published carbonate clumped isotope study minerals were digested with 103 wt.-% phosphoric acid at 25 °C in McCrea-type reaction vessels (Ghosh et al., 2006a). However, later on reaction temperatures were increased to 90 °C in several laboratories with digestions being performed using a common acid bath (Dennis and Schrag, 2010; Passey et al. 2010). Furthermore, higher H_3PO_4 densities of ~105 wt.-% were used (e.g., Henkes et al., 2013; Zaarur et al., 2011). In Frankfurt, both digestion techniques were operated (Fig. 1.3). However, due to the results described in chapter 3, we continued to digest carbonates at 90 °C in a common acid bath exclusively. We, furthermore, increased acid densities to ~106 wt.%.

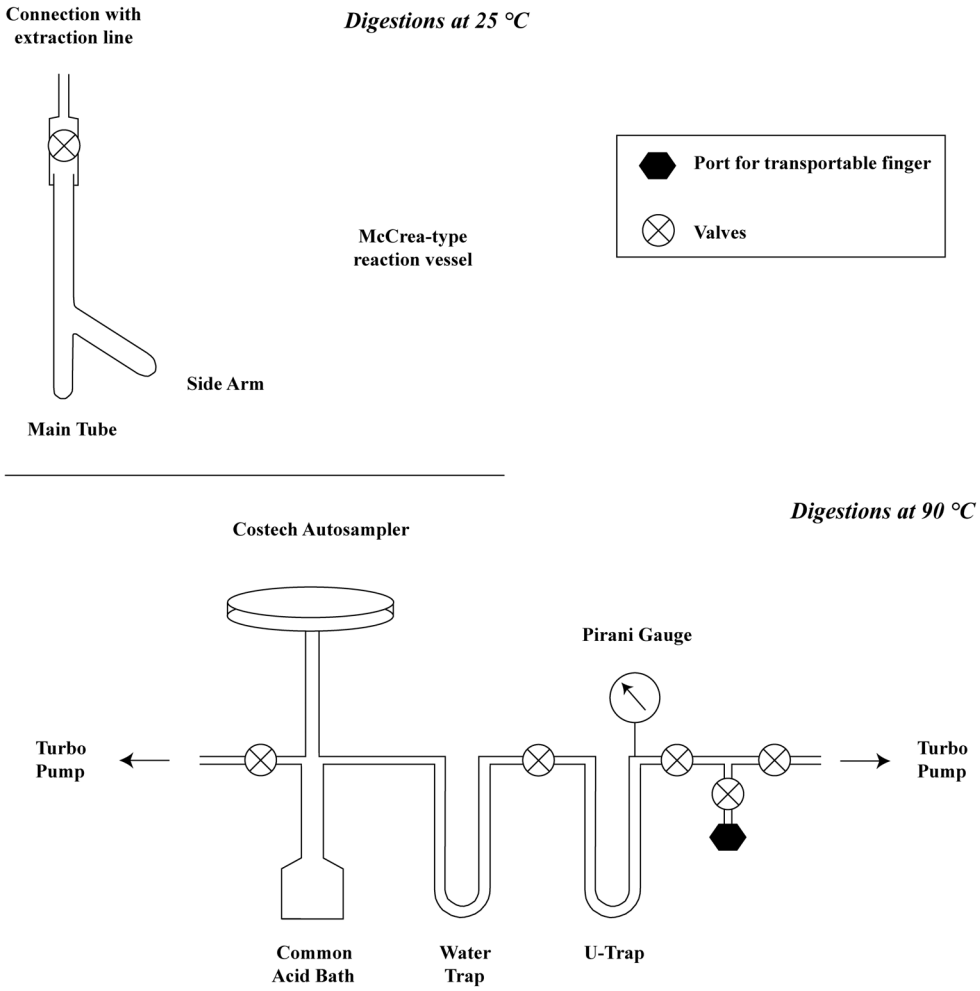

Figure 1.3 *Acid digestion techniques for carbonate clumped isotope anaylsis. McCrea-type reaction vessels are used for reactions at 25 °C. During digestion the vessel is put in a water bath at 25 °C (~12 h). Digestion at 90 °C is performed in a common acid bath (~30 min). The autosampler above the reaction vessel is loaded with carbonate samples filled in Ag capsules. The capsules fall into the stirred acid which is heated by a surrounding copper block. During the reaction analyte CO_2 is immediatelly frozen in a U-trap immerged in liquid nitrogen after passing a water trap held at −80 °C. Finally, the analyte gas is transferred into a transportable glass finger.*

1.3.2 Purification of analyte gas

Intensive purification of analyte CO_2 is necessary to obtain an accurate measurement of the small fraction of multiply substituted isotopologues in the gases (Eiler and Schauble, 2004; Ghosh et al., 2006a). Cryogenic purification of sample CO_2 is of utmost importance. Traces of water must be removed to avoid secondary re-equilibration within the gas. Water triggers the reordering of oxygen isotopes in CO_2. The abundances of the different CO_2 isotopologues will tend to a distribution that is characteristic for the temperature of re-equilibration. For this reason analyte gas is cryogenically purified using an extraction line held at high vacuum $<10^{-6}$ mbar (Fig. 1.4). CO_2 is passed at least twice over a water trap (a multiply looped helix) which is immerged in ethanol cooled to −80 °C with liquid nitrogen during gas preparation.

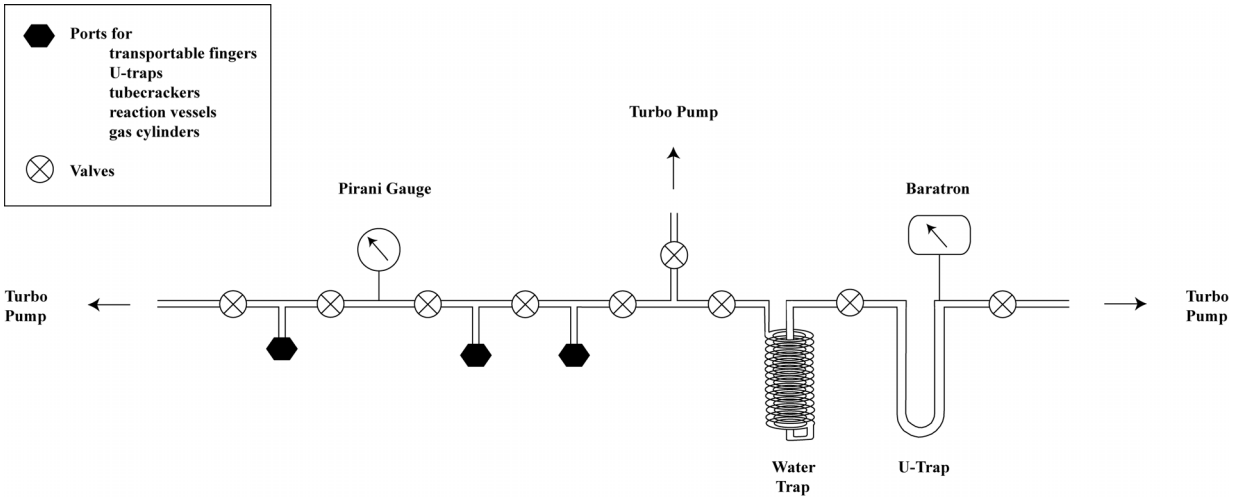

Figure 1.4 *Schematic illustration of the high-vayuum extraction line used for cryogenic purification of CO_2 at Goethe University/Frankfurt. During the preparation the water trap is immerged in ethanol cooled to −80 °C. CO_2 gas is frozen in the U-trap cooled with liquid nitrogen. Three ports can be used to connect equipment for gas transfers.*

Further purification comprises the removal of contaminant gases. This is done by gas chromatography (GC 8000 series CRYO 820; Fig. 1.5). Using He as a carrier gas (18 mL/min; purity: 99.9999%), sample CO_2 is passed through a stainless steel column (1.20 m x 2.15 mm ID) filled with Porapak Q 80/120 (Fig. 1.5(A)). During the gas transfer the column is cooled to −20 °C to fix contaminants such as hydrocarbons. At this temperature CO_2 can pass and contaminants can be successfully separated from the sample. It is essential to avoid re-equilibration triggered by traces of water that adheres on capillaries through which the analyte gases pass. For this reason, water traps cooled to −80 °C were installed both in front of and behind the GC column. We, furthermore, reverse the He flow between single sample runs

to immediately remove water that might have entered the column during gas transfer (Fig. 5(B)).

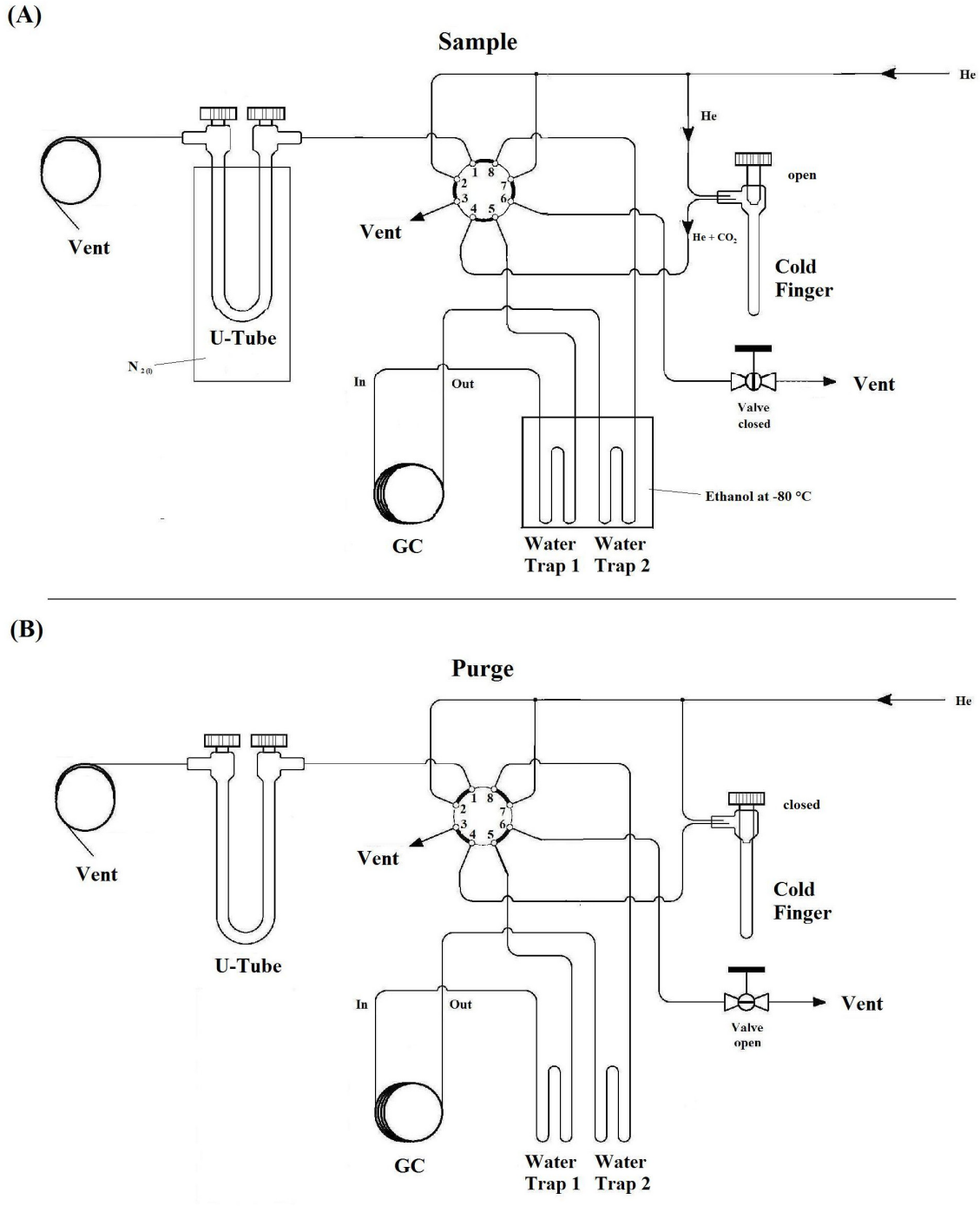

Figure 1.5 *Scheme of the gas chromatography setup. (A) Positions of valves during sample gas transfers: CO_2 is transported in a He flow from the open cold finger via the Valco valve through the first water trap held at −80 °C; the gas passes the GC column cooled to −20 °C; behind, CO_2 is transported over a second water trap at −80 °C; finally, it is transferred via the Valco valve to a U-trap immerged in liquid nitrogen; CO_2 freezes while He gas can pass through the capillary connected to the U-trap. (B) Positions of the valves between sample gas transfers: by the switch of the Valco valve the He flow is reversed to remove water or other contaminating substances on the shortest way.*

1.3.3 Mass spectrometric analysis

Clumped isotope analysis are performed using a MAT 253 gas source isotope ratio mass spectrometer (Thermo Fisher Scientific, Bremen, Germany). The Faraday cups have the following resistors: $3x10^8$ Ω, $3x10^{10}$ Ω, 10^{11} Ω for masses 44−46, respectively, and 10^{12} Ω for masses 47−49. On the instrument in Frankfurt the original stainless steel capillaries were replaced by electro-formed Ni capillaries (VICI AG, Schenkon, Switzerland; 1/32" o.d., 0.005" i.d., art. no. TEFNI.505, 122 cm x 0.127 mm i.d.). Analyte CO_2 is measured for ~3 h via the dual inlet system (10 acquisitions consisting of 10 cycles each, the integration time is 20 s; before each acquisition background determination, peak centering and press adjust of the bellows are carried out). An autosampler connected to the dual inlet system and operated with a LABVIEW script enables measurements over night.

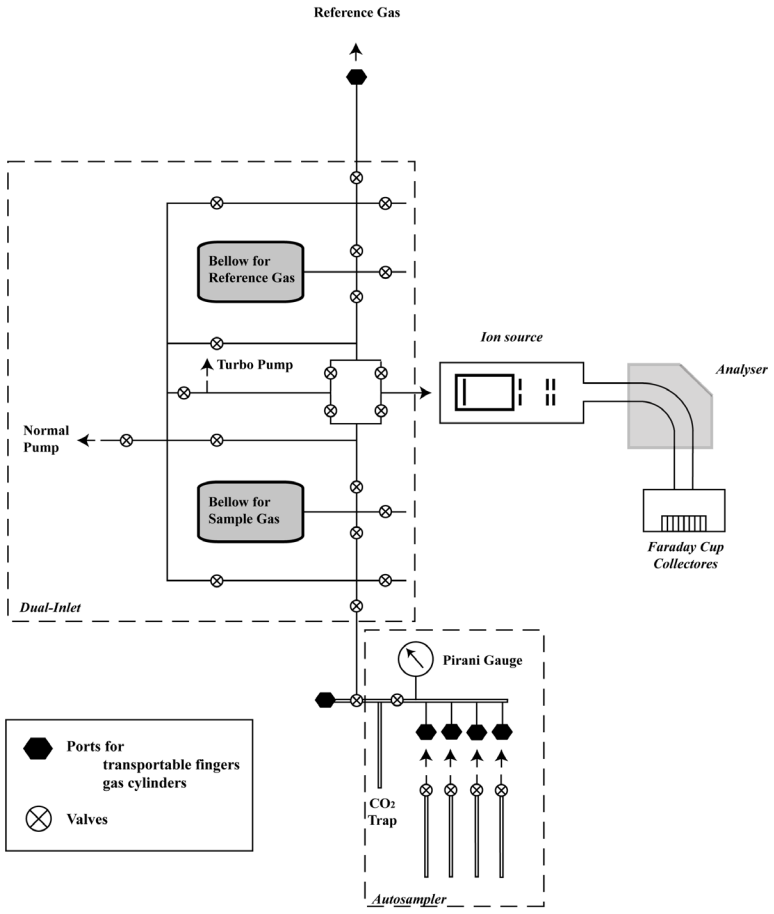

Figure 1.6 *Scheme of the mass spectrometer including autosampler. Measurements are performed using the dual inlet system. The change over switches between sample and reference CO_2 gas that is ionized in the source. Dependent on their masses the ions are deflected in the analyser and fall into the correspondent Faraday cup collectors. In order to enable measurements over night sample gases are transferred to the dual inlet via an autosampler. Controlled by a LABVIEW script fingers are opened automatically; a Dewar filled with $N_{2(l)}$ is lifted to freeze sample gas into a smaller volume to reduce gas loss; after that, CO_2 is transferred to the bellow of the dual inlet by expansion.*

1.4 Application of clumped isotope thermometry to Silurian carbonates

After establishing carbonate clumped isotope analysis at the Goethe University of Frankfurt the technique was applied to Silurian brachiopod shells from Gotland/Sweden. Published $\delta^{18}O$ and $\delta^{13}C$ records that were measured for preserved components of the exposed sedimentary succession showed large variations (Fig. 1.7; Wenzel and Joachimski, 1996; Bickert et al., 1997).

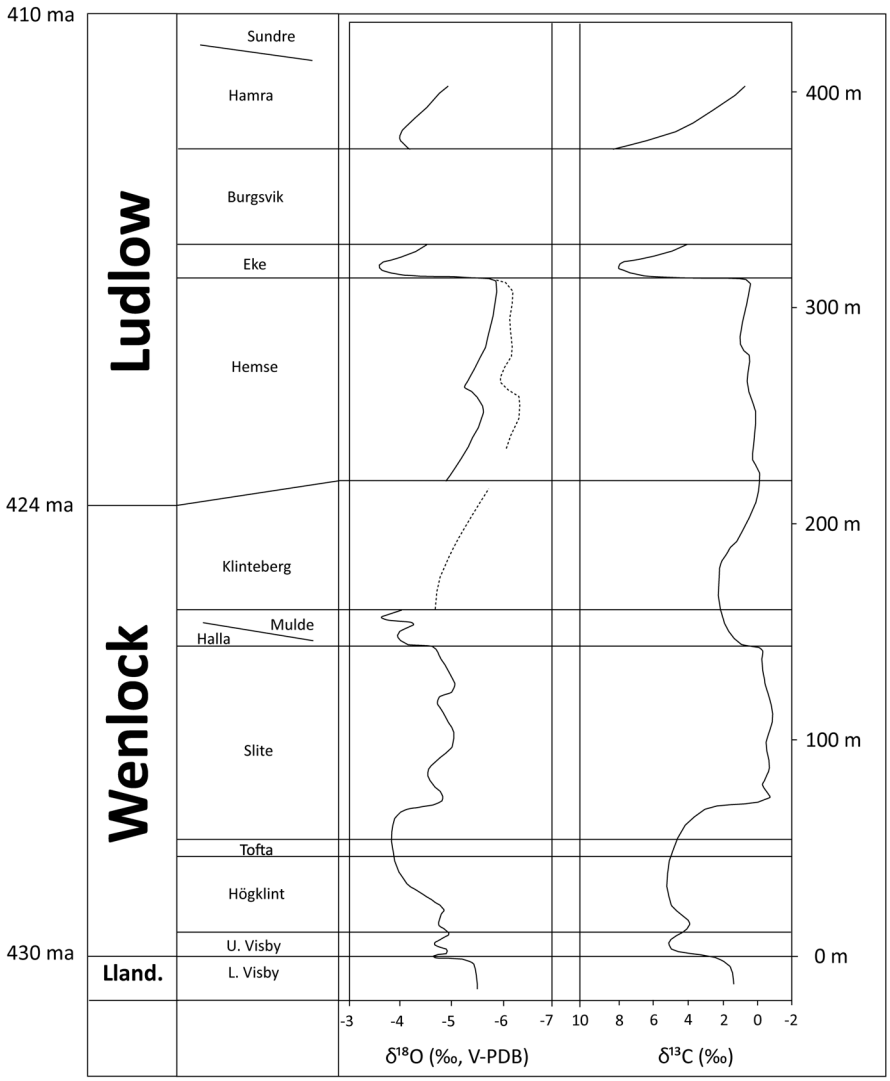

Figure 1.7 *Trends of the oxygen and carbon isotope curves based on Silurian brachiopod shells from Gotland/Sweden (after Bickert et al., 1997). Large variations of both $\delta^{18}O$ and $\delta^{13}C$ values were determined with isotopic shifts of ~2‰ and ~8‰ were observed, respectively. Furthermore, the excursions of both isotopic compositions correlate, indicating that coupled mechanisms caused the changes in the oxygen and carbon isotope ratios.*

The bulk oxygen and carbon isotope curves correlate and are coincident with sea level variations, changes of facies and minor extinction events. It is still unknown, whether the $\delta^{18}O$ excursions reflect temperature changes or $\delta^{18}O$ variations of tropical shallow water during the Silurian period (e.g., Wenzel and Joachimski, 1996; Bickert et al., 1997). Clumped isotope analysis of Silurian carbonates might help to resolve between seawater $\delta^{18}O$ and temperature variations.

The preservation quality of the fossils from Gotland has been characterized to be very high, especially the secondary layer fibres of brachiopod shell calcite (e.g., Samtleben et al., 2001). Nevertheless, it has been described that Δ_{47} compositions of ancient carbonates are prone to diagenetic alteration (e.g., Finnegan et al., 2011; Cummins et al., 2014). Furthermore, Δ_{47} data determined for sedimentary components of the carbonates of Gotland indicate that the preserved material was affected by diagenesis (Cummins et al., 2014). Nevertheless, Cummins et al. (2014) proposed temperatures and $\delta^{18}O$ values for Silurian seawater from samples derived from Gotland. They estimated lowest temperatures of ~33 °C and $\delta^{18}O$ values for the Silurian ocean of ca. −1 ‰, confirming assumptions that the oxygen isotopic composition has been buffered to (0 ± 1)‰ in the Phanerozoic time interval (e.g., Muehlenbachs et al., 2003 and references therein).

In light of the above, brachiopod shell calcite characterized by variable ultrastructural preservation and the diagenetic phases associated with the fossils were analyzed for their Δ_{47} compositions. We seek to unravel diagenetic processes and to further test assumptions of Cummins et al. (2014) concerning temperature and seawater $\delta^{18}O$ estimates for the Silurian period.

1.5 Objectives and outline of the thesis

The main targets of this thesis were

- to establish clumped isotope analysis at Goethe University of Frankfurt, including the determination of the parameters required for accurate and precise measurements;
- to calibrate the clumped isotope thermometer for various natural calcites;
- to apply the clumped isotope thermometer to Silurian carbonates from Gotland/Sweden.

Data acquired within this thesis were already published within three manuscripts (chapter 2 to 4). Furthermore, preliminary data are shown in chapter 5 and a "paper to be submitted" is presented in chapter 6.

Chapter 2 The manuscript "Background effects on Faraday collectors in gas-source mass spectrometry and implications for clumped isotope measurements" – Stefano M. Bernasconi, Bin Hu, Ulrike Wacker, Jens Fiebig, Sebastian F. M. Breitenbach, Tanja Rutz; Rapid Commun. Mass Spectrom. 2012, *27,* 603-612 results from a cooperation with the clumped isotope group at ETH Zurich. In this study a relationship between the non-linearity of Δ_{47} measurements and a negative background occurring on the m/z 47 Faraday cup collector was observed. The negative background is caused by secondary electrons generated by the m/z 44 beam. A background correction scheme was developed to account for these effects. The proposed procedure reduces time-consuming measurements of heated gases and might increase the precision of clumped isotope data.

Chapter 3 The manuscript "Clumped isotope analysis of carbonates: comparison of two different acid digestion techniques" – Ulrike Wacker, Jens Fiebig, and Bernd R. Schöne; Rapid Commun. Mass Spectrom. 2013, *27,* 1631-1642 outlines that more precise and accurate clumped isotope compositions of small samples are obtained if carbonates are reacted in a common acid bath at 90 °C. In contrast, an effect of sample size on Δ_{47} values was observed for carbonates reacted at 25 °C: higher mean Δ_{47} values and a larger scatter of data was obtained for carbonate aliquots <7 mg. Furthermore, for calcite and aragonite a $\Delta_{47}{}^{*}{}_{25-90}$ value of 0.07‰ (on the absolute scale) was determined, which is conform with the theoretical prediction (Guo et al., 2009).

Chapter 4 Δ_{47} data for a universal calibration of the clumped isotope thermometer for calcite are presented in the manuscript "Empirical calibration of the clumped isotope paleothermometer using calcites of various origins" – Ulrike Wacker, Jens Fiebig, Julian Tödter, Bernd R. Schöne, André Bahr , Oliver Friedrich, Thomas Tütken, Eberhard Gischler, and Michael M. Joachimski; Geochem. Cosmochim. Acta 2014, *141*, 127-144. The observed relationship between $1/T^2$ and Δ_{47} is not in agreement with the original Ghosh et al. (2006a) line. In contrast, it confirms the calibration of Henkes et al. (2013), as well as the theoretical prediction of Guo et al. (2009). Plausible reasons responsible for the differences between published calibration lines are discussed. However, we cannot distinctly decipher the causes for the observed discrepancies.

Chapter 5 This thesis contains unpublished preliminary results of a calibration for aragonitic bivalves. The calibration is based on heltered samples (*Arctica islandica*) and a tropical shell (*Tridacna* sp.) from the Maldives (Indian Ocean).

Chapter 6 We applied the clumped isotope paleothermometer to Silurian brachiopod shells from Gotland/Sweden and the diagenetic phases associated with the fossils: "Clumped isotope analysis applied to Silurian carbonates (Gotland/Sweden): deciphering both the alteration degree of fossil brachiopod shells and diagenetic processes" – Ulrike Wacker, Jens Fiebig, Axel Munnecke, and Michael M. Joachimski; to be submitted. SEM and CL investigations of fossil brachiopod shells were carried out for a diploma-thesis (Ulrike Wacker, 2010, FAU Erlangen-Nürnberg). We separated well-preserved shell regions to reconstruct pristine ocean water temperatures and $\delta^{18}O$ values of ambient seawater that prevailed during growth of the organisms. Furthermore, we investigated processes that occurred during diagenesis of the sedimentary rocks exposed on Gotland.

2 Background effects on Faraday collectors in gas-source mass spectrometry and implications for clumped isotope measurements

Stefano M. Bernasconi[1], Bin Hu[1,2], Ulrike Wacker[3], Jens Fiebig[3,4], Sebastian F. M. Breitenbach[1], Tanja Rutz[3]

[1] Geological Institute, ETH Zurich, Sonneggstr. 5, 8092 Zurich, Switzerland

[2] Department of Geography, Peking University, Yiheyuan Road 5, 100871 Beijing, China

[3] Department of Geosciences, Goethe-University, Altenhöferallee 1, 60438 Frankfurt am Main, Germany

[4] BiodiversityandClimate Research Center, Senckenberganlage 25, 60325 Frankfurt am Main,Germany

Published in Rapid Communications of Mass Spectrometry ***2012****, 27, 603–612*

DOI: 10.1002/rcm.6490

Abstract The measurement of the abundances of minor isotopologues by mass spectrometry requires correction of subtle non-linearities in the mass spectrometer that cause deviations in the relationship between actual and measured isotope ratios. Here we show that negative backgrounds on the Faraday cups recording the minor ion beams are the cause of the observed non-linearities in the measurement of CO_2 isotopologues, and propose a new correction procedure for clumped isotope measurements.

We carefully investigated the cause of non-linearity effects in the measurement of the abundance of $^{13}C^{18}O^{16}O$, a minor isotopologue of CO_2 with m/z 47, on two different mass spectrometers. By using gases of different composition with close to stochastic and with non-random distribution of isotopes we demonstrate that the apparent dependence of the excess abundance of the isotopologue of m/z 47 on the bulk isotopic composition of CO_2 is due to a background interference that is linearly dependent on the partial pressure of the gas in the source of the mass spectrometer.

Background determination with gas flowing into the source of the mass spectrometer is necessary for accurate clumped isotope measurements of CO_2. Background corrections can be performed accurately if the slit width of the m/z 44 Faraday cup significantly exceeds that of the one for m/z 47, using a correlation between m/z 44 signal intensity and the corresponding minimum in m/z 47 background. We propose two new correction schemes that reduce the time-consuming measurement of gases of different bulk isotopic compositions. These findings may also be relevant for the measurement of other rare isotopologues by mass spectrometry.

2.1 Introduction

Clumped isotope geochemistry is the study of the natural variations in the abundance of isotopologues containing more than one rare isotope (Eiler, 2007). It is receiving increasing interest because of its potential to solve many fundamental questions in earth and environmental sciences such as constraining budgets of atmospheric gases, and determining mechanisms of isotopic fractionation in chemical reactions or palaeoclimatological reconstructions (Eiler, 2007). The reconstruction of marine and terrestrial paleotemperatures through the analysis of fossil carbonate shells is currently the best developed of the possible applications (Ghosh et al., 2006a; Passey et al., 2010; Bristow et al., 2011; Eiler, 2011; Finnegan et al., 2011). This method is based on the fact that there is an excess abundance of carbonate isotopologues containing the two heavy isotopes ^{13}C and ^{18}O relative to their corresponding statistical distribution. This is because bonds between heavy isotopes are thermodynamically more stable than those between their lighter counterparts. This excess (expressed as the Δ_{47} value, see below for a detailed definition) is temperature-dependent and can be used to determine the temperature at which the carbonate minerals have formed, and to determine the isotopic composition of the fluid from which the mineral has precipitated (Schauble et al., 2006; Ghosh et al., 2007).

Because of the low abundance of the rare isotopes, the analytical requirements for the determination of the subtle concentration changes of isotopologues with two or more rare isotopes are very high. In particular, it requires high amplification of the signals of the minor isotopologues and, in addition, high accuracy and precision of the measurements (Eiler and Schauble, 2004; Ghosh et al., 2006a; Huntington et al., 2009; Eiler, 2011). The major limitations for a more widespread application of this method are the extremely high requirements for accuracy, and the time-consuming and rather complex procedures necessary to obtain meaningful measurements (Eiler and Schauble, 2004; Affek and Eiler, 2006; Huntington et al., 2009). The measurement of the clumped isotope composition of carbonates is carried out on CO_2 produced by reaction with phosphoric acid. Due to the low concentration of multiply substituted isotopologues (only about 46 ppm of CO_2 are formed by $^{13}C^{18}O^{16}O$) and because of the very small temperature-dependency of the Δ_{47} value, tedious gas purification procedures and long mass spectrometric counting times (ca. 2–3 h) have to be used (Eiler and Schauble, 2004; Affek and Eiler, 2006; Ghosh et al., 2006a; Ghosh et al., 2007; Guo et al., 2009; Huntington et al., 2009; Dennis and Schrag, 2010). While the automation of extraction lines (Passey et al., 2010) and the adaptation of automated commercial systems (Schmid and Bernasconi, 2010) have reduced the manpower required, increased the sample

throughput, and reduced the sample sizes necessary for accurate analysis (Schmid and Bernasconi, 2010), the analysis of clumped isotopes still remains complex due to somewhat poorly understood mass spectrometric effects.

One particularly important correction necessary to obtain accurate clumped isotope results is related to the fact that the measured excess abundance of the $^{13}C^{18}O^{16}O$ isotopologue, determined by measuring the ratio of m/z 47 to m/z 44 ions, shows an apparent dependence on the bulk isotope composition of the CO_2 (Huntington et al., 2009; Dennis et al., 2011). This is an obvious artifact produced by the mass spectrometer, the origin of which has been elusive so far (Huntington et al., 2009). Failure to properly correct for this non-linearity, however, creates significant errors in calculated clumped isotope abundances and thus it is of utmost importance to carefully monitor and correct for this effect. The currently used correction procedure involves the measurement of CO_2 gases of different bulk isotopic compositions that have been driven to a distribution of the isotopes among all isotopologues which is close to stochastic (Dennis et al., 2011). This is achieved by heating the gases at 1000 °C for 2 to 3 h in sealed quartz glass tubes (Eiler and Schauble, 2004; Huntington et al., 2009). A plot of δ^{47} vs. Δ_{47} values (for a definition of the notation, see below) can be used to determine the so-called 'heated gas line', which is used to correct all the measurements for the non-linearity effects (Huntington et al., 2009). This correction method, although relatively straightforward, requires considerable additional resources (a vacuum extraction and purification line), is time-consuming and uses a significant part of measurement time of a mass spectrometer.

Here we show that the non-linearity effects observed for clumped isotopes in the measurement of m/z 47, 48 and 49 are due to the formation of secondary electrons which create negative backgrounds on the Faraday collectors. Accurate determination of the corresponding backgrounds can be performed if the slit width of the Faraday cup collecting the major m/z 44 ion beam is wider than those of m/z 47–49 Faraday cups. In this way, the pressure-dependent backgrounds of m/z 47–49 can be monitored while mass 44 is still being collected, enabling a precise correction of measured Δ_{47} values. This background correction procedure allows for a continuous monitoring of the performance of the mass spectrometer without much effort and reduces the necessity to measure heated gases of different composition, thus simplifying the methodology while maintaining (or even improving) a high analytical quality, and permitting higher sample throughput. Finally, we discuss the use of the signal of m/z 49 for monitoring changes in backgrounds on the m/z 47 collector.

2.2 Experimental

2.2.1 Mass Spectrometers

For this study we used two Thermo Fisher Scientific (Bremen, Germany) MAT 253 mass spectrometers, one located at ETH Zuerich (ETH) and one at the Goethe University of Frankfurt (GU). The instruments are identical in their construction, except in the design of the collector array and the capillaries used to transfer the gas from the dual inlet to the source of the mass spectrometer. The ETH instrument is equipped with 8 Faraday cups, 6 of which are used to measure ions of m/z 44 to 49. The cup slit widths are 2.5 mm for the mass 44 cup, 3.5 mm for m/z 45, 1.5 mm for m/z 46 to 48 and 1.7 mm for m/z 49. Thus m/z 44 and 45 give a broader peak than the others when scanned with high voltage to determine the peak shape (Fig. 2.1(A)). The GU instrument is also equipped with 8 Faraday cups. The slit widths are 1.5 mm for m/z 44–47, 3.5 mm for m/z 48 and 4.5 mm for m/z 49, resulting in peaks of approximately the same width for m/z 44−47 ion beams (Fig. 2.1(B)). The signals are amplified through resistors with $3*10^8$ Ω for m/z 44; $3*10^{10}$ Ω for m/z 45; $1*10^{11}$ Ω (for m/z 46), and 10^{12} Ω resistors for m/z 47, 48 and 49. Both instruments are equipped with a standard dual inlet. The ETH instrument uses standard stainless steel capillaries to introduce the gas from the dual inlet to the source, whereas the GU instrument is equipped with electroformed nickel (EFNi) capillaries (22 cm * 0.127 mm i.d. (Passey et al., 2010; VICI International AG, Schenkon, Switzerland). In the Frankfurt laboratory, the capillaries were crimped to give a signal of 2 V on mass 44 for 10 mbar of gas, whereas at ETH a signal of 1.6 V is currently obtained. The sources of both instruments were tuned for linearity according to the manufacturer's instructions.

In both laboratories the heated gases were measured using the conventional dual-inlet technique. At ETH the measurements were carried out at 20000 ± 350 mV on the m/z 44 beam, and the m/z 44 signal decreased by less than 250 mV during 8 measurement cycles each of which consisted of an integration time of 26 s for sample gas and reference gas. Each sample gas was measured 10 times, and before each acquisition the reference and sample gas pressures were readjusted automatically to 20000 mV. The calculated shot noise limit for these measurements was 0.007%. In Frankfurt, sample and reference CO_2 gas were adjusted to a m/z 44 intensity of 16000 ± 150 mV prior to analysis, and the m/z 44 signal usually decreased by less than 200 mV during one acquisition. Before each new acquisition, the reference and sample gas pressures were readjusted to 16000 ± 150 mV. For a given sample gas aliquot, 10

acquisitions consisting of 10 cycles each (20 s integration time) were performed at GU with a shot noise limit of 0.008%.

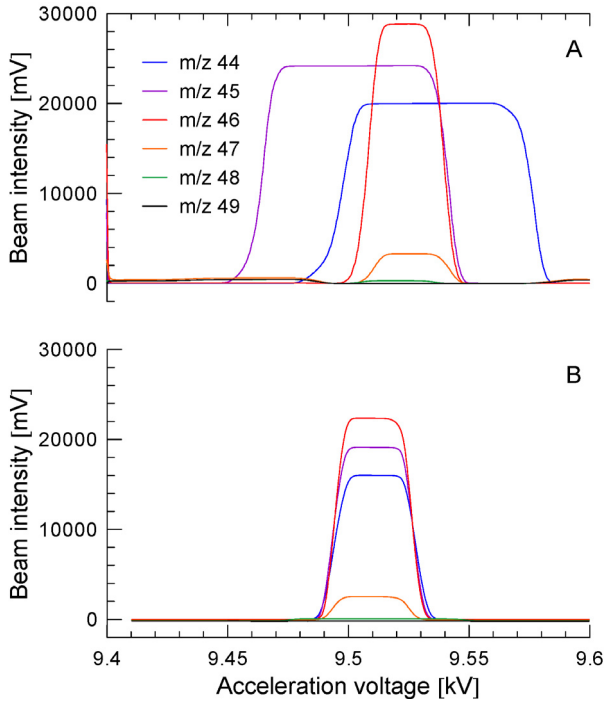

Figure 2.1 *Peak shape of the ETH (A) and GU (B) instruments obtained by acceleration voltage scanning. Note the different peak widths of the ETH instrument due to the variable width of the collectors.*

2.2.2 Background determination on masses 44-49

The background on masses 44–49 with CO_2 gas flowing into the ion source can be determined using the Thermo Scientific Isodat® software by scanning around the peak by changing the acceleration voltage (Figs. 2.2 and 2.3). For a precise determination of the background on these instruments we suggest that a scanning step of 0.0002 kV, and an integration time of 0.1 s should be chosen. This gave a more stable and consistent signal than using the software default step of 0.0008 kV. The results of the scans can be saved numerically and the minimum background value can be determined. We have studied the background of all the beams as a function of CO_2 partial pressures in the source covering the range used in our carbonate measurements (Figs. 2.4 and 2.5).

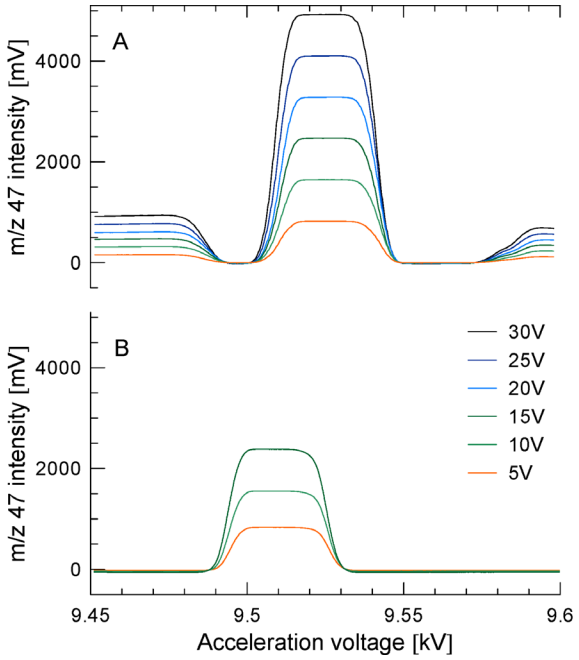

Figure 2.2 *Peak shape of m/z 47 of the ETH (A) and GU instrument (B) obtained by scanning the high voltage and different intensities on the m/z 44 beam as indicated in the legend. Note the different behavior of the background around the beam due to the different design of the collector assembly.*

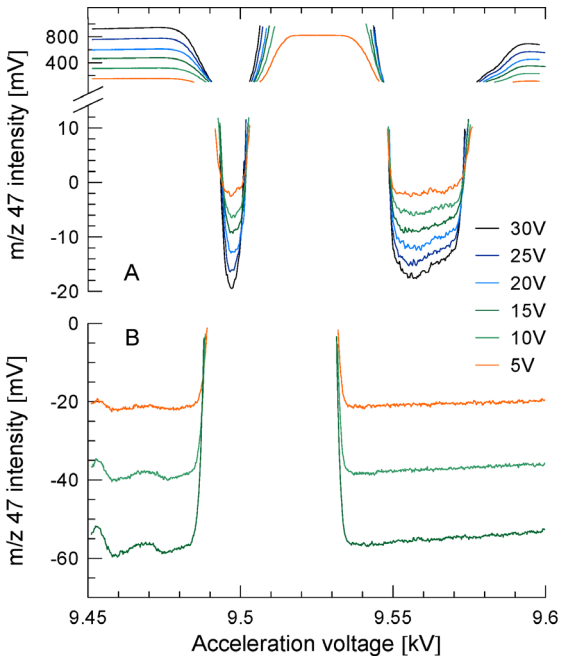

Figure 2.3 *Expanded view of the lower part of Figure 2.2, emphasizing the background: (A) ETH and (B) GU. The ETH instrument shows a narrow negative valley of maximum −20 mV for a 30 V m/z 44 beam on both sides of the mass 44 peak. The GU instrument instead shows a broad negative background reaching −60 V at 16 V m/z 44 beam. Note the decreasing minimum in the background with increasing m/z 44 signal, which is directly proportional to the amount of gas entering the source.*

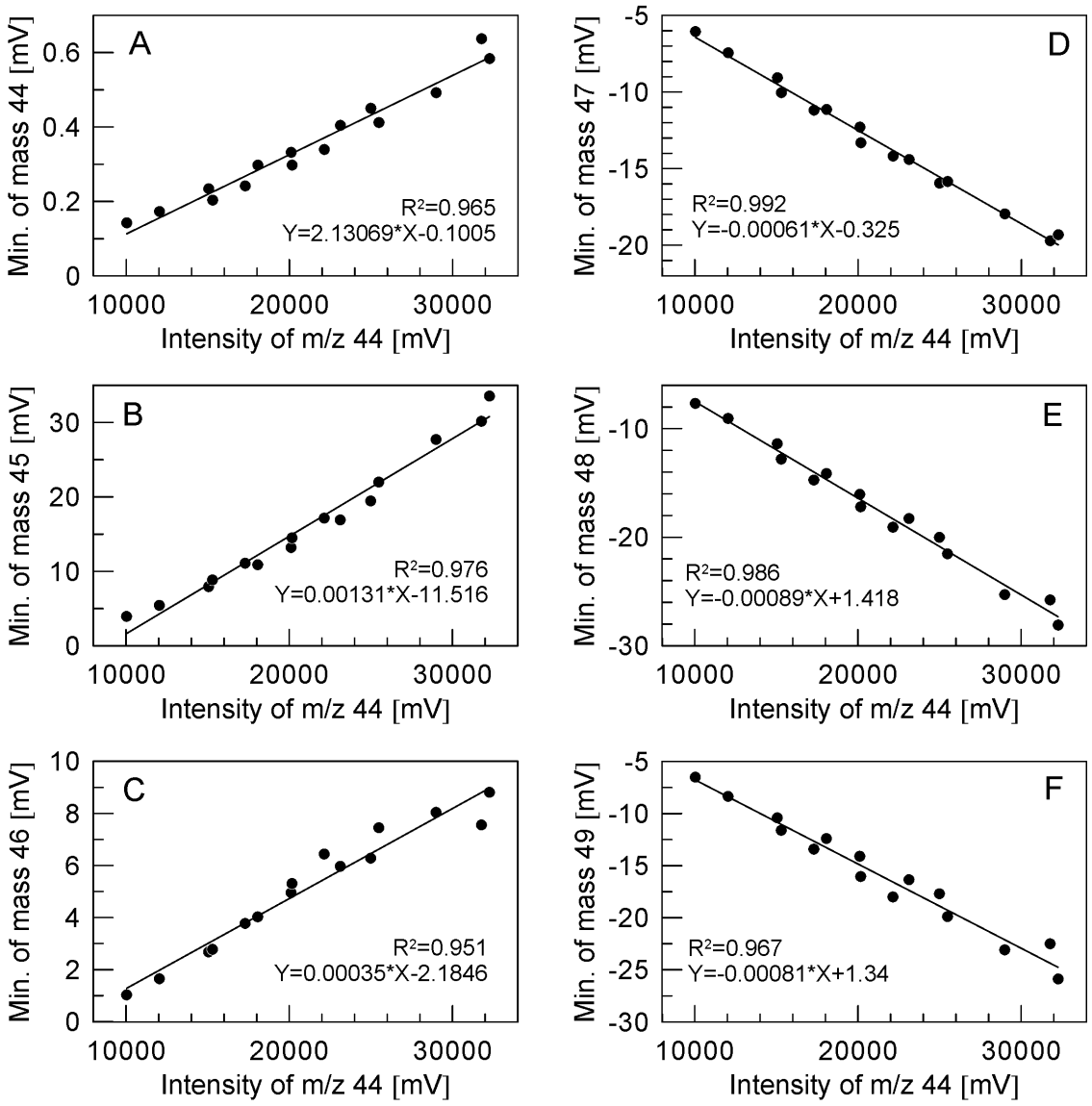

Figure 2.4 *Dependence of the backgrounds (measured as the minimum around the peak) for all six beams measured on two different days on the ETH instrument. Note the positive relationship for m/z 44 to 46 and the negative relationship for m/z 47 to 49.*

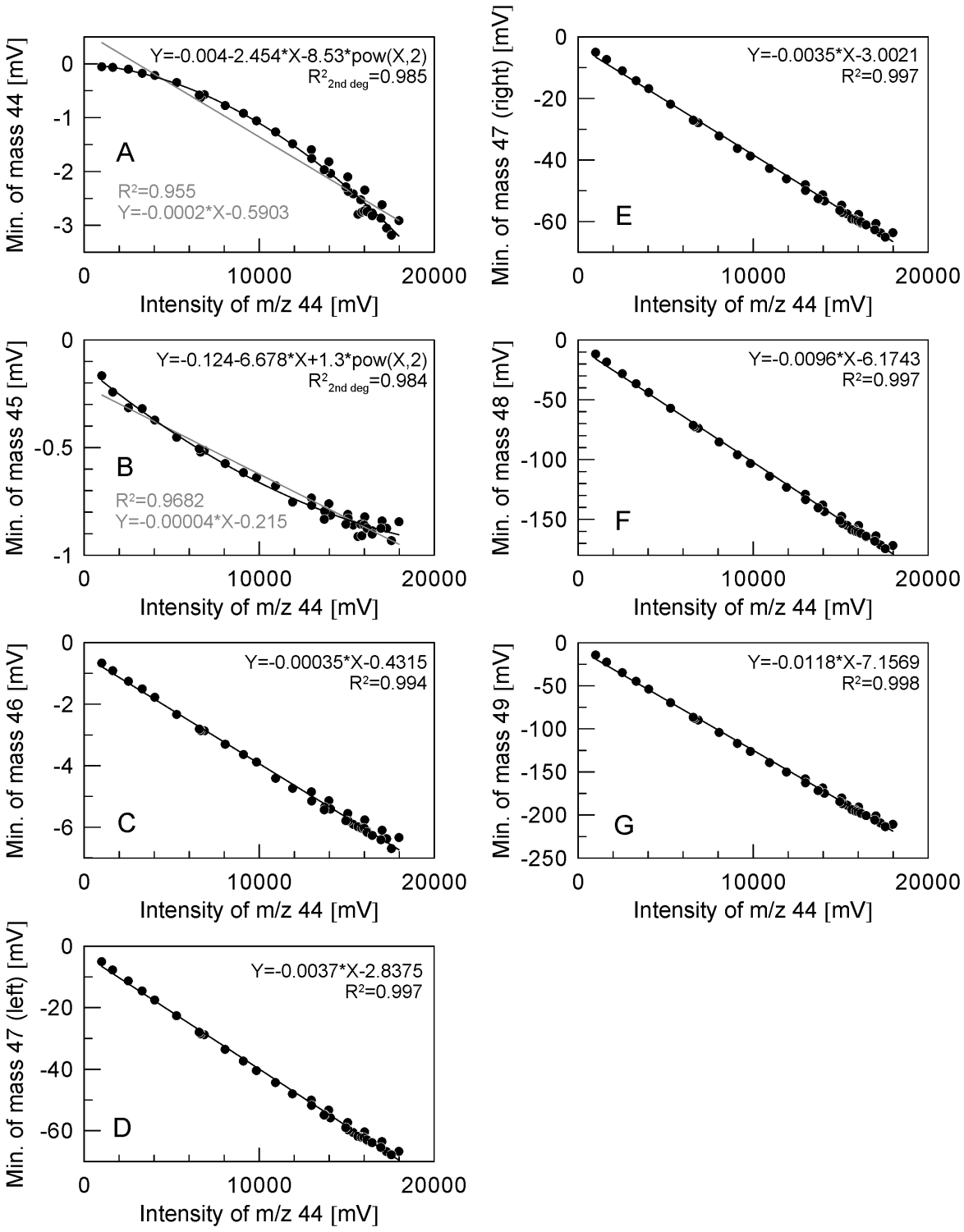

Figure 2.5 *Dependence of the backgrounds (measured right of the peak) for all six beams for GU. Note the negative correlation for all beams.*

An alternative method for the determination of the background on instruments with a collector configuration like the ETH system with a broad m/z 44 cup and narrow m/z 47 to 49 cups is the determination of the background on the high-acceleration voltage side of the peak (Fig. 2.1). When the measurement is carried out at the minimum of m/z 47 and 48 (at approximately 9.56 kV acceleration under the current conditions) the m/z 44 beam is still fully in the appropriate collector, thus allowing a rapid and direct determination of the relationship between the m/z 44 signal and the background on m/z 47 by changing the gas pressure flowing into the mass spectrometer. This is a more rapid method than the scanning one and could be easily implemented in the software using the peak jump feature. The corrections reported in this paper, however, are still based on backgrounds determined with the scan method to directly compare the two instruments.

2.2.3 Clumped isotope notation

Clumped isotope analysis aims at determining the abundance of an isotopologue containing more than one of the rare isotopes. For CO_2, for example, the multiply substituted isotopologue containing both the rare isotopes ^{13}C and ^{18}O, which can be measured with sufficient accuracy with current technology, is the one of m/z 47, corresponding predominantly to $^{13}C^{18}O^{16}O$. For geochemical applications, however, it is more convenient to measure the excess abundance relative to the amount expected for a stochastic distribution of isotopes among all isotopologues of a molecule rather than the absolute abundance. This excess is expressed with the variable Δ_{47} (Eiler and Schauble, 2004) which is defined as:

$$\Delta_{47} = \left[\left(\frac{R^{47}}{R^{47*}} - 1\right) - \left(\frac{R^{46}}{R^{46*}} - 1\right) - \left(\frac{R^{45}}{R^{45*}} - 1\right)\right] \times 1000 \quad (2.1)$$

where R^{47}, R^{46} and R^{45} are the measured abundance ratios of masses 47/44, 46/44 and 45/44 and R^{47*}, R^{46*} and R^{45*} are the corresponding stochastic abundance ratios. Stochastic abundance ratios are computed from measured $\delta^{13}C$ and $\delta^{18}O$ values. For a more detailed discussion of the calculation of Δ_{47} see Huntington et al. (2009). The bulk isotope composition of the sample with respect to the reference gas is expressed with the parameter δ^{47}:

$$\delta_{47} = \left(\frac{R^{47}\ sample}{R^{47}\ ref.gas} - 1\right) \times 1000 \quad (2.2)$$

In this study, both the δ^{47} values and the Δ_{47} data are reported relative to the composition of the reference gases of the two instruments, and are not directly comparable in absolute values as the two reference gases are different in composition. $\delta^{13}C$ and $\delta^{18}O$ values are reported in the conventional delta notation with respect to V-PDB.

2.3 Results

2.3.1 Negative backgrounds on Faraday cups

For the correction of instrumental effects on isotope abundance measurements in mass spectrometry it is necessary to correctly determine the background given by secondary electron formation in the collectors. In standard gas-source mass spectrometry, the background is generally determined by measuring the background signal on the collectors in the absence of any analyte gas, i.e. with closed changeover valve. Under these conditions, the backgrounds determined for the six CO_2 collectors in our instruments range from 0 to about 10 mV. The background depends somewhat on the source tuning and the general state (cleanliness, vacuum level) of the system, and can vary through time. Such a background measurement is generally conducted before each measurement under software control. The determined value is then subtracted from the beam intensities before the software calculates the isotope ratios. A close examination of the peak shape obtained by scanning around the peaks, however, shows that this background is not representative of the conditions when gas flows into the mass spectrometer. Figures 2.1(A) and 2.1(B) show the peak shapes for masses 44 to 49 for the ETH (m/z 44 intensity set to 20 V) and GU instrument (m/z 44 intensity set to 16 V), respectively. These were obtained by varying the acceleration voltage between 9.4 and 9.6 kV. When examined at this magnification, it is not apparent that the background is lower than zero. However, a close observation of the baseline at greater magnification shows that the background is indeed negative immediately before and after the peak. Figure 2.2 shows the m/z 47 peak shapes of both instruments for varying amounts of gas entering the source, ranging from approximately 15 to 35V on m/z 44 at ETHZ (Fig. 2.2(A)), and between 5 and 15 V at GU (Fig. 2.2(B)), respectively. Figures 2.3(A) and 2.3(B) show a blow-up of the baselines of the corresponding signals displayed in Figure 2.2. It is obvious for both instruments that the background is negative and that the background minima increase with increasing gas pressures. It is worth noting that – for a given m/z 44 signal intensity – the corresponding m/z 47 background is more negative at GU. For example, at a m/z 44 signal intensity of 10 V, the minimum is −7 mV for the ETH instrument (Fig. 2.3(A)), but −40 mV for the GU instrument

(Fig. 2.3(B)). In addition, the negative background in the ETH instrument is represented by two sharp minima centered around 9.49 and 9.56 kV acceleration voltage (Fig. 2.3(A)), whereas the minimum is much wider on the GU instrument (Fig. 2.3(B)). This effect is related to the different design of the collector assemblies at ETHZ and GU, with the m/z 46−48 collectors being placed closer to each other at ETHZ than at GU.

It should also be noted that there is a slight difference between the background on the low-acceleration voltage and that on the high-acceleration voltage side of the peak for both instruments. At ETH this difference (1 mV) seems to be independent of peak intensity, whereas it increases by up to 3 mV with increasing gas pressure at GU. To demonstrate to what extent background signals depend on the amount of gas flowing into the mass spectrometer, we plotted the intensity minimum of each background (generally found on the left of the peak, Fig. 2.3(A)) against the beam intensity on m/z 44 for both instruments (Figs. 2.4 and 2.5). The ETH instrument shows positive backgrounds on masses 44 to 46, with a robust linear positive relationship, whereas for 47, 48 and 49 the backgrounds are negative and they decrease with increasing partial pressure of gas in the source. On the GU instrument the backgrounds show a different behavior (Fig. 2.5). Backgrounds are negative and decrease with increasing gas pressure for all masses. In addition, for the minor beams 47 to 49 they are – for a given m/z 44 intensity – much more negative than at ETH. For the ETH instrument the m/z 49 background minimum values are almost identical to m/z 48 values, whereas the GU instrument exhibits m/z 49 background minima up to 30 mV more negative than the corresponding m/z 48 minima (Fig. 2.5).

2.3.2 Significance of the mass 49 signal of CO_2 measured through a 10^{12} Ω resistor

Our two instruments and, to the best of our knowledge, also most of the mass spectrometers designed for clumped isotope measurements, have an array of collectors designed to measure m/z 44 to 49. Many users of these instruments have noted that the signal on m/z 49 is commonly negative. There is a simple explanation for this effect, if the backgrounds are taken into consideration. For a CO_2 gas with an isotope composition close to the natural abundance the calculated abundance of the isotopologues of mass 47 is approximately 47.6ppm and of the isotopologue of mass 49 is 48 ppb (Eiler and Schauble, 2004). Therefore, if on our instruments the collector 47 has a signal of about 3000 mV (corresponding to a 18 V signal on m/z 44), the signal measured on collector 49 should be about 3 mV, provided that the response of the collectors is linear over the whole range. This would be the maximum signal expected on this detector. Because at 16 V on m/z 44 the negative background is about −12 mV on the ETH

system (Fig. 2.4) and about −196 mV on the GU instrument (Fig. 2.5), it becomes clear that the signal variations observed on this detector are dominated by the background changes and that the analyte gas only contributes to a small extent to the signal on the m/z 49 collector. Indeed, when monitoring the intensity of m/z 49 with changing CO_2 flow in the mass spectrometer, it was observed that the m/z 49 signal increases linearly with decreasing m/z 44 signal, clearly demonstrating that it is dominated by background issues and not by the CO_2 isotopologue of m/z 49 or isobaric non-CO_2 gases (Fig. 2.6). The variation of the contribution of ions of mass 49 related to variations in isotopic abundance would only be expected to be in the low percent range at most. Therefore, the m/z 49 signal may be considered to be a direct measure of the background even if the bulk isotopic composition of the measured CO_2 varied significantly.

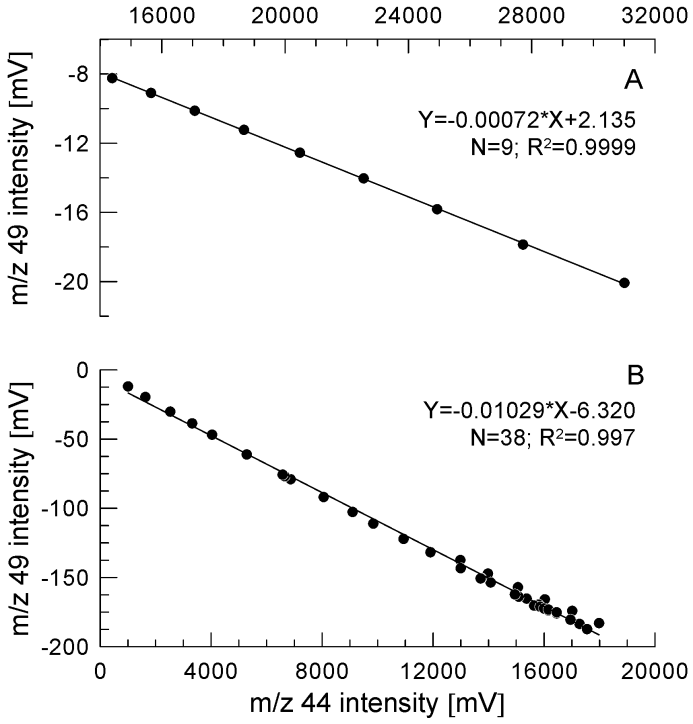

Figure 2.6 *Change in m/z 49 peak intensity with m/z 44 for ETH (A) and GU (B). Note the increasing mass 49 with decreasing peak 44 intensity, indicating that the signal is dominated by background changes.*

This is a very important finding because it potentially allows a beam-dependent background correction and a continuous monitoring of the background during the measurements. This is of particular importance for laboratories analyzing samples with the method of Schmid and Bernasconi (2010) which uses small samples that are transferred to the source from a micro volume, and thus has a strongly decreasing beam size during the measurement. The ability to continuously monitor the background on mass 49 thus allows a background-dependent

correction to be implemented and, in addition, monitoring of the background dependence between m/z 44 and 49 provides an indication of the stability of the instrument through time. It has been shown previously that the m/z 49 signal can also be influenced by contamination (Bristow et al., 2011; Finnegan et al., 2011). For this reason, it is necessary to examine the behaviour of the m/z 49 signal on both reference gas and sample to detect possible contamination.

2.4 Discussion

Origin of negative backgrounds on Faraday collectors

We propose that the negative backgrounds observed in our instruments are dominantly related to the scattering of secondary electrons generated by the m/z 44 beam. This is suggested by the observation that the negative backgrounds of m/z 47–49 increase with increasing m/z 44 beam intensity for both instruments (Figs. 2.4 and 2.5). In addition, on the GU instrument, the m/z 44 beam exhibits the most negative background if the different amplifications and slit widths of the different Faraday cups are considered. Figure 2.5 shows that for the GU instrument the negative background around the m/z 44 beam adjusted to 16 V is −2.7 mV. The negative backgrounds around the peaks 49−45 are −196.5 mV (m/z 49), −160.7 mV (m/z 48), −62.3 mV (m/z 47), −6.0 mV (m/z 46) and −0.9mV (m/z 45) (Fig. 2.5). Correcting for the different amplifications provided by the resistors, these signals would correspond to −0.065 mV, −0.054 mV, −0.02 mV, −0.02 mV and −0.01 mV, if all the Faraday cups were equipped with $3*10^8$ Ω resistors. If these signals are also normalized to a slit width of 1.5 mm, we can calculate background intensities of ca. −0.02 mV for m/z 49–46 and ca. −0.01 for m/z 45, significantly less negative than the background around the m/z 44 beam (−2.7 mV). The observation that the m/z 44 beam exhibits the most negative background is not surprising, because it comprises more than 98% of the total amount of positively charged CO_2 molecules. It seems that the production of secondary electrons is less pronounced on the ETH instrument, for which it is observed that the mass 44 background is not negative at all but that it even increases with increasing gas pressure (Fig. 2.4). This might be caused by the wider dimensions of the m/z 44 cup.

Negative backgrounds of variable magnitude were also observed on two Thermo Fisher Scientific Delta V instruments located at ETH using H_2, SO_2, CO_2, N_2 and CO (data not shown), although not on all collectors. This suggests that these effects are probably also common in other mass spectrometers, but that they are variable and should be evaluated individually for each mass spectrometer and collector design.

2.5 Background correction procedures

In the following section we describe two different procedures for background correction: one based on the (m/z 44 intensity)/(m/z 47 background) relationship determined by scanning, and one based on the (m/z 49 intensity)/(m/z 47 background) relationships. We then apply these correction schemes to existing data from both instruments, demonstrating that they can eliminate or at least significantly reduce the apparent dependence of the Δ_{47} on the bulk composition of the gas (expressed as δ^{47}). The first method produces more accurate results on the ETH instrument, while the second one yields better results on the GU instrument.

1) Correction with directly determined m/z 47 backgrounds

To carry out the background corrections, the raw data of each measurement have to be extracted from each measurement to be corrected individually. The beam intensity data exported from the raw data file of each measurement are corrected by removing first the background determined by the Isodat® software without gas flow into the source, and then by subtracting the background determined with the relationship between m/z 44 intensity and the corresponding m/z 47 background determined with the scanning procedure described above (Figs. 2.4 and 2.5). The corrected beam intensity data are then reprocessed to calculate $\delta^{13}C$, $\delta^{18}O$, δ^{47} and Δ_{47} values with a spreadsheet. The difference in the calculated $\delta^{13}C$ and $\delta^{18}O$ values with the corrected background are less than 0.02%, thus well below the analytical error. However, the changes in the calculated δ^{47} and Δ_{47} values are very large, and are strongly dependent on the bulk isotope composition of the gas. An example calculation is available as Supplementary Table S2.1 and the data are reported in Supplementary Table S2.2 (see Supporting Information).

At ETH, all the analyses to determine the heated gas line and the equilibrated gas line for exchange with water at 25 °C were carried out at 20 V on the m/z 44 signal. The gas compositions presented in Figure 2.7 were measured between November 2011 and March 2012, whereas the background determination was carried out at the beginning of June 2012 after we observed the existence of the negative backgrounds in our instruments and characterized its dependence with the signal intensity of m/z 44. Since March 2012, internal carbonate standards of various bulk and clumped isotope compositions were used to verify that the heated gas line remained stable as described in Schmid and Bernasconi (2010). On this instrument, we observe that the heated gas line is stable over long periods of time, if no changes are made to the source tuning parameters, as was also observed in other laboratories

(Huntington et al., 2009; Dennis et al., 2011). At GU, heated gas analyses were performed according to the methods outlined above. Background scans were carried out in early June 2012. We noticed no change in the m/z 49 beam intensity during reference gas measurements (set to 16 V at m/z 44) for the period end of April to mid June 2012. For the same period, a constant m/z 49 beam intensity was accompanied by an invariant heated gas regression line. In Figure 2.7 we show the effect of applying the new background correction to the analyses on the 'Heated gas line' and '25 °C equilibrated gas line' for the ETH instrument, and in Figure 2.8 we show the same effect on the May 2012 'Heated gas line' for the GU instrument.

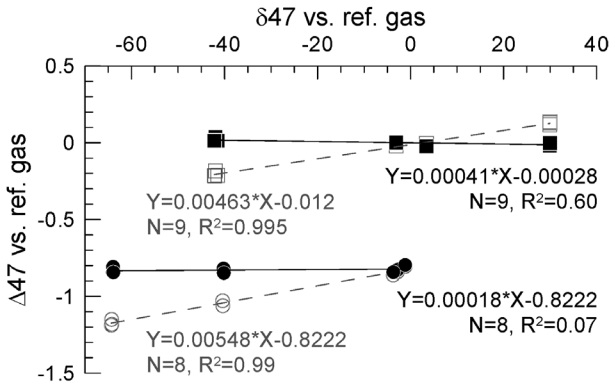

Figure 2.7 *The current 'heated gas line' (circles) and the '25 °C equilibrated gas line' (squares) of the ETH instrument calculated with the background determined by the software (open symbols) and calculated with the backgrounds determined with gas flowing in the mass spectrometer (filled symbols). The new background correction removes the dependence of Δ_{47} on d_{47} values.*

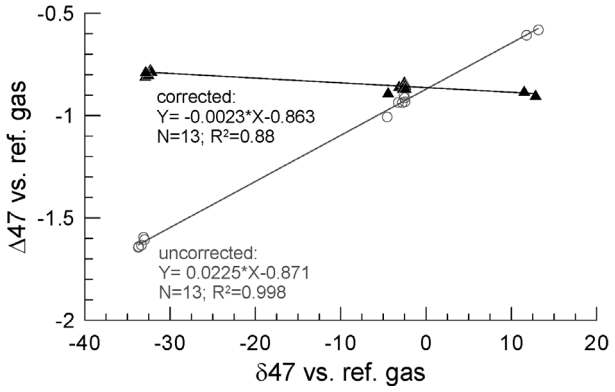

Figure 2.8 *The current heated gas line of the GU instrument calculated with the background determined by the software (circles) and recalculated with the backgrounds measured with gas flow into the source (triangles).*

For the ETH instrument, the uncorrected raw heated gas (HG) data reveal a slope of 0.00548 ± 0.00026 and an intercept of −0.8222 ± 0.0114. Applying the relationship between the m/z 47 background and the m/z 44 intensity (Fig. 4(D)) to correct raw data (after removing the corresponding, false m/z 44 background determined by the Isodat® software), the HG line is characterized by a slope of 0.00018 ± 0.00025 and an intercept of −0.8222 ± 0.0012. The most striking feature of Figure 2.7 is that the dependence of the Δ_{47} value on the δ^{47} value essentially disappears (slope 0.00018 ± 0.00025). The intercepts displayed by raw and corrected data are – within error – indistinguishable from each other, demonstrating that this correction procedure does not affect the measured Δ_{47} value of the heated reference gas. As for the heated gases, the dependence of Δ_{47} on δ^{47} values for the gases equilibrated at 25 °C with waters of different oxygen isotope composition for the ETH instrument is also removed by the correction procedure. Uncorrected 25 °C gases reveal a slope of 0.00463 ± 0.00012 and an intercept of −0.0122 ± 0.0040, which, after correction, become −0.00041 ± 0.00013 and −0.0003 ± 0.0042, respectively. As observed in other studies (Dennis et al., 2011), the uncorrected (and corrected) slopes are slightly different from those for the heated gases (Fig. 2.7). In contrast to the heated gases that have an absolute Δ_{47} of 0.0266, these gases have a theoretically determined absolute Δ_{47} of 0.9252 (Dennis et al., 2011). For a given temperature, the absolute Δ_{47} values differ from the measured ones (as represented by corresponding intercepts), because the measured Δ_{47} values are not expressed on the absolute scale, but relative to the Δ_{47} values of the reference gas used. In addition, the measured Δ_{47} values are affected by a process called 'scale compression' (Huntington et al., 2009; Dennis et al., 2011), which, in contrast to the dependence of uncorrected Δ_{47} on δ^{47} values, might be related to isotope scrambling processes occurring in the ion source.

In this respect, the positive slope reflected by uncorrected gas data can be understood as follows: the relative contribution of the background to the measured intensity of m/z 44 is the same for both reference and sample gas only if the analyte gas has the same bulk isotopic composition as the reference gas. However, as the isotope abundances are simply ratios of the beam intensities, the contribution of a constant negative m/z 47 background will increase with increasing difference in the m/z 47 beam intensity between reference gas and sample gas. As a consequence, the original erroneous background correction results in a calculated Δ_{47} value which is 0.334% lower than the actual one for a sample gas with a much more negative bulk isotope composition (e.g. for the lightest CO_2 with a δ^{47} of −63.8%) than the reference gas.

It should be noted that the background correction procedure described above not only removes the dependence of the Δ_{47} value on the bulk isotopic composition, but also that it is not accompanied by any loss in precision. This is shown by the similar errors for the uncorrected and corrected slopes and intercepts.

The same correction procedure was applied to data generated by the GU instrument, and results are presented in Figure 2.8. A first striking feature of the GU instrument is the much steeper slope of the heated gas line, which is clearly related to the much larger negative backgrounds. The uncorrected May 2012 HG line has a slope of 0.02254 ± 0.00028. The same correction applied to the heated gas data results in an improvement of the steepness of the slope, but the correction based on the direct measurement of the m/z 47 peak leads to a slight overcorrection of the data, as expressed by the negative slope of −0.00225 ± 0.00025 (Fig. 2.8; triangles).

Both datasets demonstrate that the 'non-linearity' is simply related to an improper determination of the background of the collectors. The correction procedure based on the (m/z 44 intensity)/(m/z 47 background) relationship removes the observed non-linearity completely on the ETH instrument for which the m/z 44 slit widths is nearly double the m/z 47 slit widths. The correction is demonstrated to be valid for gases with a wide range of bulk compositions (δ^{47} values ranging from −64 to +20%) and also in degree of isotopic ordering from close to stochastic distribution to equilibrium with water. However, the same procedure leads to a slight overcorrection at the GU instrument, for which the m/z 44 and 47 cups have identical slit widths. We propose that this is a result of the different cup design. When determining the m/z 47 background on the side of the peak on the GU machine using the HV scan method, the m/z 44 beam is not collected in the m/z 44 cup. This is different to conditions prevailing during measurement and during HV scans using the ETH instrument with the wide m/z 44 collector (Fig. 2.1). The fact that the m/z 47 background at GU is determined under conditions not representative of the real measurements might explain why the (m/z 44 intensity)/(m/z 47) background relationship obtained by the scan method leads to a slight overcorrection of data. This indicates that the background during measurement, when the m/z 44 beam falls into the Faraday cup, is probably slightly smaller than the one determined by peak scanning.

2) Corrections with m/z 49 intensity

As discussed above, the signal observed on m/z 49 is a close representation of the background on cup 49. Therefore, if a good correlation between the m/z 49 signal and the background 47 exists, this signal might be used to directly and continuously monitor the background on m/z 47 during the measurement, and potentially improve even further the quality of the data. In Figure 2.9 we depict the relationships between the m/z 49 signal and the m/z 47 backgrounds for the ETH (Fig. 2.9(A)) and GU (Fig. 2.9(B)) instruments. These relationships were used to correct the raw data, as with the direct determination. The results are shown in Figures 2.10(A) and 2.10(B) for ETH and GU, respectively. It is now observed for both instruments that the heated gas data is overcorrected, i.e. both corrected HG lines exhibit negative slopes significantly different from zero: −0.00172 ± 0.00025 at GU (Correction 1) and −0.0019 ± 0.0003 at ETH. However, for the GU instrument if we do not consider the absolute minimum of m/z 47, but instead the minimum to the right of m/z 47 (Fig. 2.1) and correlate it with the mass 49 intensity, a relationship is obtained that – if used for the correction of May 2012 Heated gas data – removes the heated gas slope nearly quantitatively to −0.00069 ± 0.00025 (Fig. 2.10(B), Correction 2). Such a heated gas slope is already sufficient to correct samples that have a δ^{47} value within 15% of the reference gas, introducing a maximum error of ±0.01% for the samples close to the extreme compositions.

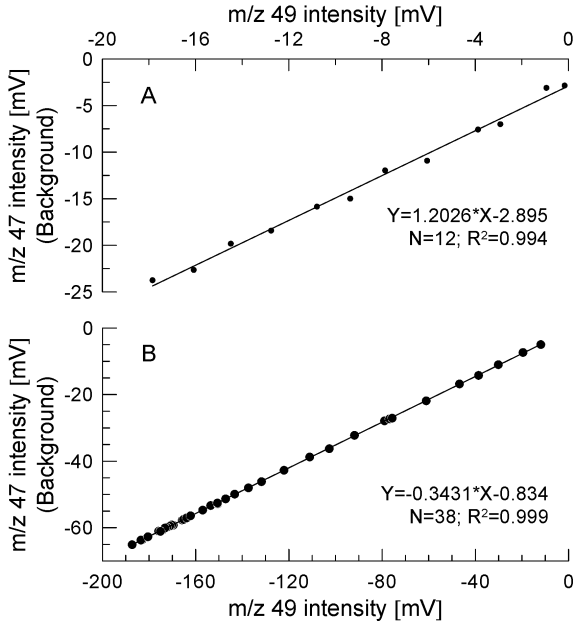

Figure 2.9 *Correlation of the m/z 49 signal with the background determined on the left side of the m/z 47 peak for the ETH (A) and GU (B) instruments. Note the excellent linear relationship.*

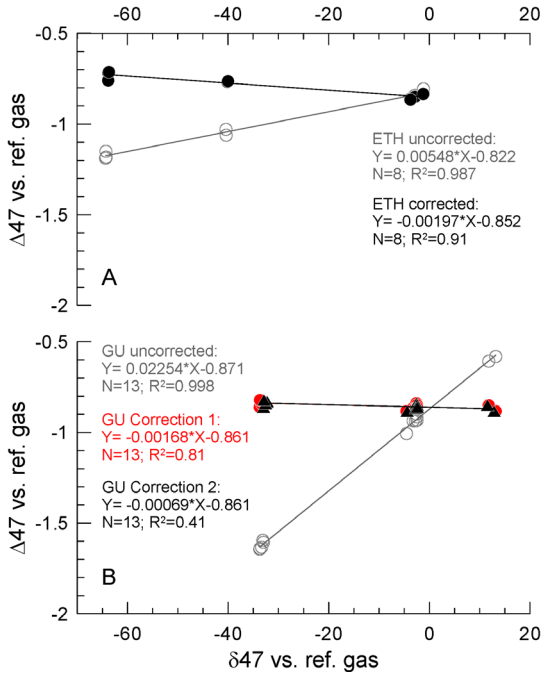

Figure 2.10 *Correction of the heated gas line (open symbols) with the m/z 49 vs. background m/z 47: ETH (A) and GU (B). Correction 1 of GU is calculated with the minimum background, correction 2 with the background on the right of the peak (for details, see text).*

At present it is not clear what the reason for the overcorrection is, but at GU it might be again related to the different slit widths of cups 44, 47 and 49. Applying the HV scan method at GU, the m/z 49 intensity vs. m/z 47 background relationship used for data correction is monitored under conditions that do not represent real measurement conditions, with the m/z 44 beam being collected by the mass 44 cup. Additional factors such as small contributions from non-CO_2 isotopologues might also be of importance, as is suggested by the observation that heated gas data is also slightly overcorrected at ETH, although the m/z 44 peak widths completely covers that of m/z 49 (Fig. 2.1). Additional studies are ongoing to better understand the behavior of the m/z 49 signal.

2.6 Conclusions and implications

The data presented in this study clearly demonstrate that the background in the collectors in both instruments is influenced by the partial pressure of CO_2 in the source, and that the background of m/z 47, 48 and 49 becomes more negative with increasing m/z 44 beam intensity.

Using the background determination with CO_2 flowing into the source, we have shown that we are able to essentially eliminate the dependence of Δ_{47} on the δ^{47} values on the ETH instrument. In addition, the intercept of the corrected linearity line is equal to the intercept determined by the uncorrected regression line. This is very important because the y-intercept is a function of the degree of scrambling of the isotopologues in the source of the mass spectrometer, and is therefore an important parameter for subsequent data correction (Huntington et al., 2009; Dennis et al., 2011). This is a further confirmation of the validity of our approach.

For an accurate correction of data it seems to be essential that the m/z 44 cup in the collector array has a wider slit width than the m/z 47 cup. Under these circumstances (m/z 44 intensity)/(m/z 47 background) correlations can be performed using the HV scan method, under analytical conditions that are comparable with those prevailing during sample gas measurements, with the m/z 44 beam being collected by the mass 44 cup. However, it might be possible that an accurate background could be performed if this prerequisite is not met. For mass spectrometers equipped with identical cups for m/z 44 and 47, more detailed investigations are necessary to evaluate if non-linearity effects can be removed by determining the m/z 47 background using strategies other than simply determining the minimum value, as described in the example above. For example, we found that the correlation of the minimum to the right of m/z 47 with the m/z 49 intensity removes the heated gas slope nearly quantitatively for the GU instrument. With a better understanding of the origin of the backgrounds better correction algorithms might be developed to improve the corrections. The corrected heated gas line for the ETH instrument still shows a small dependence between the d47 and Δ_{47} values (Fig. 2.7). This is equivalent to a 0 to 0.006% uncertainty in Δ_{47} (or 0 ~ 1.2 °C in temperature) for carbonates precipitated at the same temperature but with δ^{47} values varying between −10% (a typical value for freshwater carbonates) and +20% (typical for marine carbonates). The uncertainty can be further reduced by daily measurement of backgrounds and by using carbonate standards of contrasting bulk isotope composition and Δ_{47} values to detect and correct short-term variations in the backgrounds.

We propose that for the measurement of clumped isotopes it is not necessary to repeatedly measure heated and equilibrated gases of different composition to monitor changes in slope, but that it is sufficient to use one heated gas composition if the backgrounds are properly corrected with the methods outlined in this paper. In addition, it will still be necessary to measure gases equilibrated at 25 °C and at other temperatures in order to determine a possible compression of the Δ_{47} scale due to isotopic 'scrambling' in the source, and to calibrate the measurements across different laboratories so that all results can be projected in a common reference frame, as suggested by Dennis et al. (2011). After this frame of reference is established, the performance of the mass spectrometer can be routinely checked by the measurement of a set of reference carbonate standards that should be distributed to the community. It is important that these standards should cover a range in bulk compositions and degree of ordering encompassing the natural variability of the samples measured. The background effects observed in this study could also have implications for the measurement of other minor isotopologues in other gases and by different types of instruments where the backgrounds can significantly influence the measured abundances. In addition, our results indicate that the measurement of backgrounds without gas entering the source of the mass spectrometer is not representative of the actual background present during the measurements. Therefore, corrections using these backgrounds should be avoided.

2.7 Acknowledgements

S.M.B. and S. F. M. B. acknowledge financial support from SNF Project CRSI22_132646/1. S.M.B. andH.B. acknowledge support from SSTC Grant No. EG 03-032010. Participation of J. F. was enabled through DFG grant FI-948-4/1. We also thank Sven Hofmann (GU), Nele Meckler, Philipp Meissner, Stefan Huck, Isabel Millàn, Stewart Bishop and Maria Coray for assistance in the laboratory and Jens Radke and Johannes Schwieters for fruitful discussions. We also acknowledge Anne-Lise Jourdan and two anonymous reviewers for constructive comments.

2.8 Supplementary Information

Table S2.1 *ETH data Fig. 2.7*

NO.	$\delta^{13}C_{VPDB}$		$\delta^{18}O_{VPDB}$		δ_{47} vs ref gas		1s.e. δ_{47}	Δ_{47} vs WG		1s.e. Δ_{47}
	Original	Bg corrected	Original	Bg corrected	Original	Bg corrected		Original	Bg corrected	
HG1	-48.07	-48.08	-22.53	-22.52	-64.339	-64.022	0.008	-1.188	-0.844	0.005
HG2	-48.16	-48.17	-22.42	-22.42	-64.278	-63.964	0.007	-1.150	-0.808	0.011
HG3	-47.95	-47.96	-22.53	-22.52	-64.224	-63.909	0.007	-1.182	-0.844	0.008
HG4	-28.48	-28.48	-17.25	-17.25	-40.414	-40.216	0.012	-1.029	-0.819	0.007
HG5	-28.49	-28.50	-17.16	-17.15	-40.364	-40.162	0.009	-1.062	-0.848	0.009
HG6	-7.37	-7.37	-0.20	-0.20	-2.839	-2.823	0.009	-0.841	-0.827	0.009
HG7	-7.33	-7.33	1.36	1.36	-1.175	-1.166	0.004	-0.806	-0.796	0.003
HG8	-7.34	-7.34	-1.09	-1.09	-3.739	-3.718	0.008	-0.862	-0.843	0.009
EG1	-48.31	-48.31	-0.56	-0.56	-42.154	-41.951	0.008	-0.184	0.036	0.009
EG2	-47.64	-47.65	-0.74	-0.74	-41.707	-41.498	0.010	-0.212	0.013	0.006
EG3	-47.86	-47.87	-1.15	-1.15	-42.332	-42.120	0.011	-0.216	0.014	0.008
EG4	-48.04	-48.04	-1.06	-1.06	-42.412	-42.204	0.009	-0.214	0.013	0.012
EG5	-3.78	-3.78	1.71	1.71	3.422	3.403	0.011	-0.003	-0.023	0.009
EG6	-5.80	-5.80	-2.77	-2.78	-3.119	-3.103	0.006	-0.020	0.000	0.006
EG7	-6.98	-6.98	30.80	30.80	30.066	29.922	0.007	0.117	-0.017	0.011
EG8	-7.19	-7.19	31.04	31.04	30.119	29.972	0.010	0.135	-0.004	0.010
EG9	-7.12	-7.12	30.95	30.95	30.091	29.951	0.007	0.128	-0.003	0.010

Table S2.2 *Fra data Fig. 2.8*

Date	$\delta^{13}C$ vs VPDB	$\delta^{18}O$ vs VSMOW	δ^{47} vs WG (uncorr.)	Δ_{47} vs WG (uncorr.)	δ^{47} vs WG (corr.)	Δ_{47} vs WG (corr.)
02.05.12	-10.44	29.34	-3.243	-0.936	-3.162	-0.855
04.05.12	2.13	33.20	13.171	-0.581	12.850	-0.898
07.05.12	-29.09	17.84	-33.112	-1.595	-32.315	-0.773
	-29.17	18.05	-32.991	-1.606	-32.191	-0.779
09.05.12	-10.31	27.95	-4.555	-1.007	-4.435	-0.885
14.05.12	-10.39	29.90	-2.596	-0.898	-2.531	-0.833
	-10.35	29.98	-2.498	-0.914	-2.432	-0.848
16.05.12	-29.20	17.37	-33.722	-1.644	-32.910	-0.804
	-29.38	17.91	-33.356	-1.633	-32.545	-0.796
21.05.12	-10.40	29.77	-2.783	-0.937	-2.710	-0.863
	-10.29	29.98	-2.463	-0.932	-2.394	-0.864
23.05.12	-29.29	17.49	-33.683	-1.640	-32.853	-0.782
29.05.12	2.15	31.83	11.785	-0.607	11.511	-0.878

Table S2.3 *Fra data Fig. 10(A)*

Date	$\delta^{13}C$ vs VPDB	$\delta^{18}O$ vs VSMOW	δ^{47} vs WG (uncorr.)	Δ_{47} vs WG (uncorr.)	δ^{47}vs WG (corr. 1)	Δ_{47} vs WG (corr. 1)	δ^{47}vs WG (corr. 2)	Δ_{47} vs WG (corr. 2)
02.05.12	-10.44	29.34	-3.243	-0.936	-3.169	-0.862	-3.172	-0.865
04.05.12	2.13	33.20	13.171	-0.581	12.853	-0.895	12.866	-0.883
07.05.12	-29.09	17.84	-33.112	-1.595	-32.343	-0.801	-32.375	-0.834
	-29.17	18.05	-32.991	-1.606	-32.208	-0.797	-32.240	-0.830
09.05.12	-10.31	27.95	-4.555	-1.007	-4.427	-0.878	-4.432	-0.882
14.05.12	-10.39	29.90	-2.596	-0.898	-2.534	-0.836	-2.537	-0.839
	-10.35	29.98	-2.498	-0.914	-2.430	-0.846	-2.432	-0.848
16.05.12	-29.20	17.37	-33.722	-1.644	-32.932	-0.827	-32.964	-0.860
	-29.38	17.91	-33.356	-1.633	-32.556	-0.807	-32.588	-0.840
21.05.12	-10.40	29.77	-2.783	-0.937	-2.711	-0.864	-2.713	-0.866
	-10.29	29.98	-2.463	-0.932	-2.389	-0.859	-2.392	-0.861
23.05.12	-29.29	17.49	-33.683	-1.640	-32.857	-0.787	-32.890	-0.821
29.05.12	2.15	31.83	11.785	-0.607	11.528	-0.861	11.540	-0.850

Table S2.4 *ETH data Fig. 10(B)*

sample	original δ_{47}	original Δ_{47}	mass 49 corr δ_{47}	mass 49 corr Δ_{47}
HG1	-64.339	-1.1884397	-63.797	-0.717
HG2	-2.839	-0.841271	-63.828	-0.760
HG3	-40.414	-1.0289217	-63.680	-0.713
HG4	-64.278	-1.1502002	-40.105	-0.768
HG5	-64.224	-1.182129	-40.012	-0.763
HG6	-40.364	-1.0617314	-2.845	-0.850
HG7	-1.175	-0.8055313	-1.210	-0.834
HG8	-3.739	-0.8619977	-3.740	-0.866

The correction sheet can be downloaded from the web version of the published article.

3 Clumped isotope analysis of carbonates: comparison of two different acid digestion techniques

Ulrike Wacker[1], Jens Fiebig[1,2], and Bernd R. Schöne[3]

[1] Department of Geosciences, Goethe-University, Altenhöferallee 1, 60438 Frankfurt am Main, Germany

[2] BiodiversityandClimate Research Center, Senckenberganlage 25, 60325 Frankfurt am Main, Germany

[c] Department of Applied and Analytical Paleontology (INCREMENTS), Institute of Geosciences, University of Mainz, Johann-Joachim-Becherweg 21, 55128 Mainz, Germany

Published in Rapid Communications of Mass Spectrometry ***2013****, 27, 1631–1642*

DOI: 10.1002/rcm.6609

Abstract The kinetic nature of the phosphoric acid digestion reaction enables clumped isotope analysis of carbonates using gas source isotope ratio mass spectrometry (IRMS). In most laboratories acid digestions are performed at 25 °C in sealed vessels or at 90 °C in a common acid bath. Here we show that different Δ_{47} results are obtained depending on the digestion technique employed.

Several replicates of a biogenic aragonite and NBS 19 were reacted with 104% H_3PO_4 in sealed vessels at 25 and at 90 °C using a common acid bath. The sample size varied between 4 and 14 mg. Purification methods that are standard for clumped isotope analyses were applied to the evolved CO_2 before measuring the abundances of masses 44 to 49 relative to a reference gas by IRMS.

A systematic trend to lower and more consistent Δ_{47} values is observed for reactions at 25 °C if the sample size is increased. We suggest that secondary re-equilibration of evolved CO_2 or reaction intermediates with free water molecules preferentially occurs for relatively small samples (4–7 mg), finally yielding elevated Δ_{47} values compared with >7 mg aliquots. In contrast, no such sample size effect on Δ_{47} values is observed for carbonates that are digested at 90 °C using the common acid bath.

The determination of Δ_{47} values of carbonate samples smaller than 7 mg becomes more precise and accurate if digestions are performed at 90 °C. Based on our results we propose that the difference in phosphoric acid fractionation factor between 25 and 90 °C is 0.07% for both calcite and aragonite.

3.1 Introduction

Clumped isotope analysis has recently been advanced as a new tool to reconstruct carbonate formation temperature (Eiler, 2011 and references therein). The carbonate clumped isotope thermometer relies on the isotope exchange reaction involving the most abundant isotopologue containing two heavy isotopes $Ca^{13}C^{18}O^{16}O_2$:

$$Ca^{13}C^{16}O_3 + Ca^{12}C^{18}O^{16}O_2 = Ca^{13}C^{18}O^{16}O_2 + Ca^{12}C^{16}O_3 \quad (3.1)$$

At thermodynamic equilibrium the abundance of ^{13}C-^{18}O bonds in $CaCO_3$ is a function of the equilibrium constant of reaction (1). The equilibrium constant, in turn, largely depends on temperature (Wang et al., 2004) and hence, the determination of the abundance of ^{13}C-^{18}O bonds in the carbonate provides information about its crystallization temperature. Currently, there is no technique sensitive and precise enough to directly measure the abundance of isotopologues in carbonates participating in reaction (1). Therefore, carbonates are digested with 103% H_3PO_4 (Ghosh et al., 2006a) or 105% H_3PO_4 (Zaarur et al., 2011) and the abundance of ^{13}C-^{18}O bonds within the evolved CO_2 is measured instead. Fortunately, the acid digestion reaction is kinetically controlled such that the concentration of ^{13}C-^{18}O bonds in the evolved CO_2 remains proportional to the original abundance of corresponding bonds in the carbonate lattice (Ghosh et al., 2006a; Guo et al., 2009; Passey et al., 2010).

The temperature dependency of reaction (1) is expressed by Δ_{47} which quantifies the deviation of the abundances of isotopologues of a sample gas from a theoretical random distribution. For this purpose, measured R^{47}, R^{46} and R^{45} values are compared with their corresponding stochastic distribution ratios (R^{47*}, R^{46*}, R^{45*}) where $R^i = m_i / m_{44}$:

$$\Delta_{47} = ((R^{47}/ R^{47*} - 1) - (R^{46}/ R^{46*} - 1) - (R^{45*}/ R^{45*} - 1)) * 1000 \text{ (‰)} \quad (3.2)$$

A number of calibrations of the carbonate clumped isotope thermometer have been published, including those for synthetic and biogenic minerals (Ghosh et al., 2006a; Ghosh et al., 2007; Dennis and Schrag, 2010; Tripati et al., 2010; Thiagarajan et al., 2011), as well as speleothems (Affek et al., 2008; Daëron et al., 2011). Several modern biogenic carbonates for which growth temperatures have been determined independently confirm the relationship between T_{growth} and Δ_{47} of synthetic carbonates reported by Ghosh et al. (2006a). Amongst these are mollusks, brachiopods, corals, otholiths, foraminifera and coccoliths (see Eiler, 2007; 2011 for an overview). As a consequence, most authors refer to the Ghosh et al. (2006a) line when

applying the Δ_{47}-thermometer to fossil material (e.g., Eiler, 2007; 2011; Finnegan et al., 2011). However, discrepant results have become obvious. Dennis and Schrag (2010) failed to reproduce the temperature-Δ_{47} calibration of Ghosh et al. (2006a) for inorganically precipitated calcite. In addition, both published experimental calibrations (Ghosh et al., 2006a; Dennis and Schrag, 2010) deviate from the theoretically calculated temperature dependence (Guo et al., 2009; Schauble et al., 2006). Moreover, some marine species preferring rather cold temperatures (0–15 °C) such as some benthic foraminifera (Tripati et al., 2010) and mollusks (Henkes et al., 2013) plot below the Ghosh calibration line. The causes for these unconformities are still unclear (Eiler, 2007). According to these previous calibrations (Ghosh et al., 2006a; Dennis and Schrag, 2010; Schauble et al., 2006; Henkes et al., 2013), a Δ_{47} variation of 0.1‰ corresponds to a temperature difference of roughly 20 °C or even more. As a consequence, highly accurate and precise measurements are required, especially when applying the thermometer to the small temperature window prevailing in the marine and terrestrial realms. As stated earlier, Δ_{47} measurements of acid liberated CO_2 provide information about the temperature of carbonate crystallization because of the kinetic nature of the acid digestion reaction. However, precise measurements require that variations in kinetic fractionation factors as well as secondary bond reordering in the evolved CO_2 (e.g., due to oxygen isotope exchange between water and CO_2) are avoided. Kinetic fractionations do not only depend on temperature but can also vary with relative concentrations of reagents. For example, Wendeberg et al. (2011) observed a slight decrease in $\delta^{18}O$ of evolved CO_2 after increasing the phosphoric acid concentration from 102 to 107%. In addition, the $\delta^{18}O_{CO2}$ value varied with the $\delta^{18}O$ value of the phosphoric acid if concentrations <102% were used. In this particular case, isotopic exchange between evolved CO_2 and phosphoric acid is promoted by the presence of free water (Wendeberg et al., 2011). Furthermore, oxygen isotopic compositions of CO_2 evolved from carbonates were shown to vary slightly with the digestion method (Swart et al., 1990): systematically lower $\delta^{18}O$ values were obtained when using a common acid bath than when using sealed McCrea-type reaction vessels (McCrea, 1959). This is interpreted as being the result of O-isotopic exchange between CO_2 and phosphate polymers or free water, dissolution of CO_2 in the acid and incomplete removal of CO_2 during the extraction process. Swart et al. (1990) conclude that most accurate results for $\delta^{18}O$ analyses are obtained if the common acid bath technique is used.

In this study we compare Δ_{47} signatures of CO_2 obtained by two different carbonate digestion methods which are commonly used for clumped isotope analyses: digestions at 25 °C in

McCrea-type reaction vessels (Ghosh et al., 2006a) and digestions at 90 °C using a common acid bath (Passey et al., 2010). The main purpose is to determine whether accuracy and precision of the two techniques are consistent within the range of sample size (4–14 mg) usually addressed for clumped isotope measurements of almost pure carbonates (Ghosh et al., 2006a; Dennis and Schrag, 2010; Finnegan et al., 2011; Zaarur et al., 2011). In addition, we determine the difference in isotopic fractionations between 25 °C and 90 °C digestions.

3.2 Experimental

3.2.1 Samples and sample preparation

Two different standard materials were analyzed for their Δ_{47} signatures:

- NBS 19 (calcite, supplied by the IAEA, Vienna, Austria, and by the National Bureau of Standards, Gaithersburg, MD, USA) is a coarse-grained white marble with $\delta^{18}O$ = –2.20‰ (V-PDB) or +28.64‰ (V-SMOW) and $\delta^{13}C$ = 1.95‰ (V-PDB). NBS 19 is used as an interlaboratory standard for clumped isotope analyses (Ghosh et al., 2006a; Schmid and Bernasconi, 2010; Dennis et al., 2011). For digestions at 25 °C, NBS 19 was crushed to a fine powder and homogenized using a mortar and pestle. When not treated that way, the reaction with 104% H_3PO_4 was observed to be very slow and, sometimes incomplete, as indicated by $\delta^{13}C$ values significantly lower than 1.95‰.
- *Arctica islandica*, a bivalve with an aragonitic shell, grew near Langanes, NE Iceland, in ca. 30 m water depth at an average temperature of 6.0 ± 0.5 °C. The specimen was collected alive in August 2006. Sample material was taken from the outer layer of the most recently formed part of the shell. For this purpose, the shell was cut into two parts along the direction of growth from the umbo to the ventral marging using a Buehler low-speed precision saw equipped with a 0.4 mm thick diamond-coated saw blade. Subsequently, both shell slabs were cut perpendicularly to the growth lines. The youngest part of the valve was used for clumped isotope analyses. The periostracum and the inner shell layer were physically abraded before the two shell pieces were ground and homogenized in an oscillating disc mill. Some aliquots reacted at 25 °C were pretreated for 2 h with 1.5% H_2O_2 prior to the analysis to remove organic matter, as organic matter has been found to preclude accurate Δ_{47} analysis of some biogenic carbonates (Huntington et al., 2009).

3.2.2 Acid digestion

The concentration of the phosphoric acid used for digestion reactions was 104%. This corresponds to a density of 1.91 g/cm^3 (for the conversion of acid concentrations into acid densities we use the equation determined by Ghosh et al. (2005): y = 0.0114x + 0.723, where y is the acid density in g/cm^3 and x is the acid concentration in %). The acid was prepared by slightly modifying the method of Coplen (1983): 99% H_3PO_4 (Merck KGaA, Darmstadt, Germany, ≥99%) was heated to 150 °C, and then P_4O_{10} was slowly added to the stirred solution. After 10 h an acid aliquot was cooled to room temperature for about 1 h. The acid density was measured gravimetrically at 25 °C, and once a concentration of 104% was achieved, the acid was heated (at 150 °C) for at least three additional hours. Otherwise, either more P_4O_{10} or distilled water was added until the concentration reached 104%. The acid was stored for at least two weeks to ensure that all the water had reacted with P_4O_{10} to H_3PO_4 (Coplen et al., 1983). Before using the acid for digestion reactions, the density was controlled gravimetrically again.

Carbonate digestions at 25 °C were performed in McCrea-type reaction vessels (McCrea, 1950). 4 to 14 mg aliquots of carbonate were reacted with 7 ± 1 mL 104% H_3PO_4. The carbonate was placed into the side arm and the acid was filled in the main tube of the reaction vessel, before evacuating it for 2.5 to 3.5 h to reach a vacuum better than 10^{-3} mbar. Before starting the reaction by tipping the acid over the carbonate, the vessels were placed in a common water bath at 25.0(±0.2) °C for 1 h to ensure thermal equilibration. During the reaction, the vessels were kept in the water bath at 25 °C. The reaction time was between 16 and 20 h.

Reactions at 90 °C were performed using an automated acid bath whose design is very similar to those used at Caltech and Johns Hopkins University (Passey et a, 2010). The acid bath was was placed in a copper block surrounded with a heating band to keep the acid at a constant temperature of 90.0(±0.1) °C. The carbonate samples were filled into small Ag capsules (IVA Analysentechnik e. K., Meerbusch, Germany, art. no. 184.9921.36). These were loaded into a Zero Blank Autosampler (Costech, Valencia,CA, USA). The acid bath and the autosampler were pumped by a turbomolecular pump backed by a Membrane pump (Pfeiffer, Aßlar, Germany). After a sample was dropped in the acid, the evolved CO_2 was frozen in a U-trap cooled at liquid nitrogen temperature after passing another cold trap held at –80 °C to remove trace amounts of water. By monitoring the pressure of the evolved CO_2 we observed that the digestion of the fine grained carbonate powder of *A. islandica* takes only ~10 min, while the larger crystals of NBS 19 reacted for ~20–30 min. After manometrically determining the yield,

the extracted CO_2 was frozen into a transportable glass finger equipped with high-vacuum valves (Louwers, Hapert, The Netherlands, art code 40.200.8).

3.2.3 CO_2 cleaning procedure

The CO_2 derived from phosphoric acid digestions at both 25 and 90 °C was cleaned following the procedure described in Ghosh et al. (2006a). Briefly, the transportable glass finger containing the sample CO_2 was connected to a cryogenic vacuum extraction line, evacuated to $<10^{-6}$ mbar using a turbomolecular pump supported by a membrane pump (Pfeiffer). The CO_2 yield was determined with a capacity manometer, and then CO_2 was passed twice over a trap held at –80 °C before being frozen back into the volume of the glass finger. Afterwards, the sample was passed through a gas chromatograph (GC) purification system to remove traces of hydrocarbons. The CO_2 was entrained into a He carrier gas flow (18 mL/min; purity: 99.9999%) and purged through a 1.20 m x 2.15 mm i.d. stainless steel column packed with Porapak Q 80/120, kept at –20 °C. Before entering and after leaving the GC column the He-CO_2 gas mixture passed additional water traps held at –77 °C. The CO_2 effluent from the GC column was collected for a period of 30 min in a U-trap immersed in liquid nitrogen. After one sample had passed through the GC column the He flow was switched to a backflush mode, enabling the water traps and the column to be heated to 25 and 150 °C, respectively, for at least 15 min. In a final step, the He carrier gas was pumped away and the CO_2 was cryogenically purified one final time using the vacuum extraction line described above. For isotopic analysis, the purified CO_2 was transferred to a transportable glass finger that could be connected to the dual inlet system of the mass spectrometer.

3.2.4 Measurements

Isotopic analyses were performed at Goethe University (Frankfurt, Germany) on a MAT 253 gas source isotope ratio mass spectrometer (Thermo Fisher Scientific, Bremen, Germany) equipped with dual inlet system and six Faraday cup collectors for masses 44 to 49 (resistors: 3×10^8 Ω, 3×10^{10} Ω, 10^{11} Ω for masses 44–46, respectively, and 10^{12} Ω for masses 47–49). The original stainless steel capillaries were replaced with 4 feet long electroformed nickel (EFNi) capillaries (VICI AG, Schenkon, Switzerland; 1/32" o.d., 0.005" i.d., art. no. TEFNI.505, 122 cm x 0.127 mm ID; Passey et al., 2010).

Measurements were performed using the dual inlet system, after adjusting the sample and reference gas signals of mass 44 to (16000 ± 150) mV. Ten acquisitions consisting of ten cycles with an ion integration time of 20 s each, were used for all measurements,

corresponding to a shot-noise limit of ~0.008‰ (Merritt and Hayes, 1994). Before each acquisition, peak centering, background determination and pressure adjustments to 16 V at mass 44 were carried out. The total analysis time of one sample was about 3 h. CO_2 from Oztech (Safford, AZ, USA; $\delta^{18}O$ = +25.01‰ vs V-SMOW; $\delta^{13}C$ = –3.63‰ vs V-PDB) was used as the reference gas.

3.2.5 Data processing

We report Δ_{47} values on the absolute scale of Dennis et al. (2011). In comparison to the data correction procedure described by Huntington et al. (2009), absolute scaling of raw Δ_{47} values has the advantage that the processed data becomes comparable between labs as the Δ_{47} composition of the CO_2 reference gas (which may vary between labs) is considered. Briefly, raw data is corrected in two steps. (1) To correct for non-linearities of the mass spectrometer, CO_2 gases of different bulk isotopic compositions were measured. Prior to isotopic analysis, these were heated in quartz break-seal tubes to 1000 °C for more than 2 h to reach the characteristic distribution at this temperature. After quenching to room temperature, the gases were purified cryogenically and by GC like carbonate samples. (2) Δ_{47} values corrected for non-linearity were then converted to the absolute scale using the empirical transfer function (ETF). The ETF is determined by plotting the intercepts of linearity lines (derived from measurements of CO_2 gases of distinct bulk isotopic compositions equilibrated to at least two different temperatures) against the corresponding theoretically expected values (Wang et al., 2004). We have determined our ETF using the intercepts of CO_2 gases heated at 1000 °C and equilibrated with water at 25 °C. CO_2 and H_2O were enclosed in glass tubes, which were placed in a waterbath for at least three days at 25.0 ± 0.2 °C. After quenching with liquid nitrogen, the glass was held in an ethanol/dry-ice slush at –80 °C to release CO_2, while H_2O remained frozen. Separation between water and CO_2 was improved by passing the gas at least five times over a trap held at –80 °C using the vacuum extraction line. Afterwards, water-equilibrated gases were cleaned and measured like sample gases (Dennis et al., 2011).

Carbonates were reacted at 25 and 90 °C between April 2011 and January 2012. Instrument non-linearity was continually monitored by measuring heated gases daily and comparing the slopes of heated gas regression lines determined from blocks of nine consecutive heated gas analyses. As long as slopes of these single blocks were identical within the standard errors, all the analyses were used for the determination of the heated gas slope. If the slopes of the different blocks of analyses were changing significantly, new correction parameters were determined for each day using the running average of the heated gas line of nine consecutive

analyses. [For example, for linearity correction of the NBS 19 sample analyzed on 04 November 2011 the slope of the heated gas line (m = 0.0250) was derived using heated gas analyses carried out between 24 October 2011 and 16 November 2011 (Supplementariy Table S3.1, see Supporting Information)]. The δ^{47} and Δ_{47} values of heated gases were, however, highly correlated, with R^2-values always better than 0.99. The slopes of the heated gas lines which were used to correct carbonate data are listed in Table 3.1 along with raw and corrected carbonate Δ_{47} data.

For the determination of the ETFs we considered the intercepts of linearity lines of heated gases analyzed over a period of two months. The intercepts for April/May and June/July 2011 are statistically indistinguishable (Supplementary Table S3.1, see Supporting Information). After source cleaning a significant change in the heated gas intercept between September/October 2011 and November/December 2011 was observed, while no change occurred between November/December 2011 and January/February 2012 (Supplementary Table S3.1, see Supporting Information). Gases equilibrated at 25°C were measured frequently in November/December 2010 and, after source cleaning in September 2011. In addition, some gases were analyzed temporarily (February, March, April, July and November 2011, Supplementary Table S3.1, see Supporting Information) to test the consistency of the Δ_{47} composition of the reference gas. The intercept of the line determined by 25 °C water-equilibrated gases was constant at –0.03‰ between November 2010 and July 2011, while it was –0.06‰ after source cleaning. We therefore applied three ETFs to correct our carbonate data: y = 1.1094x + 0.9585 between November 2010 and July 2011, y = 1.0959x + 0.9910 for September 2011 and y = 1.1521x + 0.9943 from November 2011 to January 2012 (with x: intercepts of the equilibration and heated gas lines and y: theoretical equilibrium value for Δ_{47} at the corresponding equilibration temperature).

For the normalization of Δ_{47} values to acid digestions at 25 °C a difference in acid fractionation factors of +0.081‰ (Passey et al., 2010) was applied to data obtained from carbonates reacted at 90 °C, as used by Dennis et al. (2011). It should be noted that the difference of 0.081‰ was determined on the internal 'Caltech scale'. If this value is projected in the absolute reference frame using the slope of the secondary reference frame transfer function provided by Dennis et al. (2011), a value of 0.084‰ is obtained instead. Considering the precision of Δ_{47} analysis as represented by our shot noise limit, this value is indistinguishable from the +0.081‰ reported by Passey et al. (2010).

3.3 Results

$\delta^{13}C$ values, $\delta^{18}O$ values, δ^{47} values, raw Δ_{47} values, absolute Δ_{47} values and their 1σ standard errors (1 se) as well as sample size and date of analysis are listed in Table 3.1. For untreated *A. islandica* reacted at 25 °C a mean Δ_{47} value of 0.718‰ is obtained, with the total interval ranging between 0.674 to 0.772‰ and a standard error of 0.007‰ (n = 20). The mean value is statistically indistinguishable from the average obtained for sample aliquots that were treated with H_2O_2 before acid digestions (0.730 ± 0.008)‰ (n = 10), whose corresponding Δ_{47} values vary between 0.695 and 0.787‰. Altogether, an average for *A. islandica* of (0.722 ± 0.005)‰ (n = 30) is obtained. For NBS 19 digested at 25 °C, the Δ_{47} values range from 0.339 to 0.396‰ with a mean of (0.373 ± 0.004)‰ (n = 20). For both materials, distinctively lower mean Δ_{47} values are obtained if the carbonates were reacted at 90 °C, applying a correction factor of +0.081‰ (Passey et al., 2010) that accounts for the difference in acid digestion fractionation factors between reactions at 25 and 90 °C: (0.707 ± 0.003)‰ (n = 19) for *A. islandica* (total interval between 0.682 and 0.723‰) and (0.359 ± 0.004)‰ (n = 19) for NBS 19 (total interval between 0.329 and 0.391‰).

Table 3.1 *Experimental results: isotopic values reported in % deviation, sample sizes in mg. (a) Digestions at 25 °C; McCrea-type reaction vessels.*

Date of analysis	$\delta^{13}C$ (V-PDB)	$\delta^{18}O$ (V-PDB)	Sample size	δ_{47}	Δ_{47}	Δ_{47} abs	se	Slope of HG line	δ_{48}	Δ_{48}
A. islandica										
08.04.11	1.53	3.05	4.6	25.38	0.530	0.761	0.010	0.0279	64.507	24.415
26.04.11	1.56	3.28	4.9	25.66	0.548	0.772	0.013	0.0279	63.752	23.255
28.04.11	1.60	3.31	7.1	25.69	0.505	0.692	0.007	0.0290	58.068	17.728
03.05.11	1.63	3.51	4.3	26.00	0.577	0.762	0.011	0.0290	64.303	23.313
03.05.11	1.60	3.34	4.3	25.75	0.529	0.717	0.009	0.0290	60.649	20.150
03.05.11	1.69	3.39	10.2	25.87	0.521	0.705	0.010	0.0290	56.466	16.021
04.05.11	1.67	3.36	8.0	25.79	0.498	0.682	0.011	0.0290	54.985	14.672
05.05.11	1.90	3.07	4.2	25.77	0.541	0.729	0.012	0.0290	59.883	19.954
05.05.11	1.55	3.25	4.3	25.61	0.531	0.724	0.010	0.0290	62.182	21.803
06.05.11	1.67	3.11	4.1	25.62	0.564	0.760	0.009	0.0290	61.023	20.969
10.05.11	1.67	3.19	7.2	25.64	0.506	0.695	0.008	0.0290	54.969	14.980
10.05.11	1.66	3.20	9.9	25.64	0.508	0.697	0.006	0.0290	55.096	15.086
11.05.11	1.57	3.31	8.8	22.22	0.498	0.687	0.005	0.0290	54.958	14.744
31.05.11	1.60	3.05	4.8	25.43	0.528	0.703	0.012	0.0298	61.002	21.087
31.05.11	1.62	3.01	4.6	25.39	0.501	0.674	0.007	0.0298	57.110	17.416
31.05.11	1.64	3.23	4.6	25.68	0.540	0.708	0.009	0.0298	62.398	22.057
08.06.11	1.60	3.08	4.7	25.51	0.561	0.735	0.011	0.0299	61.590	21.585
08.06.11	1.64	3.12	4.8	25.59	0.562	0.733	0.010	0.0299	62.782	22.647
08.06.11	1.56	3.07	4.7	25.46	0.561	0.736	0.009	0.0299	62.641	22.611
09.06.11	1.69	3.23	14.2	25.71	0.521	0.684	0.014	0.0299	58.845	18.637
average	**1.63**	**3.21**				**0.718**				
se						**0.007**				

Table 3.1. *Continued.*

Date of analysis	$\delta^{13}C$ (V-PDB)	$\delta^{18}O$ (V-PDB)	Sample size	δ_{47}	Δ_{47}	Δ_{47} abs	se	Slope of HG line	δ_{48}	Δ_{48}
pretreated *A. islandica*										
17.05.11	1.59	3.16	5.1	25.54	0.524	0.718	0.010	0.0290	60.180	20.065
18.05.11	1.51	3.16	4.1	25.46	0.511	0.701	0.008	0.0292	64.338	24.059
19.05.11	1.64	3.09	4.9	25.55	0.550	0.741	0.010	0.0292	60.383	20.398
20.05.11	1.58	3.37	11.1	25.74	0.516	0.695	0.009	0.0293	56.040	15.657
23.05.11	1.67	3.13	4.0	25.66	0.595	0.787	0.013	0.0292	67.693	27.358
25.05.11	1.62	3.26	4.8	25.70	0.553	0.728	0.010	0.0296	63.828	23.375
26.05.11	1.66	3.36	4.2	25.85	0.561	0.731	0.007	0.0296	64.594	23.897
26.05.11	1.70	2.85	4.3	25.36	0.546	0.732	0.007	0.0296	60.177	20.686
26.05.11	1.71	3.15	4.4	25.70	0.573	0.751	0.009	0.0296	62.176	22.015
09.06.11	1.67	2.90	4.5	25.32	0.494	0.717	0.008	0.0299	58.788	19.253
average	**1.64**	**3.14**				**0.730**				
se						**0.008**				
NBS 19										
12.04.11	1.93	-2.14	4.3	19.40	0.034	0.396	0.013	0.0279	44.274	16.332
12.04.11	1.95	-2.22	4.6	19.33	0.021	0.384	0.010	0.0279	42.901	15.150
12.04.11	2.01	-2.03	4.4	19.59	0.020	0.374	0.013	0.0279	44.327	16.145
13.04.11	1.95	-2.26	4.5	19.28	0.012	0.375	0.010	0.0279	43.497	15.812
14.04.11	1.97	-2.05	5.2	19.49	-0.006	0.349	0.014	0.0279	40.182	12.171
15.04.11	1.91	-2.24	5.0	19.27	0.025	0.389	0.011	0.0279	46.020	18.228
18.04.11	1.95	-2.18	4.1	19.37	0.025	0.387	0.012	0.0279	42.245	14.444
19.04.11	1.97	-2.17	6.2	19.39	0.011	0.369	0.009	0.0280	40.530	12.745
19.04.11	1.95	-2.16	4.4	19.39	0.020	0.378	0.012	0.0280	42.644	14.779
20.04.11	1.91	-2.25	4.4	19.26	0.023	0.373	0.008	0.0286	45.142	17.393
26.04.11	1.94	-2.25	4.8	19.31	0.045	0.396	0.011	0.0286	45.681	17.915
27.04.11	1.96	-2.11	4.6	19.47	0.039	0.375	0.008	0.0290	45.631	17.580
28.04.11	1.98	-2.17	5.4	19.42	0.039	0.377	0.013	0.0290	44.897	16.992
04.05.11	1.99	-2.08	5.6	19.54	0.052	0.387	0.008	0.0290	41.304	13.307
10.05.11	2.05	-2.51	4.9	19.15	0.029	0.374	0.012	0.0290	41.910	14.756
11.05.11	1.98	-2.25	4.6	19.31	0.020	0.359	0.009	0.0290	36.232	8.730
13.05.11	2.06	-2.44	8.6	19.22	0.025	0.368	0.009	0.0290	39.234	12.024
16.05.11	2.05	-2.51	9.3	19.11	0.011	0.356	0.006	0.0290	36.933	9.929
09.06.11	2.02	-2.10	12.4	19.54	0.036	0.350	0.010	0.0299	41.524	13.563
21.06.11	2.06	-2.31	8.4	19.33	0.010	0.339	0.008	0.0294	33.261	5.943
average	**1.98**	**-2.22**				**0.373**				
se						**0.004**				

Table 3.1. *Continued.*
(b) Digestion at 90 °C; common acid bath.

Date of analysis	$\delta^{13}C$ (V-PDB)	$\delta^{18}O$ (V-PDB)	sample size	δ_{47}	Δ_{47}	Δ_{47} abs	se	slope of HG line	δ_{48}	Δ_{48}
A. islandica										
02.09.11	1.73	3.28	9.9	23.28	0.269	0.714	0.010	0.0256	44.069	8.684
05.09.11	1.53	3.27	4.0	23.06	0.257	0.707	0.011	0.0256	46.716	11.274
05.09.11	1.61	3.13	5.0	23.00	0.263	0.715	0.006	0.0256	44.957	9.856
06.09.11	1.71	3.33	9.8	23.31	0.266	0.709	0.005	0.0256	45.600	10.060
06.09.11	1.63	3.30	5.2	23.18	0.255	0.702	0.010	0.0256	45.303	9.844
06.09.11	1.60	3.25	4.2	23.09	0.248	0.696	0.011	0.0256	49.478	13.975
06.09.11	1.63	3.38	10.0	23.27	0.258	0.702	0.008	0.0256	43.964	8.387
07.09.11	1.67	3.25	6.3	23.15	0.237	0.683	0.005	0.0256	46.321	10.926
07.09.11	1.65	3.24	4.0	23.16	0.270	0.719	0.010	0.0256	47.231	11.831
07.09.11	1.67	3.34	4.5	23.29	0.278	0.723	0.009	0.0256	45.868	10.299
07.09.11	1.60	3.26	3.9	23.10	0.242	0.689	0.008	0.0256	46.437	11.018
07.11.11	1.59	3.05	6.2	22.86	0.230	0.682	0.010	0.0250	49.285	14.181
08.11.11	1.57	3.18	4.4	23.00	0.254	0.708	0.006	0.0249	51.604	16.173
10.11.11	1.63	3.12	5.7	23.00	0.263	0.719	0.011	0.0249	46.765	11.617
14.11.11	1.62	3.05	5.1	22.89	0.227	0.697	0.009	0.0243	49.193	14.101
09.01.12	1.60	3.14	8.0	22.95	0.219	0.722	0.010	0.0229	46.410	11.236
10.01.12	1.57	3.13	4.7	22.90	0.212	0.716	0.010	0.0229	47.540	12.690
11.01.12	1.59	3.20	4.3	23.00	0.212	0.712	0.000	0.0229	48.068	12.704
12.01.12	1.51	2.96	4.5	22.67	0.209	0.718	0.006	0.0229	48.068	12.704
average	**1.62**	**3.20**				**0.707**				
se						**0.003**				
NBS 19										
08.09.2011	1.98	-2.04	4.97	17.05	-0.240	0.331	0.011	0.0256	30.662	7.190
08.09.2011	1.97	-2.02	9.57	17.09	-0.212	0.361	0.009	0.0256	29.974	6.470
09.09.2011	1.97	-2.56	5.06	16.51	-0.224	0.363	0.011	0.0256	30.302	7.895
09.09.2011	2.03	-2.19	8.92	16.96	-0.228	0.347	0.006	0.0256	29.447	6.512
09.09.2011	2.02	-2.10	10.62	17.05	-0.219	0.353	0.011	0.0256	29.837	6.512
02.11.11	1.97	-2.30	5.53	16.82	-0.197	0.358	0.011	0.0253	33.544	10.526
04.11.11	1.94	-2.28	4.81	16.79	-0.210	0.349	0.011	0.0250	34.685	11.604
06.11.11	1.95	-2.21	5.17	16.89	-0.185	0.375	0.012	0.0250	33.593	10.404
07.11.2011	1.94	-2.29	4.45	16.78	-0.216	0.344	0.003	0.0250	31.550	8.564
09.11.2011	1.96	-2.30	5.13	16.79	-0.209	0.353	0.010	0.0249	34.265	11.240
10.11.2011	1.98	-2.17	7.65	16.97	-0.192	0.368	0.010	0.0249	30.609	7.397
11.11.2011	1.98	-2.18	5.24	16.92	-0.227	0.329	0.007	0.0249	32.683	9.439
14.11.2011	1.98	-2.23	4.75	16.89	-0.214	0.356	0.008	0.0243	33.949	10.779
03.01.2012	1.97	-2.17	5.63	16.94	-0.212	0.384	0.009	0.0229	33.581	10.306
04.01.2012	2.00	-2.14	8.87	16.97	-0.230	0.362	0.011	0.0229	30.857	7.593
05.01.2012	1.99	-2.25	9.25	16.88	-0.207	0.391	0.010	0.0229	30.586	7.373
09.01.2012	1.99	-2.17	7.95	16.92	-0.239	0.354	0.008	0.0229	33.231	10.102
16.01.12	1.97	-2.24	4.26	16.85	-0.218	0.379	0.011	0.0229	30.955	7.678
18.01.2012	2.04	-2.14	8.98	17.01	-0.233	0.359	0.009	0.0229	33.721	10.653
average	**1.98**	**-2.21**				**0.359**				
se						**0.004**				

3.4 Discussion

The precision of clumped isotope analysis of carbonate replicates is commonly reported as the 1σ standard error of the mean (e.g., Ghosh et al., 2006a; Huntington et al., 2009). Recently, three different laboratories analyzed NBS 19, and mean values of (0.373 ± 0.007)‰ (Harvard University, n = 7), (0.399 ± 0.005)‰ (Johns Hopkins University; n = 12) and (0.404 ± 0.006)‰ (Yale University; n = 40) were reported for Δ_{47} values with the average and accepted value being 0.392‰ (Dennis et al., 2011). In this study, the mean Δ_{47} values determined for NBS 19 at reaction temperatures of 25 and 90 °C are (0.373 ± 0.004)‰ and (0.359 ± 0.004)‰, respectively. Within errors, these values are either indistinguishable (25 °C) or nearly identical (90 °C) to the Harvard mean value. It has been postulated that the differences in NBS 19 between the three laboratories were due to possible heterogeneities of different aliquots of NBS 19. However the difference observed in our data cannot be attributed to inhomogeneities as all measured aliquots are from the same batch.

3.4.1 Correlation between sample size and Δ_{47} values

If Δ_{47} values are plotted against sample size, a systematic trend is observed for carbonates that were digested at 25 °C (Fig. 3.1). Sample aliquots <7 mg show a larger scatter in Δ_{47} values and higher corresponding mean values than >7 mg aliquots. *A. islandica* (untreated plus pretreated) <7 mg average (0.733 ± 0.006)‰ (n = 22), but (0.692 ± 0.003)‰ (n = 8) for >7 mg aliquots. Similarly, the average Δ_{47} value for NBS 19 samples <7 mg is 0.378 ± 0.003‰ (n = 16) and, therefore, clearly distinguishable from the (0.353 ± 0.006)‰ (n = 4) determined for larger (>7 mg) aliquots (Fig. 3.1, Table 3.1).

In contrast, no dependency of Δ_{47} values on sample size is observed when digesting carbonates at 90 °C (Fig. 3.1). The Δ_{47} values of small samples (<7 mg) of NBS 19 average to (0.357 ± 0.006)‰ (n = 11), indistinguishable from the mean Δ_{47} value for samples >7 mg ((0.362 ± 0.005)‰ (n = 8)). The same is observed for *A. islandica*: for small samples (<7 mg) a mean of (0.706 ± 0.003)‰ (n = 15) is calculated, which is indistinguishable from the average Δ_{47} value of large samples (>7 mg) with (0.712 ± 0.004)‰ (n = 4).

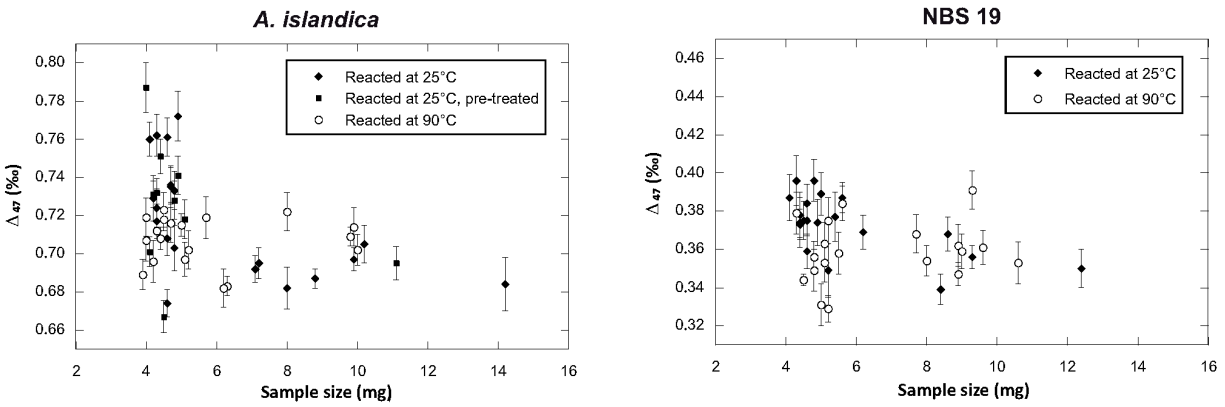

Figure 3.1 *Correlation plot of Δ_{47} values (‰) and sample size (mg) for A. islandica (a) and NBS 19 (b), respectively. For both carbonates a relatively large scatter is observed for samples between 4 and ~7 mg if acid digestion is carried out at 25 °C. Compared with the interval described by NBS 19 a larger variation in Δ_{47} values is observed for the biogenic carbonate. Using the common acid bath technique and a reaction temperature of 90 °C, no correlation between Δ_{47} values and sample size is displayed. For further discussion, see text.*

3.4.2 Potential occurrence of contaminants in sample-derived CO_2

Isobaric interferences caused by non-CO_2 additions to the sample gas will affect measured Δ_{47} values. One source of isobaric contaminants might be traces of organic matter inside carbonates, which might be partly volatilized during phosphoric acid digestion (Huntington et al., 2009). There are two evident arguments against contamination of sample gas caused by organic matter: first, we would expect more organic compounds to be volatilized if reaction temperature was increased. Hence, compared to digestions at 25 °C, a stronger sample size effect should be observed for digestions at 90 °C. These pattern are reverse to those displayed by our data. Secondly, Δ_{47} values for *A. islandica* remained unchanged regardless of whether the samples were pretreated with H_2O_2 prior to acid digestion or not (Table 3.1, Fig. 3.1(a)). For this reason it does not seem to be necessary to remove any trace amounts of organic matter from the aragonite of *A. islandica* prior to isotopic analyses. For further discussion, the datasets for untreated and H_2O_2-treated material of *A. islandica* will, therefore, be combined.

Huntington et al. (2009) used a correlation plot of δ^{48} against Δ_{48} values to control the quality of measured Δ_{47} values. As observed for Δ_{47}, Δ_{48} is also a function of the bulk isotopic composition. Likewise, heated gases describe a linear relationship between δ^{48} values and Δ_{48} values. As long as the purity of the sample gas is comparable with that of heated gases, sample-derived CO_2 gases should plot within the linear array defined by heated gases. After installation of our mass spectrometer at the end of 2009, the mass 48 signal initially was about 200 mV, but this continuously decreased to ~40 mV within two years. During the same period,

it was observed that the background of the mass 48 signal drifted to more negative values. We, therefore, applied a correction of the raw values of mass 48 intensity by adding a constant offset (roughly corresponding to the negative background) to the measured intensities of both sample and reference gas.

For a given sample δ^{48} value, we computed the deviation in Δ_{48} values (($\Delta(\Delta_{48})$ values) between sample and heated gas regression lines ($y = 0.3102x + 0.905$, $R^2 = 0.97$; after source cleaning: $y = 0.2571x + 0.4134$, $R^2 = 0.97$). These $\Delta(\Delta_{48})$ values are then plotted versus measured sample Δ_{47} values in Fig. 3.2. All the measured samples spread around $\Delta(\Delta_{48}) = 0‰$, as do the heated gases. Moreover, absolute deviations from the $\Delta(\Delta_{48}) = 0‰$ line are of the same magnitude for both the sample and the heated gases. Especially for *A. islandica*, for which the sample size effect on Δ_{47} values at 25 °C is most pronounced, the absolute variations in ($\Delta(\Delta_{48})$) values of samples reacted at 25 °C and at 90 °C are identical ($\Delta(\Delta_{48}) = 0 \pm 3‰$). Therefore, it is unlikely that elevated Δ_{47} values for 25 °C digestions are due to poor sample gas purity.

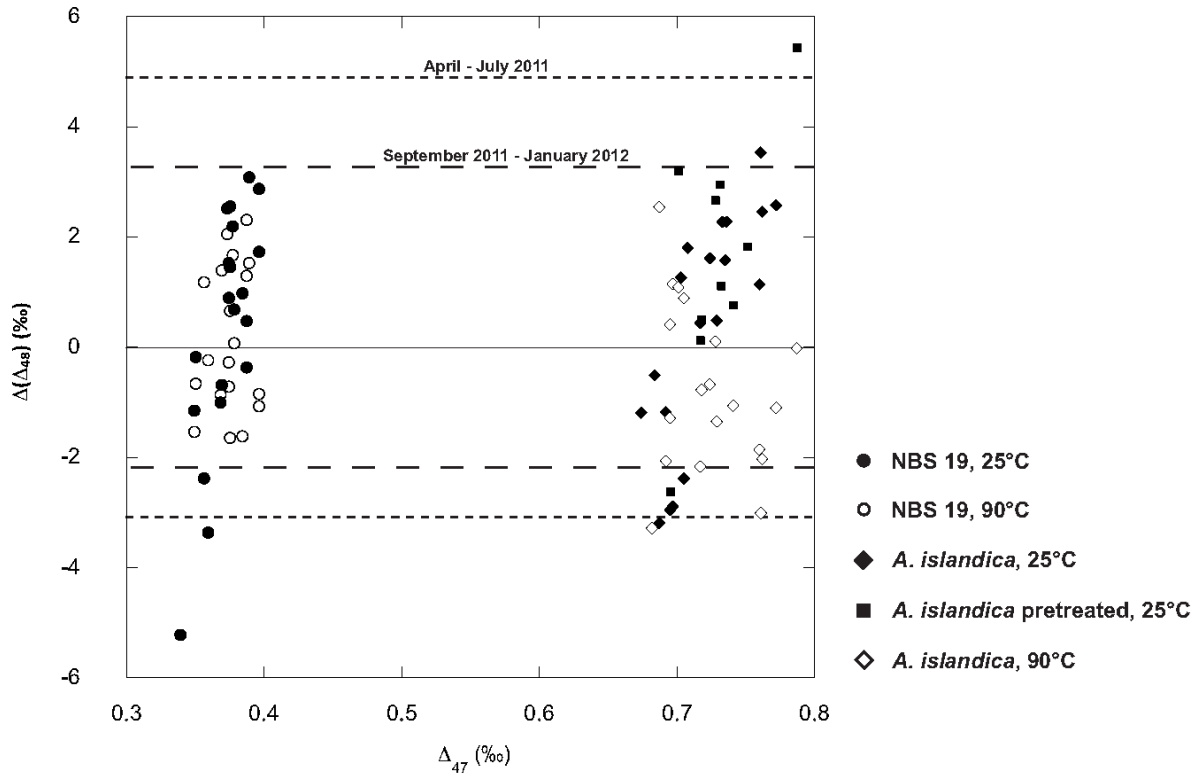

Figure 3.2 *Δ_{47} values (‰) plotted vs. the deviation in Δ_{48} between samples and heated gas regression line (expressed as $\Delta(\Delta_{48})$). The dashed lines mark the absolute Δ_{48} deviation of heated gases from the heated gas regression line observed within periods from April to July 2011 and September 2011 to January 2012. All the Δ_{48} values of carbonates scatter around $\Delta(\Delta_{48}) = 0$ and plot in the interval described by the heated gases. This indicates that the purities of sample and heated gases are indistinguishable from each other.*

3.4.3 Incomplete gas yield

Incomplete gas yield, caused either by incomplete reactions of carbonates or dissolution of CO_2 in the acid, can lead to kinetic isotope effects which might depend on sample size. Walters et al. (1971) observed that the evolved CO_2 becomes enriched in ^{18}O during the progress of the reaction between carbonate and phosphoric acid. Confirming their results, we obtained a $\delta^{18}O$ value of –2.65‰ (vs. the accepted value of –2.20‰) for coarse-grained NBS 19 that had been reacted at 25 °C for 8 h instead of the standard 16–20 h. In addition, the $\delta^{13}C$ value was significantly lower than the accepted value (1.17 vs. 1.95‰) and the Δ_{47} value of 0.451‰ was significantly higher than those obtained for the other reactions at 25 °C (0.339–0.396‰; Table 3.1). If our elevated Δ_{47} values for <7 mg aliquots were due to incomplete reactions, correlations between Δ_{47} values and the bulk oxygen and carbon isotopic compositions would be expected. Indeed, for NBS 19 a slightly negative correlation between $\delta^{13}C$ values and Δ_{47} values is observed, but there is no obvious trend between Δ_{47} values and $\delta^{18}O$ values (Fig. 3.3(b)). In addition, $\delta^{18}O$ values, $\delta^{13}C$ values and Δ_{47} values of *A. islandica* do not correlate (Fig. 3.3(a)), although the scatter of Δ_{47} values for small samples is much larger than for NBS 19. Therefore, we consider it unlikely that the sample size effect results from incomplete reactions. On the contrary, we assume that reactions were quantitative, because no systematic differences in Δ_{47} values were observed if the CO_2 was extracted after either 16 or 20 h.

Incomplete gas yields would also be observed if the evolved CO_2 is not removed quantitatively from the acid. The amount of CO_2 dissolved in the acid depends on the partial pressure of CO_2 above the acid (which, in turn, depends on the sample size), the geometry of the reaction vessel, acid viscosity and reaction temperature (Swart et al., 1990). The migration of gases in liquids can be described by diffusion laws. Fractionations between two CO_2 reservoirs that are induced by diffusion are more pronounced in $^{13}C/^{12}C$ and $^{18}O/^{16}O$ isotope ratios than in 47/44 isotopologue ratios (Eiler and Schauble, 2004). Therefore, we would expect that incomplete removal of CO_2 from the acid would be accompanied by correlations between the clumped and the bulk isotopic composition of the extracted CO_2. Since there is no trend between Δ_{47} values and $\delta^{18}O$ values for NBS 19 (Fig. 3.3(b)) and no correlations are observed between Δ_{47} values, $\delta^{18}O$ values and $\delta^{13}C$ values for *A. islandica* (Fig. 3.3(a)) it is unlikely that the sample size effect on Δ_{47} values observed for samples digested at 25 °C results from incomplete extraction of CO_2 from the acid. In addition, we found no manometric evidence for incomplete reaction yields at 25 °C.

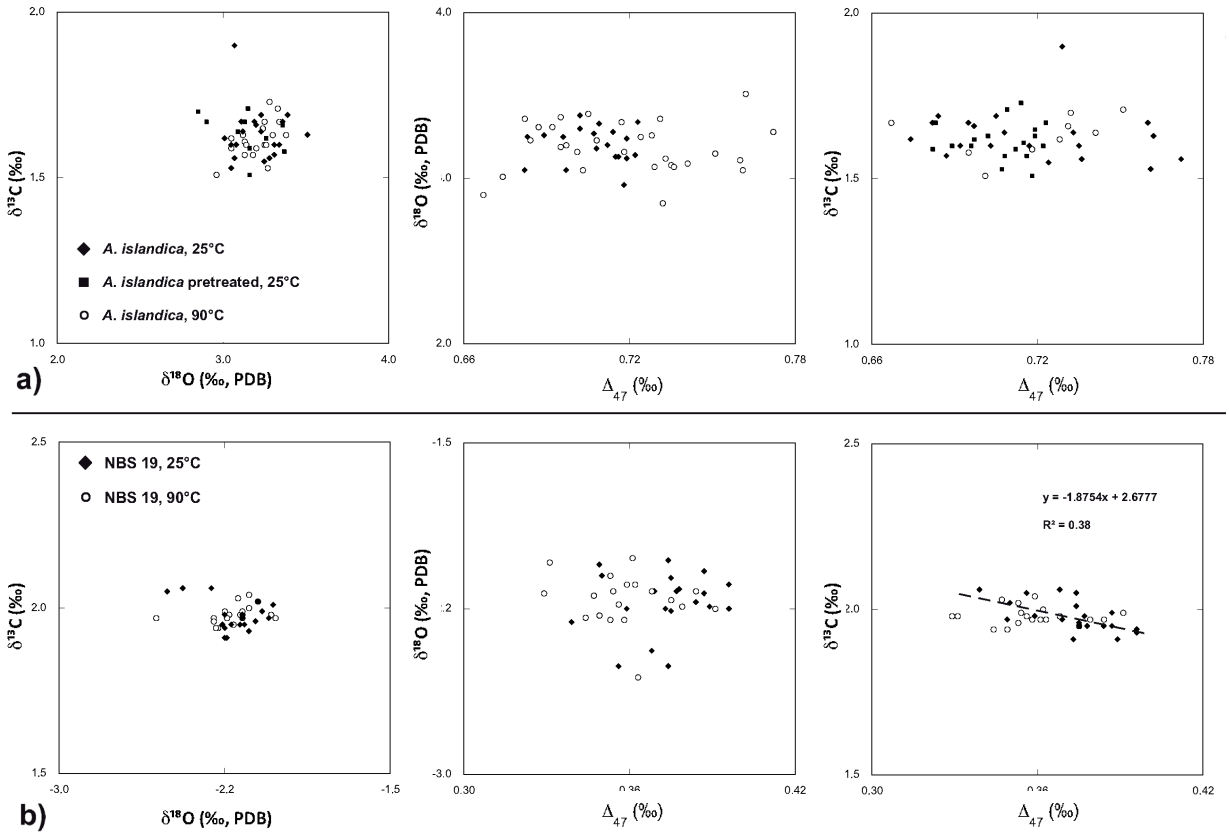

Figure 3.3 *Crossplots of $\delta^{18}O$, $\delta^{13}C$ and Δ_{47} values for A. islandica and NBS 19, respectively. Values for A. islandica do not correlate with each other (a), irrespective of the reaction temperature. CO_2 derived from 25 °C digestions of NBS 19 shows a negative trend between the Δ_{47} and $\delta^{13}C$ values (b). For further discussion, see text.*

3.4.4 Potential variations of fractionation factors during acid digestion

It is well known that the acid digestion reaction of carbonates using phosphoric acid is kinetically controlled (Ghosh et al., 2006a; Guo et al., 2009). Wendeberg et al. (2011) measured the carbon and oxygen isotopic composition of CO_2 evolved from phosphoric acid digestion of NBS 19 using variable concentrations of phosphoric acid. They observed that the $\delta^{18}O$ value of the evolved CO_2 decreased by 0.1‰ when phosphoric acid concentration was increased from 102 to 107%. They concluded that phosphoric acid concentration may affect oxygen isotope fractionation.

In general, it is assumed that the digestion proceeds via the following steps (Guo et al., 2009):

$$CaCO_3 + 2H_3PO_4 \rightarrow Ca^{2+} + 2(H_2PO_4)^- + H_2CO_3 \quad (3.3)$$

$$H_2CO_3 \rightarrow H_2O + CO_2 \quad (3.4)$$

In aqueous solutions the most common mechanism of carbonic acid decay at room temperature is the formation of a transition state complex consisting of one water molecule and one H_2CO_3 molecule. Two additional water molecules function as polarizers that lower the activation energy, and another three water molecules are involved in the decay of H_2CO_3 (Liedl et al., 1997). The decay of the carbonic acid reaction intermediate H_2CO_3 requires higher activation energies if a smaller number of water molecules is involved (Liedl et al., 1997; Lorting and Bernard, 2010; Trautermann et al., 2002). If the phosphoric acid concentration increased, free water molecules become less available, reducing reaction rates and, thereby, affecting isotopic selectivity during bond cleavage of reaction intermediates (Wendeberg et al., 2011). Therefore it might be possible that the Δ_{47} value of evolved CO_2 is also affected by the availability of free water molecules. The amount of produced water increases with increasing sample size because the formation of one CO_2 molecule also generates one water molecule. In this respect, the sample size effect expressed in Fig. 3.1 might represent a change in reaction kinetics. If sample sizes are smaller than 7 mg, the availability of free water molecules might be limited and CO_2 formation may start from different competing transition states, each of which is associated with a characteristic phosphoric acid reaction fractionation factor between carbonate and CO_2. Once water becomes available, CO_2 formation might instead proceed via a unique transition state with a constant number of water molecules being involved in the transition state. Such scenarios might explain why the scatter of data for <7 mg samples is larger than that for >7 mg samples.

The oxygen isotope fractionation factors between carbonate and CO_2 related to phosphoric acid digestion ($1000\ln\alpha_{CO2\text{-}CaCO3}$) at 25 °C are 10.25‰ for calcite and 10.57‰ for aragonite, respectively (Kim et al., 2007), while $\Delta^* = \Delta_{47,\,CO2} - \Delta_{47,\,CaCO3}$ is 0.232‰ for calcite (Guo et al., 2009). This factor has been determined on the internal 'Caltech scale'. Applying the secondary reference frame transfer function of Dennis et al. (2011), this value becomes 0.268‰ for the factor (Henkes et al., 2013). In any case, the oxygen isotope fractionation factor for carbonate digestion at 25 °C is 1–2 orders of magnitude larger than the corresponding fractionation in Δ_{47}. It can, therefore, be expected that variations in Δ_{47} values

caused by a change in the kinetic fractionation factor Δ* will be accompanied by even more pronounced variations in $\delta^{18}O$ values. However, Fig. 3.3 displays no such correlations. In conclusion, it seems unlikely that the effect of sample size on Δ_{47} values at 25 °C is caused by a variability in reaction kinetics.

3.4.5 Secondary re-equilibration

Secondary re-equilibration of evolved CO_2 can be caused by heterogeneous oxygen isotope exchange with water, which occurs relatively fast even at room temperature. In the course of this exchange reaction, original ^{13}C-^{18}O bonds in the CO_2 gas will be broken and readjusted depending on temperature and extent of exchange. If only traces of H_2O are present (e.g. adsorbed on glass walls in which the CO_2 is enclosed) mass balance constraints predict that a change in the Δ_{47} value can be observed exclusively, whereas the change in the $\delta^{18}O$ value of the CO_2 might go unnoticed. This is due to the much higher abundance of $^{12}C^{16}O^{18}O$ relative to $^{13}C^{16}O^{18}O$ isotopologues. A fully re-equilibrated gas will have a Δ_{47} value that corresponds to the temperature of exchange. The Δ_{47} value of CO_2 gas in equilibrium at 25 °C is 0.9252‰ (Wang et al., 2004). In this respect, secondary heterogeneous oxygen exchange between reaction intermediates or evolved CO_2 and water at 25 °C can shift the Δ_{47} values of CO_2 derived from NBS 19 or *A. islandica* towards higher than original values. The extent of re-equilibration may depend on several factors, such as time, difference between original Δ_{47} value of sample CO_2 and Δ_{47} value of CO_2 at thed re-equilibration temperature, the surface to volume ratio and the CO_2/H_2O concentration ratio.

Generally, secondary oxygen isotope exchange can occur within the McCrea-type reaction vessel and/or during gas purification, gas storage or mass spectrometric analyses. Heated gases were measured on a daily basis, passing the same gas purification system as well as the same bellow/capillary/source of the mass spectrometer as the sample gases. If the elevated Δ_{47} values of sample CO_2 extracted at 25 °C are due to partial re-equilibration occurring during purification and/or transfer to the ion source, elevated Δ_{47} values should also have been measured for heated gases. However, we did not notice systematically increased Δ_{47} values for the heated gases, and R^2 for the heated gas lines were always better than 0.99.

It is worth noting that the evolved CO_2 is collected in the headspace of the reaction vessel for 16 to 20 h, until the reaction is complete Ghosh et al. (2006a). During gas collection in the headspace, CO_2 might exchange oxygen with trace amounts of H_2O which might be adsorbed on the glass walls of the reactor. In addition, several authors have suggested that traces of free

water are present even at acid concentrations >100% because of ongoing polymerization/ depolymerization of phosphoric acid molecules (Such, 1971; Wachter and Hayes, 1985). Besides, according to reaction (3.4), the generation of one CO_2 molecule results in the production of one H_2O molecule. This water may interact either with the exsolving CO_2, or with reaction intermediates such as H_2CO_3 according to (3.5) and (3.6):

$$H_2{}^{18}O + H_2{}^{16}O\text{-}{}^{13}C{}^{16}O_{2(aq)} = H_2{}^{16}O + H_2{}^{18}O\text{-}{}^{13}C{}^{16}O_{2(aq)} \quad (3.5)$$

$$H_2{}^{18}O + {}^{13}C{}^{16}O{}^{16}O_{(aq)} = H_2{}^{16}O + {}^{13}C{}^{18}O{}^{16}O_{(aq)} \quad (3.6)$$

An important key factor for the extent of re-equilibration might be the residence time of CO_2 in the acid and/or in the headspace. Compared with 25 °C, the reaction rates are faster and acid viscosity is lower at 90 °C. Moreover, using the common acid bath technique at 90 °C, CO_2 is continuously removed from the acid by condensing it at liquid nitrogen temperature. As a consequence, the residence time of CO_2 in the acid is significantly lower at 90 °C and the reaction as well as CO_2 removal from the acid is complete after 30 min. We tested twice whether the effect of sample size on Δ_{47} values observed for reactions at 25 °C can be avoided if the exsolved CO_2 is immediately removed from the headspace by freezing. For this purpose, the McCrea-type reaction vessel was connected to our cryoextraction line and the evolved CO_2 was immediately collected for a period of 12 h in a U-trap cooled with liquid nitrogen after passing through a water trap held at –80 °C. We ensured the reaction was complete after 12 h by continuously monitoring the amount of released CO_2. For a small sample of NBS 19 (4.4 mg), a relatively high Δ_{47} value of 0.378‰ was obtained (higher than any value measured for samples >7 mg), whereas for the large sample of *A. islandica* (8.8 mg) a low Δ_{47} value of 0.687‰ was determined. Hence, although the residence time of the analyte gas in the reaction vessel was minimized, the results confirmed the trend of elevated Δ_{47} values for smaller sample sizes. The observation that an immediate removal of exsolved CO_2 does not affect the measured Δ_{47} values might imply that secondary re-equilibration of CO_2 does not occur within the headspace of the McCrea-type reaction vessel but, rather, takes place before the exsolution of CO_2 from the acid.

The lower the abundance of free water in the phosporic acid the lower are the reaction rates between carbonates and acid, especially at low temperatures (Loerting et al., 2010). If, as in our case, 104% H_3PO_4 is used, comparatively small gas bubbles are formed during digestions at 25 °C. If larger samples are reacted more bubbles are produced at the same time, which can

then coalesce to larger bubbles. Due to their increased buoyancy, these larger CO_2 bubbles can exsolve faster from the highly viscous H_3PO_4 than the smaller ones, thereby reducing the residence time of CO_2 in the acid and, hence, the extent of secondary re-equilibration with water. As a consequence, measured Δ_{47} values reacted at 25 °C may depend on sample size.

Heterogeneous oxygen exchange between reaction intermediates and/or dissolved CO_2 and water might even occur at 90 °C. CO_2 that has fully equilibrated with water at a temperature of 90 °C should be characterized by a Δ_{47} value of 0.651‰ (Wang et al., 2004; Dennis et al., 2011). If partial re-equilibration were to occur at 90 °C, the Δ_{47} values measured for *A. islandica* should be systematically shifted to lower values than those obtained from 25 °C reactions. However, the contrary is observed: a mean value of (0.692 ± 0.003)‰ (n = 8) is obtained from reactions of >7 mg aliquots at 25 °C, whereas the average of >7 mg aliquots reacted at 90 °C occurs 0.020‰ higher at (0.712 ± 0.004)‰ (n = 4). In addition, no sample size effect is observed at a reaction temperature of 90 °C for neither NBS 19 nor *A. islandica* (Fig. 3.1, Table 3.1). Therefore, we have no evidence that partial secondary re-equilibration occurs during the reactions at 90 °C. Compared to 25 °C, those at 90 °C are much faster with the largest proportion of evolved CO_2 being released and frozen within 5 min. Due to the enhanced reaction rate and lower acid viscosity at 90 °C, CO_2 easily exsolves from the continuously stirred acid. In addition, reaction intermediates decompose much faster at 90 °C than at 25 °C. Thus heterogeneous oxygen isotope exchange between CO_2 or reaction intermediates and traces of free water might no longer occur to a significant extent, resulting in indistinguishable mean Δ_{47} values determined for small and large sample sizes.

3.4.6 Difference in the acid fractionation factors between 90 and 25 °C

In order to compare the Δ_{47} values from reactions at 90 °C with those obtained at 25 °C we applied the empirically derived difference in the fractionation factors Δ^*_{25-90} of 0.081‰ (Passey et al., 2010). Our data can be used to address the difference in the acid fractionation factors between carbonate digestions at 25 °C and 90 °C independently. Applying the Δ^*_{25-90} value of 0.081‰, our mean Δ_{47} values (4–14 mg) at a reaction temperature of 25 °C are still 0.015‰ (*A. islandica*, aragonite) and 0.014‰ (NBS 19, calcite) higher than the corresponding averages obtained from 90 °C reactions. This would imply that the Δ^*_{25-90} values are 0.096‰ and 0.095‰ for aragonite and calcite, respectively. Recently, an identical value of 0.092‰ was determined for aragonite by Henkes et al. (2013).

However, because <7 mg aliquots reacted at 25 °C were partly affected by secondary re-equilibration with water, it is more accurate to consider only the results obtained with samples >7 mg for the calculation of the corresponding mean values (Table 3.2). At 90 °C the complete dataset can be used as no size effect is observed. In this case, reactions at 25 °C give mean values that are 0.015‰ (aragonite) and 0.006‰ (calcite) lower than those obtained at 90 °C.

Table 3.2. *Differences in acid fractionation factors between 90 and 25 °C; Δ_{47} and $\Delta_{47}^{*}{}_{25-90}$ in ‰.*

	Mineralogy	Δ_{47} abs, 25 °C, 4-14 mg	Δ_{47} abs, 90 °C, 4-14 mg	$\Delta_{47}^{*}{}_{25-90}$	Δ_{47} abs, 25°C, >7mg	Δ_{47} abs, 25°C, 4-14 mg	$\Delta_{47}^{*}{}_{25-90}$
A .islandica	aragonite	0.720	0.707	0.094	0.692	0.707	0.067
NBS 19	calcite	0.373	0.359	0.095	0.353	0.359	0.076

Therefore we conclude that the Δ^{*}_{25-90} value is not 0.081‰, but 0.066‰ for aragonite and 0.075‰ for calcite (Table 3.2). These differences in fractionation factors are very close to the theoretically predicted value of 0.069‰ (Guo et al., 2009), supporting our contention that aliquots <7 mg reacted at 25 °C should not be considered for the determination of Δ^{*}_{25-90} values.

3.4.7 Implications for discrepant calibrations

Inorganic calcite precipitation experiments for calibration of the carbonate clumped isotope (paleo)thermometer were first carried out by Ghosh et al. (2006a), and later by Dennis and Schrag (2010). In a plot of Δ_{47} vs $1/T^2$ both calibrations reveal distinct slopes, even if the original Δ_{47} values are projected to the absolute reference frame (Dennis et al., 2011). It is worth noting that the slope reported by Dennis and Schrag (2010) agrees very well with those theoretically predicted (Guo et al., 2009) and empirically derived (by analyzing mollusks and brachiopods with known growth temperatures;Henkes et al., 2013), Henkes et al. (2013) critically evaluated methodological, physicochemical and biological aspects, but found no convincing explanation why the calibration of Ghosh et al. (2006a) exhibits a higher temperature sensitivity than is displayed by their empirical calibration.

Phosphoric acid digestions of carbonate samples for the calibration datasets of Dennis and Schrag (2010) and Henkes et al. (2013) were performed at 90 °C, whereas the reactions of Ghosh et al. (2006a) were carried out at 25 °C. A closer inspection of the calibration data of

Dennis and Schrag (2010) and Ghosh et al.(2006a) is provided in Dennis et al. (2011). From their Fig. 3.3 it becomes obvious that it is only the lowest temperature precipitate of the calibration of Ghosh et al. (2006a), whose Δ_{47} value is not conform with the dataset reported by Dennis and Schrag (2010). Compared with the latter, it deviates to more positive values. Ghosh et al. (2006a) stated that sample size used for replicate analyses were around 5 mg. According to our study, this is exactly the critical range where the positive bias in Δ_{47} values appears at a digestion temperature of 25 °C. Provided that the amount of precipiated calcite at low T was limited, replicates for clumped isotope analysis of the low T precipitate might have been split into smaller aliquots than those used for the analysis of the higher T precipitates. As a consequence, their low T calibration data point would be biased by a positive offset. Unfortunately, we are not able to prove whether data used for the Ghosh et al. (2006a) calibration study are affected by a sample size effect as they did not report the exact sample sizes they used for replicate analyses.

3.5 Conclusions

A detailed comparison was carried out of carbonate clumped isotope data obtained from two different acid digestion techniques. For reactions at 25 °C in McCrea-type vessels a systematic trend to lower Δ_{47} values with increasing sample size is observed for both, *A. islandica* (aragonite) and NBS 19 (calcite). In contrast, acid digestions performed at 90 °C using a common acid bath connected to an extraction line reveal no such trend of decreasing Δ_{47} values with increasing sample size. Although we cannot unambiguously identify the source of elevated Δ_{47} values, our results imply that phosphoric acid reactions performed at 25 °C can be accompanied by secondary processes, partly altering the clumped isotopic composition of the carbonate-derived CO_2. If unrecognized, such effects might lead to erroneous results (positive bias in Δ_{47} values) especially if relatively small sample sizes are used. Therefore, laboratories using small sample sizes should investigate the effect of sample size specific for their own analytical conditions. Partial re-equilibration of CO_2 extracted at a digestion temperature of 25 °C might help to explain the discrepancy in the slopes obtained for calibrations at reaction temperatures of 25 °C (Ghosh et al.,2006a) and 90 °C (Dennis and Schrag, 2010), respectively.

3.6 Acknowledgments

The present work was made possible through DFG grant FI-948-4/1. Sven Hofmann is thanked for technical support and Tanja Rutz for analytical support.

3.7 Supplementary Information

Table S3.1 *Heated gas and water equilibrated gas data used for correction of raw Δ_{47} values.*

Heated gases			Water equilibrated gases: 25 °C		
Date	δ_{47}	Δ_{47}	**Date**	δ_{47}	Δ_{47}
04.04.11	-2.270	-0.895	**05.11.10**	6.028	0.028
05.04.11	-51.881	-2.286	**12.11.10**	10.088	0.105
05.04.11	3.758	-0.723	**12.11.10**	4.731	0.030
06.04.11	-51.911	-2.321	**15.11.10**	12.057	0.124
06.04.11	-26.849	-1.580	**15.11.10**	14.319	0.140
07.04.11	3.734	-0.724	**16.11.10**	16.419	0.208
08.04.11	-26.837	-1.573	**16.11.10**	17.031	0.202
11.04.11	16.953	-0.413	**18.11.10**	24.839	0.334
12.04.11	-21.686	-1.419	**23.11.10**	-3.058	-0.052
13.04.11	-51.860	-2.290	**24.11.10**	7.237	0.121
14.04.11	16.890	-0.424	**24.11.10**	-9.373	-0.197
15.04.11	-21866	-1.467	**25.11.10**	-3.930	-0.055
18.04.11	-51.989	-2.311	**26.11.10**	-8.337	-0.170
19.04.11	-2.376	-0.921	**29.11.10**	-19.154	-0.299
20.04.11	-39.326	-1.952	**29.11.10**	-10.953	-0.184
21.04.11	-2.453	-0.897	**30.11.10**	-0.090	-0.005
26.04.11	-39.436	-1.975	**01.12.10**	12.371	0.160
27.04.11	5.060	-0.671	**02.12.10**	-13.844	-0.255
28.04.11	-51.991	-2.400	**03.12.10**	-17.599	-0.301
29.04.11	4.844	-0.716	**08.12.10**	22.501	0.291
03.05.11	17.494	-0.391	**10.12.10**	-8.782	-0.192
04.05.11	-51.955	-2.371	**14.12.10**	16.056	0.288
05.05.11	10.619	-0.531	**16.12.10**	6.700	0.146
06.05.11	17.489	-0.386	**01.02.11**	7.874	0.154
09.05.11	-52.241	-2.373	**03.02.11**	16.255	0.385
09.05.11	-19.743	-1.401	**23.02.11**	-8.837	-0.242
10.05.11	-27.136	-1.601	**24.02.11**	-8.812	-0.247
11.05.11	-2.260	-0.902	**18.03.11**	14.619	0.316
12.05.11	-39.212	-2.004	**04.04.11**	7.397	0.144
12.05.11	-39.229	-1.959	**22.07.11**	16.552	0.317
13.05.11	-52.469	-2.379	**23.07.11**	7.689	0.090
13.05.11	-52.105	-2.356	**25.07.11**	-30.327	-0.632
16.05.11	-2.269	-0.887	**26.07.11**	6.997	0.073
17.05.11	-2.157	-0.889			
18.05.11	-29.502	-1.720			
18.05.11	-29.512	-1.676			
20.05.11	16.518	-0.346			
23.05.11	-2.231	-0.887			
24.05.11	16.787	-0.381			
26.05.12	16.947	-0.336			
30.05.11	-52.163	-2.373			
31.05.11	-27.106	-1.606			
01.06.11	17.547	-0.226			
03.06.11	-52.214	-2.382			
06.06.11	-26.761	-1.602			
06.06.11	17.606	-0.250			
07.06.11	-3.216	-0.955			
08.06.11	-29.226	-1.663			
09.06.11	-52.061	-2.348			
10.06.11	-51.892	-2.386			

Table S3.1 *Continued.*

	Heated gases			Water equilibrated gases: 25 °C	
Date	δ_{47}	Δ_{47}	**Date**	δ_{47}	Δ_{47}
14.06.11	-3.089	-0.917			
14.06.11	-29.251	-1.651			
16.06.11	-20.687	-1.457			
17.06.11	-46.254	-2.196			
21.06.11	-20.626	-1.464			
22.06.11	15.802	-0.422			
24.06.11	-3.341	-0.928			
27.06.11	15.944	-0.407			
28.06.11	-52.346	-2.456			
29.06.11	-3.313	-0.945			
30.06.11	-29.762	-1.757			
01.07.11	-52.084	-2.421			
04.07.11	-29.766	-1.771			
05.07.11	-3.482	-0.969			
06.07.11	-3.419	-0.967			
07.07.11	-20.457	-1.467			
08.07.11	-39.676	-2.037			
08.07.11	18.221	-0.346			
12.07.11	18.710	-0.252			
12.07.11	18.668	-0.270			
12.07.11	18.687	-0.246			
13.07.11	-52.258	-2.463			
After source cleaning, new tuning					
01.09.11	-17.953	-1.338	**02.09.11**	9.378	0.204
01.09.11	-38.959	-1.936	**02.09.11**	12.769	0.259
01.09.11	-51.863	-2.262	**05.09.11**	-30.289	-0.853
02.09.11	16.858	-0.474	**08.09.11**	-21.235	-0.608
02.09.11	-42.964	-2.026	**12.09.11**	-30.350	-0.854
07.09.11	-2.574	-0.967	**12.09.11**	-30.510	-0.832
12.09.11	15.439	-0.533	**14.09.11**	7.402	0.130
14.09.11	-41.948	-1.948	**14.09.11**	7.503	0.129
15.09.11	-51.961	-2.234	**20.09.11**	16.881	0.376
16.09.11	-20.041	-1.394	**30.09.11**	7.358	0.127
19.09.11	-33.080	-1.710	**22.11.11**	20.381	0.447
21.09.11	-52.092	-2.197	**24.11.11**	11.374	0.237
22.09.11	-2.691	-0.951			
23.09.11	-21.998	-1.402			
26.09.11	-3.230	-0.944			
27.09.11	-51.754	-2.225			
27.09.11	14.225	-0.543			
28.09.11	-51.792	-2.196			
28.09.11	-51.856	-2.202			
29.09.11	-3.909	-0.950			
04.10.11	-21.586	-1.399			
05.10.11	16.547	-0.445			
06.10.11	-52.160	-2.196			
24.10.11	-32.716	-1.663			
26.10.11	-2.196	-0.894			
28.10.11	-51.499	-2.157			
01.11.11	-2.663	-0.909			
04.11.11	16.214	-0.437			
08.11.11	-51.664	-2.115			

Table S3.1 *Continued.*

	Heated gases	
Date	δ_{47}	Δ_{47}
11.11.11	-29.864	-1.561
14.11.11	-29.364	-1.550
15.11.11	-2.460	-0.887
16.11.11	-51.773	-2.119
21.11.11	-51.955	-2.119
22.11.11	13.069	-0.537
24.11.11	-51.083	-2.016
24.11.11	-51.052	-1.995
28.11.11	-51.757	-2.026
28.11.11	-51.735	-2.028
30.11.11	-2.567	-0.893
22.12.11	18.385	-0.437
22.12.11	18.462	-0.407
04.01.12	15.720	-0.465
04.01.12	15.763	-0.476
06.01.12	-33.066	-1.586
11.01.12	15.874	-0.474
11.01.12	15.919	-0.464
12.01.12	-33.027	-1.634
13.01.12	-4.212	-0.940
16.01.12	-4.567	-0.961
18.01.12	15.014	-0.550
25.01.12	-32.883	-1.575
27.01.12	-3.431	-0.904
30.01.12	11.419	-0.580
01.02.12	-33.032	-1.591
03.02.12	-4.193	-0.929
05.02.12	-33.002	-1.643
06.02.12	-2.846	-0.880
08.02.12	14.879	-0.476
08.02.12	14.686	-0.457
14.02.12	-32.967	-1.554
16.02.12	-4.290	-0.962
17.02.12	15.854	-0.517
20.02.12	-32.956	-1.585
20.02.12	-32.973	-1.585

4 Empirical calibration of the clumped isotope paleothermometer using calcites of various origins

Ulrike Wacker[1], Jens Fiebig[1,2], Julian Tödter[3], Bernd R. Schöne[4], André Bahr[1], Oliver Friedrich[1,2,5], Thomas Tütken[6], Eberhard Gischler[1,2] and Michael M. Joachimski[7]

[1] Institute of Geosciences, Goethe-University, Altenhöferallee 1, 60438 Frankfurt am Main, Germany

[2] Biodiversity and Climate Research Center, Senckenberganlage 25, 60325 Frankfurt am Main, Germany

[3] Institute for Atmospheric and Environmental Sciences, Altenhöferallee 1, 60438 Frankfurt am Main, Germany

[4] Department of Applied and Analytical Paleontology (INCREMENTS), Institute of Geosciences, University of Mainz, Johann-Joachim-Becherweg 21, 55128 Mainz, Germany

[5] present address: Institute of Earth Sciences, Im Neuenheimer Feld 234-236, 69120 Heidelberg, Germany

[6] Steinmann-Institut für Geologie, Mineralogie und Paläontologie, Poppelsdorfer Schloss, University of Bonn, 53115 Bonn, Germany

[7] GeoZentrum Nordbayern, University of Erlangen-Nürnberg, Schloßgarten 5, 91054 Erlangen, Germany

Published in Geochemica et Cosmochemica Acta ***2014****, 141, 127–144*

DOI: 10.1016/j.gca.2014.06.004

Abstract We present the first universal calibration of the clumped isotope thermometer for calcites of various mineralizing types. These are an eggshell of an ostrich, a tropical bivalve, a brachiopod shell, cold seep carbonate, and three foraminifera samples that grew between 9 and 38 °C. $CaCO_3$ was digested at 90 °C using a common acid bath. Considering a difference in phosphoric acid fractionation factors between reaction at 25 and 90 °C of 0.069‰ (Guo et al., 2009), the function between growth temperature T and the excess of ^{13}C-^{18}O bonds in the evolved CO_2 is expressed by a linear regression between $1/T^2$ and absolute Δ_{47} ($R^2 = 0.9915$):

$\Delta_{47} = 0.0327 (\pm 0.0026) \times 10^6 / T^2 + 0.3030 (\pm 0.0308)$ (with Δ_{47} in ‰ and T in K).

Both the slope and intercept of our regression line deviate significantly from the first experimental calibration based on synthetic calcites digested at 25 °C (Ghosh et al., 2006a) and from several other studies having confirmed this pioneering calibration (i.e., Came et al., 2007; Tripati et al., 2010; Thiagarajan et al., 2011; Grauel et al., 2012; Saenger et al., 2012; Zaarur et al., 2013). However, our relationship between temperature and absolute Δ_{47} values is

indistinguishable from that determined by Henkes et al. (2013) if the same difference in phosphoric acid fractionation factors between 25 and 90 °C is applied to both datasets. Our study and that of Henkes et al. (2013) have in common that data were primarily projected onto the absolute scale proposed by Dennis et al. (2011) – a reference frame that allows comparison of clumped isotope data measured in different laboratories. Furthermore, at any T, our regression line lies within 0.006‰ of the theoretical calcite calibration of Guo et al. (2009). The observation that both empirical calibrations are indistinguishable from each other implies that clumped isotope data can be directly compared between laboratories and referenced to a unique temperature calibration if (1) the phosphoric acid digestion temperature is set to 90 °C, and (2) raw data are primarily projected to the absolute scale.

4.1 Introduction

Temperature reconstructions of ancient oceans, lakes and soils are of prime importance for paleoclimatic and paleoceanographic studies. The chemistry of minerals provides important insights into past conditions on Earth because isotope ratios and elemental distributions within crystals can be used for paleothermometry. This was first recognized by Urey (1947) who found that the bulk oxygen isotopic composition ($\delta^{18}O$) of carbonate depends on the water temperature prevailing during its precipitation. Since then, $\delta^{18}O$ measurements of carbonates (mostly biogenic minerals) have become an essential tool for paleoclimate reconstructions (e.g., Epstein et al., 1951, 1953; Shackleton, 1974; Elderfield and Ganssen, 2000). However, the suitability of the oxygen isotope thermometer is limited because $\delta^{18}O$ values of carbonates not only depend on temperature, but also on the oxygen isotopic composition of the water from which the carbonate precipitated (e.g., Epstein et al., 1951; Shackleton et al., 1974; Kim and O'Neil, 1997). Since these waters are in most cases no longer available, only relative temperature changes can be determined by assigning the parental water a constant isotopic composition. Absolute temperature reconstructions in the marine realm require either independent paleothermometers or models of how $\delta^{18}O$ of seawater has evolved over time (Muehlenbachs and Clayton, 1976; Gregory and Taylor, 1981; Gregory, 1991; Muehlenbachs, 1998; Kasting et al., 2006). Such models have yielded different results. It was proposed that the relative proportion of high and low-temperature alteration of the oceanic crust was invariant through time, buffering the oxygen isotopic composition of the ocean to a constant value of (0 ± 1)‰ vs. V-SMOW since the beginning of the Archean (Muehlenbachs and Clayton, 1976; Gregory and Taylor, 1981; Gregory, 1991; Muehlenbachs, 1998). In contrast, others suggested that seawater became continuously enriched in ^{18}O throughout the same interval due to a

progressive increase in hydrothermal penetration depth and pelagic sedimentation rate at midocean ridges (Kasting et al., 2006). Notably, this latter model is consistent with the hypothesis that the seawater $\delta^{18}O$ value might have increased by about +6‰ since the Paleozoic (Veizer et al., 1997, 1999). Apart from seawater–rock interactions, ice-volume effects and regional variations (e.g., evaporation and freshwater input) also influence the isotopic composition of seawater, further limiting the accuracy of the oxygen isotope paleothermometer. Since the discovery by Urey (1947), additional proxies for paleothermometry have been established such as Mg/Ca ratios (Nürnberg et al., 1996; Elderfield and Ganssen, 2000; Anand et al., 2003) and Sr/Ca ratios (Beck et al., 1992; Marshall and McCulloch, 2002; Pfeiffer et al., 2006) of marine carbonates as well as TEX_{86} measured on bulk sedimentary organic matter (Schouten et al., 2002; Wuchter et al., 2006; Kim et al., 2008). In combination with oxygen isotopes, these proxies enable both temperature and $\delta^{18}O$ estimations of ancient water masses. The most recent tool for paleotemperature estimates is the "carbonate clumped isotope thermometer". It is based on the temperature dependence of the equilibrium constant of reaction (4.1) that describes the formation of the most abundant rare carbonate isotopologue containing bonds between two heavy isotopes:

$$Ca^{13}C^{16}O_3 + Ca^{12}C^{18}O^{16}O_2 = Ca^{13}C^{18}O^{16}O_2 + Ca^{12}C^{16}O_3 \quad (4.1)$$

In natural carbonates, clumping between ^{13}C and ^{18}O occurs only in trace amounts (67 ppm, Schauble et al., 2006; Ghosh et al., 2006a), requiring highly sensitive and precise measurements. So far, no technique allows the direct determination of the abundance of doubly heavily substituted isotopologues in minerals. Therefore, CO_2 gas derived from phosphoric acid digestions of carbonate is analyzed, which still preserves information about the original ordering of ^{13}C and ^{18}O isotopes in the crystals (Ghosh et al., 2006a). Measured R^{47}, R^{46}, R^{45} on the evolved CO_2 are compared with their corresponding statistic distribution ratios R^{47*}, R^{46*}, R^{45*} (R^i = mass i/mass 44). The equilibrium constant of Eq. (4.2) is then expressed as

$$\Delta_{47} = ((R^{47}/ R^{47*} - 1) - (R^{46}/ R^{46*} - 1) - (R^{45*}/ R^{45*} - 1)) * 1000 \text{ (‰)} \quad (4.2)$$

The carbonate clumped isotope thermometer provides important information for several fields in the Earth sciences, such as reconstructing paleoclimate (e.g., Came et al., 2007; Passey et al., 2010; Csank et al., 2011; Finnegan et al., 2011; Peters et al., 2013) and paleoaltimetry (e.g., Ghosh et al., 2006b; Garzione et al., 2008; Huntington et al., 2010; Quade et al., 2011), as well

as deciphering thermal histories of rock components and lithologies during diagenetic processes (e.g., Dennis and Schrag, 2010; Huntington et al., 2011). Of course, these applications require knowledge of the temperature dependence of the equilibrium constant, K, of reaction (4.1) and the distribution of isotopologues in the CO_2 gas that is liberated from acid digestion of carbonates. This relationship has been addressed in several experimental and empirical calibration studies: inorganic calcites precipitated at controlled temperature were used for the calibrations published by Ghosh et al. (2006a), Dennis and Schrag (2010) and Zaarur et al. (2013), while the relationships between $1/T^2$ and Δ_{47} determined by Came et al. (2007), Tripati et al. (2010), Thiagarajan et al. (2011), Grauel et al. (2013) , Saenger et al. (2012), Henkes et al. (2013), as well as Eagle et al. (2013) were based on biogenic carbonates, for which growth temperatures were independently constrained. Furthermore, Affek et al. (2008) and Daëron et al. (2011) investigated the temperature dependence of clumping between ^{13}C and ^{18}O in speleothems. In addition, the theoretical temperature dependence of Δ_{47} has been computed (Schauble et al., 2006; Guo et al., 2009). Unfortunately, discrepancies between the different calibrations were reported that still persist even after projection of data to the absolute scale using the secondary reference frame (Dennis et al., 2011). At least to some extent the observed differences between the calibration lines might be related to kinetic effects that can occur in the solutions from which the carbonates precipitated. For example, this was suggested for speleothems (Affek et al., 2008; Daëron et al., 2011), but was also suspected to be of importance for marine organisms like corals and mollusks (Saenger et al., 2012; Eagle et al., 2013). Notably, calibrations performed at a digestion temperature of 90 °C (Dennis and Schrag, 2010; Henkes et al., 2013; Eagle et al., 2013) exhibit temperature sensitivities that are lower by about a factor of two when compared to calibrations based upon 25 °C reactions (Ghosh et al., 2006a; Tripati et al., 2010). Another possible explanation might, therefore, arise from changes in the analytical protocols of carbonate clumped isotope measurements over the last few years. The most important changes might be the increase of the acid digestion temperature from 25 to 90 °C and the use of a common acid bath instead of sealed reaction vessels. Wacker et al. (2013) observed that CO_2 deriving from acid digestion at 25 °C can exhibit a bias to more positive Δ_{47} values when small amounts of sample (<7 mg) are reacted, possibly pointing to secondary reequilibration of the evolved CO_2 with trace amounts of water. In contrast, no such effect was observed for reactions at 90 °C. This analytical artifact may explain the steeper slope of the Ghosh et al. (2006a) calibration provided that small aliquots were preferentially used during acid digestion of their low-temperature precipitates (Wacker et al., 2013).

In this study we present new empirical calibration data that are based on various natural calcites (several biogenic carbonates and a cold seep carbonate). These carbonates were digested at 90 °C using a common acid bath. Our results agree with the $1/T^2$ vs. Δ_{47} relationship for biogenic carbonates reported by Henkes et al. (2013) who also used a digestion temperature of 90 °C.

4.2 Materials and methods

4.2.1 Sample material

Our study is based on seven calcites of various origins (Table 4.1): we sampled an eggshell of an ostrich, a shell of a bivalve (*Spondylus* sp.), a brachiopod shell (*Dyscolia wyvillei*), and foraminifera (*Globigerinoides ruber*, *Globorotalia inflata*, *Globorotalia hirsuta*). Furthermore, a cold seep carbonate was included that formed by biologically induced precipitation (Bahr et al., 2009). Growth temperatures of the samples range from 9 to 38 °C. For all carbonates, 6 to 30 replicate measurements were made, except for the foraminifera for which each sample was analyzed only twice due to the limited amount of available material. Eagle et al. (2010) and Tripati et al. (2010) pretreated biogenic carbonates (bioapatites and foraminifera, respectively) with 1 to 3 wt.% H_2O_2 to remove traces of organic material prior to acid digestion to avoid volatilization of organic compounds potentially causing isobaric interferences with CO_2 isotopologues. However, in most studies biogenic carbonates (e.g., corals, mollusks, brachiopods) were not pretreated prior to clumped isotope analyses (e.g., Thiagarajan et al., 2011; Saenger et al., 2012; Henkes et al., 2013). Our own systematic investigations on untreated and pretreated aliquots revealed that H_2O_2 treatment was not necessary for the samples analyzed in this study. Only the foraminifera were pretreated with H_2O_2 following the protocol described by Tripati et al. (2010), because the limited sample material did not allow testing whether organic matter of untreated tests would have an influence on Δ_{47} values.

Table 4.1 *Samples, sample localities and independently constrained temperatures of growth (T_{growth} and T_{error} in °C).*

Sample	Taxa/characterization	Sample locality	Coordinates	T_{growth}	T_{error}
Eggshell	Ostrich	Germakenhof/Remagen	-	38	0.6
Bivalve mollusk	*Spondylus* sp.	Indian Ocean/ Kuramathi Island/ Rasdhoo Atoll/Maldives	4°N, 73°E	29	1
Brachiopod	*Dyscolia wyvillei*	Atlantic Ocean/ Conception Seamound	29°49.4'N, 12°19.9'W	10	1
Authigenic calcite	Cold seep carbonate	Black Sea/ Dolgovskoy Mound	44°01.130'N, 36°41.400'E	9	0.1
Foraminifera	*Globigerinoides ruber*	Arabian Sea	23°12'N, 66°49'W	26	1
Foraminifera	*Globorotalia inflata*	North Atlantic	47°11'N, 19°34'W	14	1
Foraminifera	*Globorotalia hirsuta*	North Atlantic	47°11'N, 19°34'W	9	1

4.2.1.1 Eggshell of an ostrich

The sampled eggshell was obtained from a breeding ostrich that lived in a farm in Germany (Gemarkenhof, Remagen). Schrader et al. (2009) determined that peritoneal temperatures of ostriches that live in temperate zones (Germany) vary between 37.2 and 38.1 °C. Therefore we decided to consider an average temperature of formation of 38 ± 0.6 °C. Sample material was obtained with a low-speed dental drill to prevent thermal and physical strain.

The bulk carbon and oxygen isotopic compositions of eggshells of ostriches are controlled by diet and environmental conditions of the animals (Johnson et al., 1998). According to their study, $\delta^{13}C$ values of the eggshells can be used to reconstruct the relative occurrence of C_3 and C_4 plants in the habitat of the animals. If the diet of the ostrich is composed of C_3 plants instead of C_4 plants, lower $\delta^{13}C$ values are measured for both the inorganic and organic fraction of the eggshells. $\delta^{18}O$ values of ostrich eggshells depend on body temperature (that is constant for endotherms such as ostriches) and the isotopic composition of their body water. For ostriches that are raised in controlled settings, a linear correlation between $\delta^{18}O$ values of the eggshells and $\delta^{18}O$ values of the drinking water of the animals has been observed (Johnson et al., 1998).

4.2.1.2 *Spondylus* sp.

The sampled calcitic bivalve was collected dead in 2004 at the beach of Kuramathi Island/Rasdhoo Atoll (4°N, 73°E) located in the western area of the Maldives Archipelago (NW Indian Ocean). Maximum water depths of 40 m were measured in the lagoon (Gischler, 2006). The climatic condition of this area is controlled by monsoonal influences (e.g., Storz et

al., 2013). Maximum and minimum temperature values of sea surface waters range between 29.5 and 27.8 °C (Storz et al., 2013). We refer to an annual mean temperature of 29 ± 1 °C (Storz et al., 2013). Shell material was drilled from the inner side of the valve (which is ~8 cm long, ~7 cm wide, and ~2 mm thick) using a dental drill at low speed to avoid thermal and physical strain.

Shells of bivalve mollusks consist of calcium carbonate, largely aragonite and/or calcite, and numerous different organic materials (Simkiss and Wilbur, 1989). The shell material is accreted along growing margins and typically arranged in two distinct layers that have different crystal fabrics and are separated by the myostracum. Formation of the outer and inner layers occur isolated from the ambient environment in fluid-filled compartments (Wilbur and Saleuddin, 1983), the so-called outer and inner extrapallial spaces (EPS), respectively, which are supersaturated with respect to Ca^{2+}, HCO_3^-, a number of trace elements, acidic proteins, glycoproteins, carbonic anhydrase etc. (Marin et al., 2012). Shell formation is mediated and orchestrated by the outer mantle epithelium that produces an organic scaffolding (envelope) in which a mixture of $CaCO_3$ and organics are precipitated (Wilbur and Jodrey, 1955; Lowenstam, 1981). Bivalves precipitate their shells in, or close to, isotopic equilibrium with respect to oxygen (Epstein et al., 1953; Wefer and Berger, 1991). It is mainly due to the fact that there is enough time for the DIC to equilibrate with the water before being incorporated into the carbonate (McConnaughey,1989a, b). This time is reduced by the presence of carbonic anhydrase (Uchikawa and Zeebe, GCA, 2012). The latter catalyzes the hydration reaction of respiratory CO_2 and thus minimizes potential kinetic effects. However, the stable carbon isotope values of the shell, can contain up to 10% of respiratory CO_2 (McConnaughey and Gillikin, 2008), which is typically depleted in ^{13}C as indicated by according low $\delta^{13}C$ values.

4.2.1.3 Dyscolia wyvillei

Dyscolia wyvillei is a terebratulid brachiopod dredged on RV POSEIDON cruise POS-235 (Station POS-235-DS-822, subsample 33) at the Conception Seamount in the Atlantic Ocean (29°49.4′N, 12°19.9′W). The sample was collected from a water depth of 652 mto 986 m. Based on the World Ocean Atlas 2005 (Locarnini et al., 2006), the mean annual seawater temperature at a depth of 788 m is 10 ± 1 °C. According to the Global Seawater Oxygen-18 Database a $\delta^{18}O_{water}$ value of 0.5 ± 0.5‰ (V-SMOW) can be assumed for the locality where the brachiopod lived (Schmidt et al., 1999). The ultrastructural texture of the shell was studied using an electron microprobe. This application ensured us that the sample was not affected by diagenetic and/or maturation processes. The sampled valve measures about 5 cm in length and

width. Shell thickness is about 1 to 2 mm. The valves of terebratulid brachiopods are composed of low-Mg calcite (LMC). The multi-layered skeleton is of very high structural organization (Schmahl et al., 2008) and is secreted by the outer epithelium of the mantle (Barbin and Gaspard, 1995; Schmahl et al., 2008). *Dyscolia wyvillei* possesses a punctate shell which consists of two layers: the thin primary layer (~150 μm) and the thicker secondary layer. In this study we have sampled secondary layer material. Therefore, the upper primary layer was physically removed, and the central area (1 cm × 1 cm) of the ventral valve was drilled with low speed. Secondary layer calcite consists of fibres that grow intracellularly (Williams, 1997), resulting in a composite of inorganic and organic particles (Pérez-Huerta et al., 2008). Different results were reported concerning the attainment of isotopic equilibrium within this layer: several studies indicate equilibrium precipitation for the bulk carbon and oxygen isotopes (Carpenter and Lohmann, 1995; Parkinson et al., 2005; von Allmen et al., 2010). In contrast, Auclair et al. (2003) measured near-equilibrium $\delta^{18}O$ values only on the inner side of the valve of a modern species (*Terebratalia transversa*), whereas the outer side showed large offsets to lower values by more than −4‰ and more than −6‰ for $\delta^{18}O$ and $\delta^{13}C$, respectively. These offsets have been explained by kinetic isotope effects occurring during shell precipitation (Auclair et al., 2003).

4.2.1.4 Cold seep carbonate

The cold seep carbonate was sampled at the Dolgovskoy Mound in the northeastern Black Sea (Station BS346GR; 44°01.130′N; 36°41.400′E; 2,004 m water depth, Mazzini et al., 2008; Bahr et al., 2009) during TTR Cruise 15 in 2005 onboard R/V Professor Logachev (Akhmetzanov et al., 2007). The carbonate minerals represent biologically induced precipitates which originated at active methane seep sites as a by-product of the anaerobic oxidation of CH_4 (Boetius et al., 2000; Valentine, 2002). Microbial activity due to the interaction of fluid seepage and the anaerobic oxidation of methane (Barnes and Goldberg, 1976; Reeburgh, 1976; Boetius and Wenzhöfer, 2013) leads to an increase in alkalinity and supersaturation with respect to $CaCO_3$, which subsequently results in precipitation of carbonates (e.g., Ritger et al., 1987; Bohrmann et al., 1998; Peckmann et al., 1999; Thiel et al., 2001). While the involved microbes [sulfate oxidizing bacteria and methanotrophic archaea (Hoehler et al., 1994; Thiel et al., 1999; Boetius et al., 2000; Wakeham et al., 2003)] do not actively precipitate a calcareous skeleton, it is believed that secreted polymeric cellular material provides a template for enhancing carbonate nucleation and growth (Reitner et al., 2005; Aloisi et al., 2006; Bontognali et al., 2008; Dupraz et al., 2009). The sample is characterized by two different

carbonate phases: (1) micritic high magnesium calcite cementing hemipelagic sediments, and (2) pure, yellowish, botryoidal carbonate rims that have been precipitated in direct contact to cm-thick microbial mats (Mazzini et al., 2008; Bahr et al., 2009). The relation to methane seepage is furthermore supported by the highly depleted $\delta^{13}C$ signature of the carbonates with values <−30‰ (V-PDB, Bahr et al., 2009). Since the carbonate was covered by living microbial mats, it can be assumed that carbonate precipitation occurred quite recently under the stable temperature conditions of the deep Black Sea (9.0 ± 0.1 °C, Locarnini et al., 2010). No indication for the presence of warm, deep-rooted fluids have been found that might affect the temperature conditions during carbonate precipitation (Akhmetzanov et al., 2007; Bahr et al., 2009). For clumped isotope analyses we sampled the yellowish carbonate using a hand drill (low speed). These authigenic minerals consist of pure low-Mg calcite (LMC) and contain less than 7 mol% $MgCO_3$ (Bahr et al., 2009).

4.2.1.5 Foraminifera

Δ_{47} values of the three planktic foraminiferal taxa *Globorotalia hirsuta*, *Globorotalia inflata*, and *Globigerinoides ruber* (white) have been analyzed for this study. Specimens of *G. hirsuta* and *G. inflata* were sampled from the upper 1 cm of sediment core MC575/13 from the North Atlantic (47°11′N, 19°34′W; 4577 m water depth; Kurbjeweit et al., 2000). The sample of *G. ruber* has been collected in the Arabian Sea during RV Sonne cruise 130 in April 1998 (23°12′N, 66°49′W; 569 m water depth; von Rad, 1998) from the upper 5 mm of sediment core MUC288. Foraminiferal samples were dry sieved and picked from the >200 μm size fraction. Smaller size fractions were avoided to minimize ontogenetic effects on stable isotope analyses (Friedrich et al., 2012). After crushing the individual tests, cleaning followed the protocol of Tripati et al. (2010) to remove contaminants. Due to a potentially high organic matter content of our core-top samples, the oxidative step using a cold dilute solution of 1 wt.% hydrogen peroxide was performed for 60 min. The samples were then dried in an oven at 40 °C.

Since planktic foraminifera typically show a species-specific vertical distribution in the water column (e.g., Hemleben et al., 1989; Schiebel and Hemleben, 2005), estimates of their specific depth habitat are essential for their use as paleoceanographic proxies. Of the three different taxa analyzed in this study, *G. ruber* occupies the shallowest depth habitat. This species reaches highest abundances in the upper mixed layer and typically calcifies within the upper 50 m of the water column (e.g., Fairbanks et al., 1982; Schmuker and Schiebel, 2002).

Compared to the mixed-layer species, *G. ruber*, globorotalids are generally assumed to be deep-dwelling (e.g., Hemleben et al., 1989). *Globigerinoides hirsuta* reaches their highest

standing stocks below the photic zone (Hemleben et al., 1989), calcifying typically at water depths of 500 to 800 m (e.g., Anand et al., 2003). For *G. inflata*, studies imply that this species calcifies in water depths between 100 and 400 m throughout the year (e.g., Schiebel and Hemleben, 2005; Chiessi et al., 2008). In the South Atlantic, core-top data suggest that *G. inflata* calcifies constantly within the permanent thermocline at 350–400 m water depth (Groeneveld and Chiessi, 2011).

For *G. ruber* (surface mixed layer) calcification temperatures of ~26 °C (±1 °C) have been estimated from the World Ocean Atlas 2005 (Locarnini et al., 2006). In-situ temperatures from the North Atlantic measured in the water column by conductivity, temperature and depth loggers (CTD) at the time of sampling were 8–10 °C for *G. hirsuta* (at 500–800 m) and 13–15 °C for *G. inflata* (at 200–400 m), respectively (Pfannkuche et al., 2000). These temperature ranges agree with values of the World Ocean Atlas 2005 (Locarnini et al., 2006). Therefore, we assume ~9 ± 1 °C and ~14 ± 1 °C for the calcification temperatures of these two calibration samples, respectively.

In general, tests of planktic foraminifera are multilamellar, composed of multiple layers of calcite that are deposited with each new chamber that is formed (e.g., Towe and Cifelli, 1967; Hemleben, 1969; Hemleben et al., 1989). During chamber formation, initially a cytoplasmatic bulge forms that resembles the outline of the new chamber. Along this outline, calcitic layers are formed around a primary organic membrane that built the individual layers of a foraminiferal test, a process that is finalized within hours (e.g., Hemleben et al., 1989; Bentov and Erez, 2005). Since early studies on the isotopic composition of foraminiferal tests it has been assumed that carbonate growth out of thermodynamic isotopic equilibrium is a common phenomenon and is generally more expressed in carbon than in oxygen isotopes (e.g., Erez, 1978; Wefer and Berger, 1991). Multi-species studies on the isotopic composition of benthic and planktic foraminifera support this view and have revealed deviations from equilibrium that are commonly referred to as vital effects (e.g., Erez, 1978; Grossman, 1984; Rohling and Cooke, 1999). Only a few species appear to precipitate their tests in equilibrium with seawater. In addition, ontogenetic changes in metabolism were used to explain the increase in $\delta^{18}O$ and $\delta^{13}C$ values with test size that is commonly found in planktic foraminifera (e.g., Berger et al., 1978; Spero and Lea, 1996; Friedrich et al., 2012). In addition, an influence of pH on the bulk isotopic composition of planctic foraminifera has also been described (Spero et al., 1997; Zeebe, 1999, 2007). Δ_{47} data presented by Tripati et al. (2010) suggest that kinetics do not impose any significant effects on the extent of ^{13}C-^{18}O bond ordering in foraminifera.

4.2.2 Acid digestion, gas purification, mass spectrometric analysis and data reduction

Carbonate reactions were carried out at 90 (±0.1) °C using a common acid bath that has been designed after the device built at California Institute of Technology (Passey et al., 2010). In contrast to the California Institute of Technology setup, however, we pump the acid bath using a turbomolecular pump supported by a membrane pump. Initially, the common acid bath is loaded with 105–106 wt.% H_3PO_4 (acid preparation modified by Coplen et al., 1983) and then pumped for one night. Therefore, we assume that the effective phosphoric acid concentration during carbonate digestion is >106 wt.%.

Acid digestions were performed following the description of Wacker et al. (2013): Ag capsules filled with 4–8 mg of carbonate powder are dropped in the acid, and the evolved CO_2 is frozen in liquid nitrogen for 20–30 min after subjecting it to a cryogenic cleaning step (water trap/ −80 °C). Gas yields are monitored manometrically after thawing the evolved CO_2 by heating the trap to −80 °C. Next, extracted sample gas is frozen in a transportable glass finger equipped with high vacuum valves (Louwers, Art. code 40.200.8). CO_2 is then passed through a GC to remove traces of hydrocarbons (stainless steel column: 1.20 m × 2.15 mm ID; packed with Porapak Q 80/120; −20 °C/He carrier gas: 18 ml/min; purity: 99.9999%). Two water traps were installed. Analyte CO_2 passes the first water trap before entering the GC column and the second one after the column run before being frozen for 30 min in liquid nitrogen. Between sample runs, the He flow is switched to a backflush mode, with the water traps and the gas chromatograph column being heated to 25 and 150 °C, respectively, for at least 15 min. In a final step, He and traces of water are removed by cleaning the CO_2 cryogenically using a vacuum extraction line equipped with a turbomolecular pump supported by a membrane pump (vacuum $<1 \times 10^{-6}$ mbar). During this last purification step the gas is passed twice over a trap held at −80 °C before being frozen in a glass finger which can be connected to the dual inlet system of the mass spectrometer.

Stable isotope analyses have been performed at Goethe University, Frankfurt (Germany) on a Thermo Scientific MAT 253 gas source mass spectrometer equipped with six Faraday cup collectors for masses 44 to 49 (resistors: 3×10^8 Ω, 3×10^{10} Ω, 10^{11} Ω for masses 44–46 and 10^{12} Ω for masses 47–49, respectively). Analyte CO_2 is measured against Oztech reference gas [$\delta^{18}O$ = +25.01‰ (V-SMOW) and $\delta^{13}C$ = −3.63‰ (V-PDB)] using a dual inlet system. The original stainless steel capillaries were replaced by VICI electroformed nickel (EFNi) capillaries (122 cm × 0.127 mm ID). Sample and reference gases are adjusted to mass 44 signals of 16,000 ± 150 mV. Measurements contain ten acquisitions consisting of ten cycles with an ion integration time of 20 s each, resulting in a total analysis time of about 3 h; the

corresponding shot-noise limit is ~0.008‰ (Merritt and Hayes, 1994). Before each acquisition, peak centering, background determination and pressure adjustments to 16 V at mass 44 have been made.

We report Δ_{47} values on the absolute scale of Dennis et al. (2011) that allows interlaboratory comparison of Δ_{47} values. Changes in non-linearities of the mass spectrometer were monitored by measuring "heated gases" of three different isotopic compositions per week. We followed the protocol outlined by Wacker et al. (2013). Corresponding slopes of heated gas regression lines were determined from blocks of nine consecutive heated gas analyses. If the slopes of two successive blocks were statistically identical, all analyses were considered to determine the slope of the heated gas line. If a significant change in slope occurred between successive blocks, new correction parameters for each day of analysis were determined using the running average of the heated gas line of nine subsequent measurements. For determining the ETF we refer to CO_2 gases equilibrated at 1000 °C (heated gases) and 25 °C (for >3 days isotope exchange was promoted with water; after physical separation from H_2O, CO_2 is cleaned cryogenically and by gas chromatography as described above), respectively. CO_2 gases equilibrated at 25 °C were measured in September/November 2011, and in September 2012. The intercepts of the "25 °C equilibrated gas lines" (determined in a plot of δ^{47}– Δ_{47} signatures) of both data blocks are within errors indistinguishable from each other. All heated gas and 25 °C equilibrated gas data used for the correction, as well as the slopes of heated gas lines and corresponding ETFs are shown in Table S4.1 (Supplementaries).

The difference between acid fractionation factors at 25 and 90 °C ($\Delta_{47}{}^{*}{}_{25-90}$) was experimentally determined in three different laboratories, and $\Delta_{47}{}^{*}{}_{25-90}$ values of +0.081‰ (Passey et al., 2010), +0.092‰ (Henkes et al., 2013) and +0.07‰ (Wacker et al., 2013) were proposed, respectively. Henkes et al. (2013) and Wacker et al. (2013) reported their values on the absolute scale. Henkes et al. (2013) calculated the mean $\Delta_{47}{}^{*}{}_{25-90}$ value measuring three replicates of three aragonitic samples at both 25 °C and 90 °C, respectively. For two samples the difference between acid fractionation factors was +0.099‰. For the third material a lower $\Delta_{47}{}^{*}{}_{25-90}$ value of +0.077‰ was determined. Wacker et al. (2013) measured four to eight replicates of an aragonitic and a calcitic sample and calculated $\Delta_{47}{}^{*}{}_{25-90}$ values of +0.066‰ and +0.075‰, respectively. These differences in acid fractionation factors closely confirm the theoretical value of +0.069‰ (Guo et al., 2009). We, therefore, applied the theoretical value of Guo et al. (2009) to make our data comparable to calibrations determined for carbonates digested at 25 °C.

4.3 Results

Carbonate growth temperatures (T_{growth}), isotopic data ($\delta^{13}C$, $\delta^{18}O$, δ_{47}, raw Δ_{47} and absolute Δ_{47} values and their 1σ standard errors) as well as date of analysis are presented in Table 4.2.

Table 4.2 *Measured isotopic compositions of sample material: δ_{47}, $\Delta_{47, raw}$, $\Delta_{47, abs}$ (in ‰), $\delta^{13}C$, $\delta^{18}O$ (in ‰ deviation vs. V-PDB). Growth temperatures are given in °C, sample sizes in mg.*

	Sample	T_{growth}	Sample size	δ_{47}	$\Delta_{47. raw}$	$\Delta_{47. abs}$	se $\Delta_{47. abs}$	$\delta^{13}C$	$\delta^{18}O$	Date of analysis
Eggshell	*Ostrich*	38	5.4	0.716	-0.380	0.618	0.006	-12.69	-3.60	22.03.2012
	Ostrich	38	4.8	0.730	-0.329	0.674	0.007	-12.59	-3.73	23.03.2012
	Ostrich	38	4.7	0.287	-0363	0.646	0.010	-12.82	-3.91	27.03.2012
	Ostrich	38	4.0	0.507	-0.369	0.635	0.010	-12.71	-3.79	29.03.2012
	Ostrich	38	5.4	0.662	-0.336	0.667	0.008	-12.53	-3.85	10.04.2012
	Ostrich	38	4.6	0.144	-0.377	0.634	0.012	-12.89	-3.92	17.04.2012
	Ostrich	38	7.6	0.199	-0.367	0.644	0.009	-12.90	-3.91	19.04.2012
	Ostrich	38	4.0	-0.023	-0.399	0.615	0.013	-12.85	-4.15	30.04.2012
	Ostrich	38	5.0	0.109	-0.374	0.639	0.006	-12.89	-4.01	30.04.2012
	Ostrich	38	6.2	0.088	-0.363	0.652	0.009	-12.78	-4.14	30.04.2012
	Ostrich	38	5.6	0.348	-0.355	0.654	0.009	-12.71	-3.96	30.04.2012
	Ostrich	38	4.1	0.180	-0.333	0.683	0.009	-12.84	-4.02	30.04.2012
	Ostrich	38	4.3	0.257	-0.383	0.629	0.013	-12.85	-3.89	04.05.2012
	Ostrich	38	6.0	0.523	-0.373	0.634	0.012	-12.75	-3.73	04.05.2012
	Ostrich	38	5.1	-0.287	-0.405	0.623	0.008	-13.05	-4.22	30.07.2012
Bivalve mollusk	*Spondylus* sp.	29	4.0	19.116	0.070	0.642	0.008	2.18	-0.26	23.02.2012
	Spondylus sp.	29	4.1	19.056	0.098	0.683	0.009	2.11	-0.29	06.03.2012
	Spondylus sp.	29	4.6	18.945	0.063	0.647	0.009	2.06	-0.31	13.03.2012
	Spondylus sp.	29	4.0	19,429	0.088	0.663	0.007	2.09	0.11	13.03.2012
	Spondylus sp.	29	4.1	18.925	0.019	0.616	0.009	2.02	-0.24	22.03.2012
	Spondylus sp.	29	4.1	18.544	0.024	0.637	0.008	1.94	-0.55	23.03.2012
	Spondylus sp.	29	6.0	18.860	0.044	0.653	0.009	2.01	-0.32	27.03.2012
	Spondylus sp.	29	5.2	18.627	0.055	0.660	0.007	2.03	-0.58	29.03.2012
	Spondylus sp.	29	4.4	19.167	0.083	0.679	0.004	2.13	-0.18	29.03.2012
	Spondylus sp.	29	4.0	18.800	0.064	0.660	0.008	2.01	-0.40	17.04.2012
Brachiopod	*D. wyvillei*	10	4.5	22.368	0.205	0.712	0.007	2.22	2.72	07.02.2012
	D. wyvillei	10	4.1	22.042	0.193	0.714	0.008	2.32	2.32	06.03.2012
	D. wyvillei	10	4.0	22.457	0.203	0.714	0.008	2.38	2.66	06.03.2012
	D. wyvillei	10	4.2	22.557	0.178	0.684	0.012	2.40	2.75	06.03.2012
	D. wyvillei	10	5.1	22.183	0.212	0.732	0.008	2.36	2.40	13.03.2012
	D. wyvillei	10	5.0	22.405	0.198	0.710	0.006	2.32	2.66	15.03.2012
	D. wyvillei	10	4.2	22.033	0.211	0.734	0.015	2.37	2.25	15.03.2012
	D. wyvillei	10	4.6	22.001	0.179	0.699	0.009	2.31	2.30	16.03.2012
	D. wyvillei	10	4.1	22.104	0.173	0.689	0.010	2.41	2.31	20.03.2012
	D. wyvillei	10	4.3	22.041	0.163	0.700	0.009	2.32	2.38	22.03.2012
	D. wyvillei	10	4.6	22.054	0.184	0.731	0.009	2.40	2.26	23.03.2012
	D. wyvillei	10	4.0	21.960	0.182	0.733	0.007	2.26	2.31	27.03.2012

Table 4.2 *Continued.*

	Sample	T_{growth}	Sample size	δ_{47}	$\Delta_{47.\,raw}$	$\Delta_{47.\,abs}$	se $\Delta_{47.\,abs}$	$\delta^{13}C$	$\delta^{18}O$	Date of analysis
Brachiopod	*D. wyvillei*	10	4.8	22.077	0.148	0.680	0.006	2.22	2.49	30.03.2012
	D. wyvillei	10	4.3	21.967	0.197	0.745	0.005	2.20	2.36	03.04.2012
	D. wyvillei	10	4.0	22.147	0.176	0.704	0.009	2.31	2.45	05.04.2012
	D. wyvillei	10	5.2	22.075	0.195	0.726	0.008	2.24	2.43	03.05.2012
	D. wyvillei	10	4.8	21.963	0.198	0.732	0.012	2.32	2.24	08.05.2012
	D. wyvillei	10	5.4	22.049	0.192	0.724	0.012	2.29	2.35	10.05.2012
	D. wyvillei	10	4.4	22.012	0.158	0.686	0.009	2.29	2.36	11.05.2012
	D. wyvillei	10	5.3	22.099	0.178	0.707	0.005	2.31	2.39	11.05.2012
	D. wyvillei	10	4.9	22.028	0.199	0.732	0.011	2.24	2.37	15.05.2012
	D. wyvillei	10	4.3	21.746	0.196	0.736	0.011	2.28	2.07	18.05.2012
	D. wyvillei	10	4.8	22.240	0.183	0.708	0.015	2.31	2.53	22.05.2012
	D. wyvillei	10	4.1	21.748	0.181	0.719	0.010	2.21	2.15	25.05.2012
	D. wyvillei	10	4.0	22.015	0.183	0.714	0.011	2.18	2.44	31.05.2012
	D. wyvillei	10	5.0	21.911	0.175	0.708	0.009	2.26	2.27	01.06.2012
	D. wyvillei	10	5.7	21.904	0.151	0.681	0.009	2.22	2.33	09.06.2012
Authigenic calcite	Cold seep	9	4.2	-16.374	-0.674	0.724	0.009	-33.74	0.16	01.03.2012
	Cold seep	9	4.3	-16.465	-0.669	0.732	0.011	-33.87	0.19	01.03.2012
	Cold seep	9	4.0	-16.912	-0.688	0.723	0.008	-34.08	-0.04	25.07.2012
	Cold seep	9	5.4	-16.491	-0.707	0.692	0.011	-33.99	0.32	30.07.2012
	Cold seep	9	4.6	-16.342	-0.673	0.725	0.009	-33.84	0.28	30.07.2012
	Cold seep	9	4.6	-22.990	-0.843	0.703	0.009	-41.03	0.85	30.07.2012
Foraminifera	*G. ruber*	26	4.1	15.363	-0.005	0.675	0.010	0.66	-2.39	29.03.2012
	G. ruber	26	4.1	15.315	-0.024	0.651	0.010	0.64	-2.40	05.04.2012
	G. inflata	14	4.0	19.268	0.110	0.701	0.009	0.90	1.06	13.04.2012
	G. inflata	14	4.0	19.464	0.108	0.693	0.008	1.05	1.12	13.04.2012
	G. hirsuta	9	4.0	20.400	0.154	0.705	0.005	1.05	1.97	16.02.2012
	G. hirsuta	9	4.3	20.105	0.157	0.716	0.012	1.07	1.67	17.02.2012

4.3.1 Standard materials

Two standard materials were measured regularly during the interval of calibration: NBS 19 is an interlaboratory reference material for clumped isotope analysis. Applying a $\Delta_{47}{}^{*}{}_{25-90}$ value of +0.069‰, the "accepted" Δ_{47} value reported on the absolute scale is 0.380 ± 0.017‰ (1σ standard deviation) representing the average of the mean values determined in four different laboratories (corresponding to a mean of 0.392‰ if a $\Delta_{47}{}^{*}{}_{25-90}$ value of 0.081‰ is applied, Dennis et al., 2011). Long term standard measurements of NBS 19 in our laboratory reveal a mean Δ_{47} value of 0.364 ± 0.003‰ (1σ se, n = 75). This average is clearly lower than the accepted value, but indistinguishable from the results obtained at Harvard University

0.361 ± 0.007‰ (1σ se, n = 7, corresponding to a mean of 0.373‰ if a $\Delta_{47}{}^{*}{}_{25-90}$ value of 0.081‰ is applied, Dennis et al., 2011). During the time interval of our calibration we determined an NBS 19 mean Δ_{47} value of 0.372 ± 0.003‰ (1σ se, n = 52; Supplementary S4.2).

Furthermore, we analyzed another internal standard, well-homogenized shell material of an aragonitic cold water bivalve (*Arctica islandica*) for which we measured a Δ_{47} value of 0.715 ± 0.002‰ (1σ se, n = 80) on a long term. The average that was determined during the interval of the calibration study is 0.724 ± 0.004‰ (1σ se, n = 28; Supplementary S2).

4.3.2 Regression line and statistical analyses

In Fig. 4.1 the mean Δ_{47} values for all seven calcite samples are plotted versus the inverse squared growth temperature T. In order to obtain a calibration function from these data points, a type II linear regression that considers the errors of temperatures and Δ_{47} values has been performed, yielding the following relationship ($R^2 = 0.9915$):

$$\Delta_{47} = 0.0327\ (\pm\ 0.0026)\ \text{x}\ 10^6 / T^2 + 0.3030\ (\pm\ 0.0308) \qquad \text{(with } \Delta_{47} \text{ in ‰ and T in K)} \quad (4.3)$$

The significance of the coefficient of determination, $R^2 = 0.9915$, was confirmed by an F-Test (p-value of 2×10^{-6}).

For comparison, the application of a standard simple regression procedure results in the following calibration:

$$\Delta_{47} = 0.0332\ (\pm\ 0.0015)\ \text{x}\ 10^6 / T^2 + 0.2955\ (\pm\ 0.0181) \qquad \text{(with } \Delta_{47} \text{ in ‰ and T in K)} \quad (4.4)$$

However, simple linear regression exhibits some limitations, as it implicitly assumes the values of the predictor variable (temperature) to be known exactly and furthermore requires the error of the response variable (Δ_{47}) to be constant for all data points and to be independent of temperature. Investigating the standard errors of the temperature and Δ_{47} values of our data (error bars in Fig. 4.1), we notice that the errors of Δ_{47} vary notably within the samples and, additionally, the errors of the temperature values are of non-negligible magnitude. Consequently, the output of a simple linear regression is not entirely reliable and we decided to perform a more advanced linear regression aiming at the proper consideration of all the reported errors. A least-squares solution to this non-standard regression problem is given by

York et al. (2004) who also show that a maximum-likelihood approach yields equivalent results. They present a concise and effective algorithm which we directly applied to our data points and errors, with the results being the regression relationship and its standard errors as already stated in Eq. (4.3). Compared to the standard regression line in Eq. (4.4), the consideration of errors leads to slightly modified values of intercept and slope. Though Eqs. (4.3) and (4.4) do not differ significantly, it is emphasized that the advanced regression represents a more realistic fit to the experimental data as it does not ignore the error distributions. Details concerning the procedure of non-standard linear regression and the determination of confidence intervals of the different calibration lines are reported in Appendix A.

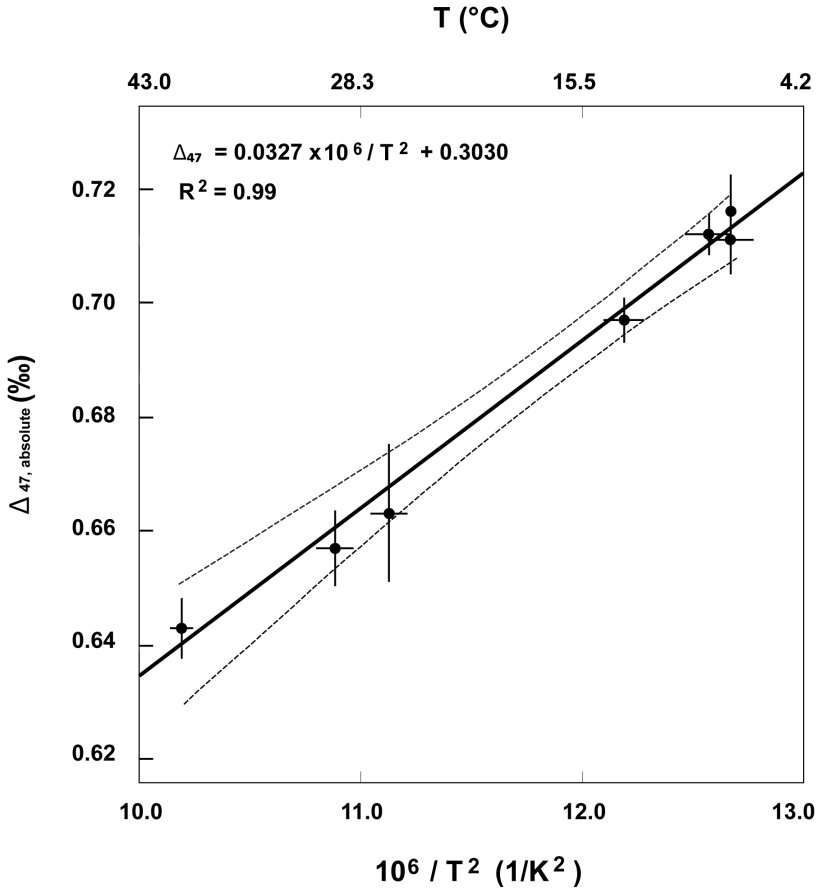

Figure 4.1 *Δ_{47} mean values of analyzed calcites plotted vs. independently constrained growth temperatures. The error bars indicate 1σ standard errors (se) derived from replicate measurements. The linear regression line expresses the calibration equation determined in this study ($\Delta_{47} = 0.0327 \times 10^6/T^2 + 0.3030$; $R^2 = 0.9915$). The 95% confidence interval of the regression line is shown.*

4.3.3 Replication of measurements

For the eggshell, the bivalve and the brachiopod shell between 11 and 30 replicates were analyzed (Table 4.2). For each sample, the absolute variations in Δ_{47} values are about 0.07‰ (Table 4.2). These variations are observed to occur both on the long and the short term. For example, on a single day (30.04.2012) we analyzed the eggshell 5 times (Table 4.2) and observed a scatter in the single Δ_{47} values of 0.068‰. Several reasons may account for the observed short and long term spread in clumped isotope data. Amongst these are (1) short and long term variations of mass spectrometric parameters, (2) heterogeneities in the phosphoric acid reaction environment, and (3) heterogeneities in the clumped and bulk isotopic compositions of samples. More detailed investigations are necessary to distinguish between these factors. However, it should be noted that absolute Δ_{47} variations of ~0.07‰ are common (e.g., Ghosh et al., 2006a; Henkes et al., 2013; Zaarur et al., 2013). As a consequence, an intensive replication of measurements of single samples is required to determine accurate mean Δ_{47} values.

A smaller scatter of ca. 0.01–0.02‰ is observed for the three foraminifera samples, for which a replication was made only twice. Considering this comparably small number, the reported estimates of the corresponding average Δ_{47} values and their standard errors (Table 4.3) exhibit a lower degree of reliability. In order to assess their impact on our calibration, we also derived a regression line without the foraminifera results (Eq. (4.5)):

$$\Delta_{47} = 0.0332\ (\pm\ 0.0028) \times 10^6 / T^2 + 0.2982\ (\pm\ 0.0330) \quad \text{(with } \Delta_{47} \text{ in ‰ and T in K)} \quad (4.5)$$

Table 4.3 *Predictor variables (T in K) and response variables (mean $\Delta_{47,\ abs}$ values in ‰) and their corresponding errors. Furthermore, weights of the different samples in %.*

Sample	$10^6/T^2$	error - $10^6/T^2$	$\Delta_{47,\ abs}$	se $\Delta_{47,\ abs}$	weights
Eggshell of an ostrich	10.32573	0.04	0.643	0.005	17
Spondylus sp.	10.94992	0.07	0.654	0.006	11
Dyscolia wyvillei	12.46848	0.09	0.713	0.004	24
Cold seep carbonate	12.55700	0.01	0.716	0.006	12
Globigerinoides ruber	11.17061	0.07	0.663	0.012	3
Globorotalia inflata	12.12359	0.09	0.697	0.004	22
Globorotalia hirsuta	12.55700	0.08	0.711	0.006	11

Both regression parameters (slope and intercept) of Eqs. (4.3) and (4.5) lie closely together within the range of their standard errors (absolute differences of 0.0005 and 0.0048, respectively, less than 20% of their standard errors). A t-test also confirms that the true parameter values are statistically identical (with p-values being around 0.8). Additionally we tested whether the resulting calibration line would differ significantly if not averaged, but single Δ_{47} values and their corresponding standard errors are used (Appendix B). However, no significant deviations between the two lines were indicated. We therefore decided not to exclude the Δ_{47} mean values obtained for the foraminifera, but to use all available information (data points together with their error estimates) to calculate the calibration regression line as given in Eq. (4.3). Furthermore, it should be noted that the number of replicate measurements used for each calibration point (between 2 and 30, see Table 4.2) is consistent with the number of replicative analyses in other calibration studies (e.g., Dennis and Schrag, 2010; Henkes et al., 2013; Zaarur et al., 2013) for which between 2 and 5 replicates were measured.

4.4 Discussion

In the following we compare the temperature dependence of Δ_{47} values determined in this study with published results and discuss potential reasons that may account for the observed inconsistencies between these calibrations.

4.4.1 Comparison of our calibration with previously published studies

A comparison of calibration data made in different laboratories becomes possible only if data are reported on the absolute scale of Dennis et al. (2011). Henkes et al. (2013) referenced their calibration data directly to the absolute scale, but this scale was not available when Ghosh et al. (2006a), Dennis and Schrag (2010) and Eagle et al. (2013) reported their calibration data. However, Dennis et al. (2011) provided an outline how data can be converted secondarily from the original "Ghosh scale" to the absolute scale, and have applied this secondary projection to the datasets of Ghosh et al. (2006a) and Dennis and Schrag (2010). Recently, Eagle et al. (2013) revised these two projections. Furthermore, they transferred their own calibration data along with those of Tripati et al. (2010) and Thiagarajan et al. (2011) to the absolute scale using the secondary reference frame as proposed by Dennis et al. (2011). In the following we refer to Eagle et al. (2013) whenever we discuss the calibrations of Ghosh et al. (2006a), Dennis and Schrag (2010), Tripati et al. (2010), Thiagarajan et al. (2011) and Eagle et al. (2013). The calibration data of Zaarur et al. (2013) also relies on the secondary reference frame.

Henkes et al. (2013) refer to a $\Delta_{47}{}^{*}{}_{25-90}$ value of +0.092‰ to correct their data, whereas the data of Dennis and Schrag (2010) and Eagle et al. (2013) were corrected using a value of +0.081‰. Throughout our study we have applied a $\Delta_{47}{}^{*}{}_{25-90}$ value of +0.069‰. In order to facilitate a comparison between our data and the data reported by these different studies, we subtracted 0.023‰ from Δ_{47} data of Henkes et al. (2013) and 0.012‰ from Δ_{47} data of Dennis and Schrag (2010) and Eagle et al. (2013).

In Fig. 4.2, our relationship between $1/T^2$ and Δ_{47} values of CO_2 obtained from acid digested calcites is compared with selected published results that were referenced primarily (Henkes et al., 2013) or secondarily (Ghosh et al., 2006a; Zaarur et al., 2013) to the absolute scale. In addition, the theoretical calibration line published by Guo et al. (2009) is shown, considering a mineral-CO_2 Δ_{47} 'acid' fractionation factor $\Delta_{63}{}^{*}$ of 0.268‰ (Henkes et al., 2013). For comparison, all experimentally and empirically derived regression lines displayed in Fig. 4.2 are accompanied with confidence intervals. All shown bands refer to a confidence level of 95%. Details concerning the regression scheme and the derivation of confidence bands are presented in Appendix A. These and other published calibration lines that were secondarily projected onto the absolute scale, as well as numerical details are provided in Table 4.4. Fig. 4.3 provides an overview over all calibrations that were made at a reaction temperature of 90 °C [our data, Dennis and Schrag (2010), Henkes et al. (2013), Eagle et al. (2013)], along with the theoretical calibration of Guo et al. (2009).

Our regression line differs from the calibration lines of Ghosh et al. (2006a), Tripati et al. (2010), Thiagarajan et al. (2011) and Zaarur et al. (2013) in that our slope is significantly shallower (Fig. 4.2; Table 4.4). Moreover, at a 95% confidence level, our slope is inconsistent with that reported by Eagle et al. (2013), even though the two slopes are similar (Fig. 4.3). On the other hand, our $1/T^2$ vs. Δ_{47} relationship is consistent with that of Henkes et al. (2013), which was additionally demonstrated by applying a X^2 test (Fig. 4.3). Both regression lines exhibit identical slopes of 0.0327 and the intercepts agree within 0.0026‰ (Table 4.4). Hence, at any temperature between 9 and 38 °C, both calibrations are identical to within less than 0.003‰ and in the same temperature interval, our calibration line differs by no more than 0.006‰ from the theoretical calibration line of Guo et al. (2009) (Fig. 4.3). Therefore, within the analytical error imposed by counting statistics (0.008‰), our calibration agrees with theoretical predictions. Finally, our calibration line is shifted by −0.02‰ relative to that reported by Dennis and Schrag (2010), but still lies within the 95% confidence interval of their line (Fig. 4.3). Hence our calibration is also consistent with their results. Additionally, the comparably small width of our confidence band indicates that we were able to refine the most

probable region. In conclusion, the temperature sensitivities of Δ_{47} signatures revealed in this study and in the calibrations of Dennis and Schrag (2010), Henkes et al. (2013) and Eagle et al., (2013) are all consistent with the theoretical prediction of Guo et al. (2009) (Fig. 4.3). However, the regression line provided by Eagle et al. (2013) plots significantly above the $1/T^2$ vs. Δ_{47} relationship determined by Henkes et al. (2013) and this study (Fig. 4.3).

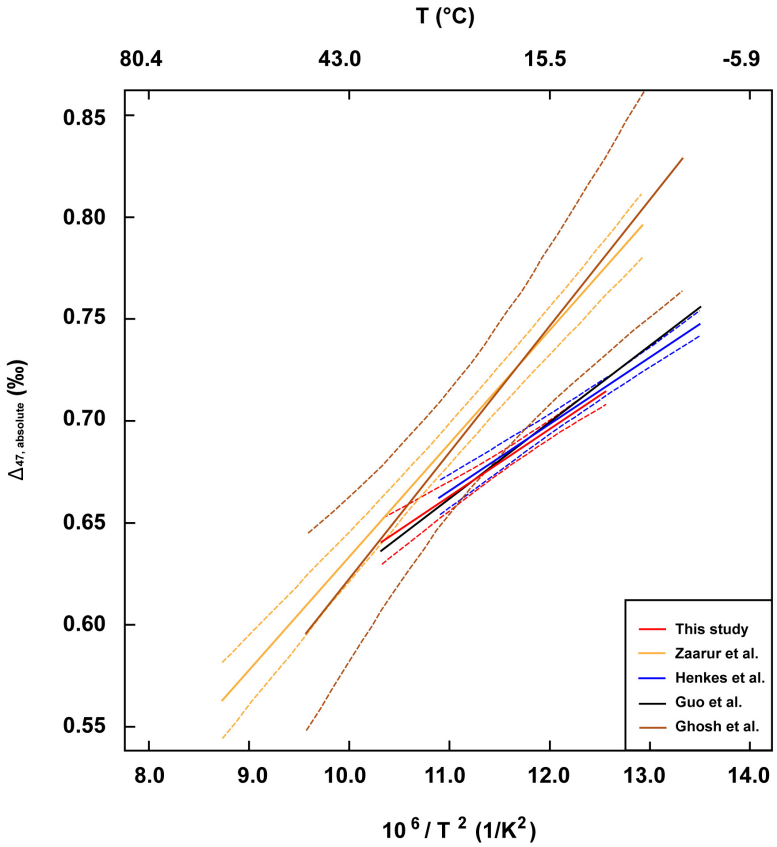

Figure 4.2 *Comparison of several calibration regression lines (including their corresponding 95% confidence intervals) determined in different laboratories. Our line (red; sample material: calcites of various origins) is indistinguishable from the $1/T^2$ vs. Δ_{47} relationship determined at Johns Hopkins University (Henkes et al., 2013; blue line; sample material: aragonitic and calcitic mollusk and brachiopod shells). Within 0.007‰, these two lines are further conform with the theoretical calibration equation of Guo et al. (2009) which was linearly interpolated for temperatures between 0 and 40 °C (black line) and which intersects our regression line and that of Henkes et al. (2013). However, the temperature sensitivities of Δ_{47} reflected by the calibrations determined for carbonates digested at 25 °C at both California Institute of Technology and Yale University are in strong disagreement and have a steeper slope (Ghosh et al., 2006a; brown line; sample material: synthetic calcites; Zaarur et al., 2013; orange line; sample material: synthetic calcites). Other published calibration lines which have been secondarily projected to the absolute scale (Dennis and Schrag, 2010; Tripati et al., 2010; Thiagarajan et al., 2011; Eagle et al., 2013), are not shown to keep the Figure clearly represented. However, comparisons and calibration parameters of all these studies are given in the text and in Table 4.*

Table 4.4 *Numerical details of several published calibration regression lines including our study. To enable the comparison of results obtained from 25 and 90 °C digestions we applied the theoretical difference of the acid fractionation factor between 25 and 90 °C reactions of 0.069‰ (Guo et al., 2009) to data made at 90 °C. Intercept and slope for Guo et al. (2009) was linearly interpolated from their polynomial equation (18) in a temperature interval of 0 to 40 °C using a Δ_{63}^{*} at 25 °C of 0.268‰.*

Study	Slope/10^6	1 se	Intercept	1 se	R^2
This study	0.0327	0.0026	0.3030	0.0307	0.9916
Zaarur et al., 2013	0.0555	0.0027	0.0780	0.0289	0.93
Eagle et al., 2013	0.0362	0.0044	0.3020	0.0527	0.7258
Henkes et al., 2013	0.0327	0.0022	0.3056	0.0278	0.84
Thiagarajan et al., 2011	0.0661	0.0053	-0.0515	0.0659	0.8703
Tripati et al., 2010	0.0524	0.0026	0.1099	0.0312	0.9068
Dennis and Schrag, 2010	0.0340	0.0038	0.3035	0.0408	0.8600
Ghosh et al., 2006a	0.0620	0.0099	0.0021	0.1095	0.8877
Guo et al., 2009	0.0374		0.2502		

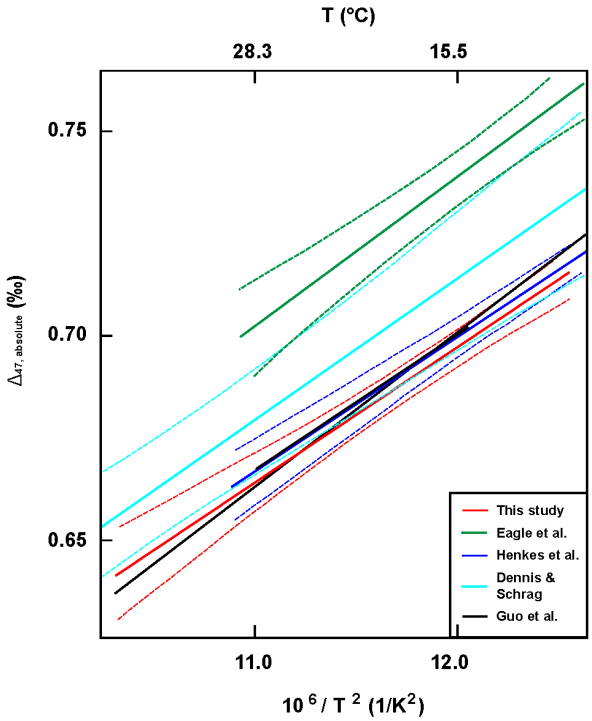

Figure 4.3 *Comparison of the regression lines determined for carbonates digested at 90 °C using a common acid bath. Our line (red; sample material: calcites of various origins) is conform with the $1/T^2$ vs. Δ_{47} relationship determined at Johns Hopkins University (Henkes et al., 2013; blue line; sample material: aragonitic and calcitic mollusk and brachiopod shells). The regression line reported from Harvard University (Dennis and Schrag, 2010; turquoise line; sample material: synthetic calcites) plots slightly above these two lines, but the overlapping 95% confidence intervals of these three calibrations indicate that their differences are not significant. The $1/T^2$ vs. Δ_{47} relationship recently reported from California Institute of Technology (Eagle et al., 2013; green line; sample material: aragonitic and calcitic mollusk shells) plots above our line and that of Henkes et al. (2013), but has a very similar slope. For comparison we included the theoretical calibration line of Guo et al. (2009) (black line) that has been linearly interpolated for temperatures between 0 and 40 °C.*

4.4.2 Potential reasons for discrepant calibrations at 90 °C and 25 °C digestion temperatures

4.4.2.1 Scaling of Δ_{47} data

Eagle et al. (2013) and Zaarur et al. (2013) secondarily projected their data to the absolute scale using interlaboratory standard materials and cylinder CO_2 gas, which were measured over the same time period as calibration samples. Transformation of the original data of Ghosh et al. (2006a), Dennis and Schrag (2010), Tripati et al. (2010) and Thiagarajan et al. (2011) was made using two-point secondary transfer functions based on CO_2 equilibrated at 1000 °C and NBS 19 or CM 2 Carrara marble, respectively (Eagle et al., 2013).

The distinct temperature sensitivities of the calibrations performed at 90 °C (Dennis and Schrag, 2010; Henkes et al., 2013; Eagle et al., 2013; this study) and 25 °C (Ghosh et al., 2006a; Tripati et al., 2010; Thiagarajan et al., 2011; Zaarur et al., 2013) persist even if all datasets are referenced to the absolute scale. As a consequence, the discrepant calibration slopes cannot be caused by differences in scaling (i.e., reporting data on the "Ghosh scale" or on the absolute scale). Furthermore, the distinct relationships between $1/T^2$ and Δ_{47} cannot be explained by interlaboratory differences either. Henkes et al. (2013) noted that any variabilities in absolute Δ_{47} values for standard materials analyzed in different laboratories (e.g., ±0.017‰ for NBS 19) are much smaller than the offset of ~0.1‰ observed for carbonates that were precipitated at ~0 °C, but reacted at temperatures of 25 and 90 °C, respectively. However, absolute Δ_{47} values resulting from secondary projections strongly depend on the accuracy of measured and accepted Δ_{47} values of interlaboratory standards. Accurate secondary transformations can only be made if standard material is available that is very homogeneous in its clumped isotopic composition. The accepted absolute Δ_{47} value of NBS 19 is 0.392‰ comprising the averages determined in three different laboratories (Dennis et al., 2011). However, the observed spread in Δ_{47} is relatively large, ranging from 0.373‰ to 0.404‰ (Dennis et al., 2011). Secondary transformations based on a heated gas and an assigned NBS 19 Δ_{47} value of 0.392‰ will, therefore, be accompanied by inaccuracies if the NBS 19 batch employed during primary data generation had a Δ_{47} value slightly different from 0.392‰. For example, Eagle et al. (2013) reported a Δ_{47} mean value of 0.352‰ for NBS 19 measured along with the calcite precipitates of Ghosh et al. (2006a). If the NBS 19 batch used during the Ghosh et al. (2006a) calibration would have had an absolute Δ_{47} of 0.404‰ instead of the assigned value of 0.392‰, secondary projection of the Ghosh et al. (2006a) data would yield a

regression line in the absolute reference frame that is shifted by −0.02 to −0.03‰ relative to its true position as reflected by applying the correct Δ_{47} value of 0.404‰. In this respect, relatively small uncertainties in assigned Δ_{47} values for NBS 19 can induce relatively large, but rather constant biases in secondarily projected Δ_{47} values.

Additional interlaboratory comparisons are necessary to identify homogeneous isotopic standards that guarantee accurate secondary projections of data. However, the isotopic heterogeneity of NBS 19 cannot be responsible for the discrepant set of calibration slopes resulting from 25 °C and 90 °C reactions.

4.4.2.2 Phosphoric acid fractionation: sensitive to the bulk or clumped isotopic composition of carbonates?

For most calibrations of the clumped isotope thermometer, carbonates were digested either at 25 °C using sealed vessels or at 90 °C using a common acid bath. The only exception is the study performed at ETH Zurich where they reacted modern foraminifera at 70 °C using a Kiel device (Grauel et al., 2013).

Notably, in a $1/T^2$ vs. Δ_{47} plot, two distinct sets of calibration regression lines were reported where analytical conditions within each set were similar. For example, a steeper slope of ca. 0.060 was determined when carbonates were digested at 25 °C (e.g., Ghosh et al., 2006a; Tripati et al., 2010; Thiagarajan et al., 2011; Zaarur et al., 2013). In contrast, shallower regression lines with slopes of ~0.034, which are comparable to the theoretically predicted temperature dependence of Δ_{47} of carbonate-liberated CO_2, were obtained at reaction temperatures of 90 °C (Dennis and Schrag, 2010; Henkes et al., 2013; Eagle et al., 2013; this study). Therefore, it is possible that the distinct sets of regression lines may be related to the two digestion temperatures used in the different studies. As a consequence, it is necessary to investigate whether the clumped isotope fractionation Δ_{47}^* between the carbonate crystal and the evolved CO_2 depends only on the digestion temperature, or if it is also a function of the bulk and/or clumped isotopic composition (Δ_{63}) of the carbonate.

Based on transition-state-theory models, Guo et al. (2009) calculated a non-ideality in clumped isotope fractionations of phosphoric acid digestions of carbonates. Their calculations suggest that the bulk isotopic composition of the carbonate has only a very small effect on Δ_{47}^* (e.g., 0.002‰ per 50‰ increase in $\delta^{13}C$ values), i.e. smaller than the precision of Δ_{47} analyses defined by counting statistics alone. The same calculations imply that the effect of Δ_{63} on Δ_{47}^* seems to be small, causing an increase of ~0.035‰ for every 1‰ increase in Δ_{63}. Δ_{63} of

naturally occurring carbonates should only vary over a range of 0.5‰ provided that their clumped isotopic composition is primarily controlled by temperature (Schauble et al., 2006). As a consequence, one may expect that the effect of Δ_{63} on Δ_{47}^* would remain negligible in Δ_{47} analyses as well.

Further support for the theoretical prediction that Δ_{47}^* is relatively insensitive to both the bulk and clumped isotopic composition of the reacted carbonate comes from calibration data. For their original calibration, Ghosh et al. (2006a) reacted two calcites (HA12 and HA4) that were precipitated at 50 °C, but exhibited a ~4‰ difference in δ_{47} values. However, the mean Δ_{47} values of these samples were identical. The same picture arises when comparing Δ_{47} values measured for *D. wyvillei* and the cold seep carbonate in this study. Both samples precipitated at very similar temperatures of 10 and 9 °C, respectively. Though their δ_{47} values differ by more than 30‰, mean Δ_{47} values are within errors indistinguishable from each other (Table 4.2).

On the other hand, if Δ_{47}^* depends on Δ_{63}, the slope of the $1/T^2$ vs. Δ_{47} relationship obtained from acid digestions at temperatures between 25 and 90 °C, should exhibit an intermediate value between 0.060, the slope characteristic for "25 °C calibrations" (Ghosh et al., 2006a; Tripati et al., 2010; Thiagarajan et al., 2011; Zaarur et al., 2013), and 0.034, the slope characteristic for "90 °C calibrations" (Dennis and Schrag, 2010; Henkes et al., 2013; Eagle et al., 2013; this study). Grauel et al. (2013) report an empirical calibration of the $1/T^2$ vs. Δ_{47} relationship using foraminifera with known growth temperatures and an acid digestion temperature of 70 °C. Their results are in agreement with the experimental calibration of Ghosh et al. (2006a) and with the empirical calibration for foraminifera of Tripati et al. (2010). Therefore, we deem it unlikely that the discrepant calibration lines are caused by variations in fractionation factors depending on the bulk isotopic composition of the carbonates and/or the degree of excess clumping between ^{13}C-^{18}O in the carbonates.

4.4.2.3 Partial re-equilibration of CO_2 at either 25 or 90 °C

As stated previously, two different sets of slopes of calibration regression lines were obtained that largely seem to depend on the carbonate digestion technique. Therefore, it might be reasonable to suspect that these two different temperature sensitivities of Δ_{47} reported in the corresponding studies are caused by systematic analytical artifacts, preferentially occurring at either 25 or 90 °C. It is well known that oxygen isotope exchange between traces of water and evolved CO_2 or intermediate products can occur during phosphoric acid digestion of carbonates (Wendeberg et al., 2011). Heterogeneous oxygen isotope exchange would also

accompany modification of the clumped isotope signature. The excess of ^{13}C-^{18}O bonds in the exchanged CO_2 will depend on reaction temperature and reaction degree. If secondary exchange proceeds to equilibrium, the evolved CO_2 will exhibit Δ_{47} values of 0.925‰ and 0.651‰ for reaction temperatures of 25 and 90 °C, respectively (Wang et al., 2004; Dennis et al., 2011). In the following, we will investigate whether re-equilibration of analyte CO_2 occurring during acid digestions either at 25 °C or at 90 °C can explain the discrepant calibration lines.

Wacker et al. (2013) observed that sample size can have an effect on Δ_{47} values if carbonates are digested in sealed vessels at 25 °C. Higher Δ_{47} mean values and a larger data scatter for samples <7 mg were found compared to larger carbonate aliquots. This possibly arises from partial secondary re-equilibration of CO_2 or reaction intermediates with trace amounts of water. On the other hand, they did not observe such a relationship for digestions at 90 °C. Conspicuously, only the Δ_{47} average of the low-temperature carbonate precipitated at 0 °C analyzed for the "25 °C calibration line" of Ghosh et al. (2006a) deviates significantly from the theoretical calculation of Guo et al. (2009) and from the $1/T^2$–Δ_{47} relationships for which a digestion temperature of 90 °C was used (Dennis and Schrag, 2010; Henkes et al., 2013; Eagle et al., 2013; this study). Ghosh et al. (2006a) reacted ~5 mg aliquots of calcite at 25 °C in sealed vessels. This is exactly the sample size where a bias towards higher mean Δ_{47} values was observed to occur in the experiments of Wacker et al. (2013). Provided that Ghosh et al. (2006a) preferentially used small aliquots for the analyses of their 0 °C precipitate, but larger aliquots for all other samples, the steeper slope obtained by Ghosh et al. (2006a) could be the result of an unnoticed sample-size effect. However, the Ghosh et al. (2006a) calibration line has been confirmed by other studies. These investigations include reactions at 25 °C (Came et al., 2007; Tripati et al., 2010; Thiagarajan et al., 2011; Saenger et al., 2012; Zaarur et al., 2013), as well as digestions at 70 °C (Grauel et al., 2013). Therefore, it seems unlikely that the discrepant calibrations obtained from the different digestion techniques are caused by an analytical artifact exclusively occurring at digestion temperatures of 25 °C. On the other hand, re-equilibration of CO_2 might preferentially occur at 90 °C. If so, the calibration line would pivot around a value of 0.651‰ with its final slope depending on the degree of re-equilibration. However, interlaboratory comparisons do not indicate that significant re-equilibration occurs at 90 °C. Calcites with different Δ_{47} values (NBS 19 and DSC-45923) were measured in several laboratories using different digestion temperatures, and no systematic difference in Δ_{47} values was observed (Dennis et al., 2011). For example, samples were digested at 25 °C in sealed vessels at Yale University, whereas carbonate reactions were

performed in a common acid bath at 90 °C at Johns Hopkins University. Applying a $\Delta_{47}{}^{*}{}_{25-90}$ value of 0.081‰ both laboratories reported indistinguishable Δ_{47} values for NBS 19 that averaged to 0.399‰ (Yale) and 0.404‰ (Johns Hopkins), respectively (Dennis et al., 2011). Considering the same $\Delta_{47}{}^{*}{}_{25-90}$ value, our long term mean Δ_{47} of NBS 19 is 0.376‰ and, therefore, even lower than the corresponding Yale average. Provided secondary re-equilibration would exclusively occur at the elevated reaction temperature of 90 °C, a trend in the opposite direction, i.e., to higher Δ_{47} values should be observed for reactions carried out at 90 °C relative to those performed at 25 °C. Likewise, carbonate samples with a Δ_{47} value >0.7‰ should exhibit a bias towards a value of 0.651‰ if re-equilibration at 90 °C is significant. However, within errors, Δ_{47} values reported for DSC-45923 analyzed at Johns Hopkins at 90 °C (0.775‰) and at Yale at 25 °C (0.781‰) were indistinguishable from each other (Dennis et al., 2011). In conclusion, we exclude that partial re-equilibration at 90 °C is responsible for the different slopes of published calibration regression lines.

4.4.3 Disequilibrium precipitation

Published calibrations of the clumped isotope thermometer are based on both synthetic calcites (Ghosh et al., 2006a; Dennis and Schrag, 2010; Zaarur et al., 2013) and biogenic calcites and aragonites (Tripati et al., 2010; Thiagarajan et al., 2011; Eagle et al., 2013; Henkes et al., 2013; this study). It is well known, that the bulk isotopic composition of biogenic carbonates can exhibit deviations from equilibrium originating from thermodynamic and kinetic effects occurring in the solution (e.g., McConnaughey, 1989a, b). Therefore, it might be possible that the same processes exert control on the extent of ^{13}C-^{18}O clumping in biogenic carbonates as well. Henkes et al. (2013) have already provided a very detailed discussion of the extent these effects may have contributed to the observed discrepancy between their empirical "mollusk-based" calibration and that of Ghosh et al. (2006a). They stated that any disequilibrium effect seen in Δ_{47} should be accompanied by even larger deviations from equilibrium in the bulk isotopic composition. However, they did not observe such large offsets of measured carbonate $\delta^{13}C$ and $\delta^{18}O$ from proposed equilibrium values. Nevertheless, they suggested that unknown differences in mineral–DIC clumped isotope fractionation between mollusks/brachiopods and other taxa might exist.

For the cold seep carbonate, *D. wyvilley*, *G. ruber* and *Spondylus* sp. $\delta^{18}O$ values of the ambient seawater in which they grew were constrained independently (Table 4.5). For these samples the oxygen isotopic compositions of calcite that precipitated in equilibrium with the

water was calculated using the temperature dependence of the bulk oxygen isotope fractionation between water and calcite (Kim and O'Neil, 1997) and independently determined crystallization temperatures of the samples (Table 4.5). The measured oxygen isotopic compositions of *D. wyvilley*, *Spondylus* sp. and the cold seep calcite are higher than the expected $\delta^{18}O_{equilibrium}$ values (Table 4.5). Vital effects might have caused the offsets from oxygen isotope equilibrium of the biogenic carbonates. Certainly, for some modern brachiopod shells offsets from equilibrium $\delta^{18}O$ signatures have been observed (e.g., Auclair et al., 2003; Yamamoto et al., 2010). For a spondylid clam, disequilibrium oxygen isotope precipitation has also been described (Maier and Titschak, 2010). The offset from $\delta^{18}O_{equilibrium}$ determined for the authigenic calcite might also point to the involvement of a kinetic effect in cold seep carbonate precipitation. The measured oxygen isotopic composition of *G. ruber* is lower than the expected equilibrium value (Table 4.5). We consider it likely that species-specific effects on $\delta^{18}O_{carbonate}$ signatures led to disequilibrium fractionation of foraminiferal calcite. For example, $\delta^{18}O_{carbonate}$ values of several species decrease with increasing pH (Spero et al., 1997), consistent with the observed negative deviation from equilibrium. The pH effect has also been described for *G. ruber* (Bijma et al., 1999). Alternatively, the observed offsets from $\delta^{18}O_{equilibrium}$ values might indicate that the oxygen isotopic composition of ambient water from which the minerals grew deviated from the assumed values listed in Table 4.5. For the brachiopod and foraminifera samples, we refer to modeled $\delta^{18}O$ values for the seawater in which these organisms grew (Table 4.5). *Spondylus* sp. lived in a monsoon-dominated environment (Maldives), where large seasonal variations in the oxygen isotopic composition of the seawater can be expected. Here, we refer to a $\delta^{18}O$ value of seawater measured by Storz et al. (2013) representing the condition that occurred in the lagoon and the fore reef area at 1 m depth during the dry winter monsoon in February (Gischler, 2006). For the water from which the cold seep carbonate precipitated, a $\delta^{18}O$ value of Black Sea bottom water at depths >500 m was used (Table 4.5; Rank et al., 1999). These relatively poorly established $\delta^{18}O_{water}$ estimates limit a more detailed evaluation to what extent kinetic effects might be important. However, even if kinetic processes might have affected the bulk oxygen isotopic composition of the investigated calcites, we deem it unlikely that they significantly affected the clumped isotopic composition of our sample set. Although the carbonates derive from distinct mineralization processes, the R^2 value describing the significance of the correlation between $1/T^2$ and Δ_{47} is 0.9915. We would not expect such a good correlation if factors other than temperature were important in controlling the extent of ^{13}C-^{18}O clumping in these carbonates. Likewise, we would not expect that our data set perfectly agrees with other calibrations that rely on

carbonates of different origins (Henkes et al., 2013) or on theoretical calculations (Guo et al., 2009). Moreover, at a 95% confidence level our calibration line supports the $1/T^2$ vs. Δ_{47} relationship of Dennis and Schrag (2010) who precipitated calcites inorganically. However, theoretical studies imply that kinetics can significantly affect the clumped isotopic composition of carbonates (Hill et al., 2014). In addition, Saenger et al. (2012) have shown that kinetic effects govern the clumped isotopic composition of certain coral skeletons. Further investigations are necessary to address in more detail to what extent the clumped isotopic compositions of natural carbonates are affected by disequilibrium processes.

Table 4.5 *Mean $\delta^{18}O_{carbonate}$ values for samples for which bulk oxygen isotope compositions of ambient water ($\delta^{18}O_{water}$) could be constrained independently. $\delta^{18}O_{equilibrium}$ values are calculated after Kim and O'Neil (1997). Isotope values are reported in ‰, T_{growth} in °C.*

Sample	T_{growth}	$\delta^{18}O_{water}$	$\delta^{18}O_{equilibrium}$	$\delta^{18}O_{carbonate}$
Spondylus sp.	29	0.5[a)]	-2.71	-0.30
Globigerinoides ruber	26	0.56[b)]	-2.05	-2.39
Dyscolia wyvillei	10	0.49[c)]	1.28	2.39
Cold seep carbonate	9	-1.77[d)]	-0.75	0.29

a) $\delta^{18}O$ of water samples taken from the lagoon and the fore reef area was measured by Storz et al. (2013).
b) Value taken from the World Ocean Atlas (2005).
c) Value taken from the Global Seawater O-18 Database.
d) Oxygen isotopic composition of Black Sea bottom water (Rank et al., 1999).

4.4.4 Isotopic mixing

Physical, biological and chemical parameters of ocean water vary over the year (e.g., productivity, temperature or isotopic and elemental compositions). These seasonalities are recorded in the chemistry of minerals precipitated from seawater, e.g., in variations of $\delta^{13}C$ and $\delta^{18}O$ signatures. A positive non-linear response of Δ_{47} values to mixing of material with different bulk, but identical clumped isotopic compositions has been described in theory and experimentally (e.g., Eiler and Schauble, 2004). However, mixing effects occurring for our sample set cannot explain the negative offset of our low-temperature samples from the Ghosh et al. (2006a) calibration because mixing will always generate higher Δ_{47} values than represented by the clumped isotope compositions of the endmembers (Eiler and Schauble, 2004; Affek and Eiler, 2006). In addition, we do not have any indication that mixing of carbonate with different bulk isotopic compositions significantly affected our calibration because (1) our regression line is highly correlated ($R^2 = 0.9915$) and (2) relatively large

variations in the bulk isotopic composition have to occur to generate positive Δ_{47} anomalies due to mixing. For example, Thiagarajan et al. (2011) calculated that the clumped isotopic composition of a sample resulting from mixing of two endmembers that exhibit identical Δ_{47} values, but are characterized by a 19‰ difference in δ_{47} values can differ by up to +0.02‰ relative to the Δ_{47} signature of the endmembers. High-resolution $\delta^{18}O$ and $\delta^{13}C$ signatures were measured on ~30 µg aliquots for the brachiopod shell (unpublished data) and the cold seep carbonate (Bahr et al., 2009). The largest variations of $\delta^{13}C$ and $\delta^{18}O$ values determined for *D. wyvillei* were 1.57‰ and 1.26‰, respectively, corresponding to a maximum δ_{47} variation of roughly 3‰. For the authigenic carbonate, differences of 5.64‰ in $\delta^{13}C$ and 0.25‰ in $\delta^{18}O$ were measured, corresponding to a maximum δ_{47} variation of roughly 6‰. Therefore, at least for these samples, Δ_{47} offsets caused by mixing are much less than 0.02‰.

4.5 Conclusions

We have determined the relationship between temperature and the extent of ^{13}C-^{18}O clumping in calcites of distinct biogenic origins (eggshell of an ostrich, tropical bivalve, brachiopod shell, cold seep carbonate, foraminifera). Although these calcites derive from different mineralization processes, a very high correlation between temperature and Δ_{47} is obtained. In a temperature range of 9 to 38 °C, this relationship is indistinguishable from another empirical calibration recently reported by Henkes et al. (2013) for mollusk and brachiopod shells and from the theoretical calcite calibration reported by Guo et al. (2009). Moreover, its 95% confidence interval overlaps with that of the Dennis and Schrag (2010) regression line after projecting the latter to the absolute scale. Based on these observations, it seems unlikely that kinetics have significantly affected the extent of ^{13}C-^{18}O clumping in the (bio)minerals analyzed in our study and in the studies of Henkes et al. (2013) and Dennis and Schrag (2010). However, for a final evaluation to what extent kinetics can affect the clumped isotopic composition of carbonates, more detailed investigations are necessary.

Our calibration line deviates significantly from relationships between $1/T^2$ and Δ_{47} of carbonates reacted at 25 °C (Ghosh et al., 2006a; Tripati et al., 2010; Thiagarajan et al., 2011; Zaarur et al., 2013). The exact cause for this discrepancy remains unclear. We strongly recommend to computing apparent carbonate formation temperatures from $1/T^2$ vs. Δ_{47} relationships established at a reaction temperature of 90 °C as long as carbonates were digested at 90 °C.

4.6 Acknowledgements

We thank S. Hofmann for technical assistance and two anonymous reviewers and associate editor Claire Rollion-Bard for constructive comments. This work has become possible through DFG grant FI-948/4-1. Participation of OF was enabled through DFG grant FR-2544/2.

4.7 Supplementary Information

Table S4.1 *HG and 25 °C equilibrated gas data. Slopes of HG lines and ETFs.*

δ_{47} and $\Delta_{47,\,raw}$ values of heated gases used for the correction of sample data.							
Date	**δ_{47}**	**$\Delta_{47,\,raw}$**	**se (internal)**	**Date**	**δ_{47}**	**$\Delta_{47,\,raw}$**	**se (internal)**
19.12.11	18.535	-0.392	0.009	**29.02.12**	-4.173	-0.989	0.007
19.12.11	18.482	-0.404	0.012	**02.03.12**	16.004	-0.559	0.007
22.12.11	18.385	-0.437	0.011	**05.03.12**	-33.319	-1.640	0.006
22.12.11	18.462	-0.407	0.004	**07.03.12**	-4.582	-0.936	0.008
04.01.12	15.720	-0.465	0.008	**07.03.12**	-4.504	-0.939	0.011
04.01.12	15.763	-0.476	0.006	**09.03.12**	10.584	-0.617	0.009
06.01.12	-33.066	-1.586	0.010	**12.03.12**	-32.751	-1.579	0.009
11.01.12	15.874	-0.474	0.007	**12.03.12**	-34.412	-1.697	0.102
11.01.12	15.919	-0.464	0.009	**14.03.12**	-5.014	-0.965	0.021
12.01.12	-33.027	-1.634	0.010	**16.03.12**	15.289	-0.520	0.009
13.01.12	-4.212	-0.940	0.010	**19.03.12**	-33.048	-1.563	0.000
16.01.12	-4.567	-0.961	0.007	**19.03.12**	-33.041	-1.555	0.008
18.01.12	15.014	-0.550	0.009	**21.03.12**	-4.446	-0.935	0.010
25.01.12	-32.883	-1.575	0.005	**21.03.12**	-4.381	-0.934	0.010
27.01.12	-3.431	-0.904	0.010	**23.03.12**	10.485	-0.625	0.010
30.01.12	11.419	-0.580	0.007	**26.03.12**	-33.318	-1.572	0.009
01.02.12	-33.032	-1.591	0.008	**26.03.12**	-33.189	-1.571	0.013
03.02.12	-4.193	-0.929	0.008	**28.03.12**	-4.167	-0.950	0.010
05.02.12	-33.002	-1.643	0.010	**30.03.12**	15.987	-0.524	0.012
06.02.12	-2.846	-0.880	0.005	**02.04.12**	-32.861	-1.606	0.007
08.02.12	14.879	-0.476	0.008	**04.04.12**	-4.086	-0.970	0.010
08.02.12	14.686	-0.457	0.006	**04.04.12**	-4.127	-0.951	0.010
14.02.12	-32.967	-1.554	0.010	**05.04.12**	10.917	-0.611	0.011
16.02.12	-4.290	-0.962	0.008	**11.04.12**	-33.382	-1.611	0.008
17.02.12	15.854	-0.517	0.008	**11.04.12**	-33.261	-1.604	0.010
20.02.12	-32956	-1.585	0.007	**13.04.12**	15.316	-0.546	0.007
20.02.12	-32.973	-1.585	0.008	**16.04.12**	-5.021	-0.969	0.011
22.02.12	-4.217	-0.954	0.005	**18.04.12**	-33.660	-1.639	0.008
22.02.12	-4.343	-0.934	0.008	**23.04.12**	-2.754	-0.909	0.009
24.02.12	15.506	-0.508	0.006	**23.04.12**	-2.687	-0.921	0.011
24.02.12	15.525	-0.507	0.008	**25.04.12**	-5.008	-0.992	0.007
27.02.12	-32.915	-1.587	0.014	**25.04.12**	-4.331	-0.945	0.009

Table S4.1 *Continued*.

Date	δ_{47}	$\Delta_{47, raw}$	se (internal)
27.04.12	10.200	-0.653	0.009
30.04.12	-33.446	-1.620	0.010
02.05.12	-3.243	-0.936	0.008
04.05.12	13.171	-0.581	0.010
07.05.12	-33.112	-1.595	0.007
07.05.12	-32.991	-1.606	0.007
09.05.12	-4.555	-1.007	0.006
14.05.12	-2.596	-0.898	0.011
14.05.12	-2.498	-0.914	0.010
16.05.12	-33.722	-1.644	0.009
16.05.12	-33.356	-1.633	0.010
21.05.12	-2.783	-0.937	0.006
21.05.12	-2.463	-0.932	0.010
23.05.12	-33.683	-1.640	0.008
29.05.12	11.785	-0.607	0.012
30.05.12	-5.229	-0.978	0.012
30.05.12	-5.324	-0.969	0.008
01.06.12	-33.731	-1.613	0.010
04.06.12	-2.515	-0.949	0.008
04.06.12	-2.621	-0.941	0.013
13.06.12	-33.593	-1.617	0.011
13.06.12	-33.220	-1.623	0.013
15.06.12	-2.883	-0.935	0.007
15.06.12	-3.080	-0.933	0.007
19.06.12	-33728	-1.646	0.009
19.06.12	-33.658	-1.638	0.009
21.06.12	-5.289	-0.970	0.007
21.06.12	-5.387	-0.980	0.009
26.06.12	-33.713	-1.629	0.010
26.06.12	-33.631	-1.618	0.009
02.07.12	-2.928	-0.948	0.008
02.07.12	-2.879	-0.913	0.014
04.07.12	-33.128	-1.610	0.008
09.07.12	-3.058	-0.930	0.010
09.07.12	-2.760	-0.928	0.007
11.07.12	-33.780	-1.620	0.010
11.07.12	-33.496	-1.637	0.005
13.07.12	13.271	-0.595	0.012
16.07.12	7.008	-0.719	0.009
19.07.12	-3.777	-0.945	0.008
25.07.12	-33.166	-1.659	0.010
30.07.12	15.915	-0.568	0.011
01.08.12	-33.762	-1.651	0.010
01.08.12	-33.670	-1.635	0.009
03.08.12	-3.718	-0.958	0.009
03.08.12	-3.723	-0.934	0.011
09.08.12	-33.517	-1.630	0.009

Slopes and R^2 of heated gas lines used during the time period of calibration.

Date	slope	R^2	intercept	se
19.12.-				
20.03.12	0.0228	0.9962	-0.846	0.005
22.03.12	0.0220	0.9959	-0.855	0.010
23.03.12	0.0217	0.9987	-0.854	0.006
27.03.12	0.0216	0.9984	-0.847	0.006
29.03.-				
30.03.12	0.0221	0.9984	-0.858	0.006
03.04.12	0.0218	0.9988	-0.867	0.005
05.04.-				
10.04.12	0.0223	0.9992	-0.869	0.005
12.04.-				
13.04.12	0.0224	0.9987	-0.865	0.005
14.04.-				
15.04.12	0.0223	0.9985	-0.867	0.005
17.04.12	0.0224	0.9988	-0.867	0.005
19.04.12	0.0223	0.9988	-0.868	0.005
30.04.12-				
09.08.12	0.0225	0.9980	-0.872	0.003

Table S4.1 *Continued*.

δ_{47} and $\Delta_{47, raw}$ values of 25 °C water equilibrated gases considered for determining the ETFs applied to sample data.			
Date	**δ_{47}**	**$\Delta_{47, raw}$**	**se (internal)**
02.09.11	9.378	0.204	0.005
02.09.11	12.769	0.259	0.006
05.09.11	-30.289	-0.853	0.006
08.09.11	-21.235	-0.608	0.009
12.09.11	-30.350	-0.854	0.010
12.09.11	-30.510	-0.832	0.009
14.09.11	7.402	0.130	0.008
14.09.11	7.503	0.129	0.007
20.09.11	16.881	0.376	0.008
30.09.11	7.358	0.127	0.009
22.11.11	20.381	0.447	0.007
24.11.11	11.374	0.237	0.008
10.09.12	-30.025	-0.780	0.007
10.09.12	-21.066	-0.584	0.009
10.09.12	15.858	0.239	0.009
17.09.12	7.353	0.111	0.015
17.09.12	13.460	0.263	0.010
17.09.12	-30.714	-0.714	0.007
Slopes and intercepts of the ETFs used during the period of calibration			
Date	**slope**	**intercept**	
nov-dec 2011	1.1670	0.9952	
jan-feb 2012	1.1521	0.9943	
mar-apr 2012	1.1233	0.9926	
may-jun 2012	1.1094	0.9918	
jul-aug 2012	1.0959	0.9910	

Table S4.2 *Carbonates measured during the analysis interval of the calibration samples.*

Date	Sample nr	Sample name	SA size	$\delta_{47,raw}$	$\Delta_{47,raw}$	m	IC HG	IC 25G	$\Delta_{47,abs}$	se	$\delta^{13}C$	$\delta^{18}O$
07.02.12	**C 980**	**D. wyvillei**	4.5	22.368	0.205	0.0228	-0.84	-0.06	0.712	0.007	2.22	2.72
	C 981	**MuStd**	4.6	22.885	0.221	0.0228	-0.84	-0.06	0.717	0.005	1.65	3.70
	C 982					0.0228	-0.84	-0.06				
	C 983					0.0228	-0.84	-0.06				
	C 984	**NBS 19**	4.6	16.875	-0.208	0.0228	-0.84	-0.06	0.381	0.012	2.04	-2.03
	C 985					0.0228	-0.84	-0.06				
08.02.12	**C 986**	**MuStd**	4.9	22.705	0.225	0.0228	-0.84	-0.06	0.726	0.007	1.60	3.56
	C 989	**MuStd**	6.0	22.814	0.224	0.0228	-0.84	-0.06	0.722	0.009	1.60	3.67
	C 990					0.0228	-0.84	-0.06				
	C 991					0.0228	-0.84	-0.06				
09.02.12	**C 992**	**NBS 19**	4.5	16.713	-0.225	0.0228	-0.84	-0.06	0.365	0.008	1.98	-2.11
	C 993					0.0228	-0.84	-0.06				
	C 996	**MuStd**	5.6	22.653	0.217	0.0228	-0.84	-0.06	0.719	0.010	1.62	3.51
	C 994					0.0228	-0.84	-0.06				
	C 995					0.0228	-0.84	-0.06				
	C 997					0.0228	-0.84	-0.06				
	C 998					0.0228	-0.84	-0.06				
10.02.12	**C 999**	**MuStd**	4.8	22.631	0.208	0.0228	-0.84	-0.06	0.708	0.011	1.56	3.55
	C 1000					0.0228	-0.84	-0.06				
	C 1004					0.0228	-0.84	-0.06				
	C 1001					0.0228	-0.84	-0.06				
	C 1002					0.0228	-0.84	-0.06				
	C 1003	**NBS 19**	5.5	16.959	-0.208	0.0228	-0.84	-0.06	0.379	0.006	2.09	-2.00
13.02.12	**C 1005**	**MuStd**	5.1	22.754	0.240	0.0228	-0.84	-0.06	0.742	0.007	1.57	3.67
	C 1006					0.0228	-0.84	-0.06				
	C 1009					0.0228	-0.84	-0.06				
	C 1007					0.0228	-0.84	-0.06				
	C 1008					0.0228	-0.84	-0.06				
	C 1010					0.0228	-0.84	-0.06				
	C 1011					0.0228	-0.84	-0.06				
14.02.12	**C 1013**	**MuStd**	5.4	22.601	0.226	0.0228	-0.84	-0.06	0.730	0.009	1.62	3.45
	C 1014					0.0228	-0.84	-0.06				
	C 1017					0.0228	-0.84	-0.06				
	C 1015					0.0228	-0.84	-0.06				
	C 1016	**NBS 19**	4.5	16.853	-0.206	0.0228	-0.84	-0.06	0.383	0.008	2.11	-2.11
	C 1018					0.0228	-0.84	-0.06				
15.02.12	**C 1019**	**MuStd**	7.8	22.865	0.226	0.0228	-0.84	-0.06	0.723	0.008	1.64	3.68
	C 1021					0.0228	-0.84	-0.06				
	C 1023					0.0228	-0.84	-0.06				
	C 1020					0.0228	-0.84	-0.06				
	C 1022	**NBS 19**	4.6	16.561	-0.235	0.0228	-0.84	-0.06	0.358	0.013	1.90	-2.17
	C 1024					0.0228	-0.84	-0.06				
	C 1025					0.0228	-0.84	-0.06				
16.02.12	**C 1026**	**MuStd**	7.4	22.910	0.197	0.0228	-0.84	-0.06	0.689	0.010	1.65	3.75
	C 1030					0.0228	-0.84	-0.06				
	C 1032					0.0228	-0.84	-0.06				
	C 1028	**NBS 19**	4.4	16.750	-0.259	0.0228	-0.84	-0.06	0.325	0.013	2.07	-2.13
	C 1031					0.0228	-0.84	-0.06				
	C 1033	**G. hirsuta**	4.0	20.400	0.154	0.0228	-0.84	-0.06	0.705	0.005	1.05	1.97
17.02.12	**C 1034**	**MuStd**	4.4	22.529	0.215	0.0228	-0.84	-0.06	0.720	0.007	1.56	3.45

Table S4.2 *Continued.*

Date	Sample nr	Sample name	SA size	$\delta_{47,raw}$	$\Delta_{47,raw}$	m	IC HG	IC 25G	$\Delta_{47,abs}$	se	$\delta^{13}C$	$\delta^{18}O$
	C 1037					0.0228	-0.84	-0.06				
	C 1036	**G. hirsuta**	4.3	20.105	0.157	0.0228	-0.84	-0.06	0.716	0.012	1.07	1.67
	C 1038	**NBS 19**	4.3	16.798	-0.222	0.0228	-0.84	-0.06	0.366	0.008	2.04	-2.09
	C 1039					0.0228	-0.84	-0.06				
	C 1046	**MuStd**	4.3	23.037	0.217	0.0228	-0.84	-0.06	0.708	0.006	1.72	3.43
	C 1049					0.0228	-0.84	-0.06				
	C 1050					0.0228	-0.84	-0.06				
23.02.12	**C 1057**	**MuStd**	4.5	22.958	0.208	0.0228	-0.84	-0.06	0.700	0.007	1.62	3.16
	C 1059	**Spondylus sp.**	4.0	19.116	0.070	0.0228	-0.84	-0.06	0.642	0.008	2.18	-0.26
	C 1061					0.0228	-0.84	-0.06				
	C 1058					0.0228	-0.84	-0.06				
	C 1060	**MuStd**	5.0	22.416	0.203	0.0228	-0.84	-0.06	0.708	0.010	1.53	3.03
	C 1062					0.0228	-0.84	-0.06				
	C 1063					0.0228	-0.84	-0.06				
28.02.12	**C 1076**	**MuStd**	4.6	22.899	0.239	0.0228	-0.84	-0.06	0.737	0.012	1.64	3.33
	C 1078					0.0228	-0.84	-0.06				
	C 1082					0.0228	-0.84	-0.06				
	C 1077					0.0228	-0.84	-0.06				
	C 1079					0.0228	-0.84	-0.06				
	C 1080					0.0228	-0.84	-0.06				
	C 1081					0.0228	-0.84	-0.06				
01.03.12	**C 1090**	**NBS 19**	5.7	16.514	-0.273	0.0228	-0.86	-0.06	0.332	0.008	2.02	-2.30
	C 1092					0.0228	-0.86	-0.06				
	C 1091	**Cold seep cc**	4.2	-16.374	-0.674	0.0228	-0.86	-0.06	0.724	0.009	-33.74	0.16
	C 1093	**NBS 19**	4.4	16.709	-0.244	0.0228	-0.86	-0.06	0.360	0.008	1.97	-2.09
	C 1094					0.0228	-0.86	-0.06				
	C 1095	**Cold seep cc**	4.3	-16.465	-0.669	0.0228	-0.86	-0.06	0.732	0.011	-33.87	0.19
02.03.12	**C 1096**	**MuStd**	4.7	22.476	0.184	0.0228	-0.86	-0.06	0.693	0.011	1.57	3.07
	C 1101					0.0228	-0.86	-0.06				
	C 1098					0.0228	-0.86	-0.06				
	C 1099					0.0228	-0.86	-0.06				
	C 1100	**NBS 19**	4.1	16.931	-0.226	0.0228	-0.86	-0.06	0.374	0.010	2.15	-2.06
	C 1103					0.0228	-0.86	-0.06				
05.03.12	**C 1104**	**MuStd**	4.2	22.472	0.189	0.0228	-0.86	-0.06	0.698	0.007	1.62	3.01
	C 1109					0.0228	-0.86	-0.06				
	C 1106					0.0228	-0.86	-0.06				
	C 1107					0.0228	-0.86	-0.06				
	C 1110					0.0228	-0.86	-0.06				
06.03.12	**C 1111**	**NBS 19**	4.0	16.497	-0.241	0.0228	-0.86	-0.06	0.369	0.010	1.97	-2.30
	C 1112	**D. wyvillei**	4.1	22.042	0.193	0.0228	-0.86	-0.06	0.714	0.008	2.32	2.32
	C 1113	**NBS 19**	4.6	16.505	-0.223	0.0228	-0.86	-0.06	0.389	0.007	2.02	-2.36
	C 1114	**D. wyvillei**	4.0	22.457	0.203	0.0228	-0.86	-0.06	0.714	0.008	2.38	2.66
	C 1115	**NBS 19**	4.5	16.820	-0.224	0.0228	-0.86	-0.06	0.380	0.012	2.01	-2.04
	C 1116	**D. wyvillei**	4.2	22.557	0.178	0.0228	-0.86	-0.06	0.684	0.012	2.40	2.75
	C 1117	**Spondylus sp.**	4.1	19.056	0.098	0.0228	-0.86	-0.06	0.683	0.009	2.11	-0.29
13.03.12	**C 1134**					0.0228	-0.86	-0.06				
	C 1136	**NBS 19**	4.1	16.435	-0.229	0.0228	-0.86	-0.06	0.384	0.005	1.97	-2.37
	C 1138	**Spondylus sp.**	4.6	18.945	0.063	0.0228	-0.86	-0.06	0.647	0.009	2.06	-0.31
	C 1135					0.0228	-0.86	-0.06				
	C 1137	**D. wyvillei**	5.1	22.183	0.212	0.0228	-0.86	-0.06	0.732	0.008	2.36	2.40
	C 1139	**Spondylus sp.**	4.0	19.429	0.088	0.0228	-0.86	-0.06	0.663	0.005	2.09	0.11
	C 1140	**MuStd**	7.0	22.841	0.225	0.0228	-0.86	-0.06	0.729	0.011	1.69	3.27
14.03.12	**C 1141**	**MuStd**	4.7	22.717	0.207	0.0228	-0.86	-0.06	0.712	0.013	1.63	3.22
	C 1144					0.0228	-0.86	-0.06				
	C 1146					0.0228	-0.86	-0.06				

Table S4.2 *Continued.*

Date	Sample nr	Sample name	SA size	$\delta_{47,raw}$	$\Delta_{47,raw}$	m	IC HG	IC 25G	$\Delta_{47,abs}$	se	$\delta^{13}C$	$\delta^{18}O$
	C 1143					0.0228	-0.86	-0.06				
	C 1145	**NBS 19**	4.3	16.657	-0.235	0.0228	-0.86	-0.06	0.371	0.013	2.09	-2.26
	C 1147					0.0228	-0.86	-0.06				
15.03.12	**C 1148**	**D. wyvillei**	5.0	22.405	0.198	0.0228	-0.86	-0.06	0.710	0.006	2.32	2.66
	C 1151	**NBS 19**	4.3	16.533	-0.226	0.0228	-0.86	-0.06	0.384	0.007	1.99	-2.29
	C 1153					0.0228	-0.86	-0.06				
	C 1149	**MuStd**	5.3	23.216	0.224	0.0228	-0.86	-0.06	0.718	0.012	1.71	3.63
	C 1150					0.0228	-0.86	-0.06				
	C 1152					0.0228	-0.86	-0.06				
	C 1154	**D. wyvillei**	4.2	22.033	0.211	0.0228	-0.86	-0.06	0.734	0.015	2.37	2.25
16.03.12	**C 1156**	**D. wyvillei**	4.6	22.001	0.179	0.0228	-0.86	-0.06	0.699	0.009	2.31	2.30
	C 1158					0.0228	-0.86	-0.06				
	C 1161					0.0228	-0.86	-0.06				
	C 1157	**MuStd**	5.4	22.638	0.232	0.0228	-0.86	-0.06	0.742	0.011	1.73	3.42
	C 1159	**NBS 19**	4.6	17.025	-0.225	0.0228	-0.86	-0.06	0.373	0.011	2.07	-1.90
	C 1160					0.0228	-0.86	-0.06				
20.03.12	**C 1168**	**MuStd**	8.7	22.707	0.227	0.0228	-0.86	-0.06	0.735	0.006	1.64	3.18
	C 1170					0.0228	-0.86	-0.06				
	C 1172					0.0228	-0.86	-0.06				
	C 1169	**D. wyvillei**	15.6	22.104	0.173	0.0228	-0.86	-0.06	0.689	0.010	2.41	-1.71
	C 1171	**NBS 19**	4.4	16.975	-0.242	0.0228	-0.86	-0.06	0.355	0.007	2.09	-1.95
	C 1173					0.0228	-0.86	-0.06				
	C 1174					0.0228	-0.86	-0.06				
22.03.12	**C 1181**	**D. wyvillei**	4.3	22.041	0.163	0.0220	-0.86	-0.06	0.700	0.009	2.32	2.38
	C 1183	**Ostrich egg**	5.4	0.716	-0.380	0.0220	-0.86	-0.06	0.618	0.006	-12.69	-3.60
	C 1185	**Spondylus sp.**	4.1	18.925	0.019	0.0220	-0.86	-0.06	0.616	0.009	2.02	-0.24
	C 1182	**NBS 19**	4.5	16.602	-0.260	0.0220	-0.86	-0.06	0.360	0.006	1.99	-2.20
	C 1184	**MuStd**	5.6	22.684	0.219	0.0220	-0.86	-0.06	0.747	0.011	1.73	3.08
	C 1186					0.0220	-0.86	-0.06				
	C 1187					0.0220	-0.86	-0.06				
23.03.12	**C 1189**	**MuStd**	10.4	22.689	0.223	0.0217	-0.86	-0.06	0.759	0.008	1.67	3.14
	C 1191					0.0217	-0.86	-0.06				
	C 1194	**Spondylus sp.**	4.1	18.544	0.024	0.0217	-0.86	-0.06	0.637	0.007	1.94	-0.55
	C 1190	**D. wyvillei**	4.6	22.054	0.184	0.0217	-0.86	-0.06	0.731	0.009	2.40	2.26
	C 1192	**NBS 19**	5.1	16.618	-0.220	0.0217	-0.86	-0.06	0.410	0.009	2.09	-2.31
	C 1193	**Ostrich egg**	4.8	0.730	-0.329	0.0217	-0.86	-0.06	0.674	0.007	-12.59	-3.73
27.03.12	**C 1201**	**D. wyvillei**	4.0	21.960	0.182	0.0216	-0.86	-0.06	0.733	0.007	2.26	2.31
	C 1203	**Ostrich egg**	4.7	0.287	-0.363	0.0216	-0.86	-0.06	0.646	0.010	-12.82	-391
	C 1206	**Spondylus sp.**	6.0	18.860	0.044	0.0216	-0.86	-0.06	0.653	0.009	2.01	-0.32
	C 1202	**MuStd**	7.1	22.538	0.202	0.0216	-0.86	-0.06	0.742	0.009	1.68	3.00
	C 1204	**NBS 19**	5.5	16.774	-0.246	0.0216	-0.86	-0.06	0.378	0.011	1.99	-2.03
	C 1205					0.0216	-0.86	-0.06				
	C1207					0.0216	-0.86	-0.06				
29.03.12	**C 1215**	**Spondylus sp.**	5.2	18.627	0.055	0.0221	-0.86	-0.06	0.660	0.007	2.03	-0.88
	C 1217	**G. ruber**	4.1	15.363	-0.005	0.0221	-0.86	-0.06	0.675	0.010	0.66	-2.39
	C 1219	**Ostrich egg**	4.0	0.507	-0.369	0.0221	-0.86	-0.06	0.635	0.010	-12.71	-3.79
	C 1216	**MuStd**	5.4	22.524	0.205	0.0221	-0.86	-0.06	0.732	0.009	1.66	3.03
	C 1218	**NBS 19**	4.0	16.986	-0.255	0.0221	-0.86	-0.06	0.354	0.004	2.10	-1.94
	C 1220					0.0221	-0.86	-0.06				.
	C 1221	**Spondylus sp.**	4.4	19.167	0.083	0.0221	-0.86	-0.06	0.679	0.004	2.13	-0.18
30.03.12	**C 1223**	**D. wyvillei**	4.8	22.077	0.148	0.0221	-0.86	-0.06	0.680	0.006	2.22	2.49
	C 1226					0.0221	-0.86	-0.06				
	C 1228					0.0221	-0.86	-0.06				
	C 1224	**MuStd**	6.2	22.722	0.213	0.0221	-0.86	-0.06	0.737	0.009	1.76	3.50

Table S4.2 *Continued.*

Date	Sample nr	Sample name	SA size	$\delta_{47,raw}$	$\Delta_{47,raw}$	m	IC HG	IC 25G	$\Delta_{47,abs}$	se	$\delta^{13}C$	$\delta^{18}O$
	C 1225					0.0221	-0.86	-0.06				
	C 1227	**NBS 19**	5.8	16.746	-0.219	0.0221	-0.86	-0.06	0.400	0.009	2.13	-2.23
03.04.12	**C 1236**	**D. wyvillei**	4.3	21.967	0.197	0.0218	-0.86	-0.06	0.745	0.005	2.20	2.36
	C 1240	**NBS 19**	5.0	16.493	-0.254	0.0218	-0.86	-0.06	0.373	0.007	2.01	-2.33
	C 1242					0.0218	-0.86	-0.06				
	C 1237	**NBS 19/25`C**				0.0218	-0.86	-0.06				
	C 1238					0.0218	-0.86	-0.06				
	C 1239	**NBS 19/25`C**				0.0218	-0.86	-0.06				
	C 1241	**NBS 19/25`C**				0.0218	-0.86	-0.06				
05.04.12	**C 1251**	**D. wyvillei**	4.0	22.147	0.176	0.0223	-0.86	-0.06	0.704	0.009	2.31	2.45
	C 1254	**G. ruber**	4.1	15.315	-0.024	0.0223	-0.86	-0.06	0.651	0.010	0.64	-2.40
	C 1252	**MuStd**	5.7	22.871	0.198	0.0223	-0.86	-0.06	0.711	0.007	1.73	3.29
	C 1253					0.0223	-0.86	-0.06				
	C 1255	**NBS 19**	6.8	16.687	-0.243	0.0223	-0.86	-0.06	0.370	0.008	2.09	-2.22
10.04.12	**C 1256**	**MuStd**	8.6	22.883	0.239	0.0223	-0.86	-0.06	0.757	0.010	1.61	3.37
	C 1258					0.0223	-0.86	-0.06				
	C 1260	**NBS 19**	6.0	16.544	-0.248	0.0223	-0.86	-0.06	0.368	0.009	1.88	-2.16
	C 1257	**Ostrich egg**	5.4	0.662	-0.336	0.0223	-0.86	-0.06	0.667	0.008	-12.53	-3.85
	C 1259					0.0223	-0.86	-0.06				
	C 1261					0.0223	-0.86	-0.06				
	C 1262					0.0223	-0.86	-0.06				
12.04.12	**C 1271**	**NBS 19/25`C**				0.0224	-0.86	-0.06				
	C 1273	**NBS 19/25`C**				0.0224	-0.86	-0.06				
	C 1276					0.0224	-0.86	-0.06				
	C 1270					0.0224	-0.86	-0.06				
	C 1272					0.0224	-0.86	-0.06				
	C 1274	**NBS 19**	4.3	16.926	-0.247	0.0224	-0.86	-0.06	0.358	0.008	2.06	-1.96
	C 1275					0.0224	-0.86	-0.06				
13.04.12	**C 1278**					0.0224	-0.86	-0.06				
	C 1279	**G. inflata**	4.0	19.268	0.110	0.0224	-0.86	-0.06	0.701	0.009	0.90	1.06
	C 1283	**NBS 19/25`C**				0.0224	-0.86	-0.06				
	C 1280	**NBS 19**	4.6	16.561	-0.244	0.0224	-0.86	-0.06	0.371	0.009	2.09	-2.35
	C 1281	**G. inflata**	4.0	19.464	0.108	0.0224	-0.86	-0.06	0.693	0.008	1.05	1.12
	C 1282	**NBS 19/25`C**				0.0224	-0.86	-0.06				
14.04.12	**C 1284**	**NBS 19/25`C**				0.0224	-0.86	-0.06				
	C 1285	**NBS 19/25`C**				0.0224	-0.86	-0.06				
15.04.12	**C 1286**	**NBS 19/25`C**				0.0224	-0.86	-0.06				
	C 1287	**NBS 19/25`C**				0.0224	-0.86	-0.06				
17.04.12	**C 1295**	**Ostrich egg**	4.6	0.144	-0.377	0.0224	-0.86	-0.06	0.634	0.012	-12.89	-3.92
	C 1298	**NBS 19**	4.9	16.664	-0.267	0.0224	-0.86	-0.06	0.343	0.007	1.96	-2.10
	C 1301	**NBS 19/25`C**				0.0224	-0.86	-0.06				
	C 1296	**NBS 19/25`C**				0.0224	-0.86	-0.06				
	C 1297	**Spondylus sp.**	4.0	18.800	0.064	0.0224	-0.86	-0.06	0660	0.008	2.01	-0.40
	C 1299					0.0224	-0.86	-0.06				
	C 1300					0.0224	-0.86	-0.06				
19.04.12	**C 1309**	**Ostrich egg**	7.6	0.199	-0.367	0.0223	-0.86	-0.06	0.644	0.009	-12.90	-3.91
	C 1311					0.0223	-0.86	-0.06				
	C 1312	**NBS 19**	7.4	16.631	-0.249	0.0223	-0.86	-0.06	0.366	0.011	1.94	-2.13
	C 1308	**NBS 19/25`C**				0.0223	-0.86	-0.06				
	C 1310					0.0223	-0.86	-0.06				
	C 1313					0.0223	-0.86	-0.06				
	C 1314					0.0223	-0.86	-0.06				
30.04.12	**C 1342**	**Ostrich egg**	4.0	-0.023	-0.399	0.0225	-0.86	-0.06	0.615	0.013	-12.85	-4.15
	C 1345	**NBS 19**	4.1	16.441	-0.270	0.0225	-0.86	-0.06	0.343	0.009	1.80	-2.16
	C 1347	**Ostrich egg**	5.0	0.109	-0.374	0.0225	-0.86	-0.06	0.639	0.006	-12.89	-4.01

Table S4.2 *Continued.*

Date	Sample nr	Sample name	SA size	$\delta_{47,raw}$	$\Delta_{47,raw}$	m	IC HG	IC 25G	$\Delta_{47,abs}$	se	$\delta^{13}C$	$\delta^{18}O$
	C 1344	**Ostrich egg**	6.2	0.088	-0.363	0.0225	-0.86	-0.06	0.652	0.009	-12.78	-4.14
	C 1346	**Ostrich egg**	5.6	0.348	-0.355	0.0225	-0.86	-0.06	0.654	0.009	-12.71	-3.96
	C 1348	**Ostrich egg**	4.1	0.180	-0.333	0.0225	-0.86	-0.06	0.683	0.009	-12.84	-4.02
03.05.12	**C 1354**	**D. wyvillei**	5.2	22.075	0.195	0.0225	-0.87	-0.06	0.726	0.008	2.24	2.43
	C 1359					0.0225	-0.87	-0.06				
	C 1355					0.0225	-0.87	-0.06				
	C 1356					0.0225	-0.87	-0.06				
	C 1358	**NBS 19**	4.3	16.722	-0.235	0.0225	-0.87	-0.06	0.383	0.014	2.08	-2.19
	C 1360					0.0225	-0.87	-0.06				
04.05.12	**C 1362**	**Ostrich egg**	4.3	0.257	-0.383	0.0225	-0.87	-0.06	0.629	0.013	-12.85	-3.89
	C 1364					0.0225	-0.87	-0.06				
	C 1367	**Ostrich egg**	6.0	0.523	-0.373	0.0225	-0.87	-0.06	0.634	0.012	-12.75	-3.73
	C 1363					0.0225	-0.87	-0.06				
	C 1365	**NBS 19**	5.4	16.913	-0.209	0.0225	-0.87	-0.06	0.406	0.007	2.11	-2.06
	C 1366					0.0225	-0.87	-0.06				
08.05.12	**C 1374**	**D. wyvillei**	4.8	21.963	0.198	0.0225	-0.87	-0.06	0.732	0.012	2.32	2.24
	C 1377	**NBS 19**	4.4	16.718	-0.207	0.0225	-0.87	-0.06	0.414	0.010	1.99	-2.13
	C 1379					0.0225	-0.87	-0.06				
	C 1375					0.0225	-0.87	-0.06				
	C 1378					0.0225	-0.87	-0.06				
10.05.12	**C 1387**	**D. wyvillei**	5.4	22.049	0.192	0.0225	-0.87	-0.06	0.724	0.012	2.29	2.35
	C 1390	**NBS 19**	4.0	16.625	-0.233	0.0225	-0.87	-0.06	0.387	0.014	1.98	-2.19
	C 1391					0.0225	-0.87	-0.06				
11.05.12	**C 1388**					0.0225	-0.87	-0.06				
	C 1394	**D. wyvillei**	4.4	22.012	0.158	0.0225	-0.87	-0.06	0.686	0.009	2.29	2.36
	C 1389	**D. wyvillei**	5.3	22.099	0.178	0.0225	-0.87	-0.06	0.707	0.005	2.31	2.39
	C 1391					0.0225	-0.87	-0.06				
	C 1392					0.0225	-0.87	-0.06				
	C 1395					0.0225	-0.87	-0.06				
12.05.12	**C 1396**					0.0225	-0.87	-0.06				
	C 1397	**NBS 19**	4.4	16.556	-0.258	0.0225	-0.87	-0.06	0.361	0.010	2.09	-2.34
	C 1398					0.0225	-0.87	-0.06				
	C 1399					0.0225	-0.87	-0.06				
15.05.12	**C 1406**	**D. wyvillei**	4.9	22.028	0.199	0.0225	-0.87	-0.06	0.732	0.011	2.24	2.37
	C 1408					0.0225	-0.87	-0.06				
	C 1411					0.0225	-0.87	-0.06				
	C 1407					0.0225	-0.87	-0.06				
	C 1409	**NBS 19**	4.9	16.750	-0.247	0.0225	-0.87	-0.06	0.369	0.011	2.07	-214
	C 1410					0.0225	-0.87	-0.06				.
	C 1412					0.0225	-0.87	-0.06				
18.05.12	**C 1419**	**D. wyvillei**	4.3	21.746	0.196	0.0225	-0.87	-0.06	0.736	0.011	2.28	2.07
	C 1421					0.0225	-0.87	-0.06				
	C 1424					0.0225	-0.87	-0.06				
	C 1420					0.0225	-0.87	-0.06				
	C 1422	**NBS 19**	4.5	16.559	-0.208	0.0225	-0.87	-0.06	0.417	0.007	2.09	-2.38
	C 1423					0.0225	-0.87	-0.06				
	C 1425					0.0225	-0.87	-0.06				
22.05.12	**C 1431**	**D. wyvillei**	4.8	22.240	0.183	0.0225	-0.87	-0.06	0.708	0.015	2.31	2.53
	C 1433	**NBS 19**	4.6	16.567	-0.252	0.0225	-0.87	-0.06	0.368	0.009	2.05	-2.29
	C 1436					0.0225	-0.87	-0.06				
	C 1432					0.0225	-0.87	-0.06				
23.05.12	**C 1434**					0.0225	-0.87	-0.06				
	C 1435					0.0225	-0.87	-0.06				
	C 1437					0.0225	-0.87	-0.06				
	C 1441					0.0225	-0.87	-0.06				

Table S4.2 *Continued.*

Date	Sample nr	Sample name	SA size	$\delta_{47,raw}$	$\Delta_{47,raw}$	m	IC HG	IC 25G	$\Delta_{47,abs}$	se	$\delta^{13}C$	$\delta^{18}O$
25.05.12	**C 1442**	**D. wyvillei**	4.1	21.748	0.181	0.0225	-0.87	-0.06	0.719	0.010	2.21	2.15
	C 1444					0.0225	-0.87	-0.06				
	C 1447					0.0225	-0.87	-0.06				
	C 1443					0.0225	-0.87	-0.06				
	C 1445	**NBS 19**	4.3	16.584	-0.229	0.0225	-0.87	-0.06	0.393	0.010	1.96	-2.21
	C 1446					0.0225	-0.87	-0.06				
	C 1448					0.0225	-0.87	-0.06				
31.05.12	**C 1458**	**D. wyvillei**	4.0	22.015	0.183	0.0225	-0.87	-0.06	0.714	0.011	2.18	2.44
	C 1460	**NBS 19**		16.728	-0.241	0.0225	-0.87	-0.06	0.375	0.011	2.00	-2.10
	C 1463					0.0225	-0.87	-0.06				
	C 1459					0.0225	-0.87	-0.06				
	C 1461	**NBS 19**	5.2	16.702	-0.245	0.0225	-0.87	-0.06	0.372	0.006	2.02	-2.14
	C 1462					0.0225	-0.87	-0.06				
	C 1464					0.0225	-0.87	-0.06				
01.06.12	**C 1466**	**D. wyvillei**	5.0	21.911	0.175	0.0225	-0.87	-0.06	0.708	0.009	2.26	2.27
	C 1468					0.0225	-0.87	-0.06				
	C 1471					0.0225	-0.87	-0.06				
	C 1467					0.0225	-0.87	-0.06				
	C 1469	**NBS 19**	5.5	16.638	-0.220	0.0225	-0.87	-0.06	0.402	0.011	2.07	-2.28
	C 1470					0.0225	-0.87	-0.06				
09.06.12	**C 1475**	**D. wyvillei**	5.7	21.904	0.151	0.0225	-0.87	-0.06	0.681	0.009	2.22	2.33
	C 1478					0.0225	-0.87	-0.06				
	C 1476					0.0225	-0.87	-0.06				
	C 1477	**NBS 19**	5.0	16.522	-0.249	0.0225	-0.87	-0.06	0.373	0.000	2.02	-2.32
	C 1479					0.0225	-0.87	-0.06				
10.07.12	**C 1553**	**NBS 19**	6.7	16.822	-0.251	0.0225	-0.88	-0.06	0.370	0.010	1.98	-1.98
	C 1556	**NBS 19**	4.9	16.774	-0.270	0.0225	-0.88	-0.06	0.351	0.006	1.98	-2.01
	C 1554					0.0225	-0.88	-0.06				
	C 1555					0.0225	-0.88	-0.06				
	C 1557					0.0225	-0.88	-0.06				
18.07.2012	**C1583**	**i. Carrara**	4.7	17.323	-0.241	0.0225	-0.88	-0.06	0.369	0.011	1.96	-1.49
	C1584					0.0225	-0.88	-0.06				
19.07.2012	**C1585**	**NBS 19**	5.7	16.858	-0.248	0.0225	-0.88	-0.06	0.372	0.011	1.99	-1.96
20.07.2012	**C1587**	**i. Carrara**	4.5	17.314	-0.259	0.0225	-0.88	-0.06	0.350	0.010	1.97	-1.49
	C1588					0.0225	-0.88	-0.06				
	C1589	**NBS 19**	4.8	15.965	-0.282	0.0225	-0.88	-0.06	0.357	0.000	1.91	-2.72
23.07.12	**C1590**					0.0225	-0.88	-0.06				
	C1592	**NBS 19**	8.3	17.001	-0.246	0.0225	-0.88	-0.06	0.371	0.013	1.99	-1.82
	C1591					0.0225	-0.88	-0.06				
24.07.12	**C1593**	**i. Carrara**	5.1	17.355	-0.245	0.0225	-0.88	-0.06	0.363	0.012	2.05	-1.53
	C1595	**NBS 19**	5.7	17.032	-0.248	0.0225	-0.88	-0.06	0.369	0.008	1.98	-1.81
	C1594	**Cold seep cc**	4.0	-16.912	-0.688	0.0225	-0.88	-0.06	0.723	0.008	-34.08	-0.04
	C1596					0.0225	-0.88	-0.06				
	C1597					0.0225	-0.88	-0.06				
25.07.12	**C1598**	**NBS 19**	4.9	16.921	-0.263	0.0225	-0.88	-0.06	0.354	0.011	1.98	-1.87
	C1599					0.0225	-0.88	-0.06				
30.07.12	**C 1606**	**Cold seep cc**	5.4	-16.491	-0.707	0.0225	-0.88	-0.06	0.692	0.011	-33.99	0.32
	C 1608	**NBS 19**	5.2	16.565	-0.253	0.0225	-0.88	-0.06	0.374	0.012	1.99	-2.24
	C 1607	**Ostrich egg**	5.1	-0.287	-0.405	0.0225	-0.88	-0.06	0.623	0.008	-13.05	-4.22
	C 1609	**Cold seep cc**	4.6	-16.342	-0.673	0.0225	-0.88	-0.06	0.725	0.009	-33.84	0.28
	C 1611	**Cold seep cc**	4.6	-22.990	-0.843	0.0225	-0.88	-0.06	0.703	0.009	-41.03	0.85

4.8 Appendices

A Details concerning the regression

This section supplies details concerning the regression procedure performed in chapter 3.2. For simplicity of the mathematical description, we refer to the n data points as $(x_i|y_i)$ and their standard errors as σ_{x_i} and σ_{y_i}, respectively.

A.1 Non-standard linear regression

As stated in chapter 3.2, the aim is to obtain a linear fit which, in contrast to simple regression, considers the different error magnitudes of the data points. The non-availablity of analytical solutions to this problem renders such a regression considerably more complex than simple regression, and many approaches have been developed, see e.g. the review by Cantrell (2008). He compares different solutions to this regression problem and finds the algorithm of York (1966) to be both consistent and effective. It is based on a least-squares approach, i.e. one obtains the regression parameters a (intercept) and b (slope) by minimizing the following so-called cost function f, containing the sum of the squared deviations of the data points $(x_i|y_i)$ from the targeted regression line $\hat{y} = a + bx$:

$$f(a,b) = \sum_{i=1}^{n} w_i (y_i - a - bx_i)^2 \quad \text{with} \quad w_i = \left(b^2\sigma_{x_i}^2 + \sigma_{y_i}^2\right)^{-1} \tag{A1}$$

The w_i can be interpreted as relative weights considering the errors of each data point. Simple linear regression is based on the same cost function, with the exception of all w_i being identical to one. York et.al. (2004) review the method of York (1966) and emphasize that this least-square estimation yields the same results as a maximum likelihood approach to the same problem and also produces the correct standard errors for the regression parameters. In addition to the application of their algorithm, we performed a direct numerical minimization (Nelder and Mead, 1965) of the cost function (A1) using the software package `R` (R Core Team, 2013) to confirm that the results are identical, underlying the reliability of the chosen regression scheme.
As a typical measure of the linear fit's goodness, we calculated the coefficient of determination,

$$R^2 = 1 - \frac{SS_{res}}{SS_{tot}} = 1 - \frac{\sum_i w_i (y_i - \hat{y}_i)^2}{\sum_i w_i (y_i - \overline{y})^2} \tag{A2}$$

where the latter term is the proportion of the residual sum of squares on the total sum of squares. In order to be consistent with our applied regression scheme, we computed both terms and $\overline{y}$ using the weights w_i from the regression scheme, resulting in $R^2 = 0.9915$.

A.2 Confidence intervals for linear regression lines

The outcome of a linear regression scheme consists of estimates for intercept ($\hat{a}$) and slope ($\hat{b}$) and their standard errors ($\hat{\sigma}_a$ and $\hat{\sigma}_b$). According to the theory of linear regression, the standard error of the regression line at any x is given by

$$\sigma_{\hat{y}(x)}^2 = \sigma^2 \left(\frac{1}{n} + \frac{(x - \overline{x})^2}{(n-1)\sigma_x^2} \right) \tag{A3}$$

The combination of both equations yields $\sigma^2 = n\left(\sigma_{\hat{a}}^2 - \overline{x}^2\sigma_{\hat{b}}^2\right)$, which allows to evaluate the error variance $\hat{\sigma}^2$ without knowledge of the y values, and subsequently equation (A3). Then $1-\alpha$ confidence intervals (with α being the level of significance) can be obtained via $\hat{y}(x) \pm t_{n-2,1-\alpha/2} \cdot \hat{\sigma}_{\hat{y}(x)}$ where $t_{n-2,p}$ represents the p-quantil of the t-distribution with $n-2$ degrees of freedom.
For our regression line, the weights w_i of the data points, an additional output of the advanced regression algorithm, are used when evaluating the statistics of the x values, i.e. for $\hat{\sigma}_x$ and $\hat{\overline{x}}$:

$$\hat{\overline{x}} = \frac{\sum_i w_i x_i}{\sum w_i} \quad , \quad \hat{\sigma}_x^2 = \frac{\sum_i w_i (x_i - \hat{\overline{x}})^2}{\sum w_i} \tag{A6}$$

with $\hat{\sigma}^2 = \frac{1}{n-2}\sum_i (y_i - \hat{y}_i)^2$ being an estimate for the overall error variance σ^2. In order to draw the confidence bands for the regression lines of the other studies, where partly only the regression parameters, their errors and the x values are available, we have to refer to the definition of the standard errors of intercept and slope,

$$\sigma_{\hat{a}}^2 = \sigma^2 \left(\frac{1}{n} + \frac{\overline{x}^2}{(n-1)\sigma_x^2} \right) \quad \text{(A4)}$$

$$\sigma_{\hat{b}}^2 = \sigma^2 \frac{1}{(n-1)\sigma_x^2} \quad \text{(A5)}$$

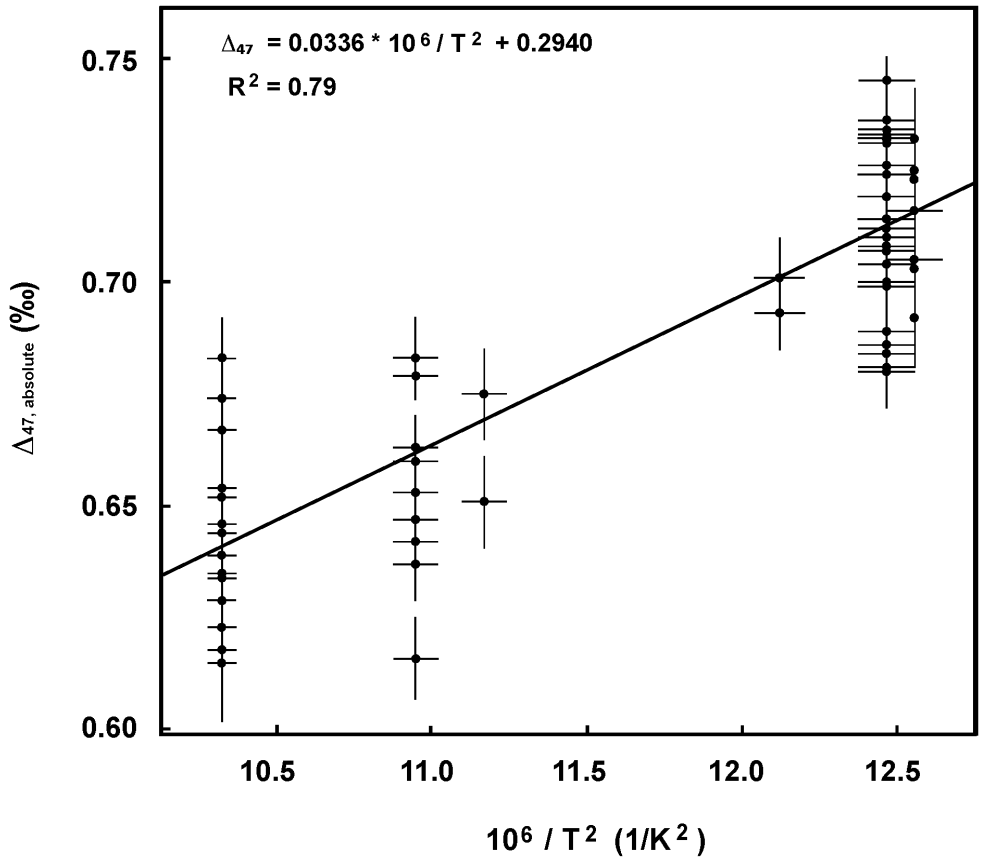

Figure A4.1 *Single Δ_{47} values of analyzed calcites plotted vs. inverse squared growth temperatures. The error bars indicate 1σ standard error (se) from ten acquisitions consisting of ten cycles. The optimat linear fit is given by the regression line (Δ_{47} = 0.0336(±0.0026)*10^6 /T^2 + 0.2940(±0.0026), R^2 = 0.7912).*

B Comparison of the regression lines obtained from mean Δ47 or single Δ47 values

The following equation was obtained applying an advanced, error-considering linear regression procedure to the mean Δ47 values of each sample (see chapter 3.2):

$$\Delta 47 = 0.0327(\pm 0.0026) \cdot \frac{10^6}{T^2} + 0.3030(\pm 0.0308) \quad \text{(with } \Delta 47 \text{ in ‰ and } T \text{ in } K\text{)} \tag{B1}$$

However, the number of replicates performed for each sample differs (see also table 2): For example, 30 aliquots were analyzed for the brachiopod shell and only two replicates were measured for each foraminifera sample. As discussed in chapter 3.3, replicating samples only twice reduces the reliability of the determined mean Δ47 value, but we also showed that excluding these samples does not alter the calibration line significantly (see chapter 3.3).
The usage of mean Δ47 values as calibration points is not only in accordance with similar studies, but is also statistically consistent in the sense that each calibration point should represent the best estimate for the corresponding sample. This estimate, together with its standard error, is the final result of an experimental procedure which itself employs a number of replicate measurements to increase the statistical significance.
However, for comparative reasons it may be worthwhile to treat each replicate as independent calibration point. Figure B1 shows the single Δ47 values measured for all seven samples (in total 68 data points). We applied the advanced linear regression scheme to determine the following $1/T^2$ vs. Δ47 relationship:

$$\Delta 47 = 0.0336(\pm 0.0011) \cdot \frac{10^6}{T^2} + 0.2940(\pm 0.0133) \quad \text{(with } \Delta 47 \text{ in ‰ and } T \text{ in } K\text{)} \tag{B2}$$

A comparison of the regression parameters given in equations (B1) and (B2) reveals that the absolute differences are 0.0009 (slope) and 0.0070 (intercept). These differences are smaller than the estimated standard errors and the parameter values in (B1) lie in the standard error range of (B2), and vice versa. Additionally, we performed a t-test concerning the equality of both slope and intercept, returning p-values of 0.08 and 0.15. Hence, from a statistical point of view, there is no evidence for a significant difference of regression line (B2) from (B1). Furthermore, the observed difference of the parameter values is of non-resolvable magnitude. Figure B2 shows both regression lines and their 95% confidence bands, visualizing the results from the statistical analysis and underlying the reliability of the calibration (B1).
This comparison supports the conclusion made in chapter 3.3 that the mean Δ47 values of the foraminifera do not have a significant influence on the calibration line and do not deteriorate its quality.

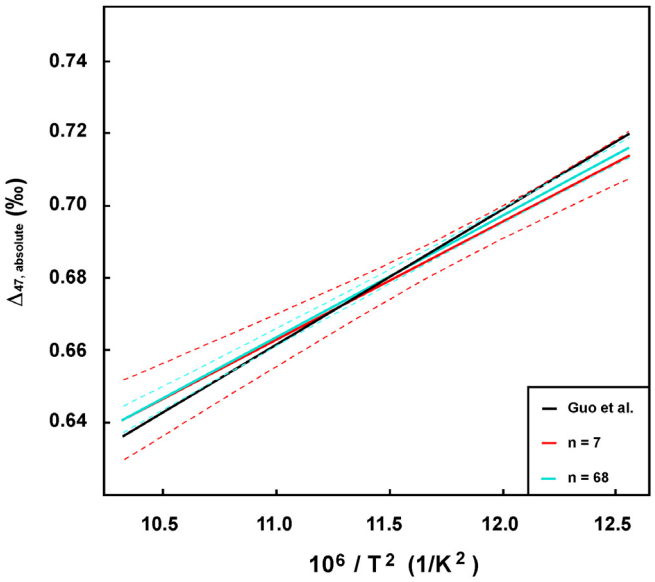

Figure A4.2 *Comparison of the calibration regression lines (including their corresponding 95% confidence intervals) obtained from either using the mean Δ_{47} values (n = 7, red line) or the single Δ_{47} values (n = 68, turquoise line). The black line shows the theoretical $1/T^2$ vs. Δ_{47} relationship of Guo et al. (2009).*

5 Empirical calibration of the clumped isotope paleothermometer based on aragonite: preliminary results

Ulrike Wacker[1], Jens Fiebig[1,2], Alan D. Wanamaker[3], Bernd R. Schöne[4]

[1] Institute of Geosciences, Goethe-University, Altenhöferallee 1, 60438 Frankfurt am Main, Germany

[2] Biodiversity and Climate Research Center, Senckenberganlage 25, 60325 Frankfurt am Main, Germany

[3] Department of Geological and Atmospheric Sciences, Iowa State University, Ames, IA 50011, USA

[4] Department of Applied and Analytical Paleontology (INCREMENTS), Institute of Geosciences, University of Mainz, Johann-Joachim-Becherweg 21, 55128 Mainz, Germany

In the following, preliminary Δ_{47} data of an aragonite calibration line based on bivalves are presented. Further investigations are necessary that approve our first results. It is not intended to publish this manuscript in its early form. This chapter is, therefore, skimped severely representing only a first draft.

Abstract We determined the relationship between growth temperatures and clumped isotopic compositions for three aragonitic bivalves (*Arctica islandica)*. These organisms grew in tanks in moderate to cold water (15, 10 and 4 °C, respectively). Additionally, a tropical aragonitic bivalve (*Tridacna* sp.) from the Maldives/Indian Ocean was included in the sample set. This organism was collected dead in surface waters exhibiting a mean annual growth temperature of 29 °C.

Preliminary results indicate that the slopes of the calibration lines for aragonitic bivalves and for various calcites (biogenic and biologically induced precipitates) that were determined in our laboratory (chapter 4), are identical. Nevertheless, relative to the calcite line an offset of ca. –0.03‰ was detected for the measured aragonites. In contrast, the preliminary mean Δ_{47} value determined for an aragonitic cold seep carbonate plots ~0.03‰ higher than the aragonite line based on bivalves. The average Δ_{47} value of the authigenic sample is, therefore, in accordance with the calcite line. However, the Δ_{47} average is based on the measurement of two replicates only and additional measurements are required to determine a statistically reliable mean Δ_{47} value. Further clumped isotope analyses are required to approve the preliminary results obtained in our study so far.

5.1 Introduction

Applying carbonate clumped isotope thermometry to fossil material requires the knowledge of correct relationships between growth temperatures of crystals and Δ_{47} values. Several calibration lines of the novel proxy have been published on the absolute scale (directly or secondarily projected). These different lines are based on synthetic (Ghosh et al., 2006a; Dennis and Schrag, 2010; Zaarur et al., 2013) and biogenic calcites (Tripati et al., 2010; Thiagarajan et al., 2011), biogenic aragonites and calcites (Eagle et al., 2013; Henkes et al., 2013), as well as biogenic and biologically induced precipitated calcites (Wacker et al., 2014). Nevertheless, discrepancies between reported calibrations occurred. The line of Ghosh et al. (2006a) was confirmed by Tripati et al. (2010), Thiagarajan et al. (2011) and Zaarur et al. (2013). In contrast, a consistently flatter slope of the $1/T^2$–Δ_{47} relationship and therefore a weaker temperature sensitivity was reported by Dennis and Schrag (2010), Eagle et al. (2013), Henkes et al. (2013) and Wacker et al. (2014). Identical calibrations were reported by Henkes et al. (2013) and Wacker et al. (2014), which are, in addition, indistinguishable from theoretical predictions regarding the relationship of $1/T^2$ and Δ_{47} values of calcite (Guo et al., 2009). No definite cause for the distinct calibrations have been found yet.

Though the calibration discrepancy has not been solved yet, it was described that different types of minerals are characterized by non-equilibriumm ^{13}C-^{18}O clumping considering the Ghosh et al. (2006a) calibration to reflect equilibrium conditions: constant positive offsets from the Ghosh et al. (2006a) line were found for otoliths (Ghosh et al., 2007) and speleothems (e.g., Affek et al., 2008; Daeron et al., 2011; Kluge et al., 2014). Furthermore, hermatypic corals (Saenger et al., 2012) plot constantly above the Ghosh et al. (2006a) line. Saenger et al. (2012) assume that this is neither caused by salinity effects nor by the presence or absence of symbionts. They suggest that kinetic effects associated with hydration and hydroxylation of CO_2 dependent on growth rates cause disequilibrium ^{13}C-^{18}O clumping, and concurrently affect $\delta^{18}O$ and $\delta^{13}C$ values of the corals. However, the studied corals were made of aragonite whereas Ghosh et al. (2006a) sampled synthetic calcites. Calculations based on thermodynamic models indicate that the aragonite calibration plots 0.02‰ above the $1/T^2$–Δ_{47} relationship of calcite (Guo et al., 2009). Nevertheless, the theoretical prediction of Guo et al. (2009) was not confirmed by the empirical calibrations of Eagel et al. (2013) and Henkes et al. (2013) which relie on both biogenic aragonite and calcite. No systematic difference was found between the clumped isotopic compositions of aragonites and calictes of each sample set. The line reported by Henkes et al. (2013) is conform with the theoretical calcite $1/T^2$–Δ_{47} relationship whereas

the calibration of Eagle et al. (2013) plots significantly above both the theoretical calcite and aragonite lines.

Here, we present Δ_{47} data that were measured for aragonitic bivalves. Three sampled organisms (*A. islandica*) lived in moderate to cold water at 15, 10 and 4 °C, respectively. Furthermore, a tropical shell (*Triadacna* sp.) from the Maldives/Indian Ocean was analyzed which grew at 29 °C. The mean Δ_{47} values of these four aragonitic samples reflect a temperature sensitivity similar to that determined for calcite (Wacker et al., 2014), but is offset from the calcite calibration line by ca. –0.03‰. However, for a modern authigenic aragonite a higher Δ_{47} value was measured that corresponds to the calcite calibration line of Wacker et al. (2014). Nevertheless, this sample was replicated only twice. Further analyses are required to test whether the observed offset of the authigenic mineral from the preliminary aragonite line is true.

5.2 Material and Methods

5.2.1 Sample material

A. islandica

Three heltered organisms were sampled for the calibration study. The organisms grew in tanks filled with ambient seawater in the Darling Marine Center (DMC) located adjacent to the tidally-influenced Damariscotta River estuary (Beirne et al., 2012). The physico-chemical parameters salinity, temperature, pH and $\delta^{13}C$ were continuously monitored. Growth periods were marked with calcein and subsampled for isotopic analysis using a hand drill at low speed to avoid thermal and physical strain.

Tridacna sp.

The bivalve derived from the Maldives Archipelago (NW Indian Ocean). The shell was collected dead. Monsoon influences control the climatic conditions of this area (e.g., Storz et al., 2013). Maximum and minimum temperature values of sea surface water range between 29.5 and 27.8 °C and a mean annual temperature of 29 ± 1 °C has been determined (Storz et al., 2013). For clumped isotope analysis inner shell material was drilled using a low-speed dental drill.

Authigenic carbonate

The authigenic carbonate was sampled from the Batumi seep area of the eastern Black Sea (Station BS377GR; 41°57.56'N; 41°17.24'E; 853 m water depth, Bahr et al., 2010) during TTR Cruise 15 in 2005 onboard R/V Professor Logachev (Akhmetzanov et al., 2007). Two phases could be distinguished (Bahr et al., 2010). (1) Micritic high-magnesium calcite that caused cementation of the sediments and (2) botroidal aragonite rims that grew recently associated with microbial mats under the stable temperature conditions of the deep Black Sea (9.0 ± 0.1 °C, Locarini et al., 2010). The yellow aragonite was sampled for clumped isotope analyses using a hand drill (low speed).

5.2.2 Acid digestion and gas preparation

Phosphoric acid digestions were performed at 90 (± 0.1) °C using a common acid bath connected to a CO_2 extraction line (Wacker et al., 2013). Acid concentrations were >106 wt.-%. Acids were prepared after Coplen et al. (1983). The evolved CO_2 gas was immediately frozen in liquid nitrogen after passing a water trap held at –80 °C. Reaction time was 20–30 min. Afterwards CO_2 was transported to the gas chormatograph (GC) using a glas finger. The GC column was held at –20 °C while sample gas was transferred through the capillaries to remove traces of hydrocarbons (stainless steel column: 1.20 m x 2.15 mm ID; packed with Porapak Q 80/120; –20 °C / He carrier gas: 18 ml/min; purity: 99.9999%). Additionally, two water traps were installed in front of and behind the column to avoid secondary re-equilibration with water adsorbed on capillaries of the system. Finally, the purified CO_2 gas was frozen in a U-tube located behind the second water trap for 30 min. Between sample runs, the He flow was switched to a backflush mode, and the water traps and the gas chromatograph column were heated to 25 and 150 °C, respectively, for at least 15 min. After that CO_2 was cleaned cryogenically using a vacuum extraction line equipped with a turbomolecular pump (vacuum $<1*10^{-6}$ mbar). The gas was passed twice over a water trap held at –80 °C; furthermore, He was removed. Finally, CO_2 was frozen in a glass finger and transferred to the the mass spectrometer.

5.2.3 Isotopic analysis

Stable isotope analyses were carried out at the Goethe University, Frankfurt (Germany). Measurements of masses 44 to 49 were performed on a Thermo Scientific MAT 253 gas source mass spectrometer equipped with six Faraday cup collectors (resistors: $3*10^8$ Ω, $3*10^{10}$ Ω, 10^{11} Ω for masses 44–46 and 10^{12} Ω for masses 47–49, respectively). The original stainless

steel capillaries of the instrument were replaced by VICI electroformed nickel (EFNi) capillaries (122 cm x 0.127 mm ID). Oztech CO_2 was used as a reference gas [$\delta^{18}O$ = +25.01‰ (V-SMOW) and $\delta^{13}C$ = –3.63‰ (V-PDB)]. Measurements were performed via the the dual inlet. Sample and reference gas were adjusted to mass 44 signals of 16,000 ± 150 mV. Analysis time was ~3 h [10 acquisitions consisting of 10 cycles with an ion integration time of 20 s each; corresponding shot-noise limit: ~0.008‰ (Meritt and Hayes, 1994)]. Before each acquisition, peak centering, background determination and pressure adjustments were carried out.

5.2.4 Data reduction

Δ_{47} data are referenced to the absolute scale (Dennis et al., 2011). The non-linearity effect on the measurement of m/z 47 were corrected by applying the "heated gas slope correction" (Huntington et al., 2009) using the protocol that was described in Wacker et al. (2013). Blocks of nine consecutive days of analyses were considered. The slopes of the heated gas lines of two consecutive blocks of nine days each were compared. If the parameters were statistically identical, all data were used for the determination of the heated gas line. Otherwise, new correction parameters were determined. In this case we used the running average of the heated gas line of nine subsequent days of measurements.

The empirical transfer functions (ETF) were determined using CO_2 gases equilibrated at 1000 °C (heated gases) and 25 °C (isotope exchange was promoted with water for >3 d; H_2O was physically separated and CO_2 was cleaned cryogenically and by gas chromatography similarly like carbonate CO_2, see chapter 5.2.2), respectively. CO_2 gases equilibrated at 25 °C was measured in September/November 2011, and in September 2012 only. The intercepts of the "25 °C equilibrated gas lines" of both data blocks are identical within errors. All heated gas and 25 °C equilibrated gas data used for the correction, as well as the slopes of heated gas lines and corresponding ETFs are shown in Table S5.1 (Supplementary information).

In order to make Δ_{47} data obtained from reactions at 90 °C comparable to data received from digestions at 25 °C, the theoretical difference in acid fractionation ($\Delta_{47}{}^{*}{}_{25-90}$) of +0.069‰ (Guo et al., 2009) was applied to reported Δ_{47} values. This value was confirmed experimentally by Wacker et al. (2013).

5.3 Results

Carbonate growth temperatures (T_{growth}), isotopic data ($\delta^{13}C$, $\delta^{18}O$, δ_{47}, $\Delta_{47,raw}$ and $\Delta_{47,abs}$ values and their 1σ standard errors) as well as date of analysis are presented in Table 5.1. The complete sample and standard sequence along the period of analysis is provided in Table S5.2 (Supplementary information).

Table 5.1 *Isotopic compositions of sample material: δ^{47}, $\Delta_{47,raw}$, $\Delta_{47,abs}$ (in ‰), $\delta^{13}C$, $\delta^{18}O$ (in ‰ deviation vs. V-PDB). T_{growth} values and their errors are given in °C, sample sizes in mg.*

Date of analysis	Sample	T_{growth}	Sample size	δ^{47}	$\Delta_{47,raw}$	$\Delta_{47,abs}$	se	$\delta^{13}C$	$\delta^{18}O$
09.01.12	*A.i*(4)	4.25±0.25	4.3	22.306	0.193	0.700	0.008	1.50	3.31
10.01.12	*A.i*(4)	4.25±0.25	4.0	22.216	0.187	0.695	0.009	1.51	3.21
13.01.12	*A.i*(4)	4.25±0.25	4.1	22.350	0.209	0.717	0.010	1.49	3.34
16.01.12	*A.i*(4)	4.25±0.25	4.7	22.278	0.181	0.687	0.007	1.52	3.27
20.01.12	*A.i*(4)	4.25±0.25	4.0	22.250	0.180	0.686	0.009	1.52	3.24
17.02.12	*A.i*(4)	4.25±0.25	9.0	22.348	0.204	0.712	0.009	1.59	2.91
average						**0.700**		**1.52**	**3.21**
se						**0.005**			
03.11.11	*A.i*(10)	10±0.25	4.6	18.835	0.141	0.680	0.009	2.16	-0.99
07.11.11	*A.i*(10)	10±0.25	4.1	18.877	0.126	0.663	0.008	2.19	-0.60
09.11.11	*A.i*(10)	10±0.25	4.3	18.968	0.127	0.663	0.007	2.17	-0.50
11.11.11	*A.i*(10)	10±0.25	6.0	18.943	0.138	0.676	0.011	2.14	-0.51
13.01.12	*A.i*(10)	10±0.25	4.1	18.580	0.102	0.693	0.009	2.02	-0.71
23.01.12	*A.i*(10)	10±0.25	4.5	18.905	0.109	0.692	0.006	2.06	-0.44
average						**0.678**		**2.12**	**-0.62**
se						**0.005**			
03.11.11	*A.i*(15)	15±0.25	4.6	18.938	0.128	0.661	0.009	2.22	-0.93
04.11.11	*A.i*(15)	15±0.25	4.2	18.845	0.151	0.691	0.008	2.18	-1.01
08.11.11	*A.i*(15)	15±0.25	4.4	19.125	0.120	0.648	0.006	2.27	-0.44
09.11.11	*A.i*(15)	15±0.25	4.2	18.824	0.137	0.680	0.011	2.21	-0.69
10.11.11	*A.i*(15)	15±0.25	4.1	18.930	0.135	0.674	0.006	2.22	-0.59
18.01.12	*A.i*(15)	15±0.25	4.1	18.867	0.103	0.686	0.008	2.20	-0.61
19.01.12	*A.i*(15)	15±0.25	4.6	18.981	0.106	0.687	0.012	2.26	-0.55
average						**0.675**		**2.22**	**-0.69**
se						**0.006**			
10.07.12	*Tridacna*	29±1	6.6	18.043	0.023	0.640	0.064	1.57	-0.97
10.07.12	*Tridacna*	29±1	4.2	17.931	0.008	0.627	0.063	1.51	-1.02
18.07.12	*Tridacna*	29±1	4.1	18.004	0.015	0.633	0.063	1.49	-0.93
23.07.12	*Tridacna*	29±1	4.5	17.897	0.019	0.639	0.064	1.51	-1.05
31.07.12	*Tridacna*	29±1	4.2	16.978	-0.020	0.620	0.062	1.46	-1.86
average						**0.632**		**1.51**	**-1.17**
se						**0.004**			
Not included in the calibration dataset:									
23.07.2012	CS arag	9±0.1	4.3	-23.006	-0.820	0.729	0.009	-41.20	0.68
31.07.2012	CS arag	9±0.1	4.0	-17.621	-0.714	0.712	0.008	-34.42	-0.69
average						**0.720**		**-37.81**	**-0.01**
se						**0.008**			

5.3.1 Reference material

Two standard materials were measured during the interval of sample analysis (Table S5.2). NBS 19 revealed a mean Δ_{47} value of 0.361 ± 0.004‰ (1σ se, n = 31) corresponding to our long-term average of 0.364 ± 0.003‰ (1σ se, n = 75). The accepted value based on a $\Delta_{47}{}^{*}{}_{25-90}$ value of +0.069‰ is 0.380 ± 0.017‰ (1σ standard deviation) and, therefore, slightly higher. However, it is indistinguishable from the mean Δ_{47} value reported from Harvard University (0.361 ± 0.007‰, 1σ se, n = 7). Within the same interval we have determined an average Δ_{47} value of 0.718 ± 0.003‰ (1σ se, n = 47) for another internal aragonitic standard (homogenized shell material of *A. islandica*). This value is identical with its long-term average of 0.715 ± 0.002‰ (1σ se, n = 80).

5.3.2 Calibration samples and authigenic aragonite

Mean Δ_{47} values obtained for the calibration material plot between 0.632 and 0.700‰ (Table 5.1). For all samples 5–7 replicative measurements were made. The absolute Δ_{47} variations determined for each aragonite range between 0.020 and 0.045‰ (Table 5.1). So far, the authigenic aragonite was measured only twice. Therefore, the preliminary mean Δ_{47} value of 0.720 ± 0.008‰ (Table 5.1) has to be evaluated critically. Further clumped isotope analyses are required to establish a significant Δ_{47} average.

5.3.3 Regression line

In Fig. 5.1 mean Δ_{47} values for the aragonitic bivalves are plotted versus their inverse squared growth temperatures T. A type II linear regression that considers the errors of $1/T^2$ and Δ_{47} values was applied to obtain a calibration function from these data points. The following relationship was obtained:

$$\Delta_{47} = 0.0329\ (\pm 0.0032) \times 10^6 / T^2 + 0.2736\ (\pm 0.0387) \qquad (\text{with } \Delta_{47} \text{ in ‰ and T in K}) \qquad (5.1)$$

The correlation coefficient R^2 is 0.9838; its significance was confirmed by an F-Test (p-value of 0.008). The weight of each sample is shown in Table 5.2.

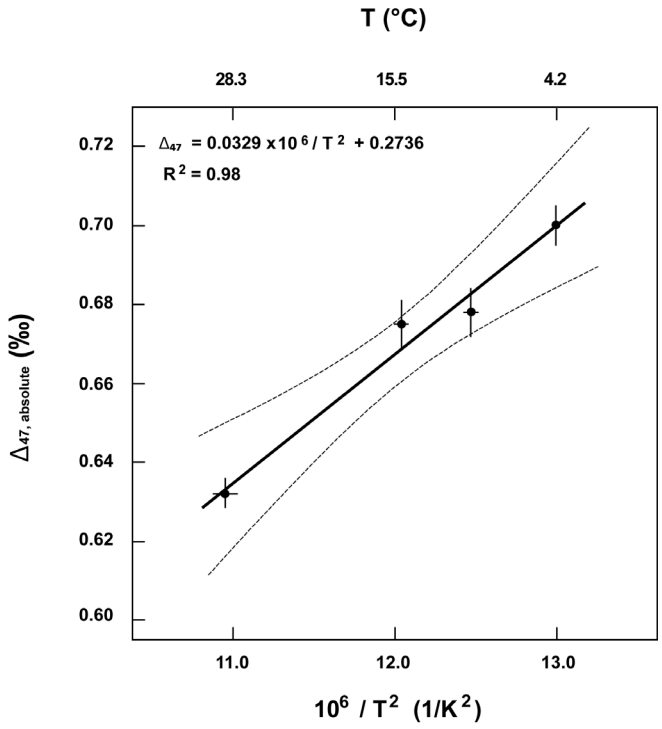

Figure 5.1 *Plot of mean Δ_{47} values against growth temperatures of the analyzed aragonitic bivalve shells. The error bars indicate 1σ standard errors (se) derived from replicative measurements. The linear regression line expresses the calibration equation determined in this study. The dashed lines mark the 95% confidence interval of the regression line.*

Table 5.2 *Predictor variables (T in K) and response variables (mean Δ_{47}, absolute values in ‰) and their corresponding errors. Furthermore, weights of the different samples in %.*

Sample	$10^6/T^2$	error - $10^6/T^2$	$\Delta_{47, absolute}$	se $\Delta_{47, absolute}$	weights
A.i.(4)	12.99064	0.02	0.700	0.005	28
A.i.(10)	12.46848	0.04	0.678	0.006	19
A.i.(15)	12.03960	0.04	0.675	0.006	19
Tridacna sp.	10.94992	0.07	0.632	0.004	34

5.4 Discussion and Outlook

5.4.1 Comparison with relevant published calibrations based on natural carbonates

Published calibrations based on digestions of natural samples at 90 °C are plotted in Fig. 5.2. The aragonite line presented in this study is compared with the two calibrations based on aragonitic and/or calcitic bivalves (Eagle et al., 2013; Henkes et al., 2013). Furthermore, the

calcite line of Wacker et al. (2014) is shown. Notably, the temperature sensitivities of Δ_{47} values reflected by all these calibrations are almost indistinguishable from each other.

However, our aragonite line plots ca. 0.03‰ below the calcite calibration of Wacker et al. (2014). According to the theoretical predictions of Guo et al. (2009) Δ_{47} values of aragonites are expected to be ~0.02‰ higher than calcite at any temperature. The hypothesis of Guo et al. (2009) is, therefore, not confirmed by the results presented in this study.

Differences between the calcite and aragonite calibration might arise from different $\Delta_{47}{}^{*}{}_{25-90}$ values for these minerals. Indeed, for calcite and aragonite a slight differences in acid fractionation factores between 90 and 25 °C reactions of only +0.009‰ has been determined by Wacker et al. (2013). Therefore, it seems unlikely that differences in $\Delta_{47}{}^{*}{}_{25-90}$ values can account for the observed offset of –0.03‰ between aragonite and calcite (Fig. 5.2).

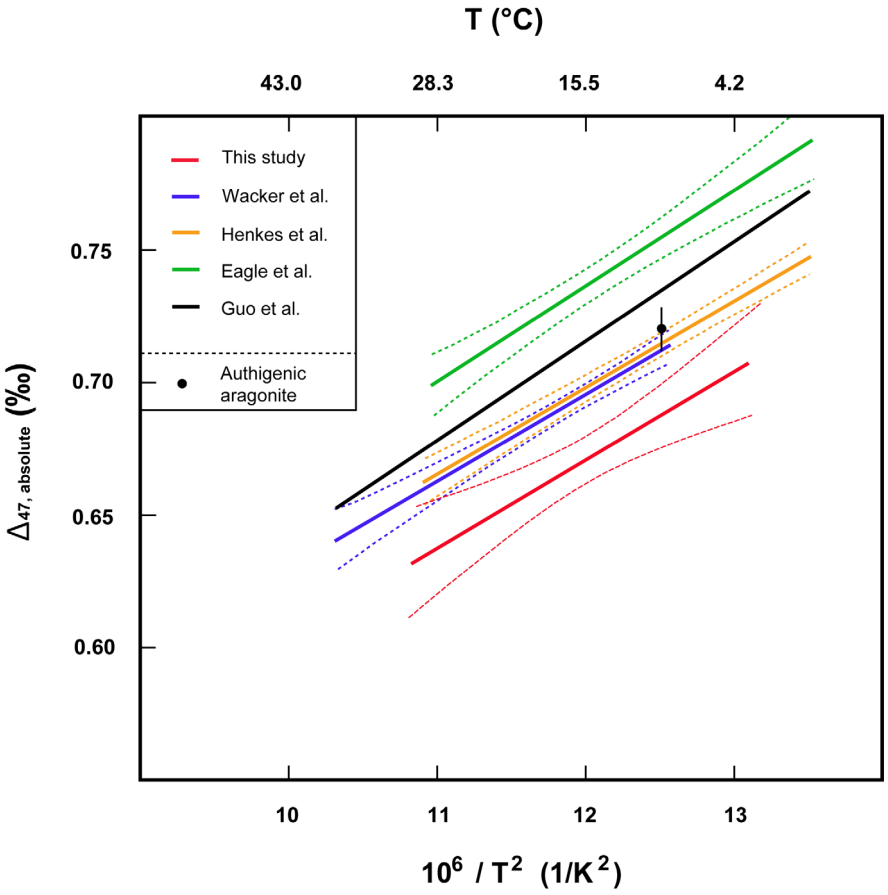

Figure 5.2 *Comparison of published calibrations determined for natural carbonates digested at 90 °C with the aragonite line determined here. Almost indistinguishable slopes were determined in all studies. However, the aragonite calibration plots significantly below the calcite line of Wacker et al. (2014) and the aragonite and/or calcite lines of Eagle et al. (2013) and Henkes et al. (2013). The black line shows the theoretical prediction of the $1/T^2$–Δ_{47} relationship of aragonites (Guo et al., 2009).*

In contrast to our results, Eagle et al. (2013) as well as Henkes et al. (2013) did not identified any significant differences between calcite and aragonite with respect to the relationship between $1/T^2$ and ^{13}C-^{18}O clumping. Furthermore, both sample sets include *A. islandica* – the taxa our aragonite line is mainly based on. This might provide a preliminary indication that the carbonates analyzed here were not affected by vital effects. Nevertheless, a larger sample set is required. Further specimen of *A. islandica*, as well as other taxa must be included to test whether the observed offset in Δ_{47} values between the different crystal structures is real.

5.4.2 Authigenic aragonite

The Δ_{47} composition of a cold seep calcite derived from the Black Sea was included in the calcite calibration line of Wacker et al. (2014). In our study, preliminary clumped isotope data were measured for an authigenic aragonite also. Both samples precipitated at the same temperature (Black Sea bottom water). Though the authigenic aragonite was measured only twice, the average Δ_{47} value of 0.720 ± 0.008‰ (Table 5.1) is indistinguishable from the authigenic calcite (0.716 ± 0.006‰; Wacker et al., 2014). Compared to our calibration line based on the studied aragonitic bivalves, the cold seep aragonite yields a significantly higher Δ_{47} value and plots on the calcite line (Fig. 5.2). Wacker et al. (2014) deemed it unlikely that kinetic effects have influenced the clumped isotopic composition of sample material included in their study since the $1/T^2$–Δ_{47} regression line of various calcites of distinct mineralization processes yielded a very high correlation coefficient. Therefore, from first measurements it might be suggested that the aragonitic cold seep carbonate also grew in equilibrium regarding ^{13}C-^{18}O clumping. If this hypothesis can be confirmed by further measurements the studied bivalves might have been influenced by disequilibrium precipitation in respect to their Δ_{47} composition. However, the preliminary Δ_{47} average of the authigenic carbonate which is based on two replicates only, is statistically not verified yet.

5.5 Acknowledgements

We thank Erin C. Beirne for providing material from heltered specimen of *A. islandica*. Eberhard Gischler and André Bahr is thanked for offering the tropical bivalve and the authigenic aragonite, respectively. We thank Sven Hofmann for technical assistance. This work has become possible through DFG grant FI-948/4-1 DFG.

5.6 Supplementary Information

Table S5.1 *HG and 25 °C equilibrated gas data. Slopes of HG lines and ETFs.*

δ_{47} and $\Delta_{47, raw}$ values of heated gases used for the correction of sample data.							
Date	**δ_{47}**	**$\Delta_{47, raw}$**	**se (internal)**	**Date**	**δ_{47}**	**$\Delta_{47, raw}$**	**se (internal)**
24.10.11	-32.716	-1.663	0.006	**16.01.12**	-4.567	-0.961	0.007
26.10.11	-2.196	-0.894	0.010	**18.01.12**	15.014	-0.550	0.009
28.10.11	-51.499	-2.157	0.007	**25.01.12**	-32.883	-1.575	0.005
01.11.10	-2.663	-0.909	0.007	**27.01.12**	-3.431	-0.904	0.010
04.11.10	16.214	-0.437	0.009	**30.01.12**	11.419	-0.580	0.007
08.11.11	-51.664	-2.115	0.007	**01.02.12**	-33.032	-1.591	0.008
14.11.11	-29.364	-1.550	0.008	**03.02.12**	-4.193	-0.929	0.008
15.11.11	-2.460	-0.887	0.010	**05.02.12**	-33.002	-1.643	0.010
16.11.11	-51.773	-2.119	0.011	**06.02.12**	-2.846	-0.880	0.005
21.11.11	-51.955	-2.119	0.007	**08.02.12**	14.879	-0.476	0.008
22.11.11	13.069	-0.537	0.005	**08.02.12**	14.686	-0.457	0.006
24.11.11	-51.083	-2.016	0.007	**14.02.12**	-32.967	-1.554	0.010
24.11.11	-51.052	-1.995	0.008	**16.02.12**	-4.290	-0.962	0.008
28.11.11	-51.757	-2.026	0.006	**17.02.12**	15.854	-0.517	0.008
28.11.11	-51.735	-2.028	0.010	**20.02.12**	-32.956	-1.585	0.007
30.11.11	-2.567	-0.893	0.011	**20.02.12**	-32.973	-1.585	0.008
02.12.11	-30.825	-1.534	0.009	**22.02.12**	-4.217	-0.954	0.005
02.12.11	-31.133	-1.505	0.007	**22.02.12**	-4.343	-0.934	0.008
06.12.11	-2.220	-0.836	0.007	**24.02.12**	15.506	-0.508	0.006
09.12.11	-51.797	-2.079	0.005	**24.02.12**	15.525	-0.507	0.008
15.12.11	-4.919	-0.915	0.010	**27.02.12**	-32.915	-1.587	0.014
19.12.11	18.535	-0.392	0.009	**29.02.12**	-4.173	-0.989	0.007
19.12.11	18.482	-0.404	0.012				
22.12.11	18.385	-0.437	0.011				
22.12.11	18.462	-0.407	0.004				
04.01.12	15.720	-0.465	0.008				
04.01.12	15.763	-0.476	0.006				
06.01.12	-33.066	-1.586	0.010				
11.01.12	15.874	-0.474	0.007				
11.01.12	15.919	-0.464	0.009				
12.01.12	-33.027	-1.634	0.010				
13.01.12	-4.212	-0.940	0.010				

Table S5.1 *Continued.*

Date	δ_{47}	$\Delta_{47, raw}$	se (internal)
02.07.12	-2.928	-0.948	0.008
02.07.12	-2.879	-0.913	0.014
04.07.12	-33.128	-1.610	0.008
09.07.12	-3.058	-0.930	0.010
09.07.12	-2.760	-0.928	0.007
11.07.12	-33.780	-1.620	0.010
11.07.12	-33.496	-1.637	0.005
13.07.12	13.271	-0.595	0.012
16.07.12	7.008	-0.719	0.009
19.07.12	-3.777	-0.945	0.008
25.07.12	-33.166	-1.659	0.010
30.07.12	15.915	-0.568	0.011
01.08.12	-33.762	-1.651	0.010
01.08.12	-33.670	-1.635	0.009
03.08.12	-3.718	-0.958	0.009
03.08.12	-3.723	-0.934	0.011
09.08.12	-33.517	-1.630	0.009

Slopes and R^2 of heated gas lines used during the time period of calibration.

Date	slope	R^2	intercept	se
03.11.-04.11.11	0.0250	0.9994	-0.837	0.008
06.11.-08.11.11	0.0249	0.9994	-0.836	0.008
09.11-14.11.11	0.0248	0.9994	-0.842	0.009
15.11.11	0.0240	0.9974	-0.838	0.016
16.11.11	0.0238	0.9966	-0.835	0.020
22.11.11	0.0236	0.9951	-0.830	0.021
23.11.-24.11.11	0.0238	0.9956	-0.818	0.019
28.11.11	0.0239	0.9951	-0.815	0.022
29.11.-30.11.11	0.0237	0.9966	-0.812	0.017
01.12.-02.12.11	0.0233	0.9987	-0.819	0.009
19.12.-20.03.12	0.0228	0.9962	-0.846	0.005
22.03.12	0.0220	0.9959	-0.855	0.010
23.03.12	0.0217	0.9987	-0.854	0.006
27.03.12	0.0216	0.9984	-0.847	0.006
29.03.-30.03.12	0.0221	0.9984	-0.858	0.006
03.04.12	0.0218	0.9988	-0.867	0.005
05.04.-10.04.12	0.0223	0.9992	-0.869	0.005
12.04.-13.04.12	0.0224	0.9987	-0.865	0.005
14.04.-15.04.12	0.0223	0.9985	-0.867	0.005
17.04.12	0.0224	0.9988	-0.867	0.005
19.04.12	0.0223	0.9988	-0.868	0.005
30.04.12-09.08.12	0.0225	0.9980	-0.872	0.003

Table S5.1 *Continued.*

δ_{47} and $\Delta_{47, raw}$ values of 25 °C water equilibrated gases considered for determining the ETFs applied to sample data.			
Date	**δ_{47}**	**$\Delta_{47, raw}$**	**se (internal)**
02.09.11	9.378	0.204	0.005
02.09.11	12.769	0.259	0.006
05.09.11	-30.289	-0.853	0.006
08.09.11	-21.235	-0.608	0.009
12.09.11	-30.350	-0.854	0.010
12.09.11	-30.510	-0.832	0.009
14.09.11	7.402	0.130	0.008
14.09.11	7.503	0.129	0.007
20.09.11	16.881	0.376	0.008
30.09.11	7.358	0.127	0.009
22.11.11	20.381	0.447	0.007
24.11.11	11.374	0.237	0.008
10.09.12	-30.025	-0.780	0.007
10.09.12	-21.066	-0.584	0.009
10.09.12	15.858	0.239	0.009
17.09.12	7.353	0.111	0.015
17.09.12	13.460	0.263	0.010
17.09.12	-30.714	-0.714	0.007
Slopes and intercepts of the ETFs used during the period of calibration			
Date	**slope**	**intercept**	
nov-dec 2011	1.1670	0.9952	
jan-feb 2012	1.1521	0.9943	
mar-apr 2012	1.1233	0.9926	
may-jun 2012	1.1094	0.9918	
jul-aug 2012	1.0959	0.9910	

Table S5.2 *Carbonates measured during the analysis interval of the calibration sample*s.

Date	Nr	Sample	SA size	δ_{47}	Δ_{47raw}	Δ_{47abs}	sd	IC HG	IC 25G	m (HG)	$\delta^{13}C$	$\delta^{18}O$
03.11.10	C 800	A.I.(10)	4.6	18.835	0.141	0.680	0.029	-0.84	-0.06	0.0250	2.16	-0.99
	C 801	MuStd	7.6	23.070	0.271	0.707	0.020	-0.84	-0.06	0.0250	1.64	3.50
	C 802	A.I.(15)	4.6	18.938	0.128	0.661	0.029	-0.84	-0.06	0.0250	2.22	-0.93
04.11.10	C 803	A.I.(15)	4.2	18.845	0.151	0.691	0.025	-0.84	-0.06	0.0250	2.18	-1.01
	C 806	NBS 19	4.8	16.794	-0.210	0.329	0.035	-0.84	-0.06	0.0250	1.94	-2.01
06.11.11	C 807	NBS 19	5.2	16.894	-0.185	0.357	0.037	-0.84	-0.06	0.0249	1.95	-1.95
07.11.11	C 808	MuStd	6.2	22.864	0.230	0.668	0.032	-0.84	-0.06	0.0249	1.59	3.73
	C 809	A.I.(10)	4.1	18.877	0.126	0.663	0.025	-0.84	-0.06	0.0249	2.19	-0.60
	C 810	NBS 19	4.5	16.776	-0.216	0.325	0.009	-0.84	-0.06	0.0249	1.94	-2.02
08.11.11	C 811	MuStd	4.4	22.996	0.254	0.692	0.020	-0.84	-0.06	0.0249	1.57	3.85
	C 814	A.I.(15)	4.4	19.125	0.120	0.648	0.020	-0.84	-0.06	0.0249	2.27	-0.44
09.11.11	C 815	A.I.(15)	4.2	18.824	0.137	0.680	0.036	-0.84	-0.06	0.0248	2.21	-0.69
	C 816	NBS 19	5.1	16.788	-0.209	0.335	0.031	-0.84	-0.06	0.0248	1.96	-2.03
	C 817	A.I.(10)	4.3	18.968	0.127	0.663	0.022	-0.84	-0.06	0.0248	2.17	-0.50
10.11.11	C 818	MuStd	5.7	23.000	0.263	0.706	0.034	-0.84	-0.06	0.0248	1.63	3.79
	C 819	A.I.(15)	4.1	18.930	0.135	0.674	0.020	-0.84	-0.06	0.0248	2.22	-0.59
	C 820	NBS 19	7.7	16.965	-0.192	0.349	0.033	-0.84	-0.06	0.0248	1.98	-1.90
11.11.11	C 821	A.I.(10)	6.0	18.943	0.138	0.676	0.034	-0.84	-0.06	0.0248	2.14	-0.51
	C 824	NBS 19	5.2	16.923	-0.227	0.310	0.023	-0.84	-0.06	00248	1.96	-2.23
14.11.11	C 825	MuStd	5.1	22.889	0.227	0.667	0.028	-0.84	-0.06	0.0248	1.62	3.72
	C 826	NBS 19	4.8	16.885	-0.214	0.326	0.025	-0.84	-0.06	0.0248	1.98	-1.96
15.11.11	C 829											
	C 832	MuStd	6.2	23.001	0.251	0.713	0.025	-0.84	-0.06	0.0240	1.59	3.84
16.11.11	C 835	MuStd	5.2	22.665	0.251	0.728	0.030	-0.84	-0.06	0.0238	1.35	3.74
	C 836											
22.11.11	C 839	MuStd	10.4	23.077	0.253	0.724	0.015	-0.84	-0.06	0.0236	1.62	3.88
23.11.12	C 843	MuStd	5.0	23.114	0.277	0.745	0.033	-0.84	-0.06	0.0238	1.64	4.18
	C 844											
	C 846											
	C 848	MuStd	5.6	23.093	0.253	0.718	0.030	-0.84	-0.06	0.0238	1.64	3.88
24.11.12	C 849	MuStd	4.0	23.029	0.267	0.736	0.035	-0.84	-0.06	0.0238	1.62	3.70
28.11.11	C 852											
	C 853	MuStd	6.1	23.053	0.263	0.728	0.018	-0.84	-0.06	0.0239	1.58	3.80
29.11.11	C 856											
	C 857	MuStd	9.8	23.139	0.251	0.717	0.033	-0.84	-0.06	0.0237	1.61	3.74
	C 858											
30.11.11	C 859	MuStd	4.9	23.105	0.282	0.754	0.021	-0.84	-0.06	0.0237	1.63	3.87
	C 862											
01.12.11	C 863	MuStd	4.3	23.059	0.237	0.714	0.016	-0.84	-0.06	0.0233	1.60	3.65
	C 864											
02.12.11	C 865	MuStd	6.9	23.098	0.262	0.741	0.034	-0.84	-0.06	0.0233	1.64	3.93
07.12.11	C 870	MuStd	6.4	23.139	0.286	0.771	0.033	-0.84	-0.06	0.0232	1.62	3.96

Table S5.2 *Continued.*

Date	Nr	Sample	SA size	δ_{47}	Δ_{47raw}	Δ_{47abs}	sd	IC HG	IC 25G	m (HG)	$\delta^{13}C$	$\delta^{18}O$
14.12.11	C 873											
15.12.11	C 874											
16.12.11	C 876											
19.12.11	C 877											
20.12.11	C 880											
21.12.11	C 883											
	C 884											
22.12.11	C 885											
	C 888											
23.12.11	C 889											
03.01.12	C 890											
	C 891	MuStd	8.5	23.022	0.258	0.737	0.031	-0.84	-0.06	0.0228	1.58	3.86
	C 892	NBS 19	5.6	16.936	-0.212	0.361	0.028	-0.84	-0.06	0.0228	1.97	-1.90
04.01.12	C 893	MuStd	8.4	22.674	0.239	0.725	0.030	-0.84	-0.06	0.0228	1.53	3.59
	C 896	NBS 19	8.9	16.968	-0.230	0.338	0.034	-0.84	-0.06	0.0228	2.00	-1.88
	C 897											
05.01.12	C 898	NBS 19	9.3	16.878	-0.207	0.371	0.032	-0.84	-0.06	0.0228	1.99	-1.98
	C 901	MuStd	9.5	23.005	0.238	0.720	0.019	-0.84	-0.06	0.0228	1.59	3.86
	C 902											
06.01.12	C 903											
	C 904											
	C 905	MuStd	7.9	22.994	0.236	0.718	0.026	-0.84	-0.06	0.0228	1.62	3.82
09.01.12	C 906	MuStd	8.0	22.950	0.219	0.713	0.033	-0.84	-0.06	0.0228	1.60	3.81
	C 907	NBS 19	8.0	16.922	-0.239	0.344	0.025	-0.84	-0.06	0.0228	1.99	-1.90
	C 910	A.I.(4)	4.3	22.306	0.193	0.700	0.024	-0.84	-0.06	0.0228	1.50	3.31
10.01.12	C 911	MuStd	4.7	22.904	0.212	0.706	0.031	-0.84	-0.06	0.0228	1.57	3.80
	C 912											
	C 914	A.I.(4)	4.0	22.216	0.187	0.695	0.027	-0.84	-0.06	0.0228	1.51	3.21
	C 915	NBS 19	5.4	16.944	-0.163	0.430	0.032	-0.84	-0.06	0.0228	1.97	-1.94
11.01.12	C 918	MuStd	4.3	23.003	0.212	0.703		-0.84	-0.06	0.0228		-37.60
12.01.12	C 919											
	C 922	MuStd	4.5	22.667	0.209	0.709	0.018	-0.84	-0.06	0.0228	1.51	3.63
13.01.12	C 922	A.I.(4)	4.1	22.350	0.209	0.717	0.033	-0.84	-0.06	0.0228	1.49	3.34
	C 924	A.I.(10)	4.1	18.580	0.102	0.693	0.029	-0.84	-0.06	0.0228	2.02	-0.71
16.01.12	C 925	NBS 19	4.3	16.850	-0.218	0.369	0.035	-0.84	-0.06	0.0228	1.97	-1.97
	C 926	A.I.(4)	4.7	22.278	0.181	0.687	0.023	-0.84	-0.06	0.0228	1.52	3.27
	C 927	CS arag	4.1	-10.328	-0.543	0.709	0.031	-0.84	-0.06	0.0228	-28.41	0.80
17.01.12	C 929	MuStd	6.5	22.955	0.230	0.725	0.015	-0.84	-0.06	0.0228	1.57	3.83
	C 930											
	C 931											
18.01.12	C 934	MuStd	4.3	23.067	0.241	0.735	0.021	-0.84	-0.06	0.0228	1.63	3.88
	C 935	A.I.(15)	4.1	18.867	0.103	0.686	0.025	-0.84	-0.06	0.0228	2.20	-0.61
	C 932	NBS 19	9.0	17.009	-0.233	0.349	0.028	-0.84	-0.06	0.0228	2.04	-1.87
19.01.12	C 936	NBS 19	4.0	16.837	-0.209	0.381	0.037	-0.84	-0.06	0.0228	1.97	-2.02
	C 937											
	C 938											

Table S5.2 *Continued.*

Date	Nr	Sample	SA size	δ_{47}	Δ_{47raw}	Δ_{47abs}	sd	IC HG	IC 25G	m (HG)	$\delta^{13}C$	$\delta^{18}O$
	C 939	A.I.(15)	4.6	18.981	0.106	0.687	0.039	-0.84	-0.06	0.0228	2.26	-0.55
20.01.12	C 940	MuStd	4.5	23.158	0.239	0.731	0.015	-0.84	-0.06	0.0228	1.62	3.97
	C 942											
	C 943	A.I.(4)	4.0	22.250	0.180	0.686	0.029	-0.84	-0.06	0.0228	1.52	3.24
23.01.12	C 944	MuStd	5.8	22.828	0.241	0.741	0.027	-0.84	-0.06	0.0228	1.55	3.72
	C 945											
	C 946											
	C 947	A.I.(10)	4.5	18.905	0.109	0.692	0.020	-0.84	-0.06	0.0228	2.06	-0.44
24.01.12	C 948	MuStd	4.2	23.014	0.233	0.727	0.019	-0.84	-0.06	0.0228	1.60	3.86
	C 949											
	C 950											
25.01.12	C 952	MuStd	6.0	23.024	0.242	0.737	0.034	-0.84	-0.06	0.0228	1.62	3.84
	C 954											
	C 955											
27.01.12	C 956											
	C 958	MuStd	4.2	22.792	0.209	0.705	0.031	-0.84	-0.06	0.0228	1.54	3.72
	C 959											
31.01.12	C 961	MuStd	4.2	23.085	0.233	0.726	0.025	-0.84	-0.06	0.0228	1.63	3.90
	C 962											
02.02.12	C 964	MuStd	5.3	22.991	0.215	0.707	0.014	-0.84	-0.06	0.0228	1.57	3.89
	C 965											
	C 966	MuStd	4.1	23.108	0.210	0.698	0.031	-0.84	-0.06	0.0228	1.59	3.99
03.02.12	C 968	MuStd	4.3	22.753	0.209	0.706	0.023	-0.84	-0.06	0.0228	1.58	3.65
	C 969											
	C 970											
06.02.12	C 974	MuStd	5.0	22.555	0.197	0.698	0.021	-0.84	-0.06	0.0228	1.58	3.46
	C 975											
	C 976											
07.02.12	C 980											
	C 981	MuStd	4.6	22.885	0.221	0.717	0.017	-0.84	-0.06	0.0228	1.65	3.70
	C 982											
	C 983											
	C 984	NBS 19	4.6	16.875	-0.208	0.381	0.039	-0.84	-0.06	0.0228	2.04	-2.03
	C 985											
08.02.12	C 986	MuStd	4.9	22.705	0.225	0.726	0.022	-0.84	-0.06	0.0228	1.60	3.56
	C 989	MuStd	6.0	22.814	0.224	0.722	0.029	-0.84	-0.06	0.0228	1.60	3.67
	C 990											
	C 991											
09.02.12	C 992	NBS 19	4.5	16.713	-0.225	0.365	0.024	-0.84	-0.06	0.0228	1.98	-2.11
	C 993											
	C 996	MuStd	5.6	22.653	0.217	0.719	0.033	-0.84	-0.06	0.0228	1.62	3.51
	C 994											
	C 995											
	C 997											
	C 998											
10.02.12	C 999	MuStd	4.8	22.631	0.208	0.708	0.036	-0.84	-0.06	0.0228	1.56	3.55

Table S5.2 *Continued.*

Date	Nr	Sample	SA size	δ_{47}	Δ_{47raw}	Δ_{47abs}	sd	IC HG	IC 25G	m (HG)	$\delta^{13}C$	$\delta^{18}O$
	C 1000											
	C 1004											
	C 1001											
	C 1002											
	C 1003	NBS 19	5.5	16.959	-0.208	0.379	0.019	-0.84	-0.06	0.0228	2.09	-2.00
13.02.12	C 1005	MuStd	5.1	22.754	0.240	0.742	0.022	-0.84	-0.06	0.0228	1.57	3.67
	C 1006											
	C 1009											
	C 1007											
	C 1008	NBS 19	4.9	16.744	-0.187	0.408	0.015	-0.84	-0.06	0.0228	1.98	-2.12
	C 1010											
	C 1011											
14.02.12	C 1013	MuStd	5.4	22.601	0.226	0.730	0.027	-0.84	-0.06	0.0228	1.62	3.45
	C 1014											
	C 1017											
	C 1015											
	C 1016	NBS 19	4.5	16.853	-0.206	0.383	0.025	-0.84	-0.06	0.0228	2.11	-2.11
	C 1018											
15.02.12	C 1019	MuStd	7.8	22.865	0.226	0.723	0.024	-0.84	-0.06	0.0228	1.64	3.68
	C 1021											
	C 1023											
	C 1020											
	C 1022	NBS 19	4.6	16.561	-0.235	0.358	0.040	-0.84	-0.06	0.0228	1.90	-2.17
	C 1024											
	C 1025											
16.02.12	C 1026	MuStd	7.4	22.910	0.197	0.689	0.031	-0.84	-0.06	0.0228	1.65	3.75
	C 1030											
	C 1032											
	C 1028	NBS 19	4.4	16.750	-0.259	0.325	0.040	-0.84	-0.06	0,0228	2.07	-2.13
	C 1031											
	C 1033											
17.02.12	C 1034	MuStd	4.4	22.529	0.215	0.720	0.023	-0.84	-0.06	0.0228	1.56	3.45
	C 1037											
	C 1036											
	C 1038	NBS 19	4.3	16.798	-0.222	0.366	0.026	-0.84	-0.06	0.0228	2.04	-2.09
	C 1039											
	C 1046	MuStd	4.3	23.037	0.217	0.708	0.019	-0.84	-0.06	0.0228	1.72	3.43
	C 1049											
	C 1050	A.I.(4)	9.0	22.348	0.204	0.712	0.028	-0.84	-0.06	0.0228	1.59	2.91
10.07.12	C 1553	NBS 19	6.7	16.822	-0.251	0.370	0.032	-0.88	-0.06	0.0225	1.98	-2.28
	C 1556	NBS 19	4.9	16.774	-0.270	0.351	0.020	-0.88	-0.06	0.0225	1.98	-2.31
	C 1554	Tridacna	6.6	18.043	0.023	0.640	0.027	-0.88	-0.06	0.0225	1.57	-0.97
	C 1555	Tridacna	4.2	17.931	0.008	0.627	0.026	-0.88	-0.06	0.0225	1.51	-1.02
	C 1557	Tridacna	4.1	18.259	0.166	0.792	0.035	-0.88	-0.06	0.0225	1.58	-0.92
18.7.12	C1583	Carrara	4.7	17.323	-0.241	0.369	0.036	-0.88	-0.06	0.0225	1.96	-1.79

Table S5.2 *Continued.*

Date	Nr	Sample	SA size	δ_{47}	Δ_{47raw}	Δ_{47abs}	sd	IC HG	IC 25G	m (HG)	$\delta^{13}C$	$\delta^{18}O$
	C1584	Tridacna	4.1	18.004	0.015	0.633	0.044	-0.88	-0.06	0.0225	1.49	-0.93
19.7.12	C1585	NBS19	5.7	16.858	-0.248	0.372	0.031	-0.88	-0.06	0.0225	1.99	-2.26
20.7.12	C1587	Carrara	4.5	17.314	-0.259	0.350	0.027	-0.88	-0.06	0.0225	1.97	-1.79
	C1589	NBS19	4.8	15.965	-0.282	0.357	0.030	-0.88	-0.06	0.0225	1.91	-3.02
23.07.12	C1590	Tridacna	4.5	17.897	0.019	0.639	0.017	-0.88	-0.06	0.0225	1.51	-1.05
	C1592	NBS 19	8.3	17.001	-0.246	0.371	0.030	-0.88	-0.06	0.0225	1.99	-2.12
	C1591	CS arag	4.3	-23.006	-0.820	0.729	0.030	-0.88	-0.06	0.0225	31.62	0.68
24.07.12	C1593	Carrara	5.1	17.355	-0.245	0.363	0.039	-0.88	-0.06	0.0225	2.05	-1.83
	C1595	NBS 19	5.7	17.032	-0.248	0.369	0.026	-0.88	-0.06	0.0225	1.98	-2.11
	C1594											
	C1596											
	C1597	Tridacna	4.6	10.739	-0.096	0.690	0.034	-0.88	-0.06	0.0225	0.55	-0.72
25.07.12	C1598	NBS19	4.9	16.921	-0.263	0.354	0.034	-0.88	-0.06	0.0225	1.98	-2.17
	C1599											
30.07.12	C 1606											
	C 1608	NBS 19	5.2	16.565	-0.253	0.374	0.038	-0.88	-0.06	0.0225	1.99	-2.54
	C 1607											
	C 1609											
	C 1611											
31.07.12	C 1612	Tridacna	4.2	16.978	-0.020	0.620	0.027	-0.88	-0.06	0.0225	1.46	-1.86
	C 1613	CS arag	4.1	-17.621	-0.714	0.712	0.027	-0.88	-0.06	0.0225	30.21	-0.69

6 Clumped isotope analysis applied to Silurian carbonates (Gotland/Sweden): deciphering both the alteration degree of fossil brachiopod shells and diagenetic processes

Ulrike Wacker[1], Jens Fiebig[1,2], Axel Munnecke[3], Michael M. Joachimski[3]

[1] Institute of Geosciences, Goethe-University, Altenhöferallee 1, 60438 Frankfurt am Main, Germany

[2] Biodiversity and Climate Research Center, Senckenberganlage 25, 60325 Frankfurt am Main, Germany

[3] GeoZentrum Nordbayern, University of Erlangen-Nürnberg, Schloßgarten 5, 91054 Erlangen, Germany

To be submitted

Abstract Clumped and bulk isotopic compositions of a set of brachiopod shells and the diagenetic phases of the inner fillings of the fossils were analyzed. Sample material derived from the Silurian succession of Gotland/Sweden which is known for a very high preservation quality including both ultrastructures and chemical compositions. Prior isotopic analyses the studied shells were investigated by cathodoluminescence (CL) and scanning electron microscopy (SEM); furthermore Mn, Fe and Sr concentrations were measured.

We have observed a variable preservation within single shells: in large areas the fossils are non-luminescent and low Mn and Fe, as well as high Sr concentrations do not indicate diagenetic alteration of shell calcite. A different picture has been obtained from ultrastructural investigations (SEM): a patchwork of pristine preserved secondary layer fibres and recrystallized or amalgamated structures indicates that the shells were affected by diagenesis. The increase of altered fibres within single samples correlates with higher clumped isotope temperatures. Because the lowest T(Δ_{47}) values of ~28 to 33 °C are reconstructed from the best preserved carbonate aliquots, we evaluate these values to reflect maximum temperatures of Silurian ocean water. Based on these samples a maximum oxygen isotopic composition for marine tropical shallow water of ca. –1‰ is determined for the studied time interval.

The clumped isotope temperatures determined from the analyzed brachiopod shells vary from ca. 30 to 90 °C. Most values plot between 40 and 60 °C indicating that measured carbonate aliquots contained various amounts of altered material. The observed correlation between Δ_{47} and $\delta^{18}O$ values indicates that the shells altered at low water–rock ratios. The $\delta^{18}O$ values of the fossils are, therefore, evaluated to reflect pristine ocean water compositions. The T(Δ_{47}) range determined for both the micritic phases and for the sparitic cements of the inner fillings of the fossils are similar to the range of temperatures estimated for the brachiopod shells. We assume that the sparitic cements precipitated during distinct diagenetic stages. They crystallized under fluid-buffered conditions from water of variable elemental and isotopic

compositions. A weak correlation between Δ_{47} and $\delta^{18}O$ values of the micritic phases implies that they lithified under rock-buffered conditions; nevertheless, in comparison to the conditions during brachiopod shell alteration, a larger fluid–rock ratio prevailed during cementation of the sediments.

6.1 Introduction

The evolution of the Earth's climate has been intensively studied because the knowledge of mechanisms that caused past climate changes can help to better predict the climate of the future. Important information has been obtained from reconstructions of ancient ocean water temperatures. Chemical compositions of minerals provide insights to past climate conditions. The oldest paleothermometer relies on the oxygen isotopic composition ($\delta^{18}O$) of minerals. This proxy has been most widely applied to carbonates to reconstruct ancient water temperatures. The fractionation of the oxygen isotopes between a crystal and the water from which the crystal grows, depends on temperature and preserves information about paleoclimate conditions (Urey, 1947). Nevertheless, the validity of the $\delta^{18}O$ paleothermometer is limited because temperature estimations require the knowledge of the oxygen isotopic composition of the water. Based on several models it has been suggested that the mean global $\delta^{18}O$ value of the ocean has been buffered to (0 ± 1)‰ (V-SMOW) since the Phanerozoic by high and low temperature alteration of oceanic crust: this hypothesis relies mostly on studies on ophiolithes (Muehlenbachs and Clayton, 1976; Gregory and Taylor, 1981; Gregory, 1991; Knauth and Roberts, 1991; Muehlenbachs, 1998; Muehlenbachs et al. 2003; Turchyn et al. 2013). However, other models have indicated that the relative proportion of hydrothermal alteration processes of oceanic crust might have varied throughout Earth's history (Veizer et al., 1999; Kasting et al., 2006; Jaffrés et al., 2007). Due to an increase of hydrothermal penetration depths and pelagic sedimentation rates at midocean ridges, ocean water might have become enriched in ^{18}O since the Mesozoic interval (e.g., Collins et al., 2003). Furthermore, short variations caused by ice-formations and regional differences (e.g., monsoonal influences) have also an effect on the oxygen isotopic composition of seawater (Frakes et al., 2005). The extent of global ice storage has varied through time and cannot exactly be constrained from the geological record. The oxygen isotope paleothermometer is, therefore, not fully reliable as long as the $\delta^{18}O$ value of ancient seawater is unknown. Nevertheless, a great number of $\delta^{18}O$ records for the Phanerozoic time interval have been measured for sediments, sedimentary rocks and their components. The general trend shows a decrease of $\delta^{18}O$ values with increasing age (Veizer et al., 1999). This might indicate a secular change of the oxygen isotopic composition

of ocean water (Veizer et al., 1999; Jaffrés et al., 2007). Furthermore, the $\delta^{18}O$ records have shown several shifts which have been interpreted to reflect glaciation events (e.g., Marshall et al., 1992) or salinity changes (e.g., Bickert et al., 1997). To unravel these mechanisms additional proxies have been developed with time that enable to constrain water temperatures independently. The youngest method is the carbonate clumped isotope thermometer (e.g., Ghosh et al., 2006a; Eiler, 2011). The abundance of clumping between the heavy isotopes ^{13}C and ^{18}O in carbonates is controlled by the growth temperatures of the crystals (e.g., Ghosh et al. 2006a; Dennis and Schrag, 2010; Tripati et al., 2010; Thiagarajan et al., 2011; Henkes et al., 2013; Zaarur et al., 2013; Wacker et al., 2014). Therefore, temperature information of past ocean water may have been preserved in the clumped isotopic compositions (Δ_{47}) of minerals. A combination of this novel proxy with the conventional $\delta^{18}O$ paleothermometer allows to estimate both the temperature during mineral growth and the oxygen isotopic composition of the water from which the crystal precipitated. As a consequence this approach offers great potential to distinguish between variations in ocean water temperature and seawater $\delta^{18}O$.

The "$\delta^{18}O$ problem" also applies to the interpretation of Silurian oxygen isotope ratios measured for the succession of sedimentary rocks exposed on Gotland/Sweden (e.g., Wenzel and Joachimski, 1996; Bickert et al., 1997; Samtleben et al., 2001; Munnecke et al., 2003). Similar $\delta^{18}O$ records were determined for well-preserved brachiopod shells composed of low magnesium calcite (Wenzel and Joachimski, 1996; Bickert et al., 1997) and carboniferous mudstones (Munnecke et al., 2003), as well as for phosphatic conodonts (Wenzel et al., 2000). This conformity might indicate that diagenetic alteration did not affect the sampled material. The records show several shifts in the oxygen isotopic composition of more than 2.5‰ (Wenzel and Joachimski, 1996; Bickert et al., 1997). If these shifts would have been caused by temperature only variations of about 12 °C (Bickert et al., 1997) and 18 °C (Wenzel and Joachimski et al., 1996) would have occurred in Silurian shallow water environments of the tropics. These variations are unrealistically high considering that 1 to 2 °C changes were reconstructed for tropical shallow waters during the last glacial–interglacial transition of the Quaternery (CLIMAP, 1981). In addition, until now no evidence for glaciated poles have been found for the studied Silurian time sequence. The published carbon isotope records are characterized by variations as well. The largest positive shift exhibits an increase in $\delta^{13}C$ values by 9‰ (Wenzel and Joachimski, 1996, Bickert et al., 1997). In addition, the $\delta^{18}O$ and $\delta^{13}C$ records correlate. They are interrelated to sea level and oxygenation states of deeper water.

Furthermore, minor extinction events in benthic and pelagic marine taxa were asocciated with the oxygen and carbon isotopic excursions (Munnecke et al, 2003).

Wenzel and Joachimski (1996) proposed a model in which the variations in the $\delta^{18}O$ and $\delta^{13}C$ values correspond to changes in sea levels. According to their interpretation a thermohaline circulation caused oxygenation of the bottom waters of the basins during sea level lowstands. Nutrients provided to the surface waters promoted an increase of the primary productivity. These conditions are recorded by high $\delta^{18}O_{carbonate}$ and $\delta^{13}C_{carbonate}$ values. In contrast, high sea levels applied to the times characterized by low carbon and oxygen isotope values. Warm saline deep waters caused an oxygen deficiency as well a storage of ^{18}O in the basins. Reduced circulations resulted in a decrease of primary productivity in the surface waters. Bickert et al. (1997) also suggested that the $\delta^{18}O$ and $\delta^{13}C$ variations determined for the Silurian succession of Gotland reflect changes in the oceanic circulation pattern. However, in contrast to Wenzel and Joachimski (1996), they proposed that salinity changes promoted the observed shifts in the oxygen and carbon isotopic records. Tropical humid periods were characterized by an estuarine circulation and up-welling of CO_2-rich deepwater that was depleted in ^{13}C. These periods were interrupted by intervals of arid climate in which downwelling of oxygenated surface waters occurred (anti-estuarine circulation).

Clumped isotope analysis was already addressed to Silurian carbonates to reconstruct both ocean water temperatures and the oxygen isotopic composition of seawater (Came et al., 2007; Finnegan et al., 2011; Cummins et al., 2014). The fossil brachiopod shells measured in the studies of Came et al. (2007) and Finnegan et al. (2011) derived from Anticosti Island (Canada) representing Early Silurian deposits (Telychian and Rhuddfordian/Aeronian, respectively). These tropical, shallow water carbonates are stratigraphically older than the deposits exposed on Gotland. In both studies an ocean water temperature of ~35 °C and a $\delta^{18}O$ value of ambient seawater of ca. –1‰ were determined. Cummins et al. (2014) analyzed brachiopod shells and rugose corals from the Telychian to Sheinwoodian that derived from the lower stratigraphic succession exposed on Gotland; their sample set includes also bryozoans, crinoids, gastropods and ostracods, as well as micritic and sparitic cements. They estimated water temperatures of ~33 °C and a $\delta^{18}O$ value of the ocean of about –1‰ from well-preserved samples. Thus, clumped isotope temperatures determined in the studies of Came et al. (2007), Finnegan et al. (2011) and Cummins et al. (2014) indicate that – compared to todays' conditions – tropical shallow water was relatively warm and that the oxygen isotopic composition of the ocean water was similar in the Early Silurian. Although these previous studies received consistent results, the influence of diagenetic alteration affecting Δ_{47} compositions of the analyzed carbonates

must be evaluated critically. According to Cummins et al. (2014) the original clumped isotopic composition of the studied fossils from Gotland was partly reset due to recrystallization. However, this is not conform with conclusions which were proposed in the literature (e.g., Wenzel and Joachimski, 1996; Bickert et al., 1997; Samtleben et al., 2001): fossil brachiopod shells from Gotland have been described to be well-preserved both ultrastructurally and geochemically. Furthermore, Finnegan et al. (2011) could reconstruct temperature and $\delta^{18}O$ variations of the ocean water during the Hirnantian glaciation applying clumped isotope analysis to Ordovician brachiopod shells collected on Anticosti Island. In contrast, Cummins et al. (2014) could not decipher a secular change in either water temperatures or the oxygen isotopic composition of ambient seawater.

In this study we applied clumped isotope analysis to Silurian brachiopod shells from Gotland and to the inner fillings of the fossils. These are micritic phases composed of sedimentary components and diagenetic cements. Furthermore, sparitic phases (sparitic cements) associated with several fossils were analyzed. Our main purpose was to evaluate to what extent the clumped isotopic composition of the shell material is indicative for pristine conditions that prevailed during growth of the organisms. In addition, previous assumptions concerning diagenetic histories of preserved Silurian fossils of Gotland published by Cummins et al. (2014) were examined. The preservation state of the studied fossils were identified using cathodoluminescence (CL) and scanning electron microscopy (SEM), as well as trace element concentrations. We tested whether the combination of these conventional tools are reliable indicators for the identification of the degree of preservation of the original clumped isotopic compositions of ancient carbonates. We, furthermore, proved the suggestions of Came et al. (2007), Finnegan et al. (2011) and Cummins et al. (2014) regarding absolute temperatures of tropical shallow water and $\delta^{18}O$ values of the ocean during the Silurian period.

6.2 Materials and methods

6.2.1 Sample material

The studied sample set includes 92 fossils derived from five stratigraphic units and 26 outcrops on the Island of Gotland/Sweden (Fig. 6.1). The fossil material derived from the collection of Axel Munnecke which has been assembled over several years. The sedimentary rocks exposed on Gotland describe an alternation of limestones, marls and, rarely, siliciclastics. For further characterization of the strata and the depositional conditions of the different beds we refer to detailed descriptions published in different studies (e.g., Jeppsson, 1990; Samtleben et al., 2001; Munnecke et al., 2003; Calner et al., 2004a; b, and references therein).

The investigated brachiopod shells belong to the extinct order Atrypida. Atrypids are highly abundant in the sedimentary succession exposed on Gotland. The shells are impuncate and consist of two layers: the thin granular primary layer (10 to 30 μm) and the fibrous secondary layer which is up to 2 mm thick. Fibre orientation of ribbed forms radiate from the apex. For most atrypids growth lamellae are common. Some orders are characterized by frills, which are long extensions of the primary and secondary layer. Frills are often broken during ontogeny or transport after death. At the anterior margin and laterally, frills are more easily preserved, which results in double or triple shell width.

6.2.2 Microscopic analyses

Longitudinal sections of brachiopod shells and the asocciated fillings were investigated for their chemical preservation using cathodoluminescence microscopy (Technosyn 8200 MK II/cold cathode). Furthermore, 34 fossils of the same sample set were screened by scanning electron microscopy (CamScan4) to identify the degree of alteration of ultrastructures. For this purpose we prepared transverse sections (Samtleben et al., 2001). In addition, for eight fossils transverse sections along the ontogenetic transects were studied to get a better overview of the preservation state of the entire shell.

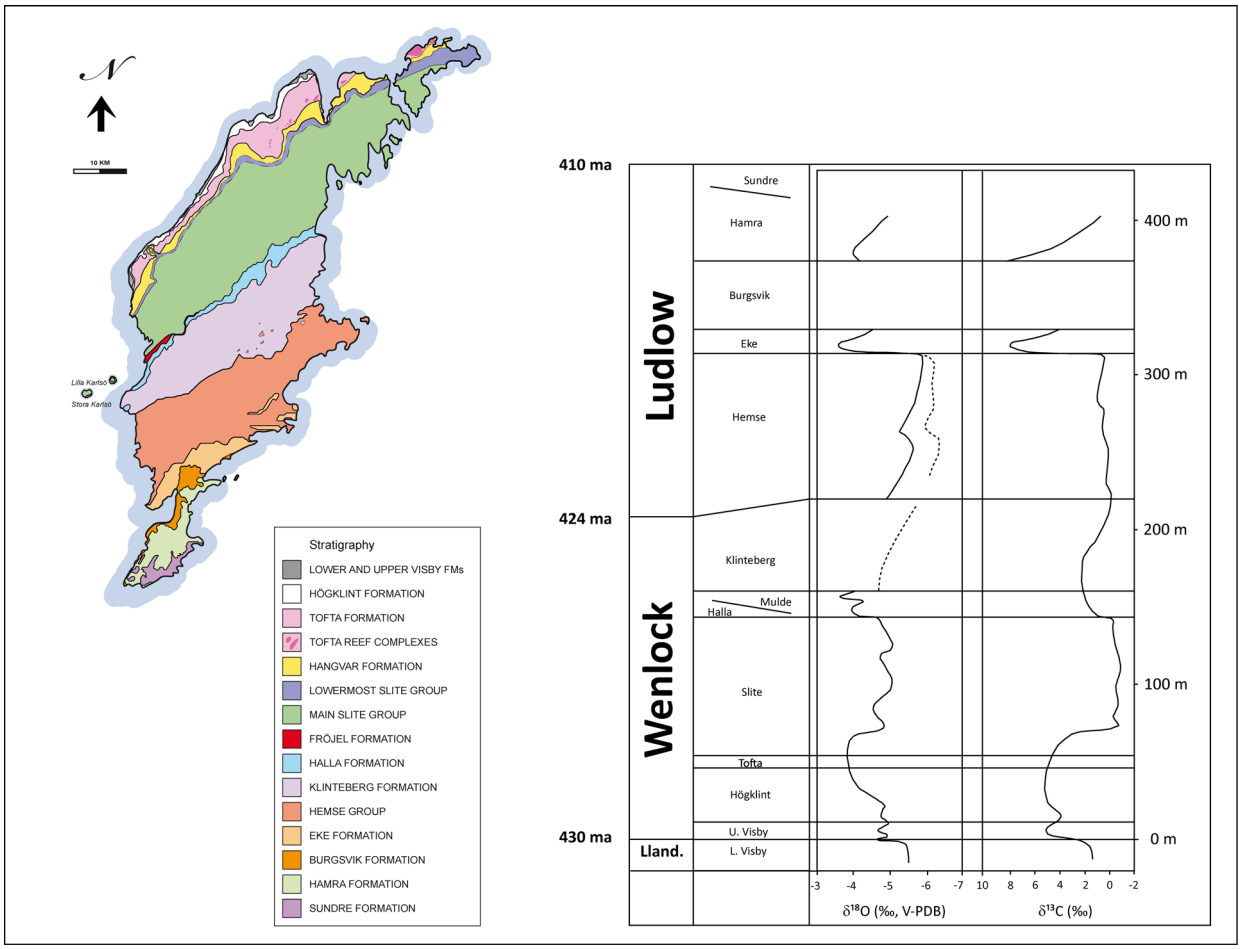

Figure 6.1 *Stratigraphic map of Gotland (modified after Calner et al., 2004). Furthermore, trends of the oxygen and carbon isotope curves determined for brachiopod shells preserved within the sedimentary rocks of Gotland (after Bickert et al., 1997). Large variations of ~2‰ and ~8‰ for $\delta^{18}O$ and $\delta^{13}C$ values were observed, respectively. The isotopic excursions of both compositions correlate, providing evidence that the shifts in oxygen and carbon isotope ratios were triggered by the same mechanisms.*

6.2.3 Sample material for elemental and isotopic analysis

33 brachiopod shells from the studied sample set were selected for clumped isotope analysis. The middle parts of the valves were sampled using either a dental drill or a scalpel. Material from the innermost area of the shells was not sampled. Furthermore, we avoided to include (1) primary layer calcite (outer shell layer) of the fossils, which is often preserved for brachiopod shells from Gotland, but which is recrystallized, and (2) matrix of the surrounding rocks: therefore, the upper surface of the fossils was removed using a scalpel. Since clumped isotope analysis requires a relatively large sample size (>4 mg) most samples were not replicated. Only

for nine shells 2 or 4 replicate measurements were made. Furthermore, for 17 samples selected areas were analyzed to study the influence of diagenetic alteration on the Δ_{47} compositions of the fossils. Additionally, we measured material from the inner fillings which are associated with the shells. Samples were taken from the micritic phases of 21 fossils. In addition, cements of 13 fossils were analyzed for their Δ_{47}, $\delta^{18}O$ and $\delta^{13}C$ compositions. From four samples large sparitic cements (diametre of about 0.5 mm) from the centre of the fossils were isolated and measured. However, for most samples we could not avoid to integrate mixtures of pristine and altered structures to obtain enough material for clumped isotope analysis.

Carbonate samples were digested at 90 °C using a common acid bath connected to an extraction line (Wacker et al., 2013). H_3PO_4 concentrations exceeded 106%. Reaction time was 20 minutes, the reaction process was monitored by a pressure control. Evolved CO_2 was immediatelly removed from the acid: during the digestion the gas was frozen in a trap cooled with liquid nitrogen, after passing a water trap held at –80 °C. Afterwards, analyte CO_2 was cleaned (1) using gas-chromatography to remove contaminants and (2) cryogenically to avoid secondary re-equilibration with water. Detailed preparation protocols are described in Wacker et al. (2013, 2014). On each day of analyses the samples were interspersed with standard materials (NBS 19 and the internal standard *A. islandica* – homogenized shell material of an aragonitic cold water bivalve). The standards werde prepared similarly like the samples.

6.2.4 Analyses of trace element concentrations

Concentrations of Mn, Fe and Sr of 31 brachiopod shells, 28 samples of the micritic phases and 19 sparitic cements were analyzed. Carbonate aliquots (284–295 μg) were taken from the homogenized sample material prepared for clumped isotope analysis. Measurements were conducted on a iCAP 6000 (Thermo Scientific^{TM}) ICP–OES at the Goethe University/Frankfurt with a combined radial and axial optical configuration. Spectral lines measured in axial mode were Al 167.07, Ba 455.40, Co 228.62, Fe 238.20, Mg 280.27, Mn 257.61, Ni 221.65, S 182.03, Ti 334.94, Y 224.31, Y 320.33, Zn 202.55, Zn 213.86, in radial mode Ca 315.89, Li 670.78, Mg 279.53, Na 589.59, Sr 421.55, Y 371.03. Calibration was done as intensity ratios using Y as an internal standard. Element concentrations were normalized to the ECRM 752-1 limestone standard (see also Greaves et al., 2005).

6.2.5 Isotopic analysis

The samples were analyzed between November 2011 and June 2012 (Table S6.2 in Supplementaries). Clumped isotope analysis was performed using a MAT 253 gas source isotope ratio mass spectrometer (Thermo Fisher Scientific, Bremen, Germany) at the Goethe University Frankfurt. The instrument is equipped with eight Faraday cup collectores with six of them being used to detect m/z 44 to 49 simultaneously. Measurements were carried out via the dual inlet system: both CO_2 sample gas and reference gas (Oztech, Safford, AZ, USA; $\delta^{18}O$ = 25.01‰ vs. V-SMOW; $\delta^{13}C$ = –3.63‰ vs. V-PDB) were set to (16,000±150) mV for m/z 44. The total analysis time of a sample gas was ca. 3 h. Measurements were composed of ten acquisitions consisting of ten cycles each (ion integration time 20 s), with peak centering, background determination and pressure adjustments before each acquisition. Δ_{47} values are reported on the absolute scale (Dennis et al., 2011) following the protocol described in Wacker et al. (2013). (1) Each week CO_2 of three different isotopic compositions equilibrated to 1000 °C ("heated gases") were measured to monitor changes of the non-linearity of the mass spectrometer. (2) CO_2 equilibrated with water at 25 °C was analyzed to identify the empirical transfer function (ETF). Water equilibrated gases were measured before and after the interval of analyses only. However, no significant changes were determined regarding the intercept of the line received in a plot of δ^{47} versus Δ_{47}. Heated gas and 25 °C gas data, as well as ETFs are presented in Table S6.1 (Supplementaries). To make Δ_{47} values comparable to clumped isotopic compositions measured for carbonates digested at 25 °C we applied a $\Delta_{47}{}^{*}{}_{25-90}$ value of +0.069‰ (Guo et al., 2009) to our data. This is the theoretical difference in acid fractionation factores between digestions at 90 and 25 °C. The $\Delta_{47}{}^{*}{}_{25-90}$ value of +0.069‰ was confirmed by experimental results (Wacker et al., 2013).

6.2.6 T(Δ_{47}) and $\delta^{18}O_w$ estimations

For clumped isotope temperature (T(Δ_{47})) calculations we refer to the calcite calibration of the clumped isotope thermometer which was determined in our laboratory (Wacker et al., 2014). Oxygen isotope ratios for ambient water ($\delta^{18}O_w$) were calculated applying the fractionation between water and calcite of Kim and O'Neil (1997), using the temperature of crystallization reflected by Δ_{47} and the measured $\delta^{18}O_{carbonate}$ value.

6.3 Results

Δ_{47}, $\delta^{18}O$ and $\delta^{13}C$ values and their standard errors, as well as trace element concentrations of the sampled brachiopod shells and the diagenetic phases are shown in Table 6.1. Furthermore, $T(\Delta_{47})$ and $\delta^{18}O_w$ estimates are included. Heated gas and water equilibrated gas data are provided in Table S6.1 (Supplementaries). Δ_{47}, $\delta^{18}O$ and $\delta^{13}C$ values of internal standard materials and samples are reported in Table S6.2 (Supplementaries). The mean Δ_{47} value of NBS 19 obtained during the interval of analysis is 0.373 ± 0.003‰ (n = 52). It corresponds to the "accepted" value of 0.380 ± 0.017‰ (1σ standard deviation) proposed by Dennis et al. (2011) considering a $\Delta_{47}{}^{*}{}_{25-90}$ value of +0.069‰. Another internal standard *A. islandica* (aragonitic bivalve) averaged to 0.723 ± 0.002‰ (n = 60), which is almost identical to our long term average of 0.715 ± 0.002‰ (1σ se, n = 80).

Table 6.1 *Geochemical data measured for the shells (B), micritic phases (M) and sparitic cements (S): $\Delta_{47,\ abs}$ ± se (in ‰), $\delta^{13}C$, $\delta^{18}O$ (in ‰ deviation vs. V-PDB) and $\delta^{18}O_w$ ± se (in ‰ deviation vs. V-SMOW). T ± se are given in °C, Mn, Fe and Sr concentrations in ppm; n is the number of replicated analysis made for homogenized material.*

Sample		n	$\Delta_{47,\ abs}$ *)	T	$\delta^{13}C$	$\delta^{18}O$	$\delta^{18}O_w$	Mn	Fe	Sr
Petsarve 14										
B	**98-47h**	2	0.602± 0.0004	58±0.3	8.29	-2.82	5.59±0.04	77	249	1762
	98-47q	1	0.622± 0.006	47±3	8.36	-3.17	3.35±0.5	102	421	2022
								96	220	1689
	98-45f	1	0.566± 0.010	79±7	8.51	-2.84	8.91±1.0	113	167	1524
								209	478	1419
								159	326	1455
	98-47m	1	0.584± 0.009	68±5	7.38	-3.88	6.13±0.8	117	214	1666
	98-47o (trace)	1	0.600± 0.010	58±6	7.80	-2.86	5.65±0.9			
	98-47o (CT)	1	0.629± 0.010	44±5	8.66	-2.74	3.24±0.9	64	113	1666
M	**98-47h M1**	1	0.601± 0.008	58±4	9.41	-4.96	3.45±0.8	481	3075	351
	98-47h M2	1	0.631± 0.008	43±4	9.49	-4.27	1.48±0.7			
	98-47o M1	1	0.604± 0.010	56±5	9.20	-5.05	3.07±0.9	219	2127	775
	98-47o M2	1	0.601± 0.009	58±5	9.13	-4.74	3.67±0.8			
	98-47p M	1	0.569± 0.009	77±6	9.10	-6.07	5.37±0.9			
	98-47m M							822	3155	181
	98-45f M							441	1766	864
								457	1824	1011
	98-47l M							246	1984	1026
	98-45q M							259	2144	1045
S	**98-47h S**	1	0.594± 0.013	62±7	5.73	-10.40	-1.38±1.1			
	98-47q S1	1	0.587± 0.012	66±7	6.32	-11.22	-1.57±1.2	1260	3213	77
	98-47q S2	1	0.574± 0.008	74±5	6.22	-10.22	0.68±0.8			
	98-47p S	1	0.595± 0.010	61±6	6.47	-9.29	-0.35±0.9			
	98-47m S							708	3290	224
	98-47l S							738	1575	127

Table 6.1 *Continued.*

	Sample	n	$\Delta_{47, abs}$ *)	T	$\delta^{13}C$	$\delta^{18}O$	$\delta^{18}O_w$	Mn	Fe	Sr
Kullunde 6										
B	**98-49b**	1	0.614± 0.010	51±5	8.43	-2.59	4.64±0.9	75	134	1543
B	**Kullu6-4 1**	1	0.548± 0.013	92±9	8.87	-2.96	10.62±1.3	91	305	1833
B	**Kullu6-4 2**	1	0.590± 0.007	64±4	8.85	-2.61	6.88±0.7			
M	**98-49b M**	1	0.593± 0.009	62±5	8.08	-6.95	2.17±0.8	457	1619	925
M	**Kullu6-4 M**	1	0.617± 0.008	50±4	8.67	-6.37	0.61±0.7	357	2760	1131
S	**98-49b S1**	1	0.565± 0.009	80±6	5.75	-10.06	1.77±0.9	1022	1643	88
S	**98-49b S2**	1	0.608± 0.006	55±3	4.66	-11.31	-3.52±0.5	999	2467	469
Skarnvik 1										
B	**97-12**	2	0.632± 0.002	42±1	-3.16	-6.78	-1.14±0.2			
B	**97-12 CT**	1	0.630± 0.008	43±4	-0.89	-5.98	-0.11±0.7	40		1595
M	**97-12 M**	1	0.604± 0.009	56±5	0.28	-5.55	2.61±0.8	176	1043	392
Tegelbruk 1										
B	**26-1b(1)**	1	0.605± 0.008	56±4	1.94	-4.67	3.44±0.7			
B	**26-1b(2)**	1	0.620± 0.006	48±3	2.26	-4.39	2.30±0.6	30		1885
B	**26-1b(3)**	1	0.652± 0.008	33±4	2.07	-4.68	-0.71±0.7			
B	**26-1b(4)**	1	0.646± 0.008	36±4	1.98	-4.24	0.26±0.7			
B	**26-1a(2)**	1	0.603± 0.008	57±4	1.16	-4.79	3.47±0.7			
B	**26-1a(3)**	1	0.624± 0.009	46±5	1.65	-4.56	1.78±0.8	20	134	2206
B	**26-1a(4)**	1	0.622± 0.007	47±3	1.85	-4.32	2.26±0.6			
M	**26-1a(1) M**	1	0.613± 0.006	52±3	2.34	-4.32	3.03±0.6	831	12027	1378
M	**26-1a M**	1	0.643± 0.008	37±4	2.41	-4.32	0.39±0.7			
M	**26-1b(3) M**	1	0.651± 0.009	34±4	1.34	-4.38	-0.30±0.8	1005	20000	1413
M	**26-1b M**	1	0.611± 0.011	53±6	1.33	-4.13	3.40±1.0			
S	**26-1b S1**	1	0.623± 0.009	47±4	2.22	-5.42	1.05±0.8	781	7648	1235
S	**26-1b S2**	1	0.598± 0.009	60±5	2.23	-5.94	2.79±0.8			
S	**26-1a S**							769	4399	746
Diupvik 1										
B	**25-1a 1**	1	0.599± 0.012	59±7	1.91	-4.15	4.48±1.1	19	80	1877
B	**25-1a 2**	1	0.608± 0.009	54±5	1.98	-3.96	3.87±0.8			
B	**Diu1**	1	0.590± 0.010	64±5	2.02	-4.51	4.92±0.9	66	399	1674
B	**Diu2**	1	0.602± 0.010	58±5	1.87	-3.84	4.51±0.9	74	561	1832
B	**Diu3**	1	0.663± 0.010	28±4	1.82	-3.43	-0.36±0.8	22	137	1694
B	**Diu4a**	1	0.598± 0.006	60±4	1.62	-4.06	4.63±0.6	59	376	1982
B	**Diu4p**	1	0.608± 0.006	54±3	1.93	-3.99	3.82±0.6			
B	**Diu5**	2	0.574± 0.002	74±1	1.61	-3.83	7.16±0.2			
B	**Diu5**	2	0.625± 0.003	45±2	1.82	-3.75	2.51±0.3			
B	**Diu5 CT**	1	0.622± 0.008	47±4	1.84	-3.81	2.75±0.7	83	203	1809
B	**Diu6 1**	1	0.577± 0.010	73±6	1.98	-3.69	7.05±1.0	116	292	1884
B	**Diu6 2**	1	0.612± 0.006	52±1	1.85	-3.87	3.57±0.5			
B	**Diu7**	2	0.566± 0.001	79±6	1.51	-4.02	7.74±0.1	41		2026
B	**Diu7 CT**	1	0.638± 0.012	39±5	1.71	-4.19	0.96±1.1	47	75	1682
B	**Diu8(1p)**	1	0.603± 0.010	57±5	1.63	-3.39	4.88±0.9	81	158	1833
B	**Diu8(2)**	1	0.609± 0.009	54±3	1.76	-3.73	3.96±0.9			
B	**Diu8(3)**	1	0.599± 0.006	59±4	1.63	-4.01	4.61±0.6			
B	**Diu8(4)**	1	0.586± 0.006	67±3	1.87	-3.71	6.11±0.6	86	168	1756
B	**Diu8(5)**	1	0.642± 0.006	38±7	1.81	-4.08	0.76±0.5			
B	**Diu8(6)**	1	0.561± 0.011	83±5	1.78	-3.93	8.37±1.0			
B	**Diu8(7)**	1	0.583± 0.009	69±4	1.86	-4.07	6.08±0.8	102	217	1749
B	**Diu8(8)**	1	0.583± 0.007	69±5	1.90	-4.00	6.13±0.6			
B	**Diu8(9.1)**	1	0.599± 0.009	59±5	1.82	-3.84	4.79±0.9			
B	**Diu8(9.2)**	1	0.624± 0.011	46±6	1.78	-4.25	2.13±1.0	62	150	1921
B	**Diu8 CT**	1	0.602± 0.011	57±1	1.91	-4.00	4.32±1.0	94	136	1830
B	**Diu 9 CT**	4	0.632± 0.002	42±1	2.13	-4.15	1.52±0.2	100	633	1969
								92	484	1909
B	**25-1b**	1	0.614± 0.008	51±4	1.67	-4.28	3.00±0.7	58	580	1730

Table 6.1 *Continued.*

	Sample	n	$\Delta_{47,\ abs}$ *)	T	$\delta^{13}C$	$\delta^{18}O$	$\delta^{18}O_w$	Mn	Fe	Sr
	25-1a M							763	1643	676
	Diu6 M	1	0.604± 0.011	57±6	2.99	-5.41	2.76±1.0	346	3091	382
	Diu7 M	1	0.618± 0.010	49±5	-3.13	-4.73	2.21±0.9	692	3721	504
	Diu8 M	1	0.620± 0.008	48±4	2.56	-4.31	2.45±0.7	417	5063	802
	Diu5 M	1	0.609± 0.010	54±5	2.33	-4.22	3.46±0.9	562	6093	991
M	**Diu3 M**	1	0.619± 0.005	48±3	2.36	-3.95	2.84±0.5	619	6449	924
	Diu1 M	1	0.641± 0.004	38±2	1.99	-3.86	1.07±0.3	982	10463	1056
	25-1b M	1	0.635± 0.008	41±4	1.83	-4.69	0.73±0.7	990	15195	868
	Diu2 M							858	2353	1186
	Diu7 M							930	3521	499
	Diu 9 CT M							242	3074	287
	25-1a S							1251	2743	303
	Diu2 S	1	0.600± 0.006	59±4	2.35	-3.76	4.78±0.6	654	1944	272
	Diu8 S	1	0.603± 0.009	57±5	2.40	-6.24	2.00±0.9	790	6880	811
S	**Diu8 CT S**	1	0.586± 0.009	67±5	2.48	-6.44	3.40±0.9	409	2770	832
	25-1b S	1	0.605± 0.007	56±4	1.85	-9.98	-1.95±0.6	1071	3281	115
	Diu5 S							976	2816	198
	Diu1 S							688	2683	289
Valbytte 1, 6										
	Val(1)-1	1	0.608± 0.009	54±5	-0.43	-4.22	3.56±0.8	39		1798
B	**Val(6)-4**	2	0.570± 0.004	77±3	-0.16	-4.80	6.57±0.4			
	Val(6)-4 CT	1	0.565± 0.007	80±5	-0.28	-4.76	7.07±0.7	41		1233
M	**Val(1)-1 M**	1	0.615± 0.009	51±4	-0.53	-4.48	2.71±0.8	281	1403	425
	Val(6)-4 M	1	0.627± 0.006	44±3	-0.90	-4.08	2.00±0.5	258	962	213
S	**Val(1)-1 S**	1	0.584± 0.006	68±4	-0.54	-10.99	-1.00±0.6	904	2102	106
	Val (6)-4 S	1	0.638± 0.007	39±3	0.16	-3.99	1.17±0.6	441	834	698
Follingbo 8										
B	**21-1d(2)**	1	0.610± 0.007	53±4	-0.64	-4.71	2.88±0.6	16		1976
M	**21-1d M**	2	0.619± 0.002	49±1	-1.20	-5.28	1.57±0.2	343	1962	248
Slitebrottet 1										
	81-1f	2	0.608± 0.008	57±7	-0.57	-4.61	3.59±1.1			
	81-1d(1)	1	0.615± 0.012	51±6	-0.87	-5.60	1.61±1.1	26		2297
	81-1d(3)	1	0.598± 0.008	60±4	-0.73	-4.91	3.83±0.7			
	81-1d(4)	1	0.632± 0.009	42±4	-0.59	-4.81	0.83±0.8			
B	**81-1e1**	1	0.620± 0.009	48±4	-0.38	-4.87	1.89±0.8	33		1690
	81-1e2	1	0.573± 0.008	75±5	-0.33	-4.35	6.76±0.8			
	81-1e3	1	0.604± 0.013	56±7	-0.31	-4.70	3.44±1.2			
	81-1f1 (recryst.)	1	0.618± 0.006	50±3	-0.73	-4.67	2.21±0.6			
	81-1f2 (recryst.)	1	0.621± 0.005	47±2	-0.73	-4.61	2.00±0.4			
	81-1d M	1	0.619± 0.011	48±6	-1.17	-5.78	1.01±1.0	218	561	285
M	**81-1f M**	1	0.589± 0.009	65±5	-1.41	-5.45	4.07±0.8	291	240	189
	81-1e M							187	355	191
	81-1d S1	1	0.586± 0.008	67±5	-1.18	-8.02	1.74±0.7	350	696	71
S	**81-1d S2**	1	0.582± 0.010	69±6	-1.21	-7.01	3.18±0.9			
	81-1e S							256	128	64
Valleviken 3										
	Valle3-1c 1	1	0.610± 0.010	53±5	-0.71	-5.05	2.55±0.9			
B	**Valle3-1c 2**	1	0.585± 0.008	67±5	-0.83	-4.85	5.08±0.7			
	Valle 3-1c 3	1	0.623± 0.008	47±4	-0.82	-5.40	1.09±0.7			
	Valle 3-1c CT	1	0.609± 0.009	53±5	-0.79	-5,27	2,39±0.8	22	62	1923
M	**Valle(3)-1c M1**		0.606± 0.009	55±5	-0.83	-6.88	1.06±0.8	288	1649	298
	Valle(3)-1c M2		0.610± 0.006	53±4	-0.89	-6,94	0.64±0.6			

Table 6.1 *Continued.*

Sample		n	$\Delta_{47, abs}$ *)	T	$\delta^{13}C$	$\delta^{18}O$	$\delta^{18}O_w$	Mn	Fe	Sr
Sigsarve 1										
B	**Sig1 5-1**	1	0.627± 0.010	44±5	1.94	-5.24	0.84±0.9	216	1006	1732
	Sig1 3	4	0.612± 0.003	52±2	2.00	-5.26	2.15±0.2	26		2297
								39	82	1784
								102	421	2022
	Sig1 1b	1	0.619± 0.013	49±7	2.09	-5.19	1.64±1.2			
M	**Sig1 3 M**							792	5708	288
S	**Sig1 3 S**							1015	1571	525
	Sig1 5-1 S1	1	0.576± 0.006	73±5	2.08	-8.67	2.07±0.6			
	Sig1 5-1 S2	1	0.559± 0.009	84±6	2.14	-8.52	3.90±0.9			
	Sig1 1 S							264	1060	1469
	Sig1 1 S							361	4143	318
	Sig1 1 S							2617	2618	94
Korpklint										
B	**Korpklint**	1	0.600± 0.010	59±6	5.01	-4.28	4.25±0.9	156	188	1267
	Korpklint	1	0.606± 0.009	55±4	4.46	-4.58	3.42±0.8			
	Korpklint	1	0.601± 0.011	58±6	4.66	-4,88	3.53±1.0			
Allhageviken 6. 4										
B	**All6**	1	0.611± 0.013	53±7	1.67	-5.34	2.18±1.2	47	153	1562
M	**All6 M1**	1	0.592± 0.010	63±6	2.55	-5.22	4.01±0.9	521	905	589
	All6 M2	2	0.617± 0.001	50±1	3.36	-4.93	2.06±0.1	562	1256	583
	All4 M							481	5338	441
	All6 M							2586	3135	137
	All4 M							2096	4007	78

*) For single measurements the internal reproducibility is given, for replicated samples se corresponds to the external reproducibility. T and $\delta^{18}O_w$ errors rely on the particular Δ_{47} errors.

6.3.1 Brachiopod shells

Preservation state analyses

In large parts investigated fossil brachiopod shells from Gotland are non-luminescent (Fig. 6.2(A)) and the fibres of secondary layer calcite show pristine shapes (Fig. 6.3(A)). However, all studied fossils also possess distinct areas that are luminescent (Fig. 6.2(B)–(C) and 6.3(B)–(C)).

Orange luminescence occur only in small areas of the investigated shells (some observable cathodoluminescence patterns are presented in Fig. 6.2(B)–(D)). In general the middle parts of most brachiopod shells show only few small orange luminescent spots. However, especially in the anterior region of many studied valves thin orange lines are common. They start between the frills and cross the shells towards the middle (Fig. 6.2(B)). In the most posterior parts of several brachiopod shells thick orange luminescent bands occur that start at the muscel scar and run towards the hinge (Fig. 6.2(C)). Dull luminescent coloures of the inner surface of the shells are common (Fig. 6.3(D)).

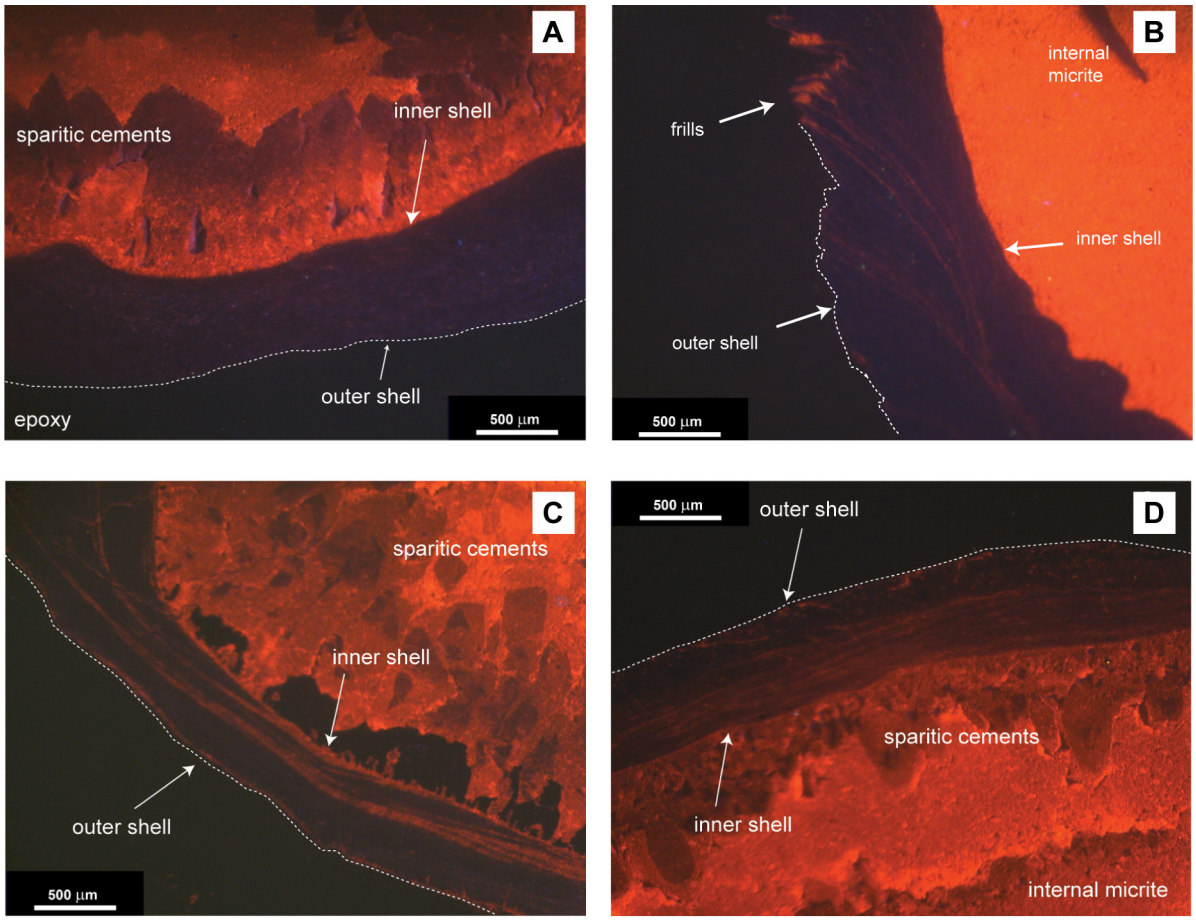

Figure 6.2 *Commonly observed cathodoluminescence pattern of the studied brachiopod fossils. (A) Non-luminescent shell material; in contrast, the sparitic cements of the filling show dull-luminescent to orange colours. (B) Thin orange lines start between the frills in the anterior part of the shell and run along growth planes towards the middle area. The adjacent micritic phase shows bright orange cathodoluminescence. (C) Orange luminescent bands in the posterior region of a valve. They start at the muscle scar and run towards the hinge. The sparitic cements are characterized by variable luminescent coloures (dull to bright orange). (D) The outer shell is almost non-luminescent while brown coloures appear in the inner area. The sparitic cements grown at the inner side of the valve are dull-brown cathodoluminescent, while the crystals towards the center of the fossil are red to orange.*

The investigated SEM sections of several samples are characterized by amalgamation of secondary layer fibres in large parts (Fig. 6.3(B)). However, these areas are mostly non-luminescent. Additionally, fibres are partly recrystallized. Instead of round shapes angular structures are visible (Fig. 6.3(C),(D)). Luminescent lines and bands (Fig. 6.2(B),(C)) are conform with recrystallized secondary layer fibres. Furthermore, for several studied shells recrystallization of fibres of the inner surfaces is observable.

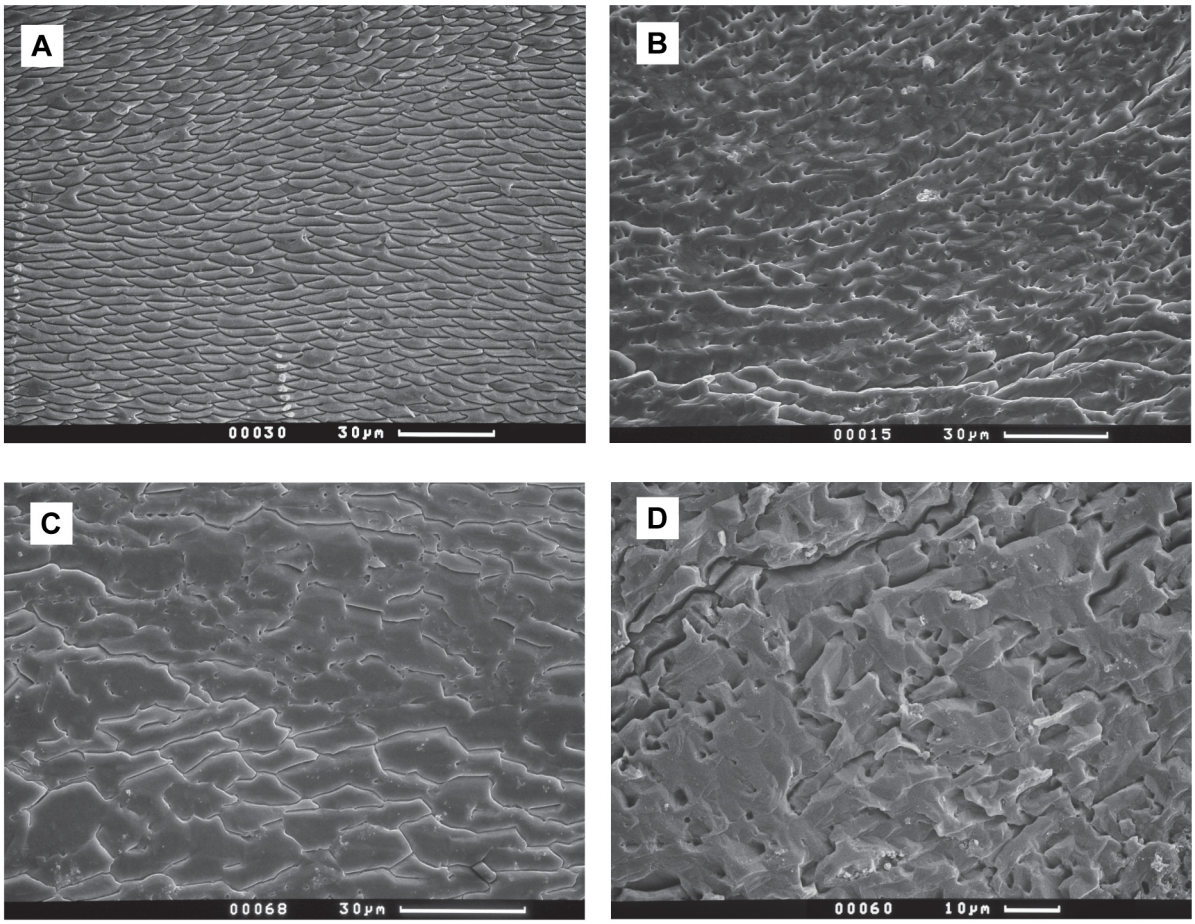

Figure 6.3 *Common states of the ultrastructural preservation observed for the studied secondary layers of the Silurian brachiopod shells. (A) Pristine preserved fibres. (B) Amalgamated fibres. No distances between single fibres are visible. (C) Recrystallized fibres. The original round shapes are replaced by angular crystals. The single fibres are still visible.(D) Intense recrystallization of secondary shell layer calcite. The original round structures of the biominerals are not observable anymore.*

Geochemistry

Most brachiopod shells are characterized by low Mn, relatively high Fe and very high Sr concentrations (Table 6.1): Mn contents reach <100 ppm, Fe concentrations range between 60 and 400 ppm, and Sr contents scatter between 1500 and 2000 ppm. These concentrations are coincident with values determined for modern counterparts (Morrison and Brand, 1986; Brand, 2003; von Allmen et al., 2010). Absolute Δ_{47} values scatter by more than 0.1‰ and plot between 0.548‰ and 0.663‰ (Table 6.1). No trends between the clumped isotopic composition and trace element concentrations are determined for the measured shells (Fig. 6.4).

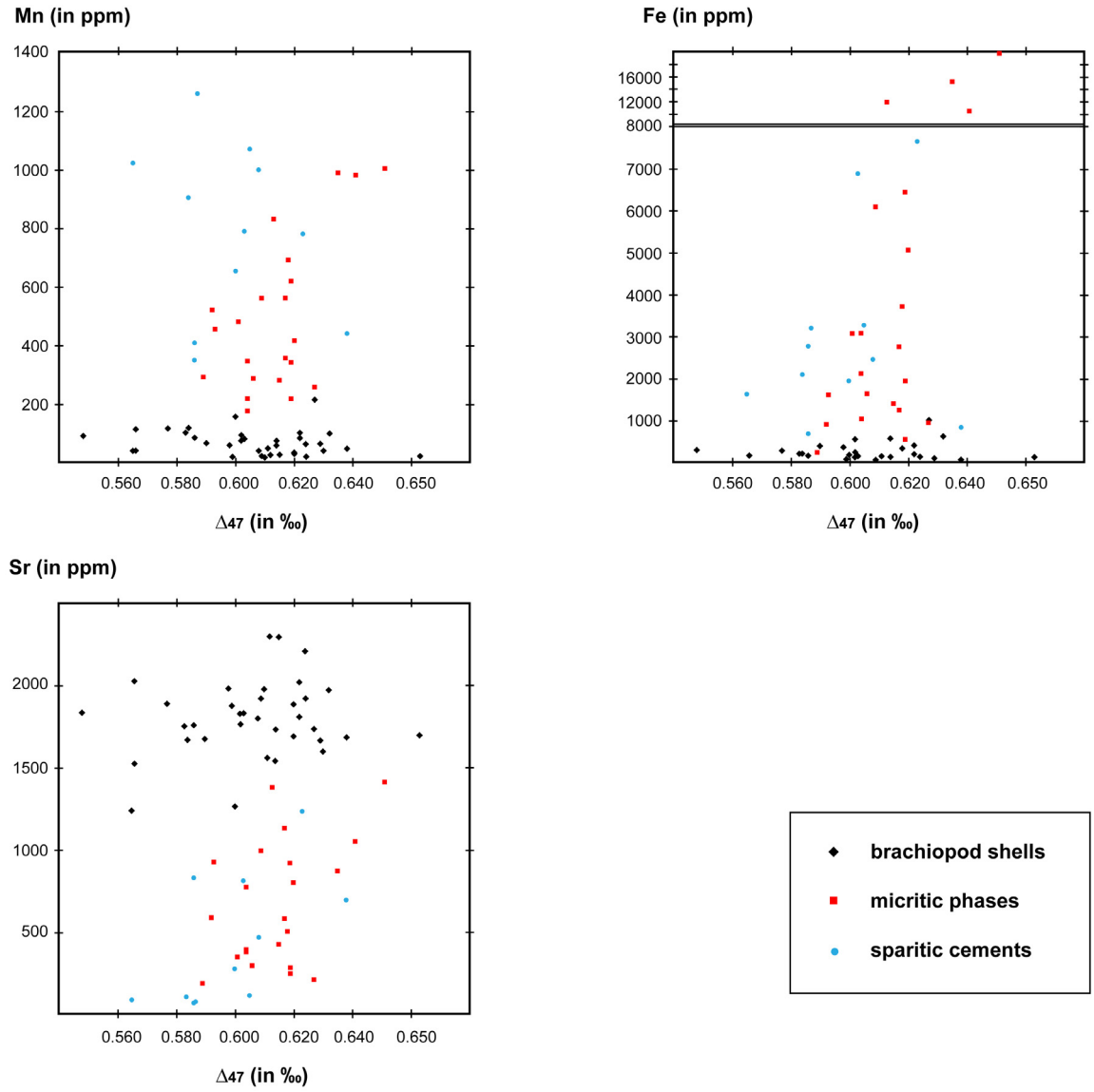

Figure 6.4 *Crossplots of clumped isotopic compositions and element concentrations of the analyzed shells and the diagenetic phases. A correlation between Δ_{47} values and element concentrations is not observed for any phase.*

Bulk oxygen and carbon isotopic compositions measured for the shells are coincident with published $\delta^{18}O$ and $\delta^{13}C$ values for the particular time intervals (e.g., Wenzel and Joachimski, 1996; Bickert et al., 1997). $\delta^{18}O$ values range from ca. –6.5 to –2.5‰, $\delta^{13}C$ values vary between ca. –3 and +9‰ (Table 6.1, Fig. 6.1).

6.3.2 Diagenetic phases

The micritic phases of the inner fillings of the studied fossils are characterized by a relatively homogenous, bright orange cathodoluminescence (Fig. 6.2(B)). Only a few shell fragments of other organisms are dull- or non-luminescent. In comparison to the micritic phases, the sparitic cements vary in their cathodoluminescence pattern (Fig. 6.2(A),(C),(D)): brown to bright orange colours occur, and in some minerals zonings are observed (Fig. 6.2(C)). The large sparitic crystals in the centre of some fossils show bright orange, homogenous luminescence; in contrast to the large cements, the smaller crystals that grew in contact with the brachiopod shells are mostly non-luminescent (Fig. 6.2(D)).

In comparison to the shells, the micritic phases are characterized by a larger variability in trace element contents (Table 6.1). Furthermore, concentrations of Mn (~200 to 1000 ppm) and Fe (~400 to 4000 ppm) are higher, and Sr concentrations are lower (~200 to 1000 ppm). In comparison to the micritic phases, Mn contents of the sparitic cements are slightly higher (~250 to 1200 ppm) and Sr contents are lower (~60 to 800 ppm); the scatter of the Fe concentrations determined for these crystals is even larger ranging from ~100 to 4000 ppm (Table 6.1).

The range of the Δ_{47} values determined for the micritic phases (between 0.592 and 0.651‰; Table 6.1) is slighty smaller than the scatter received for the brachiopod shells (0.548‰ and 0.663‰, Table 6.1). In contrast, a similar range of absolute Δ_{47} values measured for the sparitic cements (0.559 to 0.638‰; Table 6.1) and the brachiopod shells (0.548‰ and 0.663‰, Table 6.1) was obtained. For the sparitic phases lowest Δ_{47} values were measured for the large crystals in the center of some fossils. No correlation between Δ_{47} compositions and trace element concentrations of both the micritic phases and the sparitic cements is observed (Fig. 6.4).

Measured bulk oxygen isotope ratios of the mudstones are lower than those of the brachiopod shells. The difference in the oxygen isotopic composition between both phases depends on locality from which the fossils derived. For example, the difference between $\delta^{18}O$ mean values of shells and mudstones of the Diupvik outcrop is only 0.5‰, but 1.5‰ for the Petsarve samples (Table 6.1). Large variations in the bulk oxygen isotopic composition are determined for the sparitic cements: the $\delta^{18}O$ values range from –4 to –11.5‰ (Table 6.1). These variations also occur between the inner fillings of different fossils deriving from similar beds (Table 6.1). However, $\delta^{18}O$ values measured for distinct cement aliquots within a single fossil vary by only ~1‰.

6.4 Discussion

6.4.1 Preservation state of the investigated fossils

CL and SEM investigations are the common tools applied to fossil brachiopod shells to determine their preservation states. Unaltered shells are non-luminescent because concentrations of CL activating elements, e.g., Mn and REEs, are very low in oxic water where the organisms lived. However, most diagenetic processes occur under reducing conditions at which CL activators are dissolved and incorporated in diagenetically altered minerals. Alteration can be identified by CL microscopy. For example Mn^{2+} (VII) bound in carbonate crystals provokes orange cathodoluminescence (Machel et al., 1991). Nevertheless, not all altered shells show luminescence because (1) Mn^{2+} can be absent in the diagenetic fluid, or (2) Fe^{2+} can quench the effect. Cathodoluminescence does not depend on the presence of Mn^{2+} only, but also on the ratio between Mn^{2+} and Fe^{2+}. This can either result in brownish, dull colours (Savard et al., 1995; Machel et al., 1991) or in complete inhibition of luminescence (Pierson, 1981; Machel et al., 1991). The occurrence of quenching effects should not be disregarded because Mn and Fe are both stable at reducing conditions. For these reasons, it is essential to apply methods that additionally help to determine the preservation state of fossils. The investigation of ultrastructures offers direct information if biominerals were affected by alteration: angular crystals originate from recrystallization (Fig. 6.3(C), (D)) and a loss of the distances between fibres cause amalgamation (Fig. 6.3(B)). In contrast to these altered structures well-preserved fibres of secondary layer brachiopod shell calcite are characterized by round shapes (Fig. 6.3(A)). However, SEM sections represent only a very small part of the whole shell. Thus, caution has to prevail if assumptions about the preservation state of the entire fossil are made. In several studies supporting information regarding the preservation state of ancient material was obtained from trace element analyses (e.g., Mn, Fe and Sr; e.g., Popp et al., 1986; Grossman et al., 1996; Wenzel and Joachimski, 1996; Veizer et al., 1999; van Geldern et al., 2006; Finnegan et al., 2011). Well-preserved brachiopod shells are generally characterized by low Mn and Fe, but high Sr concentrations, correspondent to their abundances in oxic, marine environments. In contrast, diagenetic fluids and calcites have mostly high Mn and Fe, and low Sr concentrations depending on redox conditions (Brand and Veizer, 1980; Veizer, 1983a, b). However, trace element contents in modern brachiopod shells vary largely (Morrison and Brand, 1986; Brand, 2003; von Allmen et al., 2010). Therefore, trace element analyses of fossil material provides only limited information about the preservation state.

In general, the combined preservation state analyses applied to the studied brachiopod shells of Gotland indicate a high preservation quality. (1) Most areas of the shells are non-luminescent. (2) In large areas of the studied SEM sections pristine ultrastructures are preserved. And, (3) trace element concentrations fall in the range of modern counterparts. These observations are confirmative with results that were reported in published studies (e.g., Wenzel and Joachimski, 1996; Samtleben et al., 2001).

Furthermore, our investigations approve the conclusion made by Samtleben et al. (2001) who observed that distinct areas of brachiopod shells are susceptible to diagenetic alteration. Direct evidence for this conclusion is obtained from investigations of the ultrastructural preservation along shell transectes. The anterior and most posterior areas of the shells seem to be more prone for diagenetic alteration. In these parts the frills and the muscle scar offer pathways for diagenetic fluids which can intrude the shell and cause recrystallization. However, no remarkable increases of Mn and Fe concentrations or decreases in Sr contents were determined from recrystallized fibres (unpublished data of a diploma thesis, Ulrike Wacker, 2010, FAU Erlangen-Nürnberg). Therefore, the significance of trace element measurements for preservation state analyses seems to be relatively low. Nevertheless, the concentrations of trace elements in altered carbonates depend on the diagenetic fluids which affected the shells. Recrystallization might have occurred at a every early stage during diagenesis. Thus the elemental concentrations of the fluids might have been closely correspondent to those of seawater, so that the original marine trace element concentrations of the shells did not alter. Alternatively, alteration might have occurred at very low water–rock ratios, so that the trace element concentrations of the diagenetic fluids might have been buffered by those of the shells. As a consequence elemental concentrations within the fibres would have been preserved during recrystallization. Optical investigations do not allow to decipher diagenetic processes in more detail. Nevertheless, from combined clumped and bulk oxygen isotope analyses we obtained more detailed information about the alteration mechanisms that affected the carbonate rocks and their components (see Chapter 4.2.2).

Compared to the anterior and posterior regions, the middle parts of the valves were more resistent against alteration. This is indicated by minor luminescence (small spots which were most probably caused by bioerosion and punctual recrystallization, or lines oriented vertically to the shell surface which have been interpreted as cracks). In addition, minor degrees of recrystallization are observed in these areas. Nevertheless, within each shell well-preserved fibres alternate with amalgamated structures. Amalgamation of secondary layer fibres indicates alteration, though it is not clear whether alteration occurs due to recrystallization or

cementation. However, the observed amalgamated fibres are non-luminescent; furthermore, low Mn and Fe as well as high Sr concentrations are measured within these parts. As discussed above, this might indicate that either the bulk chemical composition was not affected by diagenetic fluids due to low water–rock ratios during diagenesis, or alternatively, that alteration occurred during a very eary stage of diagenesis under marine conditions.

6.4.2 $T(\Delta_{47})$ and $\delta^{18}O_w$ reconstructions: pristine versus altered values

6.4.2.1 $T(\Delta_{47})$ and $\delta^{18}O$ estimates for Silurian ocean water

$T(\Delta_{47})$ determined for the brachiopod shells

Clumped isotope temperatures of the sampled brachiopod shells scatter from 28 to 92 °C (Table 6.1, Fig. 6.5). The mean temperature error of the estimated values is ca. ±4 °C; $T(\Delta_{47})$ errors are shown in Table 6.1, however, in the text they are not noted explicitly. Most temperature estimates plot between 40 and 60 °C; the mean $T(\Delta_{47})$ of all analyzed samples is 56 °C. It seems unlikely that these high values reflect pristine ocean water conditions. Rather, we evaluate most fossil brachiopod shells from Gotland to be altered in their clumped isotopic compositions. This observation is conform with the results published by Cummins et al. (2014). Their $T(\Delta_{47})$ estimates scatter from 30 to 60 °C. We determined a larger temperature range as well as a higher value for the high-temperature endmember. Nevertheless, absolute Δ_{47} variations are identical within both studies indicating that the observed temperature discrepancy results from the application of different calibrations. Cummins et al. (2014) used the Ghosh et al. (2006a) $1/T^2$–Δ_{47} realtionship. In contrast, we referred to the calibration determined in our laboratory (Wacker et al., 2014). The intersection of the two lines is at a temperature of 38.8 °C corresponding to a clumped isotopic composition of 0.639‰ (using a $\Delta_{47}{}^{*}{}_{25\text{–}90}$ of +0.069‰, Guo et al., 2009). Around this Δ_{47} composition $T((\Delta_{47})$ values do not differ largely using any of the two calibrations. However, a decrease in Δ_{47} values results in an increase in the offset between temperature estimates: applying the Ghosh et al. (2006a) calibration to a Δ_{47} value of 0.550‰ a temperature of 62 °C is calculated, whereas a temperature of 91 °C is determined applying the calibration of Wacker et al. (2014). So far, it is unknown why discrepant calibrations were obtained in several differerent studies. Here, we refer to the line of Wacker et al. (2014) as this calibration was made in the same laboratory and during the same analytical time interval in which the Silurian samples of this study were analyzed. Preparation techniques and analytical conditions were identical. Furthermore, the line of Wacker et al.

(2014) is universal because several different types of calcites were measured, including a modern brachiopod shell; in addition it is indistinguishable from the calibration reported by Henkes et al. (2013) which also includes brachiopod shells. Certainly, the flatter slope of the Wacker et al. (2014) calibration line results in a lower temperature sensitivity and in larger errors of the computed T and $\delta^{18}O_w$ values.

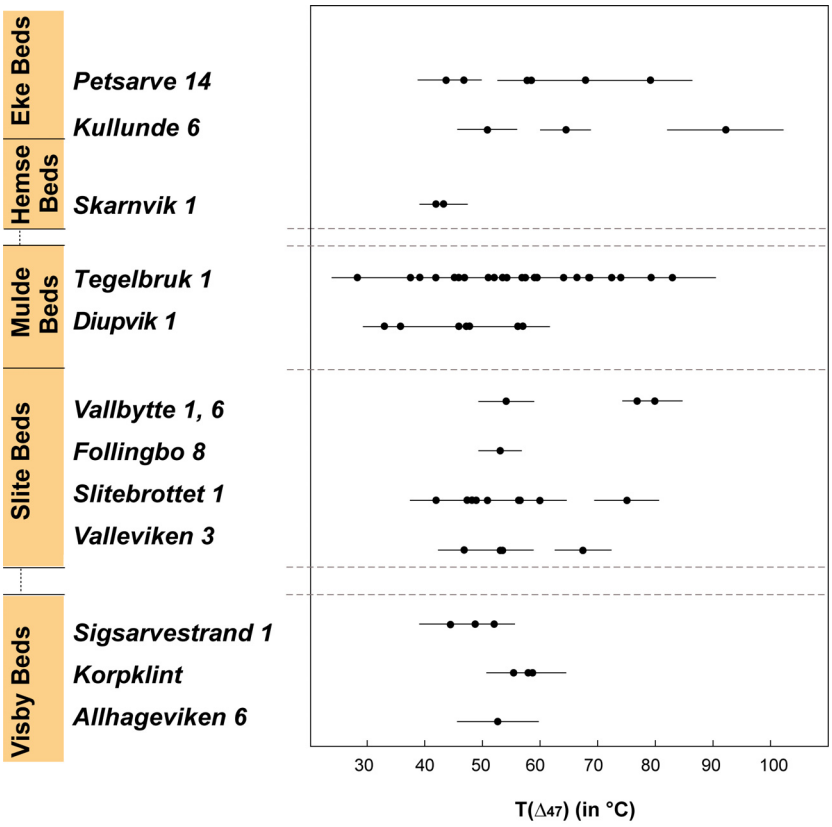

Figure 6.5 *$T(\Delta_{47})$ values estimated from the analyzed brachiopod shells deriving from different sample localities of the five stratigrafic beds.*

Deciphering pristine $T(\Delta_{47})$ values

Cummins et al. (2014) applied Δ_{47} analysis to preserved sedimentary components of the lower succession of the limestone-marl alternation exposed on Gotland. Their estimates for sea-surface temperatures are ~33 °C. They assumed that the lowest temperature estimates reflect pristine water conditions. These values are conform with $T(\Delta_{47})$ values which were reconstructed from brachiopod shells of the earliest Silurian (Came et al., 2007; Finnegan et al., 2011). In the studies of Came et al., (2007), Finnegan et al. (2011) and Cummins et al. (2014) alteration of shells were deciphered by means of visual inspection and analyses of trace element concentrations. However, Finnegan et al. (2011) argued that they cannot guarantee that

at least small amounts of sample material was contaminated with diagenetically altered calcite. Therefore, they evaluated the estimated temperatures as maximum values. The lowest T(Δ_{47}) values determined in our study are in the same range as those given by Came et al. (2007), Finnegan et al. (2011) and Cummins et al. (2014). In the following we will inspect our samples for which the lowest temperatures are reconstructed in more detail, to ascertain that these temperatures reflect pristine conditions of Silurian ocean water.

(1) The ultrastructural preservation of sample 26-1b from Tegelbruk was studied in five transverse sections along the ontogenetic transect (Fig. 6.6). Based on these investigations a decrease in the degree of preservation from the posterior to the anterior margin becomes obvious, indicated by an increase of amalgamated areas of the surfaces of sections 4 (posterior) to 1 (anterior). Only for the surface of section 5 we distinguished even larger parts of ultrastructurally altered fibres. The best preservation state is assumed for section 3 because it is adjacent to another very well preserved slice (section 4) indicating that ultrastructures of the ~1.5 mm thick slices between both surfaces are most probably well-preserved as well. From sections 4 to 1 enough material is obtained for clumped isotope analysis. The observed increase of the degree of alteration from slices 4 to 1 is almost coincident with an increase of estimated temperatures for each carbonate sample (Fig. 6.6). T(Δ_{47}) values of 33 and 36 °C are determined for the well-preserved sections in the posterior part. In contrast, for the anterior region higher T(Δ_{47}) values of 48 and 56 °C are obtained. We interprete the lower temperatures to indicate pristine conditions of Silurian ocean water. Because slice 4 is adjacent to a strongly altered section (slice 5) a larger amount of recrystallized calcite might have been included in the analyzed aliquot resulting in a slightly higher T(Δ_{47}) value.

A similar correlation between T(Δ_{47}) and the ultrastructural preservation is determined for sample 81-1d (Slitebrottet, Table 6.1). The preservation state of the secondary layer fibres was studied in four sections along the ontogenetic transect: for the most posterior section 4 only a minor amount of recrystallized fibres is observed; in contrast, recrystallization of larger areas is visible for slices 3 and 2, and section 1 exhibites both pristine and altered structures in similar amounts (Fig. 6.6). Sections 4, 3 and 1 offered enough material to measure their clumped isotopic compositions. The lowest T(Δ_{47}) value of 42 °C is determined for the best preserved slice 4, whereas the highest temperature of 60 °C is received for the most altered section 3. Nevertheless, compared to sample 26-1b a lower preservation state is determined for sample 81-1d. We, therefore, do not interpret the lowest value of 42 °C to reflect a pristine water temperature.

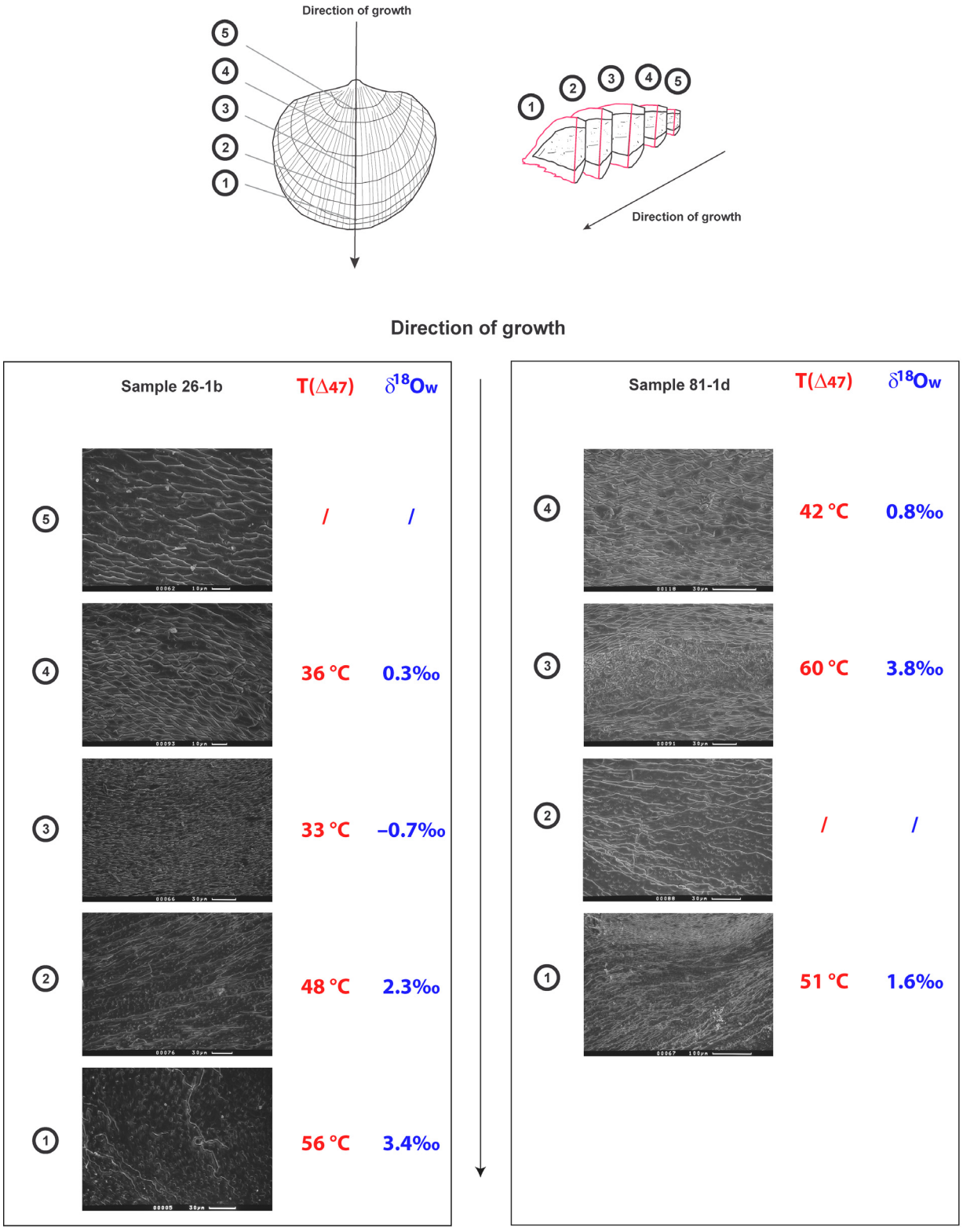

Figure 6.6 *Ultrastructural preservation along ontogenetic shell transects of two samples; the SEM slices were prepared as shown in the scheme above; investigated surfaces are marked in red. A correlation between the increase in alteration of ultrastructures and higher T(Δ_{47}) values is determined. The lowest $\delta^{18}O_w$ value is obtained for the lowest T(Δ_{47}), the highest $\delta^{18}O_w$ composition is calculated for the highest T(Δ_{47}) value. Further descriptions are given in the text.*

(2) For the investigated Diupvik samples T(Δ_{47}) values between 28 and 79 °C are determined (Table 6.1). The shells were collected from a relatively narrow time interval, and we suppose that the organisms lived under similar water conditions. Thus we assume that the temperature conditions and elemental concentrations of ambient seawater during growth of the organisms were similar. All studied samples are characterized by only minor areas of cathodoluminescence indicating a good preservation; nevertheless, for all fossils a patchwork of pristine and altered ultrastructures is observed. We, therefore, interpret the large range of T(Δ_{47}) values to result from a variability of the alteration degree of secondary layer fibres. The lowest T(Δ_{47}) value of 28 °C (Diu3, Table 6.1) is most probably calculated from a sample that contained no or only a minor amount of altered calcite, whereas material of a higher alteration degree was probably sampled from Diu7 for which the highest T(Δ_{47}) value of 79 °C is obtained (Table 6.1). Furthermore, for the Diupvik samples variations in Mn, Fe and Sr contents of ~100 ppm, >500 ppm and >300 ppm are determined, respectively (Fig. 6.7). It seems plausible that the scatter of the trace element concentrations reflects different degrees of diagenetic alteration within the shell material. However, there is no correlation between Δ_{47} values and elemental concentrations (Fig. 6.7). For three samples from Diupvik T(Δ_{47}) values lower than 40 °C are determined (Diu3, Diu7 CT, Diu8(5), Table 6.1). According to Mn, Fe and Sr contents no indication for a better preservation quality of these shells is given compared to samples for which temperatures of ~80 °C are estimated (Table 6.1). Clearly, sample Diu3, for which the lowest temperature of 28 °C is calculated, exhibits lowest Mn and Fe contents (Table 6.1). However, similar concentrations are determined for sample 25-1a for which a T(Δ_{47}) value of 59 °C is obtained (Table 6.1). Therefore, we conclude that conventional preservation state analyses are not sufficient and offer only limited use to identify diagenetic alteration of the original clumped isotopic composition of samples.

In summary, SEM investigations offer best constrains about the degree of alteration of shell calcite. Detailed studies that were made for sample 26-1b provide good evidence that shallow tropical ocean water was characterized by warm temperatures of ca. 33 ± 4 °C during growth of the organism. In contrast, the observations concerning the samples from Diupvik do not give a clear indication whether we have analyzed pristine shell material. However, even though we cannot well establish whether the lowest T(Δ_{47}) value of 28 ± 4 °C determined for Diu3 reflects an original water temperature we deem it likely that the sample contained pristine material. Nevertheless, the calculated clumped isotope temperatures should be evaluated as maximum values, since we cannot exclude that even samples characteried by low T(Δ_{47}) value contained small amounts of altererd material.

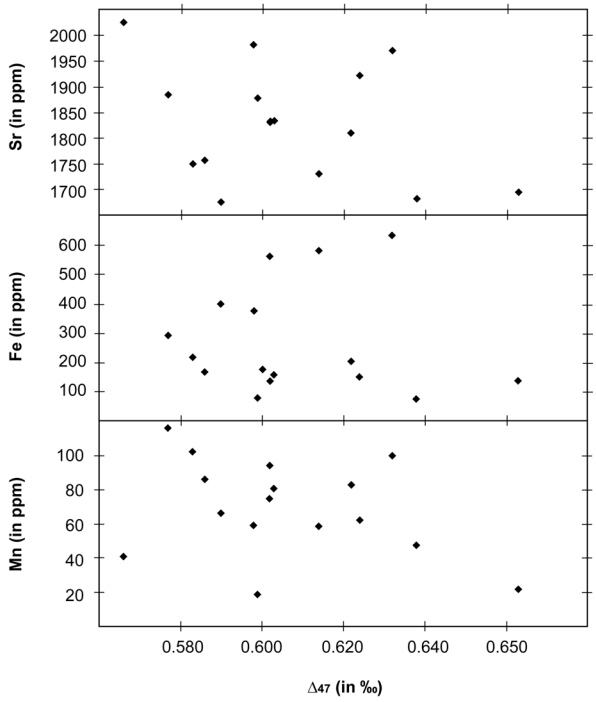

Figure 6.7 *Trace element concentrations of brachiopod shells from Diupvik plotted versus their Δ_{47} values. The variations in trace element concentrations of shells collected from a narrow time interval might indicate varying degrees of diagenetic alteration. However, no correlations between* Δ_{47} values *and element contents are displayed.*

Reconstruction of the $\delta^{18}O_w$ values of Silurian seawater

As discussed in the previous chapter the clumped isotope temperature of 33 °C estimated for sample 26-1b (section 3) is likely pristine (Fig. 6.6). Referring to the equilibrium oxygen isotope fractionation equation of Kim and O'Neil (1997) a $\delta^{18}O_w$ value for Silurian seawater of (–0.7 ± 0.7)‰ is calculated (Table 6.1, Fig. 6.6). Furthermore, for sample Diu3, which reflects the lowest $T(\Delta_{47})$ value of our sample set, a $\delta^{18}O_w$ composition of (–0.4 ± 0.8)‰ is reconstructed (Table 6.1). These values could confirm the assumption that the oxygen isotopic composition has been buffered to (0 ± 1)‰ during the Paleozoic time interval at least in the Silurian period (e.g. Muehlenbachs and Clayton, 1976; Gregory and Taylor, 1981; Gregory, 1991; Muehlenbachs, 1998; Muehlenbachs et al., 2003). Because of the variable preservation of the investigated brachiopod shells we cannot decipher whether changes in $\delta^{18}O$ values of the calcites reflect changes of the temperature or the oxygen isotopic composition of seawater or both. The reconstructed $\delta^{18}O$ seawater values are coincident with the estimates made by Cummins et al. (2014) referring to preserved sediments from Gotland, as well as those of Came et al. (2007) and Finnegan et al. (2011) studying water conditions of the earliest Silurian epoch. Because the $T(\Delta_{47})$ estimates represent maximum values, the proposed oxygen isotopic composition of Silurian ocean water are maximum values as well.

6.4.2.2 Diagenetic processes

Silurian brachiopod shells: reset of Δ_{47} values caused by recrystallization

Two mechanisms can reset the clumped isotopic composition of fossil material. These are either recrystallization and/or cementation at temperatures prevailing during burial, or solid state reordering of carbon and oxygen isotopes in a closed system (Fig. 6.8). Diffusion of atoms in the mineral lattice does not provoke visible changes of crystal morphologies (Passey and Henkes, 2012). Furthermore, alteration in a closed system does not affect the bulk isotopic compositions or the trace element concentrations (Eiler, 2011; Finnegan et al., 2011). It is, therefore, difficult to discern solid state reordering in minerals. The Conodont Alteration Index (CAI) of 1 determined for conodonts of the studied Silurian formations (Jeppsson, 1983) constrains that the rocks underwent early diagenetic processes at temperatures between 50 and 80 °C. Furthermore, well-preserved chitinozoans indicate that the temperatures during diagenesis did not exceed 100 °C (Munnecke, 1997). This is conform with the clumped isotope temperatures determined for the diagenetic phases of the sedimentary rocks (Table 6.1). At these low temperatures solid state diffusion is assumed to be negligible (Fig. 6.8; Dennis and Schrag, 2010; Eiler, 2011; Passey and Henkes, 2012). Therefore, we interpret the clumped isotopic compositions of the brachiopod shells as being altered by recrystallization. A similar conclusion was proposed by Cummins et al. (2014). In addition to the relatively low temperatures (<100 °C) that were estimated for diagenetic processes, this statement is confirmed by direct indications which are obtained from our investigations. (1) Large differences are determined for distinct samples measured from individual shells. For example, the eleven individual carbonate aliquots measured for sample Diu8, indicate a range of T(Δ_{47}) values of more than 46 °C (Table 6.1). This shows that the shells have not been altered homogeneously, but that different parts have been affected to different extents. (2) The observation that T(Δ_{47}) values increase with increasing degree of ultrastructural alteration (samples 26-1b and 81-1d; Fig. 6.6) indicates that clumped isotope compositions were reset by recrystallization and amalgamation (see discussion in Chapter 6.4.2.1).

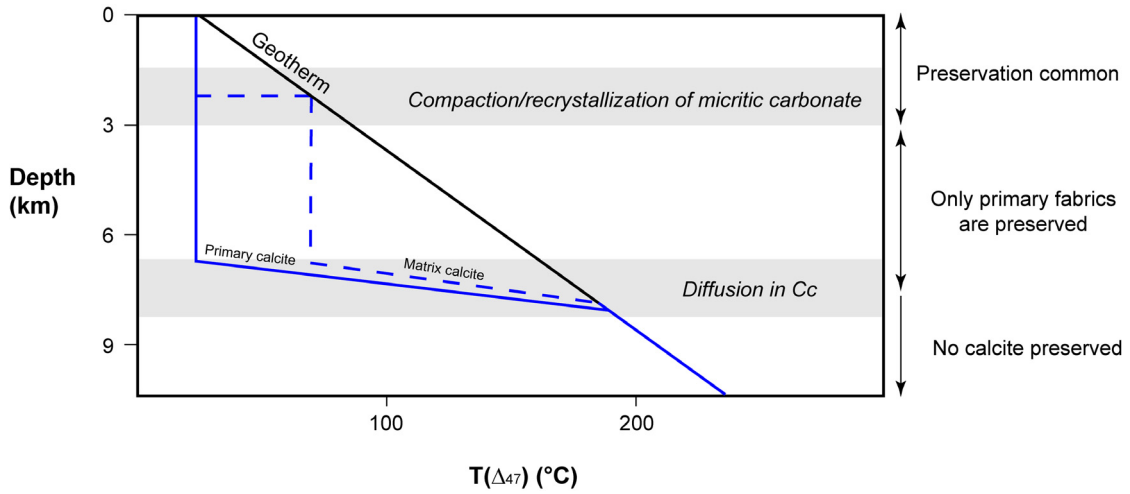

Figure 6.8 *General scheme of alteration mechanisms of the clumped isotopic composition of calcite during diagenesis (modified after Eiler, 2011). According to this model in burial depths <6 km primary calcite (such as shell material of organisms) is mostly not affected by recrystallization and alteration of Δ_{47} compositions. In contrast, clumped isotopic compositions of matrix calcite mostly alters at depth between 2 and 3 km and temperatures between 50 and 80 °C. However, buried to >6 km solid state diffusion causes reordering of isotopes and alteration of Δ_{47} values of both primary components and matrix calcite.*

Diagenetic regime: low water–rock alteration

Most T(Δ_{47}) values determined for the shells, micritic phase and sparitic cements scatter between 40 and 60 °C and the clumped isotope temperatures of these phases overlap largely (Fig. 6.9). The widest T(Δ_{47}) range is displayed for the brachiopod shells and ranges from ca. 30 to 90 °C. The values estimated for the micritic phases and the sparitic cements vary between ca. 30 and 75 °C, and ca. 40 to 80 °C, respectively. Considering a common geothermal gradient of 30 °C/km carbonates must have been exposed to burial depths of 2 km to reach diagenetic temperatures of 90 °C. The burial depths of the rocks exposed on Gotland is unknown and poorly studied. There is no evidence for soil formation, indicating that Upper Silurian and Devonian rocks may have lain above the studied succession (Munnecke, 1997). Nevertheless, Silurian carbonates exposed on Gotland might have been overlain by cretaceous deposits which might have been eroded during past glaciations. Nevertheless, more studies are needed to further clarify whether highest T(Δ_{47}) values determined for Silurian carbonates exposed on Gotland are realistic; additionally, investigations regarding burial depths of the correspondent sedimentary rocks are required. It, furthermore, needs to be examined whether hydrothermal fluids might have been involved in the diagenetic processes occuring on Gotland, which might explain elevated T(Δ_{47}) values.

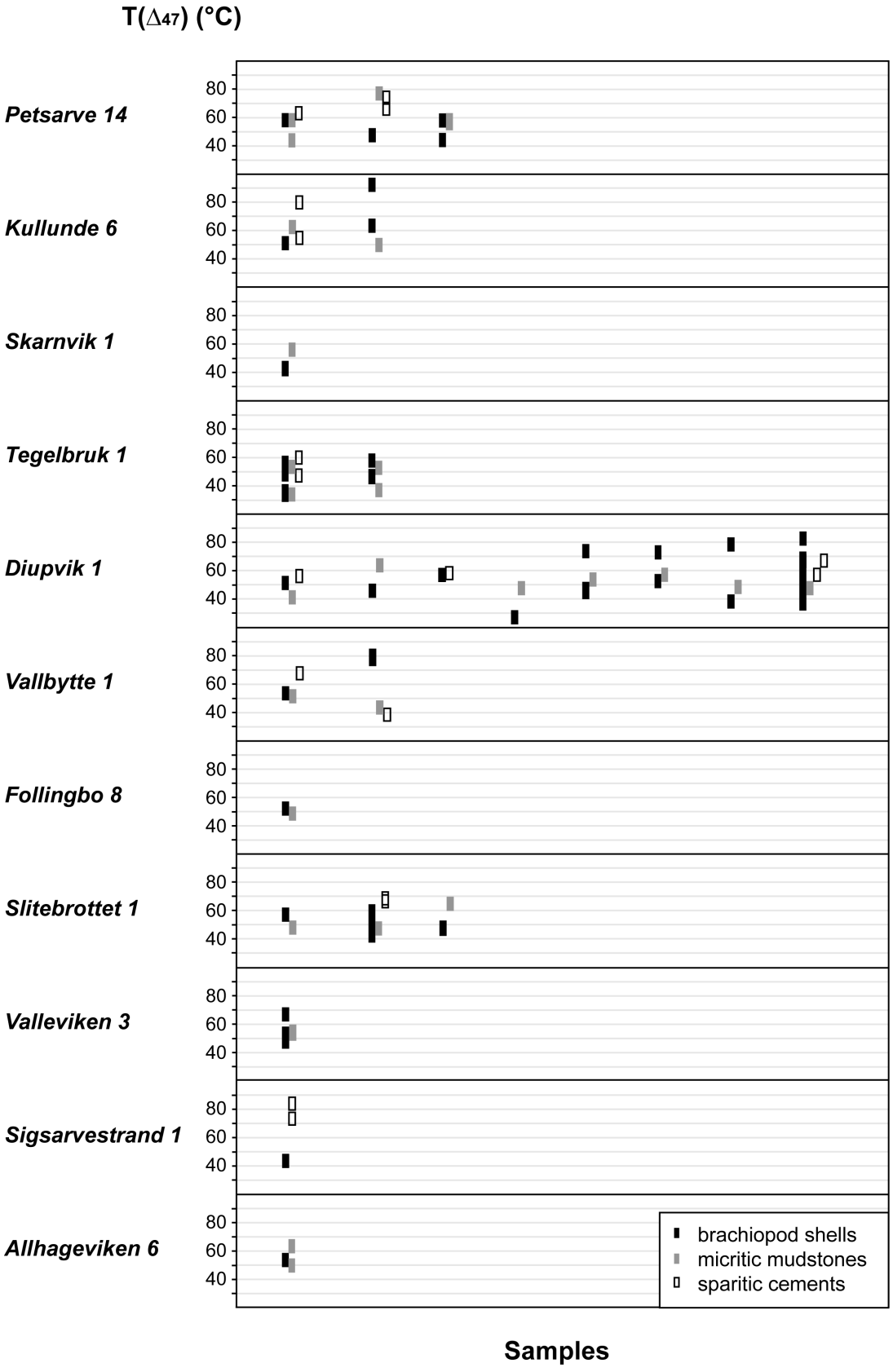

Figure 6.9 *$T(\Delta_{47})$ values determined for the different phases of each sample. Though the brachiopod shells are mostly characterized by the lowest temperatures and the sparitic cements by the highest values, $T(\Delta_{47})$ estimates of the different phases overlap largely.*

No correlation between estimated T(Δ_{47}) and measured $\delta^{18}O$ values of brachiopod shell calcite is observed (Fig. 6.10). Obviously, the reset of the Δ_{47} compositions was not accompanied by an alteration of the bulk oxygen isotopic composition. Accordingly, we infer that the alteration of the brachiopod shell chemistry occurred at low water–rock ratios, confirming the conclusion made by Cummins et al. (2014). During alteration the $\delta^{18}O$ signatures of the diagenetic fluids were buffered by the $\delta^{18}O$ value of the shell matrix. A correlion between T(Δ_{47}) and $\delta^{18}O_w$ values is displayed (Fig. 6.10) indicating that variations in the oxygen isotopic composition of the water goes along with Δ_{47} variations. Conclusively, we suggest that the oxygen isotopic compositions of the analyzed fossils from Gotland have been preserved during diagenesis, confirming assumptions made in earlier studies (e.g., Wenzel and Joachimski, 1996; Bickert et al., 1997; Samtleben et al., 2001; Munnecke et al., 2003; Cummins et al., 2014).

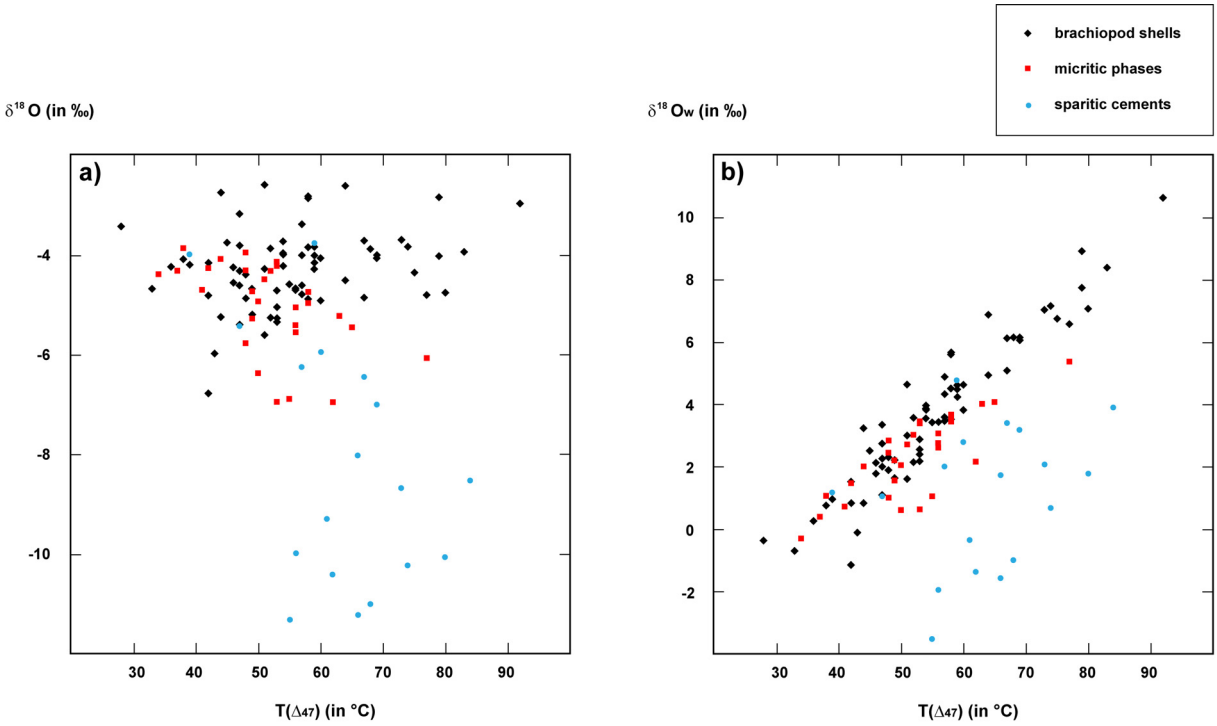

Figure 6.10 *(a) Crossplot of T(Δ_{47}) and $\delta^{18}O$ values for the different phases. No correlation is observed for the sampled shells indicating that the alteration of the clumped isotopic composition occurred decoupled from the bulk oxygen isotopic composition of the fossils. The T(Δ_{47}) estimates of the shells and the inner fillings overlap largely. $\delta^{18}O$ values of the micritic phases are slightly lower than the shells, large variations have been measured for the sparitic cements. (b) Crossplot of T(Δ_{47}) and $\delta^{18}O_w$ estimates. The correlation observed for the T(Δ_{47}) and $\delta^{18}O_w$ values of the shells shows that most likely the $\delta^{18}O$ values of the fossils did not alter. A weaker correlation determined for the micritic phases indicate that the $\delta^{18}O$ values represent conditions during early lithification. The large variations of the cements result from several distinct precipitation events at different T and from water with different $\delta^{18}O$ compositions. For further explanations, see text.*

$T(\Delta_{47})$ and $\delta^{18}O_w$ values: brachiopod shells vs. diagenetic phases

Fig. 6.9 illustrates that the clumped isotope temperatures which are reconstructed from the shells are mostly similar or lower than the estimates for both the micritic phases and the sparitic cements; generally, the $T(\Delta_{47})$ values of the micritic phases are in the same range or lower than the temperature estimates for the sparitic cements.

The micritic phases are composed of a mixture of diagenetic cements that caused the lithification of the sedimentary marine components. The sedimentary components might have been partly chemically altered. Therefore, bulk and clumped isotopic compositions most probably reflect mixed values of the compositions of a marine and diagenetic endmember. The $\delta^{18}O$ values of the studied micritic phases are mostly close to the values of the surrounding brachiopod shells being either identical or lower by up to 1‰ (Table 6.1). Furthermore, SEM observations indicate that the components were affected by only minor compaction, if at all (Munnecke, 1997). Therefore, it was assumed that cementation occurred at a very early diagenetic stage. Fig. 6.10 indicates a weak correlation between $T(\Delta_{47})$ values and $\delta^{18}O_w$ estimates of the micritic phases. An integration of all these observations leads to the conclusion that the micritic phases were cemented under rock–buffered early marine diagenetic conditions. The scatter of the Δ_{47} values might be due to different extents of mixing of varying proportions of diagenetic cements and pristine or altered components within each sample. Furthermore, several diagenetic events, each of which occurred at different temperatures, might have affected the micritic phase after lithification; the $\delta^{18}O$ values of the diagenetic fluids might have been buffered by the oxygen isotopic composition of ambient carbonate crystals.

The different cathodoluminescence patterns and the variations of Mn, Fe and Sr concentrations (Table 6.1) of the sparitic cements show that these minerals represent several cement generations. This is confirmed by clumped isotope data because $T(\Delta_{47})$ estimates of the cements scatter largely (Fig. 6.10). The small crystals which grew in contact with the shells and for which dark brown cathodoluminescence is observed, are considered to have precipitated at an early diagenetic stage. In contrast, large sparitic calcites (diameters of up to 5 mm) grew in the centres of the cement fillings of four fossils (98-47h; 98-47q; 98-49b S1; Sig1-5). For these crystals homogeneous, bright orange cathodoluminescence is observed providing evidence that the minerals precipitated during one single diagenetic event. Since these minerals are characterized by the highest clumped isotope temperatures determined for the sparitic cements we assume that they represent the diagenetic endmembers, i.e., that they preserved information about peak temperatures of diagenetic processes. In contrast to the brachiopod shells and the micritic phases no correlation is observed between the $T(\Delta_{47})$ and the $\delta^{18}O_w$ values of the

cements (Fig. 6.10). This gives further evidence, that the distinct cement generations grew during several diagenetic events at different temperatures. The fluids from which they precipitated must have been characterized by variable oxygen isotopic and elemental compositions.

6.5 Conclusions

SEM, CL and trace element analyses indicate that the studied Silurian brachiopod shells from Gotland/Sweden are partly preserved, ultrastructurally and chemically. Nevertheless, at least in parts all investigated fossils were affected by diagenetic alteration. Clear evidence for this statement is obtained from SEM observations: most studied sections are characterized by a patchwork of pristine, recrystallized and amalgamated secondary layer fibres. A similar picture is received from clumped isotope analysis. A large range in $T(\Delta_{47})$ values between 30 and 90 °C is determined for the sampled shells. However, lowest temperature estimates correspond to ultrastructurally well-preserved material, whereas higher temperatures are obtained from material containing increased amounts of altered structures. We, therefore, evaluate the lowest $T(\Delta_{47})$ values of the analyzed shells to reflect pristine seawater temperatures. This conclusion confirms previous assumptions published earlier that warm conditions (~35 °C) have prevailed in tropical, shallow water settings and that the ocean had an oxygen isotopic composition close to –1‰ during the Silurian. Clumped and bulk oxygen isotopic analyses of the shells, the micritic phases and the sparitic cements help to make assumptions concerning diagenetic processes. We propose that the shells altered at low water–rock ratios. We, therefore, evaluate amalgamated and recrystallized material as being reset in its clumped isotopic composition, whereas the bulk oxygen isotopic composition has been preserved. The cements of the inner fillings of the fossils formed at several distinct events during diagenesis. The large crystals in the centers of the sparitic cements of some samples most probably represent the diagenetic endmembers indicating peak temperatures during diagenesis of ~90 °C. The clumped and bulk oxygen isotopic compositions of the micritic phases result from endmember-mixing between the marine (brachiopod shells) and diagenetic (sparitic cements in the centers) endmembers. The micritic phases lithified during early marine diagenesis.

6.6 Acknowledgements

We thank Sven Hofmann for technical assistance. This work has become possible through DFG grant FI-948/4-1 DFG.

6.7 Supplementary information

Table S6.1 *HG and 25 °C equilibrated gas data. Slopes of HG lines and ETFs.*

δ_{47} and $\Delta_{47, raw}$ values of heated gases used for the correction of sample data.							
Date	**δ_{47}**	**$\Delta_{47, raw}$**	**se (internal)**	**Date**	**δ_{47}**	**$\Delta_{47, raw}$**	**se (internal)**
24.10.11	-32.716	-1.663	0.006	**16.01.12**	-4,567	-0,961	0,007
26.10.11	-2.196	-0.894	0.010	**18.01.12**	15,014	-0,550	0,009
28.10.11	-51.499	-2.157	0.007	**25.01.12**	-32,883	-1,575	0,005
01.11.10	-2.663	-0.909	0.007	**27.01.12**	-3,431	-0,904	0,010
04.11.10	16.214	-0.437	0.009	**30.01.12**	11,419	-0,580	0,007
08.11.11	-51.664	-2.115	0.007	**01.02.12**	-33,032	-1,591	0,008
14.11.11	-29.364	-1.550	0.008	**03.02.12**	-4,193	-0,929	0,008
15.11.11	-2.460	-0.887	0.010	**05.02.12**	-33,002	-1,643	0,010
16.11.11	-51.773	-2.119	0.011	**06.02.12**	-2,846	-0,880	0,005
21.11.11	-51.955	-2.119	0.007	**08.02.12**	14,879	-0,476	0,008
22.11.11	13.069	-0.537	0.005	**08.02.12**	14,686	-0,457	0,006
24.11.11	-51.083	-2.016	0.007	**14.02.12**	-32,967	-1,554	0,010
24.11.11	-51.052	-1.995	0.008	**16.02.12**	-4,290	-0,962	0,008
28.11.11	-51.757	-2.026	0.006	**17.02.12**	15,854	-0,517	0,008
28.11.11	-51.735	-2.028	0.010	**20.02.12**	-32,956	-1,585	0,007
30.11.11	-2.567	-0.893	0.011	**20.02.12**	-32,973	-1,585	0,008
02.12.11	-30.825	-1.534	0.009	**22.02.12**	-4,217	-0,954	0,005
02.12.11	-31.133	-1.505	0.007	**22.02.12**	-4,343	-0,934	0,008
06.12.11	-2.220	-0.836	0.007	**24.02.12**	15,506	-0,508	0,006
09.12.11	-51.797	-2.079	0.005	**24.02.12**	15,525	-0,507	0,008
15.12.11	-4.919	-0.915	0.010	**27.02.12**	-32,915	-1,587	0,014
19.12.11	18.535	-0.392	0.009	**29.02.12**	-4,173	-0,989	0,007
19.12.11	18.482	-0.404	0.012	**02.03.12**	16,004	-0,559	0,007
22.12.11	18.385	-0.437	0.011	**05.03.12**	-33,319	-1,640	0,006
22.12.11	18.462	-0.407	0.004	**07.03.12**	-4,582	-0,936	0,008
04.01.12	15.720	-0.465	0.008	**07.03.12**	-4,504	-0,939	0,011
04.01.12	15.763	-0.476	0.006	**09.03.12**	10,584	-0,617	0,009
06.01.12	-33.066	-1.586	0.010	**12.03.12**	-32,751	-1,579	0,009
11.01.12	15.874	-0.474	0.007	**12.03.12**	-34,412	-1,697	0,102
11.01.12	15.919	-0.464	0.009	**14.03.12**	-5,014	-0,965	0,021
12.01.12	-33.027	-1.634	0.010	**16.03.12**	15,289	-0,520	0,009
13.01.12	-4.212	-0.940	0.010	**19.03.12**	-33,048	-1,563	0,000

Table S6.1 *Continued.*

Date	δ_{47}	$\Delta_{47, raw}$	se (internal)
19.03.12	-33.041	-1.555	0.008
21.03.12	-4.446	-0.935	0.010
21.03.12	-4.381	-0.934	0.010
23.03.12	10.485	-0.625	0.010
26.03.12	-33.318	-1.572	0.009
26.03.12	-33.189	-1.571	0.013
28.03.12	-4.167	-0.950	0.010
30.03.12	15.987	-0.524	0.012
02.04.12	-32.861	-1.606	0.007
04.04.12	-4.086	-0.970	0.010
04.04.12	-4.127	-0.951	0.010
05.04.12	10.917	-0.611	0.011
11.04.12	-33.382	-1.611	0.008
11.04.12	-33.261	-1.604	0.010
13.04.12	15.316	-0.546	0.007
16.04.12	-5.021	-0.969	0.011
18.04.12	-33.660	-1.639	0.008
23.04.12	-2.754	-0.909	0.009
23.04.12	-2.687	-0.921	0.011
25.04.12	-5.008	-0.992	0.007
25.04.12	-4.331	-0.945	0.009
27.04.12	10.200	-0.653	0.009
30.04.12	-33.446	-1.620	0.010
02.05.12	-3.243	-0.936	0.008
04.05.12	13.171	-0.581	0.010
07.05.12	-33.112	-1.595	0.007
07.05.12	-32.991	-1.606	0.007
09.05.12	-4.555	-1.007	0.006
14.05.12	-2.596	-0.898	0.011
14.05.12	-2.498	-0.914	0.010
16.05.12	-33.722	-1.644	0.009
16.05.12	-33.356	-1.633	0.010
21.05.12	-2.783	-0.937	0.006
21.05.12	-2.463	-0.932	0.010
23.05.12	-33.683	-1.640	0.008
29.05.12	11.785	-0.607	0.012
30.05.12	-5.229	-0.978	0.012
30.05.12	-5.324	-0.969	0.008
01.06.12	-33.731	-1.613	0.010
04.06.12	-2.515	-0.949	0.008
04.06.12	-2.621	-0.941	0.013
13.06.12	-33.593	-1.617	0.011

Slopes and R^2 of heated gas lines used during the time period of calibration.

Date	slope	R^2	intercept	se
15.11.11	0.0240	0.9974	-0.838	0.016
16.11.11	0.0238	0.9966	-0.835	0.020
22.11.11	0.0236	0.9951	-0.830	0.021
23.11.-24.11.11	0.0238	0.9956	-0.818	0.019
28.11.11	0.0239	0.9951	-0.815	0.022
29.11.-30.11.11	0.0237	0.9966	-0.812	0.017
01.12.-02.12.11	0.0233	0.9987	-0.819	0.009
19.12.-20.03.12	0.0228	0.9962	-0.846	0.005
22.03.12	0.0220	0.9959	-0.855	0.010
23.03.12	0.0217	0.9987	-0.854	0.006
27.03.12	0.0216	0.9984	-0.847	0.006
29.03.-30.03.12	0.0221	0.9984	-0.858	0.006
03.04.12	0.0218	0.9988	-0.867	0.005
05.04.-10.04.12	0.0223	0.9992	-0.869	0.005
12.04.-13.04.12	0.0224	0.9987	-0.865	0.005
14.04.-15.04.12	0.0223	0.9985	-0.867	0.005
17.04.12	0.0224	0.9988	-0.867	0.005
19.04.12	0.0223	0.9988	-0.868	0.005
30.04.12-09.08.12	0.0225	0.9980	-0.872	0.003

Table S6.1 *Continued.*

δ_{47} and $\Delta_{47, raw}$ values of 25 °C water equilibrated gases considered for determining the ETFs applied to sample data.			
Date	**δ_{47}**	**$\Delta_{47, raw}$**	**se (internal)**
02.09.11	9.378	0.204	0.005
02.09.11	12.769	0.259	0.006
05.09.11	-30.289	-0.853	0.006
08.09.11	-21.235	-0.608	0.009
12.09.11	-30.350	-0.854	0.010
12.09.11	-30.510	-0.832	0.009
14.09.11	7.402	0.130	0.008
14.09.11	7.503	0.129	0.007
20.09.11	16.881	0.376	0.008
30.09.11	7.358	0.127	0.009
22.11.11	20.381	0.447	0.007
24.11.11	11.374	0.237	0.008
10.09.12	-30.025	-0.780	0.007
10.09.12	-21.066	-0.584	0.009
10.09.12	15.858	0.239	0.009
17.09.12	7.353	0.111	0.015
17.09.12	13.460	0.263	0.010
17.09.12	-30.714	-0.714	0.007
Slopes and intercepts of the ETFs used during the period of calibration			
Date	**slope**	**intercept**	
nov-dec 2011	1.1670	0.9952	
jan-feb 2012	1.1521	0.9943	
mar-apr 2012	1.1233	0.9926	
may-jun 2012	1.1094	0.9918	
jul-aug 2012	1.0959	0.9910	

Table S6.2 *Carbonates measured during the analysis interval of the Silurian sample*s.

Date	Nr	Sample	Size	δ_{47}	Δ_{47raw}	Δ_{47abs}	sd	IC HG	IC 25G	m HG	$\delta^{13}C$	$\delta^{18}O$
15.11.11	C 829	25-1a 1	4.1	14.733	-0.045	0.599	0.039	-0.84	-0.06	0.0240	1.91	-4.15
	C 832	MuStd	6.2	23.001	0.251	0.713	0.025	-0.84	-0.06	0.0240	1.59	3.84
16.11.11	C 835	MuStd	5.2	22.665	0.251	0.728	0.030	-0.84	-0.06	0.0238	1.35	3.74
	C 836											
22.11.11	C 839	MuStd	10.4	23.077	0.253	0.724	0.015	-0.84	-0.06	0.0236	1.62	3.88
23.11.12	C 843	MuStd	5.0	23.114	0.277	0.745	0.033	-0.84	-0.06	0.0238	1.53	3.75
	C 844	25-1a 2	4.6	15.005	-0.034	0.608	0.027	-0.84	-0.06	0.0238	1.64	4.18
23.11.12	C 846											
	C 848	MuStd	5.6	23.093	0.253	0.718	0.030	-0.84	-0.06	0.0238	1.64	3.88
24.11.12	C 849	MuStd	4.0	23.029	0.267	0.736	0.035	-0.84	-0.06	0.0238	1.62	3.70
28.11.11	C 852											
	C 853	MuStd	6.1	23.053	0.263	0.728	0.018	-0.84	-0.06	0.0239	1.58	3.80
29.11.11	C 856											
	C 857	MuStd	9.8	23.139	0.251	0.717	0.033	-0.84	-0.06	0.0237	1.61	3.74
	C 858	98-47h	4.0	22.302	0.130	0.599	0.032	-0.84	-0.06	0.0237	8.39	-3.11
30.11.11	C 859	MuStd	4.9	23.105	0.282	0.754	0.021	-0.84	-0.06	0.0237	1.63	3.87
	C 862							-0.84	-0.06			
01.12.11	C 863	MuStd	4.3	23.059	0.237	0.714	0.016	-0.84	-0.06	0.0233	1.60	3.65
	C 864	Sig1 5-1	4.2	13.628	-0.057	0.627	0.033	-0.84	-0.06	0.0233	1.94	-5.24
02.12.11	C 865											
07.12.11	C 870											
14.12.11	C 873											
15.12.11	C 874											
16.12.11	C 876											
19.12.11	C 877											
20.12.11	C 880											
21.12.11	C 883											
	C 884	98-47q	4.6	22.228	0.144	0.622	0.019	-0.84	-0.06	0.0235	8.36	-3.17
22.12.11	C 885	MuStd	9.7	23.082	0.259	0.734	0.031	-0.84	-0.06	0.0235	1.49	3.80
	C 888	Sig1 3	4.3	14.170	-0.034	0.636	0.024	-0.84	-0.06	0.0235	2.01	-4.80
23.12.11	C 889											
03.01.12	C 890											
	C 891	MuStd	8.5	23.022	0.258	0.737	0.031	-0.84	-0.06	0.0235	1.58	3.86
	C 892	NBS 19	5.6	16.936	-0.212	0.361	0.028	-0.84	-0.06	0.0235	1.97	-1.90
04.01.12	C 893	MuStd	8.4	22.674	0.239	0.725	0.030	-0.84	-0.06	0.0235	1.53	3.59
	C 896	NBS 19	8.9	16.968	-0.230	0.338	0.034	-0.84	-0.06	0.0235	2.00	-1.88
	C 897											
05.01.12	C 898	NBS 19	9.3	16.878	-0.207	0.371	0.032	-0.84	-0.06	0.0233	1.99	-1.98
	C 901	MuStd	9.5	23.005	0.238	0.720	0.019	-0.84	-0.06	0.0233	1.59	3.86
	C 902	Sig1 3	4.0	13.544	-0.086	0.601	0.031	-0.84	-0.06	0.0233	2.01	-5.36
06.01.12	C 903											
	C 904											
	C 905	MuStd	7.9	22.994	0.236	0.718	0.026	-0.84	-0.06	0.0233	1.62	3.82
09.01.12	C 906	MuStd	8.0	22.950	0.219	0.713	0.033	-0.84	-0.06	0.0228	1.60	3.81
	C 907	NBS 19	8.0	16.922	-0.239	0.344	0.025	-0.84	-0.06	0.0228	1.99	-1.90
	C 910											
10.01.12	C 911	MuStd	4.7	22.904	0.212	0.706	0.031	-0.84	-0.06	0.0228	1.57	3.80
	C 912	Valle3-1c1	5.2	11.152	-0.139	0.610	0.033	-0.84	-0.06	0.0228	-0.71	-5.05
	C 914											

Table S6.2 *Continued.*

Date	Nr	Sample	Size	δ_{47}	Δ_{47raw}	Δ_{47abs}	sd	IC HG	IC 25G	m HG	$\delta^{13}C$	$\delta^{18}O$
	C 915	NBS 19	5,4	16.944	-0.163	0.430	0.032	-0.84	-0.06	0.0228	1.97	-1.94
11.01.12	C 918											
12.01.12	C 919	Valle3-1c 2	5.3	11.227	-0.159	0.585	0.025	-0.84	-0.06	0.0228	-0.83	-4.85
	C 922	MuStd	4.5	22.667	0.209	0.709	0.018	-0.84	-0.06	0.0228	1.51	3.63
13.01.12	C 922											
	C 924											
16.01.12	C 925	NBS 19	4.3	16.850	-0.218	0.369	0.035	-0.84	-0.06	0.0228	1.97	-1.97
	C 926											
	C 927											
17.01.12	C 929	MuStd	6.5	22.955	0.230	0.725	0.015	-0.84	-0.06	0.0228	1.57	3.83
	C 930	Val(1)-1	5.7	12.298	-0.115	0.608	0.028	-0.84	-0.06	0.0228	-0.43	-4.22
	C 931	Sig1 3	4.2	13.493	-0.087	0.609	0.027	-0.84	-0.06	0.0228	1.97	-5.36
18.01.12	C 934	MuStd	4.3	23.067	0.241	0.735	0.021	-0.84	-0.06	0.0228	1.63	3.88
	C 935											
	C 932	NBS 19	9.0	17.009	-0.233	0.349	0.028	-0.84	-0.06	0.0228	2.04	-1.87
19.01.12	C 936	NBS 19	4.0	16.837	-0.209	0.381	0.037	-0.84	-0.06	0.0228	1.97	-2.02
	C 937	Sig1 3	4.2	13.369	-0.094	0.603	0.029	-0.84	-0.06	0.0228	1.99	-5.50
	C 938											
	C 939											
20.01.12	C 940	MuStd	4.5	23.158	0.239	0.731	0.015	-0.84	-0.06	0.0228	1.62	3.97
	C 942	81-1f	5.0	11.670	-0.122	0.616	0.024	-0.84	-0.06	0.0228	-0.58	-4.68
	C 943											
23.01.12	C 944	MuStd	5.8	22.828	0.241	0.741	0.027	-0.84	-0.06	0.0228	1.55	3.72
	C 945	Sig1 1b	4.0	13.799	-0.071	0.619	0.042	-0.84	-0.06	0.0228	2.09	-5.19
	C 946	81-1f	4.0	11.838	-0.133	0.600	0.019	-0.84	-0.06	0.0228	-0.56	-4.53
	C 947											
24.01.12	C 948	MuStd	4.2	23.014	0.233	0.727	0.019	-0.84	-0.06	0.0228	1.60	3.86
	C 949	98-47h 2	5.1	13.464	-0.095	0.600	0.025	-0.84	-0.06	0.0228	2.03	-5.44
	C 950											
25.01.12	C 952	MuStd	6.0	23.024	0.242	0.737	0.034	-0.84	-0.06	0.0228	1.62	3.84
	C 954											
	C 955											
27.01.12	C 956											
	C 958	MuStd	4.2	22.792	0.209	0.705	0.031	-0.84	-0.06	0.0228	1.54	3.72
	C 959											
31.01.12	C 961	MuStd	4.2	23.085	0.233	0.726	0.025	-0.84	-0.06	0.0228	1.63	3.90
	C 962											
02.02.12	C 964	MuStd	5.3	22.991	0.215	0.707	0.014	-0.84	-0.06	0.0228	1.57	3.89
	C 965											
	C 966	MuStd	4.1	23.108	0.210	0.698	0.031	-0.84	-0.06	0.0228	1.59	3.99
03.02.12	C 968	MuStd	4.3	22.753	0.209	0.706	0.023	-0.84	-0.06	0.0228	1.58	3.65
	C 969											
	C 970											
06.02.12	C 974	MuStd	5.0	22.555	0.197	0.698	0.021	-0.84	-0.06	0.0228	1.58	3.46
	C 975	Diu1	4.4	14.429	-0.082	0.590	0.030	-0.84	-0.06	0.0228	2.02	-4.51
	C 976	Diu2	4.4	14.998	-0.058	0.602	0.032	-0.84	-0.06	0.0228	1.87	-3.84
07.02.12	C 980											
	C 981	MuStd	4.6	22.885	0.221	0.717	0.017	-0.84	-0.06	0.0228	1.65	3.70
	C 982											
	C 983	Diu3	4.2	15.428	0.004	0.663	0.032	-0.84	-0.06	0.0228	1.82	-3.43
	C 984	NBS 19	4.6	16.875	-0.208	0.381	0.039	-0.84	-0.06	0.0228	2.04	-2.03
	C 985											
08.02.12	C 986	MuStd	4.9	22.705	0.225	0.726	0.022	-0.84	-0.06	0.0228	1.60	3.56

Table S6.2 *Continued.*

Date	Nr	Sample	Size	δ_{47}	Δ_{47raw}	Δ_{47abs}	sd	IC HG	IC 25G	m HG	$\delta^{13}C$	$\delta^{18}O$
	C 989	MuStd	6,0	22.814	0.224	0.722	0.029	-0.84	-0.06	0.0228	1.60	3.67
	C 990	Val(1)-1 S	7,1	5.042	-0.301	0.584	0.019	-0.84	-0.06	0.0228	-0.54	-10.99
	C 991	Sig1 5-1 S1	4,5	10.088	-0.193	0.576	0.019	-0.84	-0.06	0.0228	2.08	-8.67
09.02.12	C 992	NBS 19	4,5	16.713	-0.225	0.365	0.024	-0.84	-0.06	0.0228	1.98	-2.11
	C 993	98-47h S	6,5	11.901	-0.136	0.594	0.040	-0.84	-0.06	0.0228	5.73	-10.40
	C 996	MuStd	5,6	22.653	0.217	0.719	0.033	-0.84	-0.06	0.0228	1.62	3.51
	C 994	Val(1)-1 M	5,3	11.940	-0.117	0.615	0.027	-0.84	-0.06	0.0228	-0.53	-4.48
	C 995	Sig1 5-1S2	5,4	10.295	-0.203	0.559	0.028	-0.84	-0.06	0.0228	2.14	-8.52
	C 997	98-47h M1	5,4	21.335	0.085	0.601	0.026	-0.84	-0.06	0.0228	9.41	-4.96
	C 998	98-47h M2	5,4	22.172	0.130	0.631	0.025	-0.84	-0.06	0.0228	9.49	-4.27
10.02.12	C 999	MuStd	4,8	22.631	0.208	0.708	0.036	-0.84	-0.06	0.0228	1.56	3.55
	C 1000	98-49b	4,5	22.886	0.132	0.614	0.031	-0.84	-0.06	0.0228	8.43	-2.59
	C 1004	Diu4a	4,3	14.509	-0.073	0.598	0.020	-0.84	-0.06	0.0228	1.62	-4.06
	C 1001	Korbklint	4,1	17.666	0.001	0.600	0.032	-0.84	-0.06	0.0228	5.01	-4.28
	C 1002	Diu4p	4,3	14.897	-0.056	0.608	0.019	-0.84	-0.06	0.0228	1.93	-3.99
	C 1003	NBS 19	5,5	16.959	-0.208	0.379	0.019	-0.84	-0.06	0.0228	2.09	-2.00
13.02.12	C 1005	MuStd	5,1	22.754	0.240	0.742	0.022	-0.84	-0.06	0.0228	1.57	3.67
	C 1006	26-1b(2)	4,3	14.814	-0.047	0.620	0.020	-0.84	-0.06	0.0228	2.26	-4.39
	C 1009	26-1b(1)	4,0	14.188	-0.075	0.605	0.024	-0.84	-0.06	0.0228	1.94	-4.67
	C 1007	26-1b(3)	5,5	14.361	-0.030	0.652	0.026	-0.84	-0.06	0.0228	2.07	-4.68
	C 1008											
	C 1010	26-1b(4)	4,7	14.725	-0.027	0.646	0.027	-0.84	-0.06	0.0228	1.98	-4.24
	C 1011											
14.02.12	C 1013	MuStd	5,4	22.601	0.226	0.730	0.027	-0.84	-0.06	0.0228	1.62	3.45
	C 1014	26-1a(3)	4,3	14.035	-0.061	0.624	0.029	-0.84	-0.06	0.0228	1.65	-4.56
	C 1017	81-1d(3)	4,3	11.271	-0.147	0.598	0.025	-0.84	-0.06	0.0228	-0.73	-4.91
	C 1015	26-1a(4)	4,4	14.490	-0.053	0.622	0.022	-0.84	-0.06	0.0228	1.85	-4.32
	C 1016	NBS 19	4,5	16.853	-0.206	0.383	0.025	-0.84	-0.06	0.0228	2.11	-2.11
	C 1018	81-1d(4)	9,2	11.548	-0.111	0.632	0.029	-0.84	-0.06	0.0228	-0.59	-4.81
15.02.12	C 1019	MuStd	7,8	22.865	0.226	0.723	0.024	-0.84	-0.06	0.0228	1.64	3.68
	C 1021	81-1d(1)	6,7	10.423	-0.152	0.615	0.038	-0.84	-0.06	0.0228	-0.87	-5.60
	C 1023	21-1d(2)	4,2	11.585	-0.129	0.610	0.022	-0.84	-0.06	0.0228	-0.64	-4.71
	C 1020	26-1a(2)	4,2	13.287	-0.097	0.603	0.025	-0.84	-0.06	0.0228	1.16	-4.79
	C 1022	NBS 19	4,6	16.561	-0.235	0.358	0.040	-0.84	-0.06	0.0228	1.90	-2.17
	C 1024	26-1a(1) M	5,2	14.970	-0.049	0.613	0.020	-0.84	-0.06	0.0228	2.34	-4.32
	C 1025	26-1b(3) M	5,5	13.940	-0.040	0.651	0.029	-0.84	-0.06	0.0228	1.34	-4.38
16.02.12	C 1026	MuStd	7.x	22.910	0.197	0.689	0.031	-0.84	-0.06	0.0228	1.65	3.75
	C 1030											
	C 1032											
	C 1028	NBS 19	4,4	16.750	-0.259	0.325	0.040	-0.84	-0.06	0.0228	2.07	-2.13
	C 1031											
	C 1033											
17.02.12	C 1034	MuStd	4,4	22.529	0.215	0.720	0.023	-0.84	-0.06	0.0228	1.56	3.45
	C 1037											
	C 1036											
	C 1038	NBS 19	4,3	16.798	-0.222	0.366	0.026	-0.84	-0.06	0.0228	2.04	-2.09
	C 1039											
	C 1046	MuStd	4,3	23.037	0.217	0.708	0.019	-0.84	-0.06	0.0228	1.72	3.43
	C 1049											
	C 1050											
23.02.12	C 1057	MuStd	4,5	22.958	0.208	0.700	0.022	-0.84	-0.06	0.0228	1.62	3.46
	C 1059											
	C 1061											

Table S6.2 *Continued.*

Date	Nr	Sample	Size	δ_{47}	Δ_{47raw}	Δ_{47abs}	sd	IC HG	IC 25G	m HG	$\delta^{13}C$	$\delta^{18}O$
	C 1058											
	C 1060	MuStd	5.0	22.416	0.203	0.708	0.031	-0.84	-0.06	0.0228	1.53	3.03
	C 1062											
	C 1063											
28.02.12	C 1076	MuStd	4.6	22.899	0.239	0.737	0.039	-0.84	-0.06	0.0228	1.64	3.33
	C 1078	Diu5	3.9	15.393	-0.079	0.568	0.023	-0.84	-0.06	0.0228	1.79	-3.76
	C 1082	Val(6)-4	4.8	11.636	-0.173	0.558	0.028	-0.84	-0.06	0.0228	-0.20	-5.03
	C 1077	Diu6 1	5.2	15.232	-0.075	0.577	0.033	-0.84	-0.06	0.0228	1.98	-3.69
	C 1079											
	C 1080	Diu7	5.0	14.321	-0.109	0.562	0.040	-0.84	-0.06	0.0228	1.47	-4.06
	C 1081	Kullu6-4 1	4.1	22.876	0.074	0.548	0.041	-0.84	-0.06	0.0228	8.87	-2.96
01.03.12	C 1090	NBS 19	5.7	16.514	-0.273	0.332	0.025	-0.86	-0.06	0.0228	2.02	-2.30
	C 1092	Diu5	4.1	14.476	-0.099	0.580	0.026	-0.86	-0.06	0.0228	1.43	.3.89
	C 1091											
	C 1093	NBS 19	4.4	16.709	-0.244	0.360	0.026	-0.86	-0.06	0.0228	1.97	-2.09
	C 1094	Diu6 2	4.3	14.944	-0.060	0.612	0.018	-0.86	-0.06	0.0228	1.85	-3.87
	C 1095											
02.03.12	C 1096	MuStd	4.7	22.476	0.184	0.693	0.035	-0.86	-0.06	0.0228	1.57	3.07
	C 1101	Val(6)-4	5.8	12.205	-0.149	0.582	0.039	-0.86	-0.06	0.0228	-0.13	-4.56
	C 1098	Diu7	4.0	14.487	-0.107	0.570	0.034	-0.86	-0.06	0.0228	1.54	-3.97
	C 1099	Kullu6-4 2	4.0	23.247	0.110	0.590	0.023	-0.86	-0.06	0.0228	8.85	-2.61
	C 1100	NBS 19	4.1	16.931	-0.226	0.374	0.033	-0.86	-0.06	0.0228	2.15	-2.06
	C 1103											
05.03.12	C 1104	MuStd	4.2	22.472	0.189	0.698	0.022	-0.86	-0.06	0.0228	1.62	3.01
	C 1109	98-45f	4.3	22.652	0.076	0.566	0.033	-0.86	-0.06	0.0228	8.51	-2.84
	C 1106	97-12	4.5	6.906	-0.219	0.639	0.036	-0.86	-0.06	0.0228	-3.26	-6.69
	C 1107											
	C 1110	Korbklint	4.0	16.805	-0.023	0.606	0.027	-0.86	-0.06	0.0228	4.46	-4.58
06.03.12	C 1111	NBS 19	4.0	16.497	-0.241	0.369	0.030	-0.86	-0.06	0.0228	1.97	-2.30
	C 1112											
	C 1115	NBS 19	4.5	16.820	-0.224	0.380	0.038	-0.86	-0.06	0.0228	2.01	-2.04
	C 1114											
	C 1113	NBS 19	4.6	16.505	-0.223	0.389	0.023	-0.86	-0.06	0.0228	2.02	-2.36
	C 1116											
	C 1117											
13.03.12	C 1134											
	C 1136	NBS 19	4.1	16.435	-0.229	0.384	0.017	-0.86	-0.06	0.0228	1.97	-2.37
	C 1138											
	C 1135											
	C 1137											
	C 1139											
	C 1140	MuStd	7.0	22.841	0.225	0.729	0.034	-0.86	-0.06	0.0228	1.69	3.27
14.03.12	C 1141	MuStd	4.7	22.717	0.207	0.712	0.040	-0.86	-0.06	0.0228	1.63	3.22
	C 1144	Korbklint	4.0	16.675	-0.030	0.601	0.034	-0.86	-0.06	0.0228	4.66	-4.88
	C 1146	97-12	4.0	6.917	-0.230	0.626	0.032	-0.86	-0.06	0.0228	-3.06	-6.86
	C 1143	Diu5	4.1	15.334	-0.049	0.614	0.017	-0.86	-0.06	0.0228	1.86	-3.52
	C 1145	NBS 19	4.3	16.657	-0.235	0.371	0.041	-0.86	-0.06	0.0228	2.09	-2.26
	C 1147	Diu5	4.0	14.765	-0.042	0.636	0.022	-0.86	-0.06	0.0228	1.77	-3.98
15.03.12	C 1148											
	C 1151	NBS 19	4.3	16.533	-0.226	0.384	0.023	-0.86	-0.06	0.0228	1.99	-2.29
	C 1153	Diu8(3)	4.1	14.562	-0.080	0.599	0.019	-0.86	-0.06	0.0228	1.63	-4.01
	C 1149	MuStd	5.3	23.216	0.224	0.718	0.038	-0.86	-0.06	0.0228	1.71	3.63
	C 1150	Diu8(1p)	4.1	15.227	-0.061	0.603	0.032	-0.86	-0.06	0.0228	1.63	-3.39

Table S6.2 *Continued.*

Date	Nr	Sample	Size	δ_{47}	Δ_{47raw}	Δ_{47abs}	sd	IC HG	IC 25G	m HG	$\delta^{13}C$	$\delta^{18}O$
	C 1152	Diu8(2)	4.0	14.992	-0.061	0.609	0.030	-0.86	-0.06	0.0228	1.76	-3.73
	C 1154											
16.03.12	C 1156											
	C 1158	Diu8(4)	4.1	15.106	-0.079	0.586	0.020	-0.86	-0.06	0.0228	1.87	-3.71
	C 1161	Diu8(6)	4.1	14.767	-0.109	0.561	0.033	-0.86	-0.06	0.0228	1.78	-3.93
	C 1157	MuStd	5.4	22.638	0.232	0.742	0.035	-0.86	-0.06	0.0228	1.73	3.42
	C 1159	NBS 19	4.6	17.025	-0.225	0.373	0.036	-0.86	-0.06	0.0228	2.07	-1.90
	C 1160	Diu8(5)	4.4	14.713	-0.038	0.642	0.019	-0.86	-0.06	0.0228	1.81	-4.08
20.03.12	C 1168	MuStd	8.7	22.707	0.227	0.735	0.021	-0.86	-0.06	0.0228	1.64	3.18
	C 1170	Diu8(7)	4.0	14.712	-0.091	0.583	0.028	-0.86	-0.06	0.0228	1.86	-4.07
	C 1172	Diu8(8)	4.8	14.824	-0.088	0.583	0.021	-0.86	-0.06	0.0228	1.90	-4.00
	C 1169											
	C 1171	NBS 19	4.4	16.975	-0.242	0.355	0.021	-0.86	-0.06	0.0228	2.09	-1.95
	C 1173	Diu8(9.1)	6.5	14.926	-0.072	0.599	0.029	-0.86	-0.06	0.0228	1.82	-3.84
	C 1174	Diu8(9.2)	4.3	14.485	-0.059	0.624	0.034	-0.86	-0.06	0.0228	1.78	-4.25
22.03.12	C 1181											
	C 1183											
	C 1185											
	C 1182	NBS 19	4.5	16.602	-0.260	0.360	0.018	-0.86	-0.06	0.0220	1.99	-2.20
	C 1184	MuStd	5.6	22.684	0.219	0.747	0.034	-0.86	-0.06	0.0220	1.73	3.08
	C 1186	Diu 9 CT	4.0	14.923	-0.070	0.614	0.024	-0.86	-0.06	0.0220	2.11	-4.13
	C 1187	Diu 9 CT	4.5	14.724	-0.054	0.637	0.032	-0.86	-0.06	0.0220	2.22	-4.44
23.03.12	C 1189	MuStd	10.4	22.689	0.223	0.759	0.025	-0.86	-0.06	0.0217	1.67	3.14
	C 1191	All6	5.4	13.207	-0.115	0.611	0.042	-0.86	-0.06	0.0217	1.67	-5.34
	C 1194											
	C 1190											
	C 1192	NBS 19	5.1	16.618	-0.220	0.410	0.030	-0.86	-0.06	0.0217	2.09	-2.31
	C 1193											
27.03.12	C 1201											
	C 1203											
	C 1206											
	C 1202	MuStd	7.1	22.538	0.202	0.742	0.028	-0.86	-0.06	0.0216	1.68	3.00
	C 1204	NBS 19	5.5	16.774	-0.246	0.378	0.035	-0.86	-0.06	0.0216	1.99	-2.04
	C 1205	Diu 9 CT	5.5	14.928	-0.046	0.647	0.020	-0.86	-0.06	0.0216	2.12	-4.16
	C1207	Diu 9 CT	5.5	15.176	-0.056	0.630	0.018	-0.86	-0.06	0.0216	2.06	-3.85
29.03.12	C 1215											
	C 1217											
	C 1219											
	C 1216	MuStd	5.4	22.524	0.205	0.732	0.028	-0.86	-0.06	0.0221	1.66	3.02
	C 1218	NBS 19	4.0	16.986	-0.255	0.354	0.013	-0.86	-0.06	0.0221	2.10	-1.94
	C 1220											
	C 1221											
30.03.12	C 1223											
	C 1226	98-47m	4.9	20.416	0.026	0.584	0.027	-0.86	-0.06	0.0221	7.38	-3.88
	C 1228	98-47trace	4.3	21.925	0.074	0.600	0.032	-0.86	-0.06	0.0221	7.80	-2.86
	C 1224	MuStd	6.2	22.722	0.213	0.737	0.030	-0.86	-0.06	0.0221	1.76	3.50
	C 1225	81-1e1	4.9	11.662	-0.136	0.620	0.028	-0.86	-0.06	0.0221	-0.38	-4.87
	C 1227	NBS 19	5.8	16.746	-0.219	0.400	0.028	-0.86	-0.06	0.0221	2.13	-2.23
03.04.12	C 1236											
	C 1240	NBS 19	5.0	16.493	-0.254	0.373	0.021	-0.86	-0.06	0.0218	2.01	-2.33
	C 1242	81-1e2	5.5	12.207	-0.169	0.573	0.026	-0.86	-0.06	0.0218	-0.33	-4.35
	C 1237											
	C 1238	Valle 3-1c 3	5.7	10.666	-0.158	0.623	0.027	-0.86	-0.06	0.0218	-0.82	-5.40

Table S6.2 *Continued.*

Date	Nr	Sample	Size	δ_{47}	Δ_{47raw}	Δ_{47abs}	sd	IC HG	IC 25G	m HG	$\delta^{13}C$	$\delta^{18}O$
	C 1239											
	C 1241											
05.04.12	C 1251											
	C 1254											
	C 1252	MuStd	5.7	22.871	0.198	0.711	0.022	-0.86	-0.06	0.0223	1.73	3.29
	C 1253	81-1e3	4.8	11.907	-0.142	0.604	0.041	-0.86	-0.06	0.0223	-0.31	-4.70
	C 1255	NBS 19	6.8	16.687	-0.243	0.370	0.026	-0.86	-0.06	0.0223	2.09	-2.22
10.04.12	C 1256	MuStd	8.6	22.883	0.239	0.757	0.031	-0.86	-0.06	0.0223	1.61	3.37
	C 1258											
	C 1260	NBS 19	6.0	16.544	-0.248	0.368	0.028	-0.86	-0.06	0.0223	1.88	-2.16
	C 1257											
	C 1259											
	C 1261											
	C 1262											
12.04.12	C 1271											
	C 1273											
	C 1276											
	C 1270											
	C 1272											
	C 1274	NBS 19	4.3	16.926	-0.247	0.358	0.026	-0.86	-0.06	0.0224	2.06	-1.96
	C 1275											
13.04.12	C 1278											
	C 1279											
	C 1283											
	C 1280	NBS 19	4.6	16.561	-0.244	0.371	0.028	-0.86	-0.06	0.0224	2.09	-2.35
	C 1281											
	C 1282											
14.04.12	C 1284											
	C 1285											
15.04.12	C 1286											
	C 1287											
17.04.12	C 1295											
	C 1298	NBS 19	4.9	16.664	-0.267	0.343	0.022	-0.86	-0.06	0.0224	1.96	-2.10
	C 1301											
	C 1296											
	C 1297											
	C 1299											
	C 1300											
19.04.12	C 1309											
	C 1311											
	C 1312	NBS 19	7.4	16.631	-0.249	0.366	0.034	-0.86	-0.06	0.0223	1.94	-2.13
	C 1308											
	C 1310											
	C 1313											
	C 1314											
30.04.12	C 1342											
	C 1345	NBS 19	4.1	16.441	-0.270	0.343	0.028	-0.86	-0.06	0.0225	1.80	-2.16
	C 1347											
	C 1344											
	C 1346											
	C 1348											
03.05.12	C 1354											
	C 1359	Diu5 CT	5.1	14.994	-0.058	0.622	0.025	-0.87	-0.06	0.0225	1.84	-3.81

Table S6.2 *Continued.*

Date	Nr	Sample	Size	δ_{47}	Δ_{47raw}	Δ_{47abs}	sd	IC HG	IC 25G	m HG	$\delta^{13}C$	$\delta^{18}O$
	C 1355	97-12 CT	5.0	10.003	-0.164	0.630	0.026	-0.87	-0.06	0.0225	-0.89	-5.98
	C 1356	Diu8 CT	4.2	14.841	-0.079	0.602	0.033	-0.87	-0.06	0.0225	1.91	-4.00
	C 1358	NBS 19	4.3	16.722	-0.235	0.383	0.043	-0.87	-0.06	0.0225	2.08	-2.19
	C 1360	Diu7 CT	4.1	14.480	-0.055	0.638	0.039	-0.87	-0.06	0.0225	1.71	-4.19
04.05.12	C 1362											
	C 1364	Val(6)-4CT	4.1	11.827	-0.181	0.565	0.022	-0.87	-0.06	0.0225	-0.28	-4.76
	C 1367											
	C 1363	Valle3-1c CT	4.3	10.821	-0.163	0.609	0.028	-0.87	-0.06	0.0225	-0.79	-5.27
	C 1365	NBS 19	5.4	16.913	-0.209	0.406	0.021	-0.87	-0.06	0.0225	2.11	-2.06
	C 1366	98-47o	5.1	22.951	0.127	0.629	0.032	-0.87	-0.06	0.0225	8.66	-2.74
08.05.12	C 1374											
	C 1377	NBS 19	4.4	16.718	-0.207	0.414	0.031	-0.87	-0.06	0.0225	1.99	-2.13
	C 1379	All6 M1	7.1	14.186	-0.103	0.592	0.031	-0.87	-0.06	0.0225	2.55	-5.22
	C 1375	Valle(3)-1c M1	6.4	9.079	-0.205	0.606	0.029	-0.87	-0.06	0.0225	-0.83	-6.88
	C 1378	98-47o M1	5.7	21.006	0.061	0.604	0.031	-0.87	-0.06	0.0225	9.20	-5.05
10.05.12	C 1387											
	C 1390	NBS 19	4.0	16.625	-0.233	0.387	0.044	-0.87	-0.06	0.0225	1.98	-2.19
	C 1391	98-47o M2	5.4	21.272	0.064	0.601	0.028	-0.87	-0.06	0.0225	9.13	-4.74
11.05.12	C 1388	Val (6)-4 S	4.1	13.140	-0.086	0.638	0.021	-0.87	-0.06	0.0225	0.16	-3.99
	C 1394											
	C 1389											
	C 1391	Val(6)-4 M	7.7	11.979	-0.121	0.627	0.018	-0.87	-0.06	0.0225	-0.90	-4.08
	C 1392	All6 M2	10.4	15.497	-0.052	0.616	0.031	-0.87	-0.06	0.0225	3.53	-4.93
	C 1395	Diu6 M	9.8	14.442	-0.087	0.604	0.034	-0.87	-0.06	0.0225	2.99	-5.41
12.05.12	C 1396	Valle(3)-1c M2	8.4	8.970	-0.204	0.610	0.020	-0.87	-0.06	0.0225	-0.89	-6.94
	C 1397	NBS 19	4.4	16.556	-0.258	0.361	0.031	-0.87	-0.06	0.0225	2.09	-2.34
	C 1398	97-12 M	7.6	11.591	-0.151	0.604	0.028	-0.87	-0.06	0.0225	0.28	-5.55
	C 1399	Diu7 M	7.8	9.065	-0.196	0.618	0.033	-0.87	-0.06	0.0225	-3.13	-4.73
15.05.12	C 1406											
	C 1408	26-1a M	6.4	15.050	-0.038	0.643	0.026	-0.87	-0.06	0.0225	2.41	-4.32
	C 1411	26-1b M	6.9	14.140	-0.087	0.611	0.035	-0.87	-0.06	0.0225	1.33	-4.13
	C 1407	81-1d S1	4.6	7.527	-0.258	0.586	0.026	-0.87	-0.06	0.0225	-1.18	-8.02
	C 1409	NBS 19	4.9	16.750	-0.247	0.369	0.035	-0.87	-0.06	0.0225	2.07	-2.14
	C 1410	21-1d M	8.5	11.107	-0.143	0.625	0.030	-0.87	-0.06	0.0225	-0.74	-5.06
	C 1412	26-1b S1	5.5	13.681	-0.087	0.623	0.027	-0.87	-0.06	0.0225	2.22	-5.42
18.05.12	C 1419											
	C 1421	26-1b S2	6.1	13.117	-0.122	0.598	0.028	-0.87	-0.06	0.0225	2.23	-5.94
	C 1424	81-1d S2	9.7	8.540	-0.239	0.582	0.032	-0.87	-0.06	0.0225	-1.21	-7.01
	C 1420	81-1d M	4.5	9.915	-0.175	0.619	0.036	-0.87	-0.06	0.0225	-1.17	-5.78
	C 1422	NBS 19	4.5	16.559	-0.208	0.417	0.021	-0.87	-0.06	0.0225	2.09	-2.38
	C 1423	21-1d M	6.2	9.723	-0.186	0.612	0.022	-0.87	-0.06	0.0225	-1.65	-5.50
	C 1425	98-49b S2	10.2	9.867	-0.187	0.608	0.019	-0.87	-0.06	0.0225	4.66	-11.31
22.05.12	C 1431											
	C 1433	NBS 19	4.6	16.567	-0.252	0.368	0.027	-0.87	-0.06	0.0225	2.05	-2.29
	C 1436	81-1f1	5.7	11.528	-0.140	0.618	0.020	-0.87	-0.06	0.0225	-0.73	-4.67
	C 1432	98-49b M	5.6	17.871	-0.019	0.593	0.028	-0.87	-0.06	0.0225	8.08	-6.95
23.05.12	C 1434	98-47q S1	8.5	11.589	-0.166	0.587	0.039	-0.87	-0.06	0.0225	6.32	-11.22
	C 1435	81-1f M	5.8	9.992	-0.200	0.589	0.028	-0.87	-0.06	0.0225	-1.41	-5.45
	C 1437	81-1f2	7.0	11.593	-0.135	0.621	0.015	-0.87	-0.06	0.0225	-0.73	-4.61
	C 1441											
25.05.12	C 1442											
	C 1444	Diu8M	10.6	15.187	-0.056	0.620	0.025	-0.87	-0.06	0.0225	2.56	-4.31
	C 1447	Diu2 S	4.1	15.531	-0.066	0.600	0.020	-0.87	-0.06	0.0225	2.35	-3.76

Table S6.2 *Continued.*

Date	Nr	Sample	Size	δ_{47}	Δ_{47raw}	Δ_{47abs}	sd	IC HG	IC 25G	m HG	$\delta^{13}C$	$\delta^{18}O$
	C 1443	Diu5M	10.1	15.045	-0.068	0.609	0.031	-0.87	-0.06	0.0225	2.33	-4.22
	C 1445	NBS 19	4.3	16.584	-0.229	0.393	0.031	-0.87	-0.06	0.0225	1.96	-2.21
	C 1446	Diu8 S	4.8	12.980	-0.121	0.603	0.030	-0.87	-0.06	0.0225	2.40	-6.24
	C 1448	Diu3M	7.8	15.368	-0.052	0.619	0.016	-0.87	-0.06	0.0225	2.36	-3.95
31.05.12	C 1458											
	C 1460	NBS 19		16.728	-0.241	0.375	0.034	-0.87	-0.06	0.0225	2.00	-2.10
	C 1463	98-49b S1	5.2	12.236	-0.172	0.565	0.029	-0.87	-0.06	0.0225	5.75	-10.06
	C 1459	Diu1M	10,8	15.109	-0.039	0.641	0.012	-0.87	-0.06	0.0225	1.99	-3.86
	C 1461	NBS 19	5.2	16.702	-0.245	0.372	0.019	-0.87	-0.06	0.0225	2.02	-2.14
	C 1462	All6 M2	7.4	15.149	-0.058	0.618	0.034	-0.87	-0.06	0.0225	3.18	-4.93
	C 1464	98-47q S2	4.6	12.537	-0.157	0.574	0.025	-0.87	-0.06	0.0225	6.22	-10.22
01.06.12	C 1466											
	C 1468	98-47p M	7.7	19.791	0.002	0.569	0.027	-0.87	-0.06	0.0225	9.10	-6.07
	C 1471	Diu8 CT S	4.5	12.829	-0.140	0.586	0.030	-0.87	-0.06	0.0225	2.48	-6.44
	C 1467	Kullu6-4M	6.3	19.095	0.030	0.617	0.025	-0.87	-0.06	0.0225	8.67	-6.37
	C 1469	NBS 19	5.5	16.638	-0.220	0.402	0.035	-0.87	-0.06	0.0225	2.07	-2.28
	C 1470	98-47p S	4.7	13.785	-0.110	0.595	0.032	-0.87	-0.06	0.0225	6.47	-9.29
09.06.12	C 1475											
	C 1478	25-1b M	6.0	14.062	-0.068	0.635	0.025	-0.87	-0.06	0.0225	1.83	-4.69
	C 1476	25-1b	5.0	14.321	-0.081	0.614	0.025	-0.87	-0.06	0.0225	1.67	-4.28
	C 1477	NBS 19	5.0	16.522	-0.249	0.373	0.030	-0.87	-0.06	0.0225	2.02	-2.32
	C 1479	25-1b S	4.5	8.485	-0.220	0.605	0.022	-0.87	-0.06	0.0225	1.85	-9.98

7 Summary and outlook

7.1 Summary

Clumped isotope analysis of CO_2 gas and carbonates was successfully established at the Goethe University of Frankfurt. This is proven by long-term reproducibilities of standard materials which are comparable to other laboratories. For example, our mean Δ_{47} composition of NBS 19 yields an average on a long term which is in the range of the "accepted value".

The installation of the clumped isotope technique comprised (1) the elaboration of gas preparation protocols as well as digestion techniques, and (2) the identification of mass spectrometric parameters and data reduction protocols to receive accurate and precise Δ_{47} values. During the course of the dissertation the following preparation protocols and analytical setups were applied.

(1) Initially phosphoric acid digestions of carbonate samples were performed at 25 °C in McCrea-type reaction vessels. However, we changed to reaction temperatures of 90 °C using a partly automated common acid bath.

(2) CO_2 gases were cleaned cryogenically on an extraction line held at high vacuum to prevent secondary re-equilibration with water. Furthermore, sample gases were passed through a GC to remove contaminants that provoke isobaric interferences with m/z 47.

(3) Sample CO_2 was analyzed on a Thermo Scientific MAT 253 gas source mass spectrometer (Thermo Fisher Scientific, Bremen, Germany) that is equipped with six Faraday cup collectores for the measurement of masses 44–49 (resistors: $3*10^8$ Ω, $3*10^{10}$ Ω, 10^{11} Ω for masses 44-46 and 10^{12} Ω for masses 47–49, respectively). The original stainless steel capillaries were replaced by electroformed Ni-capillaries. Sample CO_2 was measured versus Oztech reference gas using a dual inlet system. Mass 44 signals were adjusted to (16000 ± 150) mV. Ten acquisitions consisting of ten cycles each were run (ion integration time: 20 s; shot-noise limit: ~0.008‰); before each acquisition peak centering, background determination and pressure adjustments was made.

(4) Δ_{47} values were directly referenced to the absolute scale (Dennis et al., 2011). For this purpose, clumped isotope data were corrected for a non-linearity of the mass spectrometer using heated gases. Afterwards, Δ_{47} values were referenced to the absolute scale by applying the empirical transfer function (ETF) which was constructed using gases equilibrated at distinct temperatures (25 and 1000 °C).

During the course of this study the following methodological results were obtained.

(1) In cooperation with ETH Zurich the non-linearity of the mass spectrometers was investigated. The non-linearity affects the measurements of CO_2 isotopologues by creating deviations between actual and measured 47/44 isotopologue ratios. It arises from from negative background interferences on the m/z 47 Faraday cup collector. The negative background increases linearly with increasing intensity of the m/z 44 ion beam. A correction scheme was proposed which can be applied if the m/z 44 cup has a wider slit width than the m/z 47 collector. The proposed background correction is less time-consuming compared to the non-linearity correction procedure using heated gases.

(2) For carbonates digested at 25 °C in sealed vessels a sample size effect was observed. For samples <7 mg higher mean Δ_{47} values were obtained than for larger aliquots. Furthermore, Δ_{47} data of small samples showed a larger scatter. No sample size effect was determined for carbonates digested in a common acid bath at 90 °C. To avoid such methodological artefacts on Δ_{47} measurements we recommend to react samples at 90 °C in a common acid bath instead of using digestions at 25 °C in sealed vessels.

(3) Differences in acid fractionation factores between 90 and 25 °C digestions ($\Delta_{47}{}^{*}{}_{25-90}$) of 0.066‰ and 0.075‰ were obtained for aragonite and calcite, respectively. Δ_{47} data obtained only from samples >7 mg reacted at 25 °C were considered for the determination of the $\Delta_{47}{}^{*}{}_{25-90}$ values. Our $\Delta_{47}{}^{*}{}_{25-90}$ values approximate the theoretical prediction of 0.069‰ for calcite (Guo et al., 2009). However, the $\Delta_{47}{}^{*}{}_{25-90}$ values are lower than the difference in acid fractionation factors between 90 and 25 °C reported by Henkes et al. (2013) who determined a $\Delta_{47}{}^{*}{}_{25-90}$ value of 0.092‰ on the absolute scale.

The relationship between growth temperatures and ^{13}C-^{18}O clumping in carbonates has been investigated in several studies. However, discrepant results have been published (e.g., Ghosh et al., 2006a; Guo et al., 2009; Dennis and Schrag, 2010; Tripati et al., 2010; Thiagarajan et al., 2011; Eagle et al., 2012; Henkes et al., 2013; Zaarur et al., 2013). In this thesis further calibration data based on natural calcites are presented. Preliminary calibration data was also produced for aragonitic bivalves.

(1) For the calcite calibration material of various origins (biominerals: shell of a brachiopod and a bivalve, eggshell of an ostrich and foraminifera tests; biologically induced precipitates: cold seep carbonate) were sampled. The following universal relationship between the inverse squared temperature of growth and absolute Δ_{47} was determined: $\Delta_{47} = 0.0327\ (\pm\ 0.0026) * 1/T^2 + 0.3030\ (\pm\ 0.0308)$ (with Δ_{47} in ‰ and T in K; the

theoretical $\Delta_{47}{}^{*}{}_{25-90}$ value of Guo et al. (2009) was applied to the Δ_{47} data). The line is identical with the "90 °C calibration" reported by Henkes et al. (2013) as well as with the theoretical prediction of Guo et al. (2009). Furthermore, at least the slope of our calibration is comparable with the slopes of the "90 °C lines" determined by both Dennis and Schrag (2010) and Eagle et al. (2012); nevertheless, the intercepts differ. In contrast to the calibrations based on 25 °C digestions (e.g., Ghosh et al., 2006a) the temperature sensitivity of our line is lower. The best achievable analytical precision of Δ_{47} analysis yields a precision of ±3 °C, instead of ±2 °C resulting from the Ghosh et al. (2006a) line. It seems unlikely that kinetic effects or isotopic mixing cause the observed discrepancies. Furthermore, no evidence was found the clumped isotope fractionation between CO_2 and calcite dependent on the isotopic composition of samples.

(2) Preliminary Δ_{47} data of aragonitic bivalves indicate that the temperature sensitivity of the aragonite calibration is identical with the sensitivity of the calcite line determined in this study. However, the intercept plots 0.03‰ lower. For verification of the aragonite line additional investigations are required.

Clumped isotope analysis was applied to Silurian brachiopod shells from Gotland/Sweden (1) to decipher both ocean water temperatures and $\delta^{18}O$ values of ancient seawater, and (2) to determine the susceptibility of the clumped isotopic composition to diagenetic processes.

(1) For shell calcite for which SEM observations indicated a good state of preservation, $T(\Delta_{47})$ values of ~28 to 33 °C are determined for tropical shallow water in the Silurian period. From these samples $\delta^{18}O$ values of ca. –1‰ are reconstructed for Silurian seawater. These results are conform with previously published clumped isotope data of Silurian carbonates and may strengthen the assumption that the oxygen isotopic composition has been buffered to (0 ± 1)‰ since the Paleozoic time interval.

(2) Variable degrees of ultrastructural preservation of investigated brachiopod shells coincide with a large range and scatter of $T(\Delta_{47})$ values. Our results show that the shells altered at low water–rock ratios during rock–buffered diagenesis. The $\delta^{18}O$ values are assumed to reflect pristine ocean water compositions. The sparitic phases represent different cement generations that grew from several fluids at varying temperatures during fluid–buffered diagenesis; the micritic phases lithified during rock–buffered diagenesis; nevertheless, a more open system prevailed compared to conditions during the alteration of the brachiopod shells. This study indicates that significant information

regarding diagenetic alteration of $\delta^{18}O$ compositions of fossil material as well as reconstructions of diagenetic processes are obtained from clumped isotope analysis.

7.2 Outlook

Laboratory developments At the Goethe University of Frankfurt we established the original technique for clumped isotope measurements of CO_2 gas first developed by John M. Eiler and his group at Caltech. In order to reduce the menpower to operate this technique a fully automated device is currently constructed in Frankfurt. A similar system was set up at Caltech Institute and later in other laboratories (Passey et al., 2010; Henkes et al., 2013). We will, furthermore, study microvolume measurements to evaluate if the large sample sizes required for clumped isotope analysis can be reduced (single measurements: ~4 mg resulting in ~20 mg for replications). An alternative way to reduce sample sizes and to increase sample throughput would be the change to the method developed at ETH Zurich using a Kiel IV carbonate device (Schmid and Bernasconi, 2010).

Correction for non-linearities We have already started to correct the non-linearity of the mass spectrometer using a new background correction procedure based on simultaneous monitoring of m/z 49 ion beam intensities and corresponding m/z 47 "off-peak" backgrounds (Fiebig et al., 2014, Abstract). These are determined before and after each acquisition for both reference and the sample gas. An improved precision of Δ_{47} data was obtained. Nevertheless, no impact on mean Δ_{47} values of standard materials and re-analyzed calibration samples was observed. Therefore, the non-linearity correction procedure via heated gases as applied to Δ_{47} data reported in this dissertation are evaluated to be accurate as well.

Calibration of the carbonate clumped isotope thermometer It is of utmost importance that the clumped isotope community solves the "calibration issue" regarding the carbonate clumped isotope thermometer. The reasons for the discrepant lines which were determind have to be discovered. Inter-laboratory comparisons might help to unravel the causes for the different reported calibration lines. For this reason, Stefano M. Bernasconi from the ETH Zurich already supplied a set of standard materials which describe a large range in Δ_{47} compositions to several laboratories. We will further investigate the relationship between $1/T^2$ and Δ_{47} values of aragonites. Samples measured before will be re-analyzed and additional samples of various origins will be added.

Application to Silurian brachiopod shells The application of clumped isotope analysis to Silurian brachiopod shells shows that Δ_{47} values of fossil material are prone to diagenetic alteration. Conventional techniques to determine the preservation state of the samples (CL, SEM, trace element concentrations) do not give sufficient indication whether clumped isotopic compositions reflect original ocean water signatures. Calculated $T(\Delta_{47})$ values are interpreted to reflect only highest seawater temperature estimates. Therefore, it is essential to find new methods that help to distinguish between pristine and altered Δ_{47} values.

Recently, we have studied the boron isotopic composition ($\delta^{11}B$) of the investigated brachiopod shells from Gotland/Sweden. High resolution boron isotope compositions were measured using a laser ablation multi-collector inductively coupled mass spectrometer (LA-MC-ICP-MS). Preliminary results show that the $\delta^{11}B$ values are prone to diagenetic alteration. The depths transects of a shell indicated that for material characterized by orange cathodoluminescent colours lower $\delta^{11}B$ ratios are measured. Furthermore a large scatter of more than 2‰ is observed in regions of variable preservation (Fig. 7.1, red squares and black diamonds). In contrast, no significant variations are determined from non-luminescent areas (Fig. 7.1, yellow circles). Further investigations will be made to evaluate whether $\delta^{11}B$ analysis can help to discern diagenetic alteration of fossil material.

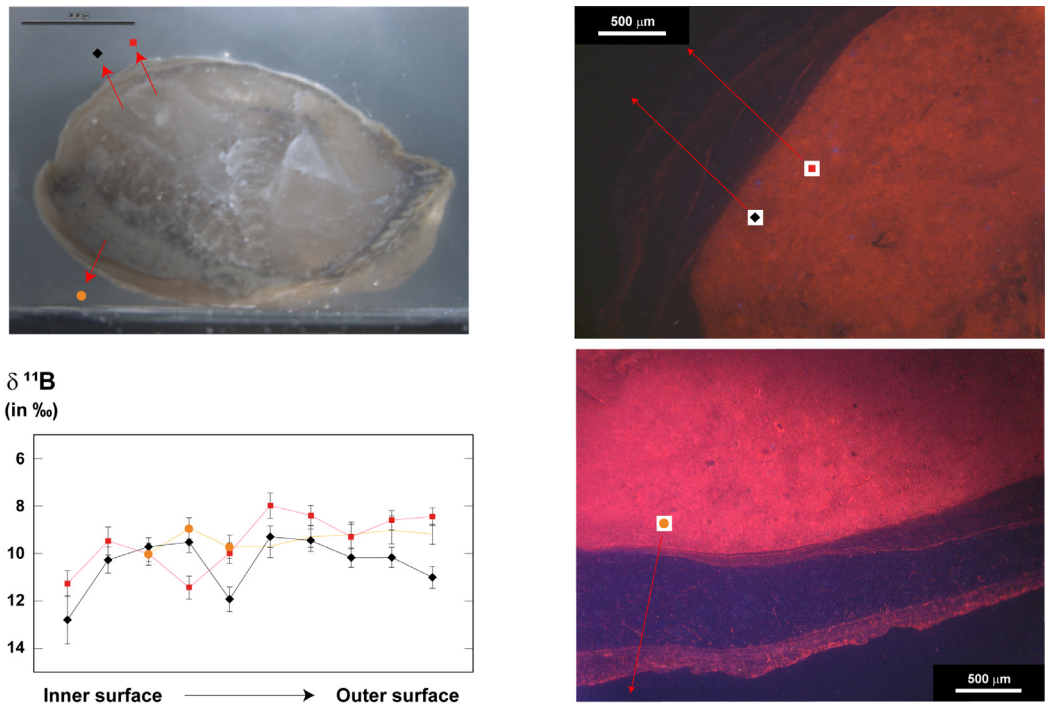

Figure 7.1 *$\delta^{11}B$ values of three depth transects of sample 17-1. Cathodouminescence is observed in the analyzed area of the dorsal valve (a). Depths transects of this area indicate a large scatter of $\delta^{11}B$ values (red squares and black diamonds). In contrast, constant values are measured along a transect of a non-luminescent area (b) of the ventral valve (yellow circles).*

We will, furthermore, investigate whether we can decipher diagenetic alteration processes that affected shell material in more detail. We have already applied high-resolution $^{87}Sr/^{86}Sr$ and $\delta^{11}B$ analyses to the different phases of the sample Val(1)-1 (shell, micritic phase, cements; Fig. 7.2). The following conclusions have been made: (1) For non-cathodoluminescent shell material most likely pristine $\delta^{11}B$ values are recorded. (2) The large orange cathodoluminescent cements in the center of the fossil are characterized by $\delta^{11}B$ and $^{87}Sr/^{86}Sr$ compositions that are typical for meteoric fluids. (3) The boron and radiogenic strontium isotopic ratios of the micritic phase plot between those of the marine and the meteoric endmembers. However, conspicuously the $^{87}Sr/^{86}Sr$ value is much closer to a marine composition than the $\delta^{11}B$ value indicating that the boron isotopic composition of shell carbonate is more prone to diagenetic alteration than the $^{87}Sr/^{86}Sr$ values. In contrast to the $^{87}Sr/^{86}Sr$ ratio, the $\delta^{11}B$ value was not buffered by the boron isotopic composition of the rock. (4) Small non-cathodoluminescent cements grew in direct contact with the brachiopod shell. Their $^{87}Sr/^{86}Sr$ compositions are identical to the values of shell (marine endmember). We, therefore, conclude that these cements precipitated at a very early diagenetic stage from marine fluids. However, since the $\delta^{11}B$ values of these different cement generations are identical, the boron isotopic compositions of the cements must have been altered during the formation of the sparitic cements. Further studies are required to test the usability of mutiproxy approaches for deciphering geological mechanisms such as diagenetic processes.

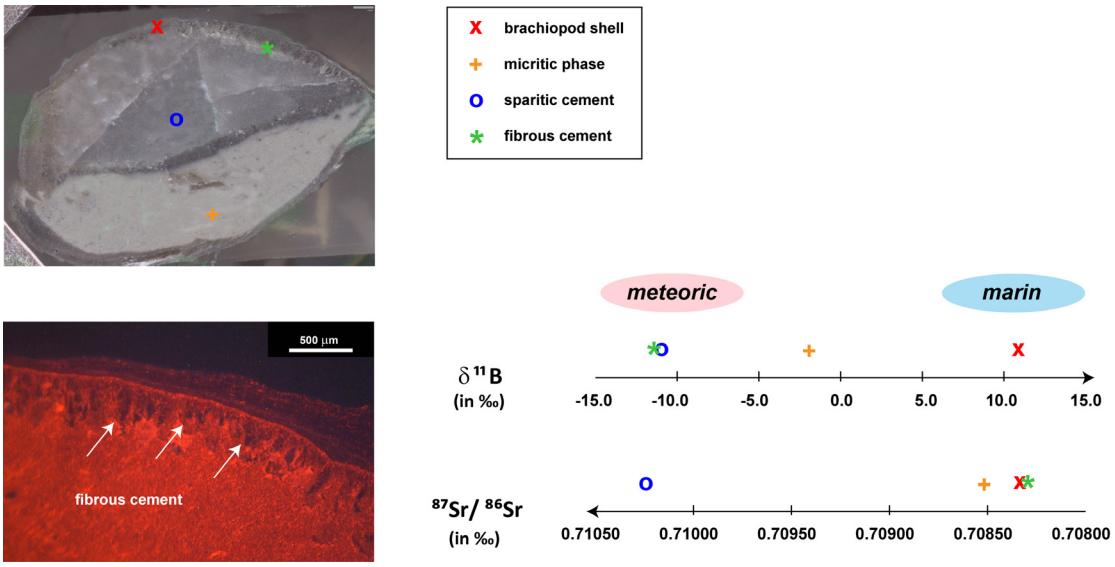

Figure 7.2 *$\delta^{11}B$ and $^{87}Sr/^{86}Sr$ values of the different phases of sample Val(1)-1. The shell represents the marine phase, whereas the sparitic cements typifies the diagenetic endmember. The $\delta^{11}B$ and $^{87}Sr/^{86}Sr$ values of the micritic phase indicate mixing between both endmembers. The non-luminescent fibrous cements grew from marine fluids. Combined $\delta^{11}B$ and $^{87}Sr/^{86}Sr$ isotope analyses can help to decipher diagenetic processes and sources of fluids.*

8 References

Affek H.P. and Eiler J.M., Abundance of mass 47 CO_2 in urban air, car exhaust, and human breath, Geochim. Cosmochim. Acta **70**, 2006, 1–12.

Affek H.P., Bar-Matthews M., Ayalon A., Matthews A. and Eiler J.M., Glacial/interglacial temperature variations in Soreq cave speleothems as recorded by 'clumped isotope' thermometry, Geochim. Cosmochim. Acta **72**, 2008, 5351–5360.

Aloisi G., Gloter A., Krüger M., Wallmann K., Guyot F. and Zuddas P., Nucleation of calcium carbonate on bacterial nanoglobules, Geology **34**, 2006, 1017–1020.

Akhmetzanov A. M., Ivanov M., Kenyon N. H. and Mazzini A. (Eds) (2007) Deep-water cold seeps, sedimentary environments and ecosystems of the Black and Tyrrhenian Seas and Gulf of Cadiz, 72. UNESCO, Paris. p. 140.

Anand P., Elderfield H. and Conte M.H., Calibration of Mg/Ca thermometry in planktonic foraminifera from a sediment trap time series, Paleoceanography **18**, 2003, DOI: 10.1029/2002PA000846.

Auclair A.C., Joachimski M.M. and Lécuyer C., Deciphering kinetic, metabolic and environmental controls on stable isotope fractionations between seawater and the shell of *Terebratalia transversa* (Brachiopoda), Chem. Geol. **202**, 2003, 59–78.

Bahr A., Pape T., Abbeg F., Bohrmann G., van Weering T., and Ivanov M.K., Authigenic carbonates from the eastern Black Sea as an archive for shallow gas hydrate dynamics e Results from the combination of CT imaging with mineralogical and stable isotope analyses, Marine and Petrol. Geol. **27**, 2010, 1819–1829.

Bahr A., Pape T., Bohrmann G., Mazzini A., Haeckel M., Reitz A. and Ivanov M.K., Authigenic carbonate precipitates from the NE Black Sea: a mineralogical, geochemical, and lipid biomarker study, Int. J. Earth Sci. **98**, 2009, 677–695.

Barbin V. and Gaspard D., Cathodoluminescence of recentarticulate brachiopod shells. Implications for growth stages and diagenesis evaluation, Geobios **28** (SUPPL. 1), 1995, 39–45.

Barnes R.O. and Goldberg E.D., Methane production and consumption in anaerobic marine sediments, Geology **4**, 1976, 297–300.

Beck J.W., Edwards L., Ito E., Taylor F.W., Recy J., Rougerie F., Joannot P. and Henin C., Sea-surface temperature from coral skeletal strontium/calcium ratios, Science **257**, 1992, 644–647.

Beirne E.C., Wanamaker Jr. A.D. and Feindel S.C., Experimental validation of environmental controls on the $\delta^{13}C$ of *Arctica islandica* (ocean quahog) shell carbonate, Geochim. Cosmochim. Acta **84**, 2012, 395–409.

Bentov S. and Erez J., Novel observations on biomineralization processes in foraminifera and implications for Mg/Ca ratio in the shells, Geology **33**, 2005, 841–844.

Berger W.H., Killingley J.S. and Vincent E., Stable isotopes in deep-sea carbonates: box core ERDC-92, west equatorial Pacific, Oceanol. Acta **1**, 1978, 203–216.

Bickert T., Pätzold J., Samtleben C. and Munnecke A., Paleoenvironmental changes in the Silurian indicated by stable isotopes in brachiopod shells from Gotland, Sweden, Geochim. Cosmochim. Acta **61**, 1997, 2717–2730.

Bigeleisen J. and Mayer M.G., Calculation of equilibrium constants for isotopic exchange reactions. J. Chem. Phys. **15,** 1947, 261–267.

Bigeleisen J., Statistical mechanics of isotopic systems with small quantum corrections. I. General considerations and the rule of the geometric mean, J. Chem. Phys. **23(12)**, 1955, 2264–2267.

Bijma J., Spero H.J., Lea D.W. and Archer D., reassessing foraminiferal stable isotope geochemistry: impact of the oceanic carbonate system (experimental results), In: Fischer G. and Wefer G., (Eds.), Use of Proxies in Paleoceanography, 1999, Springer.

Boetius A., Ravenschlag K., Schubert C.J., Rickert D., Widdel F., Gieseke A., Amann R., Jorgensen B.B., Witte U. and Pfannkuche O., A marine microbial consortium apparently mediating anaerobic oxidation of methane, Nature **407**, 2000, 623–626.

Boetius A. and Wenzhöfer F., Seafloor oxygen consumption fuelled by methane from cold seeps, Nature Geosci. **6**, 2013, 725–734.

Bohrmann G., Greinert J., Suess E. and Torres M., Authigenic carbonates from the Cascadia subduction zone and their relation to gas hydrate stability, Geology **26**, 1998, 647–650.

Bontognali T.R.R., Vasconcelos C., Warthmann R.J., Dupraz C., Bernasconi S.M. and McKenzie J.A., Microbes produce nanobacteria-like structures, avoiding cell entombment, Geology **36**, 2008, 663–666.

Brand, U. and Veizer, J., Chemical diagenesis of a multicomponent carbonate system. I. trace elements. J. Sediment. Petrol., 51, 1980, 1219–1236.

Brand U., Carbon, oxygen and strontium isotopes in Paleozoic carbonate components: An evaluation of original seawater-chemistry proxies, Chem. Geol. **204(1-2)**, 23–44.

Brand, U., Posenato R., Came R., Affek H.P., Angiolini L., Azmy K. and Farabegoli E., The end Permian mass extinction: a volcanic CO_2 – climatic global catastrophe*,* Chem. Geol.*,* 2012, 322–323.

Bristow T.F., Bonifacie M., Derkowski A., Eiler J.M. and Grotzinger J.P., Hydrothermal origin for isotopically anomalous cap dolostone cements from south China. Nature **474**, 2011, 68–71.

Calner M., Jeppsson L. and Munnecke A., Field Guide to the Silurian of Gotland - Part I. Erlanger Geol. Abh. **5**, 2004a, 113–131.

Calner M., Jeppsson L. and Munnecke A., Field Guide to the Silurian of Gotland - Part II. Erlanger Geol. Abh. **5**, 2004b, 133–151.

Came R., Eiler J.M., Veizer J., Azmy K., Brand U. and Weidman C., Coupling of surface temperatures and atmospheric CO2 concentrations during the Paleozoic era, Nature **449**, 2007, 198–201.

Cantrell, C.A., Technical Note: Review of methods for linear least-squares fitting of data and application to atmospheric chemistry problems, Atmos. Chem. Phys. **8**, 2008, 5477-5487.

Carpenter S.J. and Lohmann K.C., $\delta^{18}O$ and $\delta^{13}C$ values of modern brachiopod shells, Geochim. Cosmochim. Acta **59**, 1995, 3749–3764.

Chiessi C.M., Mulitza S., Paul A., Pätzold J., Groeneveld J. and Wefer G., South Atlantic interocean exchange as the trigger for the Bolling warm event, Geology **36**, 2008, 919–922.

CLIMAP Project Members, Seasonal reconstructions of the Earths surface at the last glacial maximum. GSA Map and Chart Ser. MC-36, 1981, Boulder, Colorado.

Collins W.J., Slab pull, mantle convection, and Pangaean assembly and dispersal, Earth Planet. Sci. Lett. **205**, 2003, 225–237.

Coplen T.B., Kendall C. and Hopple J., Comparison of stable isotope reference samples, Nature **302**, 1983, 236–238.

Csank A.Z., Tripati A.K., Patterson W.P., Eagle R.A., Rybczynski N., Ballantyne A.P. and Eiler J.M., Estimates of Arctic land surface temperatures during the early Pliocene from two novel proxies, Earth Planet. Sci. Lett. **304**, 2011, 291–299.

Cummins R.C., Finnegan S., Fike D.A., Eiler J.M. and Fischer W.W., Carbonate clumped isotope constraints on Silurian ocean temperature and seawater $\delta^{18}O$, Geochim. et Cosmochim. Acta **140**, 2014, 241–258.

Daëron M., Guo W., Eiler J.M., Genty D., Blamart D., Boch R., Drysdale R., Maire R., Wainer K. and Zanchetta G., $^{13}C^{18}O$ clumping in speleothems: observations from natural caves and precipitation experiments, Geochim. Cosmochim. Acta **75**, 2011, 3303–3317.

Dennis K.J. and Schrag D.P., Clumped isotope thermometry of carbonatites as an indicator of diagenetic alteration, Geochim. Cosmochim. Acta **74**, 2010, 4110–4122.

Dennis K.J., Affek H.P., Passey B.H., Schrag D.P. and Eiler J.M., Defining an absolute reference frame for 'clumped' isotope studies of CO_2, Geochim. Cosmochim. Acta **75**, 2011, 7117–7131.

Dupraz C., Reid R.P., Braissant O., Decho A.W., Norman R.S. and Visscher P.T., Processes of carbonate precipitation in modern microbial mats, Earth-Sci. Rev. **96**, 2009, 141–162.

Eagle R.A., Schauble E.A., Tripati A.K., Tütken T., Hulbert R.C. and Eiler J.M., Body temperatures of modern and extinct vertebrate from ^{13}C–^{18}O bond abundances in bioapatit, PNAS **107**, 2010, 10377–10382.

Eagle R.A., Eiler J.M., Tripati A.K., Ries J.B., Freitas P.S., Hiebenthal C., Wanamaker A.D., Jr., Taviani M., Elliot M., Marenssi S., Nakamura K., Ramirez P. and Roy K., The influence of

temperature and seawater carbonate saturation state on ^{13}C–^{18}O bond ordering in bivalve mollusks, Biogeoscience **10**, 2013, 4591–4606.

Eiler J.M. and Schauble E., $^{18}O^{13}C^{16}O$ of earth's atmosphere, Geochim. Cosmochim. Acta **68**, 2004, 4767–4777.

Eiler J.M., 'Clumped-isotope' geochemistry – The study of naturally-occurring, multiply-substituted isotopologues. Earth Planet. Sci. Lett. **262**, 2007, 309–327.

Eiler J.M., Paleoclimate reconstruction using carbonate clumped isotope thermometry. Quatern. Sci. Rev. 2011, **30**, 3575–3588.

Elderfield H. and Ganssen G., Past temperature and $\delta^{18}O$ of surface ocean waters inferred from foraminiferal Mg/Ca ratios, Nature **405**, 2000, 442–445.

Erez J., Vital effect on stable-isotope composition seen in foraminifera and coral skeletons, Nature **273**, 1978, 199–202.

Epstein S., Buchsbaum R., Lowenstam H.A. and Urey H.C., Carbonate-water isotopic temperature scale, Bull. Geol. Soc. Am. **62**, 1951, 417–426.

Epstein S., Buchsbaum R., Lowenstam H.A. and Urey H.C., Revised carbonate–water isotopic temperature scale, Bull. Geol. Soc. Am. **64**, 1953, 1315–1325.

Fairbanks R.G., Sverlove M., Free R., Wiebe P.H. and Be A.W.H., Vertical-distribution and isotopic fractionation of living planktonic foraminifera from the Panama Basin, Nature **298**, 1982, 841–844.

Ferry, J.M., Passey B.H., Vasconcelos C., and Eiler J.M., Formation of dolomite at 40–80 °C in the Latemar carbonate buildup, Dolomites, Italy, from clumped isotope thermometry, Geology **39(6)**, 2011, 571–574.

Fiebig J., Luedecke T., Loeffler N., Methner K., Wacker U. and Hofmann S., Background Correction for Clumped Isotope Analysis of CO_2 Based on m/z = 49 Ion Beam Intensity, Abstract – Goldschmidt Conf. 2014.

Finnegan S., Bergmann K., Eiler J.M., Jones D.S., Fike D.A., Eisenman I., Hughes N.C., Tripati A.K. and Fischer W.W., The magnitude and duration of late Ordovician-Early Silurian glaciation, Science **331**, 2011, 903–906.

Frakes L.A., Francis J.E. and Syktus J.I., Climate modes of the Phanerozoic. Cambridge Univ. Press, 2005.

Friedrich O., Schiebel R., Wilson P.A., Weldeab S., Beer C.J., Cooper M.J. and Fiebig J., Influence of test size, water depth, and species ecology on Mg/Ca, Sr/Ca, $\delta^{18}O$ and $\delta^{13}C$ in nine modern species of planktic foraminifers, Earth Planet. Sci. Lett. **319–320**, 2012, 133–145.

Garzione C.N., Hoke G.D., Libarkin J.C., Withers S., MacFadden B., Eiler J.M., Ghosh P. and Mulch A., Rise of the Andes, Science **6**, 2008, 1304–1307.

Ghosh, P., Patecki M., Rothe M. and Brand, W.A., Calcite-CO_2 mixed into CO_2-free air: a new CO_2-in-air stable isotope reference material for the VPDB scale. Rapid Commun. Mass Spectrom. **19**, 2005, 1097–1119.

Ghosh P., Adkins J., Affek H.P., Balta B., Guo W., Schauble E.A., Schrag D.P. and Eiler J.M., $^{13}C–^{18}O$ bonds in carbonate minerals: a new kind of paleothermometer, Geochim. Cosmochim. Acta **70**, 2006a, 1439–1456.

Ghosh P., Garzione C.M. and Eiler J.M., Rapid uplift of the altiplano revealed through $^{13}C–^{18}O$ bonds in paleosol carbonates, Science **27**, 2006b, 511–515.

Ghosh P., Eiler J.M., Campana S.E. and Feeney R. F., Calibration of the carbonate 'clumped isotope' paleothermometer for otoliths. Geochim. Cosmochim. Acta **71**, 2007, 2736–2744.

Gischler E., Sedimentation on Rasdhoo and Ari atolls, Maldives, Indian Ocean, Facies **52**, 2006, 341–360.

Grauel A.-L., Schmid T.W., Hu B., Bergami C., Capotondi L., Zhou L. and Bernasconi S.M., Calibration and application of the 'clumped isotope' thermometer to foraminifera for high-resolution climate reconstructions, Geochim. Cosmochim. Acta **108**, 2013, 125–140.

Greaves M., Barker S., Daunt C. and Elderfield H., Accuracy, standardization, and interlaboratory calibration standards for foraminiferal Mg/Ca thermometry, Geochem., Geophys., Geosyst. **6(2)**, Q02D13.

Gregory R.T. and Taylor H.P., An oxygen isotope profile in a section of Cretaceous oceanic crust, Samail Ophiolite, Oman: evience for $\delta^{18}O$ buffering of the oceans by deep (>5 km) seawater hydrothermal circulation at mid-ocean ridges, J. Geophys. Res. **86**, 1981, 2737–2755.

Gregory R. T. (1991) Oxygen isotope history of seawater revisited: timescales for boundary event changes in the oxygen isotopic composition of seawater. In Stable Isotope geochemistry: A Tribute to Samuel Epstein (eds. H. P. Taylor, J. R. O'Neil and I. R. Kaplan). Geochem. Soc. Spec. Publ. 3. pp. 65–76.

Groeneveld J. and Chiessi C.M., Mg/Ca of *Globorotalia inflata* as a recorder of permanent thermocline temperatures in the South Atlantic, Paleoceanography **26**, 2011, DOI: 10.1029/2010PA001940.

Grossman E.L., Stable isotope fractionation in live benthic foraminifera from the Southern California Borderland, Palaeogeogr. Palaeoclimatol. Palaeoecol. **47**, 1984, 301–327.

Grossman, E.L., Zhang, C. and Yancey, T.E., Stable-isotope stratigraphy of brachiopods from Pennsylvanian shales in Texas, Geol. Soc. Am. Bull. 103, 1991, 953–965.

Guo W., Mosenfelder J.L., Goddard W.A., III and Eiler J.M., Isotopic fractionations associated with phosphoric acid digestion of carbonate minerals: insights from first-principles theoretical modeling and clumped isotope measurements, Geochim. Cosmochim. Acta **73**, 2009, 7203–7225.

Hemleben C., Zur Morphogenese planktonischer Foraminiferen, Zitteliana **1**, 1969, 91–133.

Hemleben C., Spindler M. and Anderson O.R., Modern Planktonic Foraminifera, 1989, Springer-Verlag; New York, pp. 1–363.

Henkes G.A., Passey B.H., Wanamaker A.D., Jr., Grossman E.L., Ambrose W.G., Jr. and Carroll M.L., Carbonate clumped isotope compositions of modern marine mollusk and brachiopod shells, Geochim. Cosmochim. Acta **106**, 2013, 307–325.

Hill P.S., Tripati and Schauble E.A., Theoretical constraints on the effects of pH, salinity, and temperature on clumped isotope signatures of dissolved inorganic carbon species and precipitating carbonate minerals, Geochim. Cosmochim. Acta **125**, 2014, 610–652.

Hoehler T., Alperin M., Albert D.B. and Martens C.S., Field and laboratory studies of methane oxidation in an anoxic marine sediment: evidence for a mehanogen-sulfate reducer consortium, Global Biogeochem. Cycles **8**, 1994, 451–463.

Huntington K.W., Eiler J.M., Affek H.P., Guo W., Bonifacie M., Yeung L.Y., Thiagarajan N., Passey B.H., Tripati A.K., Daëron M. and Came R., Methods and limitations of 'clumped' CO_2 isotope (Δ_{47}) analysis by gas-source isotope ratio mass spectrometry. J. Mass Spectrom. **44**, 2009, 1318 –1329.

Huntington K.W., Wernicke B.P. and Eiler J.M., Influence of climate change and uplift on Colorado Plateau paleotemperatures from carbonate clumped isotope thermometry, Tectonics **29**, 2010, DOI: 10.1029/2009TC002449.

Huntington K.W., Budd D.A., Wernicke B.P. and Eiler J.M., Use of clumped-isotope thermometry to constrain the crystallization temperature of diagenetic calcite, J. Sediment. Res. **81**, 2011, 656–669.

Jaffrés J.B.D., Shields G.A. and Wallmann K., The oxygen isotope evolution of seawater: A critical review of a long-standing controversy and an improved geological water cycle model for the past 3.4 billion years, Earth Sci. Rev. **83**, 2007, 83–122.

Jeppsson, L., Silurian conodont faunas from Gotland, Fossils Strata **15**, 1983, 121–144.

Jeppsson L., An oceanic model for lithological and faunal changes tested on the Silurian record, J. Geol. Soc. London, **147**, 1990, 663–674.

Johnson B.J., Fogel M.L. and Miller G.H., Stable isotopes in modern ostrich eggshell: a calibration for paleoenvironmental applications in semi-arid regions of southern Africa, Geochim. Cosmochim. Acta **62**, 1998, 2451–2461.

Kasting J.F., Howard M.T., Wallmann K., Veizer J., Shields G. and Jaffrés J., Paleoclimates, ocean depth, and the oxygen isotopic composition of seawater, Earth Planet. Sci. Lett. **252**, 2006, 82–93.

Kim S.T. and O'Neil J.R., Equilibrium and nonequilibrium oxygen isotope effects in synthetic carbonates, Geochim. Cosmochim. Acta **61**, 1997, 3461–3475.

Kim J.-H., Schouten S., Hopmans E.C., Donner B. and Sinninghe Damsté J.S., Global sediment core-top calibration of the TEX_{86} paleothermometer in the ocean, Geochim. Cosmochim. Acta **72**, 2008, 1154–1173.

Kim S.-T, Mucci A. and Taylor B.E., Phosphoric acid fractionation factors for calcite and aragonite between 25 and 75°C: Revisited. Chem. Geol. **246**, 2007, 135–146.

Kluge T., Affek H.P., Zhang Y.G., Dublyanski Y., Spötl C., Immenhauser A. and Richter D.A., Clumped isotope thermometry of cryogenic cave carbonates. Geochim. et Cosmochim. Acta **126**, 2014, 541–554.

Knauth L. P. and Roberts S. K. (1991) The hydrogen and oxygen isotope history of the Silurian-Permian hydrosphere as determined by direct measurement of fossil water. In Stable Isotope Geochemistry: A Tribute to Samuel Epstein (eds. H. P. Taylor, Jr., J. R. O'Neil and I. R. Kaplan). Geochem. Soc. pp. 91–104.

Kurbjeweit F., Schmiedl G., Schiebel R., Hemleben Ch., Pfannkuche O., Wallmann K. and Schäfer P., Distribution, biomass and diversity of benthic foraminifera in relation to sediment geochemistry in the Arabian Sea, Deep Sea Res. Part II: Top. Stud. Oceanograph. **47**, 2000, 2913–2955.

Liedl K.R., Sekušak S. and Mayer, E., Has the dimer of carbonic acid a lower energy than its constituents water and carbon dioxide? J. Am. Chem. Soc. **119**, 1997, 3782–3784.

Locarnini R.A., Mishonov A.V., Antonov J.I., Boyer T.P., Garcia H.E., Baranova O.K., Zweng M.M. and Johnson D.R., World Ocean Atlas 2009, In: Levitus S., (Ed), NOAA Atlas NESDIS 68. Temperature, 2010, U.S. Government Printing Office; Washington, D.C., 184, (vol. 1).

Locarnini R.A., Mishonov A.V., Antonov J.I., Boyer T.P. and Garcia H.E., World Ocean Atlas 2005, In: Levitus S., (Ed), NOAA Atlas NESDIS 61. Temperature, 2006, US Government Printing Office; Washington, DC, 182, (vol. 1).

Loerting T. and Bernard J., Aqueous carbonic acid (H_2CO_3). Chem. Phys. Chem. **11**, 2010, 2305–2309.

Lowenstam H.A., Minerals formed by organisms, Science **211**, 1981, 1126–1131.

Loyd S., Corsetti F., Eiler J.M., and Tripati A.K., Determining the diagenetic conditions of concretion formation: Assessing temperatures and pore-waters using clumped isotopes, J. Sediment. Res. Curr. Ripp. **82**, 2012, 1006-1016.

Machel, H.G., Mason, R.A., Mariano, A.N. and Mucci, A., 1991. Causes and emission of luminescence in calcite and dolomite. In: C.E. Barker and O.C. Kopp (Eds): Luminescence Microscopy and Spectroscopy: Qualitative and Quantitative Applications. SEPM Short Course 25, 9-25.

Maier E. and Titschak J., *Spondylus gaederopus*: a new Mediterranean climate archive – based on high-resolution oxygen and carbon isotope analyses, Palaeogeogr. Palaeoclimatol. Palaeoecol. **291**, 2010, 228–238.

Marin F., Le Roy N. and Marie B., The formation and mineralization of mollusk shell, Frontiers Biosci. **S4**, 2012, 1099–1125.

Marshall J.D., Climatic and oceanographic isotopic signals from the carbonate rock record and their preservation. Geol. Mag. **129**, 1992, 143–160.

Marshall J.F. and McCulloch M.T., An assessment of the Sr/Ca ratio in shallow water hermatypic corals as a proxy for sea surface temperature, Geochim. Cosmochim. Acta **66**, 2002, 3263–3280.

Merritt D.A., Hayes J.M., Factors controlling precision and accuracy in isotope-ratio-monitoring mass spectrometry. Anal. Chem. **66**, 1994, 2336–2347.

Mazzini A., Ivanov M., Nermoen A., Bahr A., Bohrmann G., Svensen H. and Planke S., Complex plumbing systems in the near subsurface. geometries of authigenic carbonates from Dolgovskoy Mound (Black Sea) constrained by analogue experiments, Mar. Petrol. Geol. **25**, 2008, 457–472.

McConnaughey T., ^{13}C and ^{18}O isotopic disequilibrium in biological carbonates: I. Patterns, Geochim. Cosmochim. Acta **53**, 1989a, 151–162.

McConnaughey T., ^{13}C and ^{18}O isotopic disequilibrium in biological carbonates: II. In vitro simulation of kinetic isotope effects, Geochim. Cosmochim. Acta **53**, 1989b, 163–171.

McConnaughey T.A. and Gillikin D.P., Carbon isotopes in mollusk shell carbonates, Geo-Mar. Lett. **28**, 2008, 287–299.

McCrea J.M., On the Isotopic Chemistry of carbonates and a paleotemperature scale. J. Chem. Phys. **18**, 1950, 849–857.

Merritt D.A. and Hayes J.M., Factors controlling precision and accuracy in isotope-ratio-monitoring mass spectrometry, Anal. Chem. **66**, 1994, 2336–2347.

Morrison J.O. and Brand U., Geochemistry of Recent marine invertebrates, Geosci. Can. **13(4)**, 1986, 237–254.

Muehlenbachs K. and Clayton R.N., Oxygen isotope composition of oceanic crust and its bearing on seawater, J. Geophys. Res. **81**, 1976, 4365–4369.

Muehlenbachs K., The oxygen isotopic composition of the oceans, sediments and the seafloor, Chem. Geol. **145**, 1998, 263–273.

Muehlenbachs K., Furnes H., Fonneland H.C. and Hellevang B., Ophiolites as faithful records of the oxygen isotope ratio of ancient seawater: the Solund-Stavfjord Ophiolite Complex as a Late Ordovician example. Geol. Soc., London, Spec. Pub. **218**, 2003, 401–414.

Munnecke, A., Bildung mikritischer Kalke im Silur auf Gotland. Courier Forschungsinst. Senckenberg **198**, 1997, 1-71.

Munnecke A., Samtleben C. and Bickert T., The Ireviken Event in the lower Silurian of Gotland, Sweden – relation to similar Palaeozoic and Proterozoic events. Palaeogeogr. Palaeoclimatol. Palaeoecol. **195**, 2003, 99–124.

Nelder J.A. and Mead R., A simplex algorithm for function minimization, Comp. J. **7**, 1965, 308-313.

Nürnberg D., Bijma J. and Hemleben C., Assessing the reliability of magnesium in foraminiferal calcite as a proxy for water mass temperatures, Geochim. Cosmochim. Acta **60**, 1996, 803–814.

Passey B.H., Levin N.E., Cerling T.E., Brown F.H. and Eiler J.M., High-temperature environments of human evolution in East Africa based on bond ordering in paleosol carbonates, Proc. Natl. Acad. Sci. **107**, 2010, 11245–11249.

Passey, B.H. and Henkes G.A., Carbonate clumped isotope bond reordering and geospeedometry, Earth Planet. Sci. Lett. **351-352**, 2012, 223–236.

Parkinson D., Curry G.B., Cusack M. and Fallik A.E., Shell structure, patterns and trends of oxygen and carbon stable isotopes in modern brachiopod shells, Chem. Geol. **219**, 2005, 193–235.

Peckmann J., Thiel V., Michaelis W., Clari P., Gaillard C., Martire L. and Reitner J., Cold seep deposits of Beauvoisin (Oxfordian; southeastern France) and Marmorito (Miocene; northern Italy): microbially induced authigenic carbonates, Int. J. Earth Sci. **88**, 1999, 60–75.

Pérez-Huerta A., Cusack M., Ball A., Williams C.T. and Mackay S., Deciphering the distribution of organic components in brachiopod shells by confocal laser scanning microscopy, J. Microsci. **230**, 2008, 94–99.

Peters N.A., Huntington K.W. and Hoke G.D., Hot or not? Impact of seasonally variable soil carbonate formation on paleotemperature and O-isotope records from clumped isotope thermometry, Earth Planet. Sci. Lett. **361**, 2013, 208–218.

Pfannkuche O., Müller T. J., Nellen W. and Wefer G. (2000). Ostatlantik 1998, Cruise No. 42. Meteor Ber 00–1. p. 259.

Pfeiffer M., Timm O., Dullo W.-C. and Garbe-Schönberg D., Paired coral Sr/Ca and $\delta^{18}O$ records from the Chagos Archipelago: Late twentieth century warming affects rainfall variability in the tropical Indian Ocean, Geology **34**, 2006, 1069–1072.

Pierson, B.J., The control of cathodoluminescence in dolomite by iron and manganese. Sedimentol. **28**, 1981, 601–610.

Popp, B.N., Anderson, T.F. and Sandberg, P.A., Brachiopods as indicators of original isotopic compositions in some Paleozoic limestones, Geolog. Soc. Am. Bull. **97(10)**, 1262–1269.

Quade J., Breecker D.O., Daëron M. and Eiler J.M., The paleoaltimetry of Tibet: an isotopic perspective, Am. J. Sci. **311**, 2011, 77–115.

R Core Team, R: A language and environment for statistical computing. R Foundation for Statistical Computing, 2013, Vienna, Austria. URL http://www.R-project.org/.

Rank D., Öszoy E. and Salihoglu I., Oxygen-18, deuterium and tritium in the Black Sea and the Sea of Marmara, J. Environ. Radioact. **43**, 1999, 231–245.

Reeburgh W.S., Methane consumption in Cariaco Trench waters and sediments, Earth Planet. Sci. Lett. **28**, 1976, 337–344.

Reitner J., Peckmann J., Reimer A., Schumann G. and Thiel V., Methane-derived carbonate build-ups and associated microbial communities at cold seeps on the lower Crimean shelf (Black Sea), Facies **51**, 2005, 66–79.

Ritger S., Carson B. and Suess E., Methane-derived authigenic carbonates formed by subduction-induced pore-water expulsion along the Oregon/Washington margin, Geol. Soc. Am. Bull. **98**, 1987, 147–156.

Rohling E.J. and Cooke S., Stable oxygen and carbon isotopes in foraminiferal carbonate shells, In: Sen Gupta B.K., (Ed), Modern Foraminifera, 1999, Kluwer Academic Publishing; Dordrecht, 239–258.

Saenger C., Affek H.P., Felis T., Nhiagarajan N., Lough J.M. and Holcomb M., Carbonate clumped isotope variability in shallow water corals: temperature dependence and growth-related vital effects, Geochim. Cosmochim. Acta **99**, 2012, 224–242.

Samtleben C., Munnecke A., Bickert T. and Pätzold J., Shell succession, assemblage and species dependent effects on the C/O-isotopic composition of brachiopods – examples from the Silurian of Gotland, Chem. Geol. **175**, 2001, 61–107.

Savard, M., Veizer, J. and Hinton, R., Cathodoluminescence at low Fe and Mn concentrations: a SIMS study of zones in natural calcites. J. Sediment. Res. **A65**, 1995, 208–213.

Schauble E.A., Ghosh P. and Eiler J.M., Preferential formation of $^{13}C–^{18}O$ bonds in carbonate minerals, estimated using first-principles lattice dynamics, Geochim. Cosmochim. Acta **70**, 2006, 2510–2529.

Schiebel R. and Hemleben C., Modern planktic foraminifera, Paläontol. Z. **79**, 2005, 135–148.

Schmahl W.W., Grieshaber E., Merkel C., Kelm K., Deutschle J., Neuser R.D., Göetz A.J., Sehrbrock A. and Mader W., Hierarchical fibre composite structure and micromechanical properties of phosphatic and calcitic brachiopod shell biomaterials – an overview, Mineral. Mag. **72**, 2008, 541–562.

Schmid T.W. and Bernasconi S., An automated method for clumped-isotope$_0$ measurements on small carbonate samples. Rapid Commun. Mass Spectrom. **24**, 2010, 1955–1963.

Schmidt, G.A., Bigg, G.R., and Rohling, E.J. (1999). Global Seawater Oxygen-18 Database. http://www.giss.nasa.gov./data/o18data/.

Schmuker B. and Schiebel R., Planktic foraminifers and hydrography of the eastern and northern Caribbean Sea, Mar. Micropaleontol. **46**, 2002, 387–403.

Schouten S., Hopmans E.C., Schefuss E. and Sinninghe Damsté J.S., Distribuional variations in marine crenarchaeotal membrane lipids: a new tool for reconstructing ancient sea water temperatures?, Earth Planet. Sci. Lett. **204**, 2002, 265–274.

Schrader L., Fuhrer K. and Oetow S., Body temperatures of ostriches (Struthio camelus) kept in an open stable during winter time in Germany, J. Therm. Biol. **34**, 2009, 366–371.

Shackleton N.J., Attainment of isotopic equilibrium between ocean water and the benthonic foraminiferal genus *Uvigerina*: isotopic changes in the ocean during the last glacial, Cent. Natl. Rech. Sci. Colloq. Int. **219**, 1974, 203–209.

Simkiss K. and Wilbur K.M., Biomineralization. Cell Biology and Mineral Deposition, 1989, Academic Press; San Diego etc., 337p.

Spero H.J. and Lea D.W., Experimental determination of stable isotope variability in *Globigerina bulloides*: implications for paleoceanographic reconstructions, Mar. Micropaleontol. **28**, 1996, 231–246.

Spero H.J., Bijma J., Lea D.W. and Bernis B.E., Effect of seawater carbonate concentration on foraminiferal carbon and oxygen isotopes, Nature **390**, 1997, 497–500.

Swanson, E.M., Wernicke B.P., Eiler J.M. and Losh S., Temperatures and fluids on faults based on carbonate clumped-isotope thermometry, Am. J. Sci., **312(1)**, (2012), 1–21.

Storz D., Gischler E., Fiebig J., Eisenhauer A. and Garbe-Schönberg D., Evaluation of oxygen isotope and Sr/Ca ratios from a Maldivian scleractinian coral for reconstruction of climate variability in the northwestern Indian Ocean, Palaios **28**, 2013, 42–55, DOI: 10.2110/palo.2012.p12-034r.

Such J.E., Linear polyphosphoric acids, in *Mellor's Comprehensive Treatise on Inorganic and Theoretical Chemistry*, vol. **VIII**, suppl. III, (Eds: A. A. Eldridge, G. M. Dyson, A. J. E. Welch, D. A. Pantony). John Wiley, New York, 1971.

Swart P.K., Burns S.J. and Leder J.J., Fractionation of the stable isotopes of oxygen and carbon in carbon dioxide during the reaction of calcite with phosphoric acid as a function of temperature and technique. Chem. Geol. **86**, 1990, 89–96.

Thiagarajan N., Adkins J. and Eiler J.M., Carbonate clumped isotope thermometry of deep-sea corals and implications for vital effects, Geochim. Cosmochim. Acta **75**, 2011, 4416–4425.

Thiel V., Peckmann J., Richnow H.H., Luth U., Reitner J. and Michaelis W., Molecular signals for anaerobic methane oxidation in Black Sea seep carbonates and a microbial mat, Mar. Chem. **73**, 2001, 97–112.

Thiel V., Peckmann J., Seifert R., Wehrung P., Reitner J. and Michaelis W., Highly isotopically depleted isoprenoids: molecular markers from ancient methane venting, Geochim. Cosmochim. Acta **63**, 1999, 3959–3966.

Towe K.M. and Cifelli R., Wall ultrastructure in the calcareous foraminifera: crystallographic aspects and a model for calcification, J. Paleontol. **41**, 1967, 742–762.

Trautermann C.S., Voegele A.F., Loerting T., Kohl I., Hallbrucker A., Mayer E. and Liedl K.R., Towards the experimental decomposition rate of carbonic acid (H_2CO_3) in aqueous solution. Chem. Eur. J. **8**, 2002, 66–73.

Tripati A.K., Eagle R.A., Thiagarajan N., Gagnon A.C., Bauch H., Halloran P.R. and Eiler J.M., ^{13}C–^{18}O isotope signatures and 'clumped isotope' thermometry in foraminifera and coccoliths, Geochim. Cosmochim. Acta **74**, 2010, 5697–5717.

Turchyn A.V., Alt J.C., Brown S.T., DePaolo D.J., Coggon R.M., Chi G., Bédard J.H. and Skulski T., Reconstructing the oxygen isotope composition of late Cambrian and Cretaceous hydrothermal vent fluid. Geochim. Cosmochim. Acta **123**, 2013, 440–458.

Uchikawa J. and Zeebe, R.E., The effect of carbonic anhydrase on the kinetics and equilibrium of the oxygen isotope exchange in the CO_2-H_2O system: Implications for $\delta^{18}O$ vital effects in biogenic carbonates, Geochim. Cosmochim. Acta **95**, 2012, 15-34.

Urey H.C., The thermodynamic properties of isotopic substances, J. Chem. Soc. 1947, 562–581.

Valentine D.L., Biogeochemistry and microbial ecology of methane oxidation in anoxic environments: a review, Antonie Van Leeuwenhoek **81**, 2002, 271–282.

van Geldern R., Joachimski M.M., Day J., Jansen U., Alvarez F., Yolkin E.A. and Ma X.-P., Carbon, oxygen and strontium isotope records of Devonian brachiopod shell calcite. Paleogeogr. Paleoclimatol. Palaeoecol. **240(1-2)**, 2006, 47–67.

Veizer, J., Chemical diagenesis of carbonates: theory and application of trace element technique, SEPM Short Course No. 10, 1983a, 3-1)-3–100.

Veizer, J., Trace elements and isotopes in sedimentary carbonates. In: Reeder, R.J. (Ed.), Carbonates: Mineralogy and Chemistry: Revs. in Mineral. **11**, 1983b, pp. 265–299.

Veizer J., Bruckschen P., Pawellek F., Diener A., Podlaha O.G., Carden G.A.F., Jasper T., Korte C., Strauss H., Azmy K. and Ala D., Oxygen isotope evolution of Phanerozoic seawater, Palaeogeogr. Palaeoclimatol. Palaeoecol. **132**, 1997, 159–172.

Veizer J., Ala D., Azmy K., Bruckschen P., Buhl D., Bruhn F., Carden G.A.F., Diener A., Ebneth S., Godderis Y., Jasper T., Korte C., Pawellek F., Podlaha O.G. and Strauss H., $^{87}Sr/^{86}Sr$, $\delta^{13}C$ and $\delta^{18}O$ evolution of Phanerozoic seawater, Chem. Geol. **161**, 1999, 59–88.

von Allmen K., Nägler T.F., Pettke T., Hippler D., Grieshaber E., Logan A., Eisenhauer A. and Samankassou E., Stable isotope profiles (Ca, O, C) through modern brachiopod shells of *T. septentrionalis* and *G. vitreus*: Implications for calcium isotope paleo-ocean chemistry, Chem. Geol. **269**, 2010, 210–219.

von Rad U. (1998) Sonne Cruise SO-130 – MAKRAN II, Sonne Cruise Report 130, 152 pp.

Wachter E.A. and Hayes J.M., Exchange of oxygen isotopes in carbon dioxide-phosphoric acid systems. *Chem. Geol.* **52**, 1985, 365–374.

Wacker U., Fiebig J. and Schöne B.R., Clumped isotope analysis of carbonates comparison of two different acid digestion techniques, Rapid Commun. Mass Spectrom. **27**, 2013, 1631–1642.

Wakeham S.G., Lewis C.M., Hopmans E.C., Schouten S. and Sinninghe Damste J.S., Archaea mediate anaerobic oxidation of methane in deep euxinic waters of the Black Sea, Geochim. Cosmochim. Acta **67**, 2003, 1359–1374.

Walters Jr L.J., Claypool G.E. and Choquette P.W., Reaction rates and $\delta^{18}O$ variation for the carbonate-phosphoric acid preparation method. Geochim. Cosmochim. Acta **36**, 1971, 129–140.

Wang Z., Schauble E.A. and Eiler J.M., Equilibrium thermodynamics of multiply substituted isotopologues of molecular gases, Geochim. Cosmochim. Acta **68**, 2004, 4779–4797.

Wefer G. and Berger W.H., Isotope paleontology: growth and composition of extant calcareous species, Mar. Geol. **100**, 1991, 207–248.

Wendeberg M., Richter J.M., Rothe M. and Brand W.A., $\delta^{18}O$ anchoring to VPDB: calcite digestion with ^{18}O-adjusted ortho-phosphoric acid, Rapid Commun. Mass Spectrom. **25**, 2011, 851–860.

Wenzel, B. and Joachimski, M.M.,. Carbon and oxygen isotopic composition of Silurian brachiopods (Gotland/Sweden): Palaeoceanographic implications, Paleogeogr. Paleoclimatol. Paleoecol. **122(1–4)**, 1996, 143–166.

Wenzel B., Lécuyer C. and Joachimski M.M., Comparing oxygen isotope records of silurian calcite and phosphate – $\delta^{18}O$ compositions of brachiopods and conodonts, Geochim. et Cosmochim. Acta **64**, 2000, 1859–1872.

Wilbur K.M. and Jodrey L.H., Studies on Shell Formation. V. The inhibition of shell formation by carbonic anhydrase inhibitors, Biol. Bull. **108**, 1955, 359–365.

Wilbur K. M. and Saleuddin A. S. M. (1983) Shell formation. In The Mollusca (eds. A. S. M. Saleuddin and K. M. Wilbur). vol. 4. Physiology, Part I. 235-287.

Williams A. (1997) Shell structure. In Treatise on Invertebrate Paleontology, Part H, Brachiopoda, Vol. 1: Introduction (eds. A. Williams, M. A. James, C. C. Emig, S. Mackay, M. C. Rhodes, B. L. Cohen, A. B. Gawthrop, L. S. Peck, G. B. Curry, A. D. Ansell, M. Cusack, D. Walton, C. H. C. Brunton, D. I. MmacKinnon and J. R. Richardson (Eds.). The Geolog. Soc. Am. pp. 267–320.

Wuchter C., Schouten S., Wakeham S.G. and Sinninghe Damsté J.S., Archaeal tetraether membrane lipid fluxes in the northeastern Pacific and the Arabian Sea: implications for TEX_{86} paleothermometry, Paleoceanography **21**, 2006, DOI: 10.1029/2006PA001279.

Yamamoto Y.K., Asami R. and Iryu Y., Within-shell variations in carbon and oxygen isotope compositions of two modern brachiopods from a subtropical shelf environment off Amami-o-shima, southwestern Japan, Geochem. Geophys. Geosyst. **11** (10), 2010, 1–16.

Yeung, L.Y., Affek H.P., Hoag K.J., Guo W., Wiegel A.A., Atlas E.L., Schauffler S.M., Okumura M., Boering K.A. and Eiler J.M., Large and unexpected enrichment in stratospheric $^{16}O^{13}C^{18}O$ and its meridional variation, Proc. Natl. Acad. Sci. USA, **106(28)**, 2009, 11496–11501.

Yeung L.Y., Young E.D. and Schauble E.A., Measurements of $^{18}O^{18}O$ and $^{17}O^{18}O$ in the atmosphere and the role of isotope-exchange reactions, *J. Geophys. Res*, **117**(D18), 2012, 306.

York, D., Least-squares fitting of a straight line, Can. J. Phys. **44**, 1966, 1079–1086..

York D., Evensen N.M., Lopez Martinez M. and De Basabe Delgado J., Unified equations for the slope, intercept, and standard errors of the best straight line, Am. J. Phys. **72** (3), 2004, 367–375.

Zaarur S., Olack G. and Affek H.P., Paleo-environmental implication of clumped isotopes in land snail shells. *Geochim. Cosmochim. Acta* **75**, 2011, 6859–68692.

Zaarur S., Affek H.P. and Brandon M.T., A revised calibration of the clumped isotope thermometer, Earth Planet. Sci. Lett. **382**, 2013, 47–57.

Zeebe R.E., An explanation of the effect of seawater carbonate concentration on foraminiferal oxygen isotopes, Geochim. Cosmochim. Acta **63**, 1999, 2001–2007.

Zeebe R.E., An expression for the overall oxygen isotope fractionation between the sum of dissolved inorganic carbon and water, Geochem. Geophys. Geosyst. **8**, 2007, 1–7.

Zusammenfassung

Clumped isotope Thermometrie an Karbonaten ermöglicht die Bestimmung von Temperaturen während der Mineralisation und somit die Rekonstruktion von physiko-chemischen Bedingungen des umgebenden Wassers. Das *clumped isotope Thermometer* basiert auf der relativen Verteilung des doppelt-substituierten schweren Isotopologs $^{13}C^{18}O^{16}O^{16}O^{2-}$ im Karbonatkristall. Die Abweichung der Häufigkeit dieser CO_3^{2-}-Gruppe von der zu erwartenden statistischen Verteilung im Mineral ist temperaturabhängig. Es gibt jedoch keine Methode, die eine direkte Messung der Karbonatisotopologe ermöglicht. Stattdessen werden die Proben mit Phosphorsäure in CO_2 überführt, das mittels Gas-Massenspektrometrie analysiert werden kann. Die Abweichung zur statistischen Verteilung des CO_2 Gases wird über den Δ_{47}-Wert dargestellt:

$$\Delta_{47} = ((R^{47}/ R^{47*} - 1) - (R^{46}/ R^{46*} - 1) - (R^{45*}/ R^{45*} - 1)) * 1000 \text{ (‰)} \qquad \text{(Z1)}$$

In dieser Studie wurde die Analysetechnik für die *clumped isotope Thermometrie* an Karbonaten an der Goethe Universität in Frankfurt am Main erfolgreich aufgebaut. Dies ist über die Kurz- und Langzeitreproduzierbarkeit von Standardmaterialien und Proben belegbar. Außerdem wurde für NBS 19 ein Δ_{47}-Mittelwert bestimmt, der den Ergebnissen aus anderen Laboren entspricht und im Bereich des akzeptierten Wertes liegt. Die Häufigkeit von $^{13}C^{18}O^{16}O^{16}O^{2-}$- und $^{13}C^{18}O^{16}O$-Isotopologen in natürlichen Kristallen bzw. Gasen ist mit 67 bzw. 45 ppm sehr gering (Ghosh et al., 2006a). Dies erschwert die Probenaufbereitung und die Analytik. Zum einen muss vermieden werden, dass das Probengas mit Wasser in Kontakt kommt. H_2O bewirkt im Austausch mit CO_2 eine Re-equilibrierung und die Neuanordnung der Isotope in den Molekülen. Diese nähert sich an die Verteilung der Isotopologe an, die für die vorherrschende Temperatur charakteristisch ist. Deswegen wird das Analysengas an einer Glas-Extraktionsanlage unter Hochvakuum ($<10^{-6}$ mbar) gereinigt. Es wird mehrfach über Wasserfallen gegeben, die mit flüssigem Stickstoff gekühlt sind. Zusätzliche H_2O-Fallen sind an sämtlichen Präparationsgeräten installiert worden. Zudem wurden die ursprünglichen Edelstahlkapillaren des Massenspektrometers durch elektropolierte Ni-Kapillaren ausgetauscht, da diese weniger Wasser an ihrer inneren Oberfläche adsorbieren. Des Weiteren müssen Substanzen, die isobare Interferenzen mit m/z 47 ($^{13}C^{18}O^{16}O$) bewirken, mit Hilfe von Gas-Chromatographie abgetrennt werden. Die CO_2-Analyse erfolgt an einem Gas-Massenspektrometer MAT 253. Über ein duales Einlasssystem, werden abwechselnd Analyse- und Referenzgas in die Quelle transferiert und deren Isotopenverhältnisse R^{45}, R^{46}, R^{47}

bestimmt (Analysezeit: ~3 h). Die hier vorgestellten Δ_{47}-Werte sind mittels equilibrierter Gase direkt auf die absolute Skala von Dennis et al. (2011) transformiert worden, um für die Kompression, die von der Zusammensetzung des Referenzgases abhängt zu korrigieren und für Fraktionierungen, die systematisch in der Quelle auftreten. Dies ermöglicht schließlich einen Vergleich der Ergebnisse mit Δ_{47}-Daten aus anderen Laboren. Der Nicht-Linearitätseffekt für die Messung von m/z 47 wurde mittels sogenannter „heated gas-Geraden“ (1000 °C Gase) korrigiert.

Im Zuge dieser Arbeit konnte in Kooperation mit Stefano Bernasconi und seinem Forschungsteam an der ETH Zürich gezeigt werden, dass der Nicht-Linearitäteffekt durch Sekundärelektronen des m/z 44 Ionenstrahls hervorgerufen wird. Die Elektronen treffen auf den Kollektor für m/z 47 und bewirken einen negativen Untergrund. Eine Abhängigkeit zwischen der Steigung der “heated gas-Geraden” und dem negativen Untergrund auf dem Kollektor für m/z 47 wurde festgestellt. Außerdem wurde beobachtet, dass der negative Untergrund bei zunehmender Intensität des m/z 44 Ionenstrahls größer wird. Somit kann die Nicht-Linearität über die Messung des negativen Untergrundes auf dem Kollektor m/z 47 ermittelt werden. Dies reduziert die zeitaufwendige Bestimmung dieser Effekte über „heated gas Geraden“. Eine Korrekturmethode wurden vorgestellt, die jedoch nur angewendet werden kann, wenn der Kollektor für m/z 44 einen breiteren Spalt hat, als der für m/z 47. Da dies für das Massenspektrometer in Frankfurt nicht zutrifft, konnte diese Methode nicht angewendet werden. Stattdessen wurden Δ_{47}-Daten bezüglich der Nicht-Linearität weiterhin mit Hilfe von „heated gas-Geraden“ korrigiert.

CO_2-Analysegas aus Karbonaten wird mittels eines Phosphorsäureaufschlusses einer Proben generiert. Seit den Anfängen der *clumped isotope Analytik* an Karbonaten hat sich die Technik jedoch verändert. Ghosh et al. (2006a) verwendeten Reaktionsgefäße des McCrea-Typs und reagierten bei 25 °C für ca. 12 h. Heute werden Proben in den meisten Laboren bei 90 °C für ca. 30 min in einem *common acid bath* reagiert (z. B., Passey et al., 2010). In der vorliegenden Arbeit wurde ein Vergleich dieser Techniken durchgeführt, bei dem signifikante Unterschiede festgestellt wurden. Für CO_2-Gase aus Säurereaktionen bei 25 °C wurde eine Abhängigkeit des Δ_{47}-Wertes von der Probenmenge festgestellt. Im Vergleich zu Proben >7 mg wurden für Proben <7 mg höhere Δ_{47}-Mittelwerte bestimmt. Außerdem wurde für große Probenmengen eine geringere Streuung und somit prezisere Δ_{47}-Werte ermittelt. Dagegen trat dieser Effekt für Karbonate, die bei 90 °C reagiert wurden, nicht auf. Wir vermuten, dass bei Proben <7 mg die bei 25 °C reagiert werden, sekundäre Re-equilibrierung von CO_2 oder Zwischenprodukten mit

freiem Wasser in der Säure stattfindet. Diese Prozesse könnten mit der Verweildauer des Gases in der Säure zusammenhängen. Dass dieser Effekt bei 90 °C nicht auftritt, könnte mit der geringeren Reaktionszeit und der sehr kurzen Verweildauer des Analysengases in der Säure zusammenhängen. Unsere Beobachtungen zeigen, dass durch eine Erhöhung der Reaktionstemperatur von 25 auf 90 °C methodische Artefakte vermieden werden können, und genaue Δ_{47}-Werte für Karbonat-CO_2 bestimmt werden.

Die Umstellung auf höhere Temperaturen der Phosphorsäurereaktion hatte außerdem zur Folge, dass der Unterschied zwischen Fraktionierungsfaktoren bei 25 und 90 °C ($\Delta_{47}{}^{*}{}_{25-90}$) ermittelt werden musste, um einen Vergleich mit früheren Ergebnissen und mit Resultaten aus Laboren, die weiterhin Proben bei 25 °C reagieren, zu ermöglichen. Der theoretische $\Delta_{47}{}^{*}{}_{25-90}$-Wert ist 0.069‰ (Guo et al., 2009). Allerdings ermittelte Henkes et al. (2013) einen $\Delta_{47}{}^{*}{}_{25-90}$-Wert von 0.092‰ für *clumped isotope Daten*, die auf die absolute Skala projiziert worden waren. Unsere absoluten Δ_{47}-Daten bestätigen jedoch die Berechnung von Guo et al. (2009). In der vorliegenden Arbeit wurden $\Delta_{47}{}^{*}{}_{25-90}$-Werte von jeweils 0.066‰ bzw. 0.075‰ für Aragonit bzw. Kalzit bestimmt. Auf Grund der oben beschriebenen Abhängigkeit der Δ_{47}-Zusammensetzung von der Probenmenge, wurden für die Berechnungen der Δ_{47}-Mittelwerte der Karbonate, die bei 25 °C reagiert wurden, nur Proben >7 mg berücksichtigt.

Die Häufigkeiten von $^{13}C^{18}O^{16}O^{16}O^{2-}$-Isotopologen im Karbonatkristall sind nicht identisch mit den gemessenen Häufigkeiten von $^{13}C^{18}O^{16}O$-Isotopologen in den Analysegasen, da während der Säurereaktion Fraktionierungen auftreten. Sie sind jedoch proportional zueinander. Für die erste Kalibrierung des *Karbonat-clumped isotope-Thermometers* wurden synthetische Kalzite, die zwischen 0 und 50 °C ausgefällt wurden, analysiert (Ghosh et al., 2006a). Ghosh et al. (2006a) ermittelten eine lineare Abhängigkeit zwischen $1/T^2$ und Δ_{47}, die – bei bester analytischer Präzision – eine Sensitivität des Thermometers von ±2 °C aufweist. Diese Kalibrierung wurde durch Messungen rezenter biogener und synthetischer Karbonate in mehreren Studien bestätigt (z. B., Came et al., 2007; Tripati et al., 2010; Thiagarajan et al., 2011; Grauel et al., 2013; Zaarur et al., 2013). Allerdings bestimmmten Dennis und Schrag (2010) für synthetische Kalzite (7.5–77 °C) eine geringere Temperaturabhängigkeit (±3 °C), die theoretischen Berechnungen enspricht (Guo et al., 2009). Auch die später publizierten Kalibrierungsgeraden von Eagle et al. (2013) und Henkes et al. (2013) bestätigen die Steigung von Dennis und Schrag (2010). Allerdings treten Diskrepanzen zwischen den Achsenabschnitten dieser Geraden auf.

Teil dieser Arbeit war die Ausarbeitung einer weiteren Kalibrierung des *Karbonat-clumped isotope-Thermometers*. Dafür wurden kalzitische Biominerale (Brachiopodenschale, Muschelschale, Eischale eines Strauß, Foraminiferenschalen) und ein authigener Kalzit (*cold seep carbonate* – biologisch-induziert gefällte Minerale) analysiert, die zwischen 9 und 38 °C wuchsen. Die hier ermittelte universelle Kalibrierungsgerade ist identisch mit der theoretischen Berechnung von Guo et al. (2009) und mit der empirischen Geraden von Henkes et al. (2013), die auf aragonitische Muschelschalen und kalzitische Brachiopodenschalen beschränkt ist. Dieses Ergebnis ist von großer Wichtigkeit, da in der Henkes et al. (2013) Studie und in unserer Arbeit Kalibrierungsdaten zum ersten mal direkt auf die absolute Skala transferiert wurden; außerdem wurden für beide Studien gleiche Säurereaktionstechniken angewendet. Des Weiteren ist die Steigung unserer Geraden ebenfalls identisch bzw. zumindest vergleichbar mit der von Dennis und Schrag (2010) bzw. Eagle et al. (2013). Alle diese empirischen Studien beziehen sich auf eine Reaktion der Karbonate mit Phosphorsäure bei 90 °C. Im Gegensatz dazu wurden die Proben, die von Ghosh et al. (2006a), Came et al. (2007), Tripati et al. (2010) Thiagarajan et al. (2011) and Zaarur et al. (2013) analysiert wurden, bei 25 °C aufgeschlossen. Unsere Ergebnisse bestätigen somit die Vermutung, dass die unterschiedlichen Säurereaktionstemperaturen Auswirkungen auf Δ_{47}-Werte haben könnten. Allerdings resultieren die unterschiedlichen Steigungen der Kalibrierungsgeraden im Wesentlichen aus den verschiedenen Δ_{47}-Werten der kalttemperierten Karbonatproben, die in den jeweiligen Studien gemessen wurden. Zum jetzigen Zeitpunkt ist jedoch unklar, durch welchen Mechanismus dieser Sachverhalt verursacht werden könnte. Dieser Frage sollte in weiteren Untersuchungen nachgegangen werden. Es ist unwahrscheinlich, dass Ungleichgewichts-fällungen in der *clumped isotope-Zusammensetzung* oder *isotopic mixing-Effekte* Einfluss auf die in unserer Studie analysierten Kalzite hatten, da die Δ_{47}-Mittelwerte verschiedenartiger Proben, für die unterschiedliche Mineralisationsprozesse galten, auf einer Geraden plotten, die einen Korrelationskoeffizient R^2 von 0.9915 aufweist.

Erste Ergebnisse einer Kalibrierung an aragonitischen Muschelschalen bestätigen die Steigung der hier ermittelten Kalzit-Geraden des *clumped isotope-Thermometers*. Diese ist jedoch um –0.03‰ verschoben. Weitere Untersuchungen sind nötig, um den beobachteten Unterschied von ^{13}C-^{18}O *clumping* zwischen Kalzit und Aragonit zu überprüft.

In der hier präsentierten Arbeit wurde die *clumped isotope-Analytik* auf silurische Karbonate aus Gotland/Schweden angewendet. Für die Rekonstruktion von Temperaturen im marinen, tropischen Milieu im Silur, sowie für die Bestimmung der Sauerstoffisotopie des damaligen Ozeanwassers, wurde die Δ_{47}-Zusammensetzung kalzitischer Brachiopodenschalen gemessen.

Allerdings konnte mit Hilfe von Rasterelektronen- und Kathodolumineszenzmikroskopie (REM und KL) festgestellt werden, dass alle untersuchten Fossilien in Teilbereichen diagenetisch alteriert waren. Nichtsdestotrotz konnten gut erhaltene Bereiche in einigen Schalen mittels detaillierter REM Studien separiert werden. Die *clumped isotope-Temperaturen* $T(\Delta_{47})$ dieser Proben entsprechen den niedrigsten Werten unseres Datensatzes. Sie ergeben ~28 bis 33 °C und stellen sehr wahrscheinlich primäre Temperaturen des Oberflächenwassers dar. Für diese Proben wurden $\delta^{18}O$-Werte von ca. –1‰ für umgebendes silurisches Ozeanwasser ermittelt. Da angenommen wird, dass während des untersuchten Zeitintervalls die Pole eisfrei waren, geben unsere Ergebnisse Hinweise darauf, dass das Meerwasser seit dem Paläozoikum wie heute bei einem $\delta^{18}O$-Wert von (0 ± 1)‰ gepuffert war. Es sollte jedoch berücksichtigt werden, dass die ermittelten *clumped isotope-Temperaturen* Maximalwerte darstellen, da nicht ausgeschlossen werden kann, dass die analysierten Proben Spuren von alteriertem Kalzit enthielten. Somit stellen die rekonstruierten $\delta^{18}O$-Werte ebenso Maximalwerte dar. Des Weiteren ist der Fehler der berechneten Sauerstoffisotopie mit ungefähr ±1‰ sehr groß. Somit betrachten wir die rekonstruierten $\delta^{18}O$-Werte kritisch. Es kann nicht eindeutig ausgeschlossen werden, dass der Ozean im Silur eine geringeren Sauerstoffisotopie aufwies.

Die Größenordnung der $T(\Delta_{47})$-Werte, die für die Brachiopodenschalen bestimmt wurden, reicht von circa 30 bis 90 °C. Dieses große Interval entspricht der variablen Erhaltung der einzelnen Fossilien, die mittels REM- und KL-Analysen ermittelt wurde. Um die diagenetischen Prozesse, durch die die Brachiopodenschalen alterierten, zu rekonstruieren, wurden, neben den Schalen, zusätzlich die sekundären Phasen der Fossilfüllung analysiert (mikritische Phasen und sparitische Zemente). Da die Δ_{47}- und $\delta^{18}O$-Werte der Brachiopodenschalen nicht korrelieren, kann angenommen werden, dass die Sauerstoffisotopie während der Alteration der *clumped isotope-Zusammensetzung* nicht verändert wurde. Die Überprägung fand bei geringem Wasser–Gesteins-Verhältnis statt, weshalb der $\delta^{18}O$-Wert von der *bulk-Zusammensetzung* der Schale gepuffert war (*rock–buffered diagenesis*). Es kann somit davon ausgegangen werden, dass die gemessenen $\delta^{18}O$-Werte der Brachiopodenschalen Bedingungen des silurischen Meerwassers widerspiegeln. Der $T(\Delta_{47})$-Bereich, den die diagenetischen Phasen abdecken, entspricht dem Intervall, das für die Brachiopodenschalen bestimmt wurde (~30–90 °C). Die verschiedenen Zementgenerationen präzipitierten aus verschiedenen Lösungen in offenen Systemen. Die Lithifizierung der mikritischen Phase erfolgte während der frühen Diagenese. Es wird angenommen, dass während dieses Prozesses offenere Bedingungen bei größerem Wasser–Gesteins-Verhältnis herrschten, als bei der Alteration der Brachiopodenschalen.

Curriculum Vitae

Day/Place of birth	* 28.05.1984 in Nürnberg (Germany)
Education/School	
09/1990 – 07/1994	Primary school in Altdorf
09/1994 – 06/2003	Grammar school: Leibniz-Gymnasium Altdorf
06/2003	A-levels
University training	
10/2003 – 09/2004	Studies in chemistry at the Friedrich-Alexander-Universität (FAU) – Erlangen/Nürnberg (Germany)
10/2004 – 07/2010	Studies in geology/paleontology at the Friedrich-Alexander-Universität (FAU) – Erlangen/Nürnberg (Germany) Diploma thesis: High-resolution stable carbon and oxygen isotope records from Silurian brachiopod shells (Gotland/Sweden): distinguishing influences of seawater parameters, physiology and diagenesis
07/2010 – 08/2010	Assistant for Dr. Jens Fiebig at the Goethe Universität – Frankfurt (Germany)
09/2010 – 11/2013	Reasearch associate at the Goethe Universität – Frankfurt (Germany)
07/2010 – 08/2014	Dissertation Supervisor: Dr. Jens Fiebig; DFG – Project FI 948/4-1

Conference abstracts as a lead author

1. *Talk* U. Wacker, A. Munnecke, M.M. Joachimski: Stable carbon and oxygen isotope values from Silurian brachiopod shells from Gotland (Sweden): primary or diagenetically altered signals? – Paleozoic Seas Symposium/Graz 2009. – Awarded for the best talk.

2. *Talk* U. Wacker, A. Munnecke, M.M. Joachimski: Fossil brachiopod shells: reliable archives of seawater temperatures? – 2nd International Sclerochronology Conference ISC 2010. – Awarded for the second best student talk.

3. Poster U.Wacker, J. Fiebig, B.R. Schoene, A. Bahr: Clumped isotope analyses of NBS 19 and modern marine carbonates: first results from Frankfurt university – 2nd International Workshop on Clumped Isotopes, London 2011.

4. *Talk* U. Wacker, J. Fiebig, B.R. Schoene*:* Sample size affects ^{13}C-^{18}O clumping in CO_2 derived from phosphoric acid digestion of carbonates. – American Geophysical Union, Fall Meeting 2011, San Francisco.

5. *Poster* U. Wacker, J. Fiebig, A. Munnecke, M.M. Joachimski, B.R. Schoene: Clumped isotope signatures of Silurian brachiopod shells: pristine signals or diagenetic overprints? – European Mineralogical Conference[2], Frankfurt 2011.

6. *Talk* U. Wacker, J. Fiebig, A. Munnecke, M.M. Joachimski, B.R. Schoene: Clumped isotope analysis of modern carbonates and Silurian brachiopods – Sixth International Symposium on Isotopomers ISI, Washington 2012.

7. *Talk* U. Wacker, J. Fiebig, A. Munnecke, M.M. Joachimski, B.R. Schoene: Clumped isotopes applied to Silurian brachiopod shells, Gotland/Sweden – Goldschmid Conference, Montreál 2012.

8. *Short talk* U. Wacker, J. Fiebig, B.R. Schoene, A.D. Wanamaker: Empirical calibration of the "carbonate clumped isotope thermometer": biogenic calcite and aragonite – 3nd International Workshop on Clumped Isotopes, Harvard 2013.

9. *Talk* U. Wacker, J. Fiebig, B.R. Schoene: A comparison of two carbonate digestion techniques: sealed vessels vs common acid bath – 3nd International Workshop on Clumped Isotopes, Harvard 2013.

10. *Talk* U. Wacker, J. Fiebig, Clumped isotopes, $\delta^{18}O$, $\delta^{13}C$, $\delta^{11}B$, $^{87}Sr/^{86}Sr$: A multiproxy approach applied to Silurian brachiopod shells – Goldschmid Conference, Florence 2013.

List of publications

1. Background effects on Faraday collectors in gas-source mass spectrometry and implications for clumped isotope measurements" – Stefano M. Bernasconi, Bin Hu, **Ulrike Wacker**, Jens Fiebig, Sebastian F. M. Breitenbach, Tanja Rutz; Rapid Commun. Mass Spectrom. 2012, *27,* 603-612.

2. Clumped isotope analysis of carbonates: comparison of two different acid digestion techniques" – **Ulrike Wacker**, Jens Fiebig, and Bernd R. Schöne; Rapid Commun. Mass Spectrom. 2013, *27,* 1631-1642.

3. Empirical calibration of the clumped isotope paleothermometer using calcites of various origins" – **Ulrike Wacker**, Jens Fiebig, Julian Tödter, Bernd R. Schöne, André Bahr , Oliver Friedrich, Thomas Tütken, Eberhard Gischler, and Michael M. Joachimski; Geochem. Cosmochim. Acta 2014, *141*, 127-144.

4. Clumped isotope analysis applied to Silurian carbonates (Gotland/Sweden): deciphering both the alteration degree of fossil brachiopod shells and diagenetic processes" – **Ulrike Wacker**, Jens Fiebig, Axel Munnecke, and Michael M. Joachimski; to be submitted.